



Unraveling the functional relevance of the Ubiquitin-specific peptidase 22 for necroptotic cell death

Dissertation

zur Erlangung des Doktorgrades der Naturwissenschaften

vorgelegt beim Fachbereich 14 Biochemie, Chemie und Pharmazie
der Johann Wolfgang Goethe-Universität
in Frankfurt am Main

von

Jens Rödiger

aus Rüsselsheim

Frankfurt am Main, 2020

(D30)

Vom Fachbereich 14 der Johann Wolfgang Goethe-Universität als Dissertation
angenommen.

Dekan: Prof. Dr. Clemens Glaubitz
Gutachter 1: Prof. Dr. Volker Dötsch
Gutachter 2: Prof. Dr. Simone Fulda

Datum der Disputation:

Table of contents

1	Abstract.....	1
2	Introduction	3
2.1	The ubiquitin code and its players	3
2.1.1	Ubiquitination	3
2.1.2	Deubiquitinating enzymes.....	5
2.2	Ubiquitin-specific peptidase 22	7
2.3	Programmed cell death.....	10
2.3.1	Tumor necrosis factor receptor superfamily	11
2.3.2	NF- κ B pro survival signaling.....	11
2.3.3	Apoptosis	12
2.3.3.1	Intrinsic apoptosis.....	12
2.3.3.2	Extrinsic apoptosis.....	13
2.3.4	Necroptosis.....	15
2.3.5	The necroptotic core machinery	16
2.3.5.1	Receptor-interacting protein kinase 1.....	17
2.3.5.2	Receptor-interacting protein kinase 3.....	19
2.3.5.3	Mixed lineage kinase domain-like protein.....	20
2.3.6	Necroptosis in cancer	24
3	Aim of the study	27
4	Materials and Methods.....	28
4.1	Materials	28
4.1.1	Cell lines	28
4.1.1.1	Human cell lines	28
4.1.1.2	Stable transfected human cell lines.....	28
4.1.2	Murine cell lines	29
4.1.3	Cell culture reagents.....	30
4.1.3.1	Media.....	30
4.1.3.2	Media supplements and additional cell culture reagents.....	30

4.1.3.3	Cell death-inducing drugs	31
4.1.3.4	Inhibitors	31
4.1.3.5	Fluorescent dyes	31
4.1.4	Western blot-related materials	31
4.1.4.1	Western blot reagents	31
4.1.4.2	Buffers for Western blotting	32
4.1.4.3	Primary antibodies for Western blotting.....	34
4.1.4.4	Secondary antibodies for Western blotting.....	35
4.1.5	Mass spectrometry buffers and materials.....	35
4.1.6	Immunofluorescence-related materials.....	36
4.1.6.1	Buffers for immunofluorescence	36
4.1.6.2	Primary antibodies for immunofluorescence	36
4.1.6.3	Secondary antibodies for immunofluorescence.....	37
4.1.7	Material for cloning, DNA transfection and transduction.....	37
4.1.7.1	Plasmids	37
4.1.7.2	Mutagenesis primer	38
4.1.7.3	Cloning reagents and kits	39
4.1.7.4	Bacterial growth media	40
4.1.7.5	Oligonucleotides for generation of CRISPR/Cas9 knockout cells	40
4.1.7.6	Reagents for transfection and transduction.....	40
4.1.8	Small-interfering RNA (siRNA)	41
4.1.9	Kits.....	41
4.1.10	Chemicals	42
4.1.11	Consumables.....	43
4.1.12	Equipment.....	44
4.1.13	Software.....	46
4.2	Methods	46
4.2.1	Cell culture.....	46
4.2.2	Freezing and thawing of cell lines.....	47
4.2.3	Counting, seeding and treatment of cell lines.....	47
4.2.4	Generation of genetically modified cell lines.....	47
4.2.4.1	CRISPR/Cas9-derived USP22 and RIPK3 knockout cell lines.....	47
4.2.4.2	Site directed mutagenesis	48
4.2.4.3	Generation of stable cell lines using the T-REx™ system.....	48
4.2.4.4	Generation of stable cell lines using the Sleeping Beauty vector system	49

4.2.5	Transfection of cells.....	50
4.2.5.1	Transfection with Lipofectamine	50
4.2.5.2	Transfection with FuGENE HD.....	50
4.2.5.3	Reverse RNAiMAX.....	51
4.2.6	Western Blot analysis	51
4.2.6.1	Cell lysis	51
4.2.6.2	Determination of protein concentration.....	51
4.2.6.3	SDS Page and Western blotting.....	51
4.2.6.4	Detection of proteins.....	52
4.2.7	Determination of cell death	53
4.2.8	Immunoprecipitations.....	53
4.2.9	<i>In vivo</i> (de)ubiquitination immunoprecipitations.....	53
4.2.10	Complex-I and -II immunoprecipitations	54
4.2.11	Enrichment of ubiquitinated proteins using Tandem Ubiquitin Binding Entities.....	54
4.2.12	Immunofluorescence	55
4.2.13	Mass spectrometry (MS) analysis.....	55
4.2.13.1	Sample preparation	55
4.2.13.2	Analysis	56
4.2.13.3	Peptide identification	56
5	Results	57
5.1	USP22 governs necroptotic signaling by regulating RIPK3 ubiquitination and phosphorylation	57
5.1.1	USP22 regulates necroptosis in HT-29 cells	57
5.1.2	Loss of USP22 induces resistance to necroptotic cell death in RIPK3-expressing HeLa cells	70
5.1.3	USP22 controls RIPK3 ubiquitination during necroptosis induction.....	73
5.1.4	USP22 mediates RIPK3 ubiquitination and controls necroptosis through RIPK3 K518 ubiquitination.....	76
5.1.5	RIPK3 K518R hypersensitizes HT-29 cells to TBZ-induced necroptosis	85
6	Discussion.....	88
6.1	USP22 controls TBZ-induced necroptotic cell death in human tumor cell lines.....	88
6.2	USP22-mediated deubiquitination of RIPK3	89
6.3	USP22-mediated RIPK3 K518 ubiquitination regulates necroptosis progression....	90
6.4	USP22 affects RIPK3 phosphorylation during TBZ-induced necroptosis	92
6.5	Limitations and outlook	94

6.5.1	Dissecting the signaling cascade leading to delayed necroptotic cell death upon loss of USP22	94
6.5.2	Detailed investigation of USP22-mediated RIPK3 ubiquitination during necroptosis progression	94
6.5.3	Unraveling the effects of USP22-mediated changes on RIPK3 phosphorylation 95	
6.5.4	Evaluating the effects of USP22 on necroptosis-induced antitumor immunity .	96
7	Summary (Deutsche Zusammenfassung).....	98
8	References.....	103
9	Acknowledgements	119
10	Curriculum vitae.....	120
11	Erklärung	123

List of abbreviations

A20	Tumor necrosis factor, alpha-induced protein 3
aa	Amino acid
ABD	Antibody dilution
ADAM17	ADAM Metallopeptidase Domain 17
AIF	Apoptosis-inducing factor
AML	Acute myeloid leukemia
Apaf-1	Apoptotic protease-activating factor-1
APL	Acute promyelocytic leukemia
ATCC	American Type Culture Collection
ATG5	Autophagy protein 5
ATG7	Ubiquitin-like modifier-activating enzyme
ATP	Adenosine triphosphate
ATXN7	Ataxin 7
ATXN7L3	Ataxin 7 like 3
AXL	AXL Receptor Tyrosine Kinase
B	Smac mimetics
BAK	BCL2 Antagonist/Killer 1
BAX	BCL-2-associated X protein
BCL-2	B-cell lymphoma 2
BH3	BCL-2 homology 3
Bid	BH3-interacting domain death agonist
BMDCs	Bone marrow-derived dendritic cells
BR	Brace region
BRAF	B-Raf Proto-Oncogene, Serine/Threonine Kinase
BSA	Bovine serum albumin
CARDs	Caspase-recruitment domains
CDC37	Hsp90 co-chaperone Cdc37
CDK	Cyclin-dependent kinase
cFLIP	FLICE-like inhibitory protein
CHIP	HSC70-interacting protein
clAP1	Cellular inhibitor of apoptosis protein 1
CIM	clAP interaction motif
CLL	Chronic lymphocytic leukemia
CO ₂	Carbon dioxide
CRISPR	Clustered Regularly Interspaced Short Palindromic Repeats
CSN5	COP9 signalosome 5
CYLD	Ubiquitin carboxyl-terminal hydrolase CYLD
Dab	Dabrafenib
DAMPs	Damage-associated molecular patterns
DAPK	Death-associated protein kinase
DDs	Death domains
DEDs	Death effector domains
DISC	Death-inducing signaling complex
Dox	Doxycycline

Drp1	Dynamamin 1 Like
DRs	Death receptors
DSMZ	German Collection of Microorganisms and Cell Cultures
dsRNA	Double-stranded ribonucleic acid
DTT	Dithiothreitol
DUBm	Deubiquitinating module
DUBs	Deubiquitinating enzymes
ECL	Enhanced chemo-luminescence
EDTA	Ethylenediaminetetraacetic acid
ENY2	ENY2 Transcription And Export Complex 2 Subunit
ERK	Extracellular signal-regulated protein kinases
ESCRT	Endosomal Sorting Complex Required for Transport
FADD	Fas-associated protein with death domain
FAS	CD95 ligand
FBP1	Far Upstream Binding Protein 1
FCS	Fetal calf serum
FU	Fluorouracil
H2B	Histone 2B
H3	Histone 3
HCC	Hepatocellular carcinoma
HCD	Higher energy C-trap dissociation
HCL	Hydrochloric acid
HEPES	4-(2-hydroxyethyl)-1-piperazineethanesulfonic acid
HOIL-1	Central catalytic component E3 ubiquitin-protein ligase RNF31
HOIP	RANBP2-Type And C3HC4-Type Zinc Finger Containing 1)
HSP90	Heat Shock Protein 90
HSV-1	Herpes-simplex-virus 1
IFNs	Interferons
IKK α /IKK β	Inhibitor of nuclear factor κ B kinase subunits α/β
IL-1 β	Interleukin-1 β
IP	Inositol phosphate
IP	Immunoprecipitation
IPMK	Inositol polyphosphate multikinase
ISG15	Interferon-stimulated gene 15
ITPK1	Inositol-tetrakisphosphate 1-kinase
JAMMs	JAB1/MPN/MOV34 family
K	Lysine
KD	Kinase domain
KO	Knockout
LC3B	Microtubule-associated proteins 1A/1B light chain 3B
LGC	Laboratory of the Government Chemist
LIR	LC3-interacting motif
LOP	Loperamide hydrochloride
LUBAC	Linear ubiquitin chain-assembly complex
M1	Initiator methionine
MAPK	Mitogen-activated protein kinase
MEFs	Mouse embryonic fibroblasts

mg	Milligram
MINDY	Motif interacting with Ub-containing novel DUB
MJDs	Machado-Josephin domain proteases
ml	Milliliter
MLKL	Mixed lineage kinase domain-like protein
mM	Millimolar
MMTV	Mouse mammary tumor virus
MOMP	Mitochondrial outer membrane permeabilization
MS	Mass spectrometry
mTOR	Mammalian target of rapamycin
NaCl	Sodium chloride
NEDD8	Neural precursor cell expressed, developmentally downregulated 8
NEDP1	NEDD8-specific protease 1
NEMO	NF- κ B essential modulator
NF- κ B	Nuclear factor-kappa B
NIK	NF- κ B inducing kinase
NSA	Necrosulfonamide
OTUs	Ovarian tumor proteases
p115	General vesicular transport factor
p16INK4A	p16 cyclin-dependent kinase inhibitor 4a
p21	Cyclin-dependent kinase inhibitor 1
PAM	Protospacer adjacent Motif
PBS	Phosphate-buffered saline
PCR	Polymerase chain reaction
PDA	Pancreatic ductal adenocarcinoma
PD-L1	Programmed cell death 1 ligand 1
PELI1	Pellino E3 Ubiquitin Protein Ligase 1
Pen	Penicillin
PEP	Posterior error probability
PGAM5	Phosphoglycerate Mutase Family Member 5
PI	Propidium iodide
PIC	Protease inhibitor cocktail
PINK1	PTEN Induced Kinase 1
PIPs	Phosphatidylinositol phosphates
PKR	Double-stranded RNA-dependent protein kinase
PMSF	Phenylmethylsulfonyl fluoride
polyI:C	Polycytidylic acid
PPM1B	Protein Phosphatase, Mg ²⁺ /Mn ²⁺ Dependent 1B
PsKD	Pseudo kinase like domain
PTEN	Phosphatase and tensin homolog
PTM	Post translational modification
PyVT	Polyoma Virus middle T antigen
Q79	Polyglutamine (79 repeats)
qRT	Quantitative real-time
R	Arginine
RCAN1	Regulator of Calcineurin 1
REEP5	Receptor expression-enhancing protein 5

RHD	Reticulon homology domain
RHIMs	RIPK homotypic interaction motifs
RIPK	Receptor-interacting protein kinase
RNF4	RING-Type E3 Ubiquitin Transferase RNF4
ROS	Reactive oxygen species
SAGA	Spt-Ada-Gcn5 acetyltransferase
SB	Sleeping Beauty
SDS	Sodium dodecyl sulfate
SDS-PAGE	SDS-polyacrylamide gel electrophoresis
SEN1	Sentrin/SUMO-specific protease 1
SHARPIN	SHANK Associated RH Domain Interactor
SILAC	Stable isotope labeling of amino acids in cell culture
SIRT1	Sirtuin 1
SMAC	Second mitochondria-derived activator of caspases
Sp1	Transcription Factor Sp1
STING	Stimulator of interferon genes
Strep	Streptomycin
SUMO	Small ubiquitin-related modifier
T	TNF α
TAB2/3	TAK1-binding proteins 2 and 3
TAK1	Transforming growth factor- β -activated kinase 1
tBid	Truncated Bid
TBK1	TANK Binding Kinase 1
TBS	Tris-buffered saline
TEMED	Tetramethylethylenediamine
TLRs	Toll-like receptors
TNF α	Tumor necrosis factor α
TNFR-SF	Tumor Necrosis Factor Receptor Superfamily
TRADD	TNFR1-associated via death domain
TRAF2	TNF receptor-associated factor 2
TRAIL	TNF-related apoptosis inducing ligand
TRIF	Toll/Interleukin-1 receptor domain-containing adaptor inducing interferon- β
Trx1	Thioredoxin-1
TUBE	Tandem Ubiquitin Binding Entities
Ub	Ubiquitin
UbicREST	Ubiquitin Chain Restriction Analysis
UbL	Ubiquitin like
UCHs	Ubiquitin C-terminal hydrolases
UHD	Ubiquitin hydrolase domain
UHPLC	Ultra-High-Performance-Liquid-Chromatography
UHRF1	Ubiquitin-Like PHD And RING Finger Domain-Containing Protein 1
USP22	Ubiquitin-specific peptidase 22
USPs	Ubiquitin-specific proteases
VCPIP	Valosin-containing protein p97/p47 complex-interacting protein
XIAP	X-linked inhibitor of apoptosis protein
ZBP1	Virus-mediated activation of Z-DNA binding protein-1
ZNF	Zinc-finger motif

zVAD.fmk	N-benzyloxycarbonyl-Val-Ala-Asp(O-Me)fluoromethylketone
μg	Microgram
μl	Microliter
μM	Micromolar
2g	Two guide RNAs
4HB	Four helical bundle domain

List of tables

Table 1 Human cell lines	28
Table 2 Stable transfected human cell lines.....	28
Table 3 Murine cell lines.....	29
Table 4 Media.....	30
Table 5 Media supplements and additional cell culture reagents.....	30
Table 6 Cell death-inducing drugs.....	31
Table 7 Inhibitors and reagents.....	31
Table 8 Fluorescent dyes	31
Table 9 Western Blot reagents.....	31
Table 10 Buffers for Western blotting.....	32
Table 11 Primary antibodies for Western blotting	34
Table 12 Secondary antibodies for Western blotting.....	35
Table 13 Mass spectrometry buffers	35
Table 14 Mass spectrometry reagents and equipment	35
Table 15 Buffers for immunofluorescence.....	36
Table 16 Primary antibodies for immunofluorescence	36
Table 17 Secondary antibodies for immunofluorescence	37
Table 18 Plasmids.....	37
Table 19 List of mutagenesis primers	38
Table 20 Cloning reagents	39
Table 21 Bacterial growth media.....	40
Table 22 List of oligonucleotides for generation of small guide RNAs (sgRNAs).....	40
Table 23 List of reagents for transfection and transduction	40
Table 24 List of siRNA constructs	41
Table 25 List of kits	41
Table 26 List of chemicals.....	42
Table 27 List of consumables.....	43
Table 28 List of equipment.....	44
Table 29 List of software	46
Table 30 Taq polymerase PCR cycle conditions.....	49
Table 31 Phusion polymerase PCR cycle conditions.....	49

List of figures

Figure 1 The ubiquitination process and its complexity.....	4
Figure 2 Ubiquitin-specific peptidase 22 (USP22) and its function in Spt-Ada-Gcn5-acetyltransferase (SAGA) complex.	9
Figure 3 Schematic simplified overview of the extrinsic and intrinsic apoptotic pathway.	14
Figure 4 Necroptotic key players and their architecture.	16
Figure 5 Schematic overview of necroptotic signaling and its regulation via ubiquitin.	24
Figure 6 USP22 knockdown decreases TBZ-induced necroptotic cell death in HT-29 cells..	58
Figure 7 CRISPR/Cas9-mediated knockout (KO) of USP22 in HT-29 cells increases H2Bub1 levels.	58
Figure 8 USP22 knockout (KO) decreases TBZ-induced necroptotic cell death in HT-29 cells.	59
Figure 9 Loss of USP22 in HT-29 cells does not affect NF- κ B activation upstream of I κ B α	60
Figure 10 Loss of USP22 in HT-29 cells does not affect TB-induced apoptosis.	61
Figure 11 Stable reconstitution of USP22 in USP22 KO HT-29 cells re-sensitizes USP22 KO HT-29 cells for TBZ-induced necroptosis.	62
Figure 12 HT-29 USP22 KO (2g) cells display a comparable number of cells re-expressing USP22 PAM, USP22 PAM C185S or USP22 PAM C185A.	63
Figure 13 USP22 KO reduces TBZ-induced necroptotic cell death in acute lymphoblastic leukemia (ALL) Jurkat cells.	64
Figure 14 CRISPR/Cas9-mediated knockout of USP22 in NB4 cells does not affect TB-induced apoptotic cell death.	64
Figure 15 CRISPR/Cas9-mediated knockout of USP22 does not alter TBZ-induced cell death in MEF cells and the macrophage cell lines Raw264.7 or J774A.1.	65
Figure 16 USP22 KO reduces TRAIL(BZ)-and FasL(BZ)-induced necroptotic cell death in HT-29 cells.	67
Figure 17 USP22 KO leads to increased TBZ-induced RIPK3 phosphorylation in HT-29 cells.	69
Figure 18 USP22 knockdown in RIPK3-expressing HeLa cells induces resistance to TBZ-induced necroptotic cell death.	70
Figure 19 USP22 KO in HeLa TRex RIPK3 does not affect complex-I or -II formation.	71
Figure 20 USP22 KO leads to increased TBZ-induced RIPK3 phosphorylation in HT-29 cells.	72
Figure 21 USP22 interacts with RIPK3 independently of TBT treatment.	73
Figure 22 Increased RIPK3 ubiquitination in USP22 KO HT-29 cells during TBZ-induced necroptosis.	74

Figure 23 USP22 KO in HT-29 cells does not alter TBZ-induced RIPK1 ubiquitination.....	75
Figure 24 Ubiquitin remnant profiling identifies RIPK3 K518 as USP22-dependent ubiquitin target during necroptosis.....	76
Figure 25 SILAC incorporation does not alter the resistance of HT-29 USP22 KO cells to TBZ-induced necroptosis or the expression levels of necroptotic core proteins.	77
Figure 26 USP22-dependent modification of RIPK3 lysine residue 518 amplifies TBZ-induced necroptotic responses in RIPK3-reconstituted HeLa cells.	79
Figure 27 siRNA-mediated knockdown of USP22 in RIPK3-K518R or RIPK3 3xKR reconstituted HeLa cells does not affect sensitivity to TBZ-induced necroptotic cell death. ..	80
Figure 28 Mutation of RIPK3 lysine residue 518 alter RIPK3 phosphorylation upon TBZ-induced necroptosis in RIPK3-reconstituted HeLa cells.....	82
Figure 29 Mutation of RIPK3 lysine residue 518 amplifies necrosome formation upon TBZ-induced necroptosis in RIPK3-reconstituted HeLa cells.....	83
Figure 30 Mutation of RIPK3 lysine residue 518 decreases RIPK3 ubiquitination upon TBZ-induced necroptosis in RIPK3-reconstituted HeLa cells.....	84
Figure 31 RIPK3 KO HT-29 cells are resistant against TBZ-induced necroptosis.	85
Figure 32 RIPK3 K518R hypersensitize HT-29 cells for TBZ-induced necroptosis.	86
Figure 33 RIPK3 K518R amplifies necrosome formation upon TBZ-induced necroptosis in HT-29 cells.	87
Figure 34 USP22 controls necroptotic cell death by regulating RIPK3 phosphorylation and RIPK3 K518 ubiquitination.	93

1 Abstract

Ubiquitination is regarded as one of the key post-translational modifications in nearly all biological processes, endowed with numerous layers of complexity. Deubiquitinating enzymes (DUBs) dynamically counterbalance ubiquitination events by deconjugating ubiquitin signals from substrates. Dysregulation of the ubiquitin code and its negative regulators drive various pathologies, such as neurological disorders and cancer.

The DUB ubiquitin-specific peptidase 22 (USP22) is well-known for its essential role in the human Spt-Ada-Gcn5 acetyltransferase (SAGA) complex, mediating the removal of monoubiquitination events from Histone 2A and 2B (H2A and -B), thereby regulating gene transcription. In cancer, USP22 was initially described as a part of an 11-gene expression signature profile, predicting tumor metastasis, reoccurrence and death after therapy in a wide range of tumor cells. However, novel roles for USP22 have emerged recently, accrediting USP22 essential roles in regulating tumor development as well as apoptotic cell death signaling.

One of the hallmarks of cancer is the evasion of cell death, especially apoptosis, a form of programmed cell death (PCD). Necroptosis, a regulated form of necrosis, is regarded as an attractive therapeutic strategy to overcome apoptosis-resistance in tumor cells, although a profound understanding of the exact signaling cascade still remains elusive. Nevertheless, several ubiquitination and deubiquitination events are described in fine-tuning necroptotic signaling.

In this study, we describe a novel role for USP22 in regulating necroptotic cell death signaling in human tumor cell lines. USP22 depletion significantly delayed TNF α /Smac mimetic/zVAD.fmk (TBZ)-induced necroptosis, without affecting TNF α -induced nuclear factor-kappa B (NF- κ B) signaling or TNF α -mediated extrinsic apoptosis. Intriguingly, re-expression of USP22 wildtype in the USP22 knockout background could re-sensitize HT-29 cells to TBZ-induced necroptosis, whereas re-constitution with the catalytic inactive mutant USP22 Cys185Ser did not rescue susceptibility to TBZ-induced necroptosis, confirming the USP22 DUB-function a pivotal role in regulating necroptotic cell death. USP22 depletion facilitated ubiquitination and unexpectedly also phosphorylation of Receptor-interacting protein kinase 3 (RIPK3) during necroptosis induction, as shown by Tandem Ubiquitin Binding Entities (TUBE) pulldowns and *in vivo* (de)ubiquitination immunoprecipitations. To substantiate our findings, we performed mass-spectrometric ubiquitin remnant profiling and identified the three novel USP22-regulated RIPK3 ubiquitination sites Lysine (K) 42, K351 and K518 upon TBZ-induced necroptosis. Further assessment of these ubiquitination sites unraveled, that mutation of K518

in RIPK3 reduced necroptosis-associated RIPK3 ubiquitination and additionally affected RIPK3 phosphorylation upon necroptosis induction. At the same time, genetic knock-in of RIPK3 K518R sensitizes tumor cells to TNF α -induced necroptotic cell death and amplified necrosome formation.

In summary we identified USP22 as a new regulator of TBZ-induced necroptosis in various human tumor cell lines and further unraveled the distinctive role of DUBs and (de)ubiquitination events in controlling programmed cell death signaling.

2 Introduction

2.1 The ubiquitin code and its players

2.1.1 Ubiquitination

Ubiquitin (Ub) is a 76 amino acid (aa) long protein, highly conserved among eukaryotes and, as its name implies, ubiquitously expressed. Ubiquitin post-translationally modifies the vast majority of cellular proteins during their life-time and is thereby dictating a plethora of cellular processes. An orchestrated enzymatic cascade consisting of E1 ubiquitin-activating enzymes [1], E2 ubiquitin-conjugating enzymes [2] and E3 ubiquitin ligases [3], tightly regulates the covalent attachment of mono-ubiquitin or multiple ubiquitin molecules to the target substrate. This conjugation process is commonly defined as ubiquitination.

Ubiquitination is initiated by an E1-activating enzyme, which catalyzes the adenylation of the C-terminus of ubiquitin at the cost of adenosine triphosphate (ATP), forming a highly reactive thioester, which is directly transferred to the cysteine of an E2-conjugating enzyme [4]. Subsequently, an E3 ligase recruits E2 conjugating enzymes, loaded with activated ubiquitin and mediates the ligation between the C-terminus of ubiquitin and a lysine residue of the substrate protein, creating a stable isopeptide bond [5, 6] (Figure 1A). Substrates can be modified either by mono-ubiquitination or by poly-ubiquitination. Ubiquitin itself has eight ubiquitination sites, consisting of seven lysines and a methionine at the N-terminus, which can all be targeted for self-conjugation of ubiquitin. This generates a total of eight different homotypic ubiquitin chains, namely the initiator methionine (M1), K6, K11, K27, K29, K33, K48 or K63 chains (Figure 1B) [7-11]. Whereas K48- and K63- linked poly-ubiquitination are well characterized for their role in regulating protein degradation [11] and cell signaling [12], the specific role for the residual linkage types still remains to be further characterized [8, 9]. Meanwhile, ubiquitin chains can also be heterotypic by mixing of linkages, which amplifies the complexity of ubiquitination. Two types of heterotypic chains exist: Firstly, mixed ubiquitin chains, generated by diverse linkage types within the same ubiquitin chain and secondly, branched ubiquitin chains, generated through ubiquitination of multiple lysines within the very same ubiquitin molecule. Furthermore, several (~10) ubiquitin-like proteins, comprised of e.g. the interferon-stimulated gene 15 (ISG15) [13], the small ubiquitin-related modifier (SUMO) [14] and the neural precursor cell expressed, developmentally downregulated 8 (NEDD8) [15], exist. Ubiquitin-like proteins can be linked to either a lysine of an existing ubiquitin chain, ligated to a lysine residue of a substrate protein directly or modified with ubiquitin themselves, generating a comprehensive crosstalk among ubiquitin-signaling and ubiquitin-like pathways.

For instance, RING-Type E3 Ubiquitin Transferase RNF4 (RNF4) promotes genomic stability by poly-ubiquitination of SUMOylated proteins [16]. Moreover, ubiquitin-NEDD8 hybrid chains are formed in response to proteotoxic stress, protecting the cell from proteotoxicity [17].

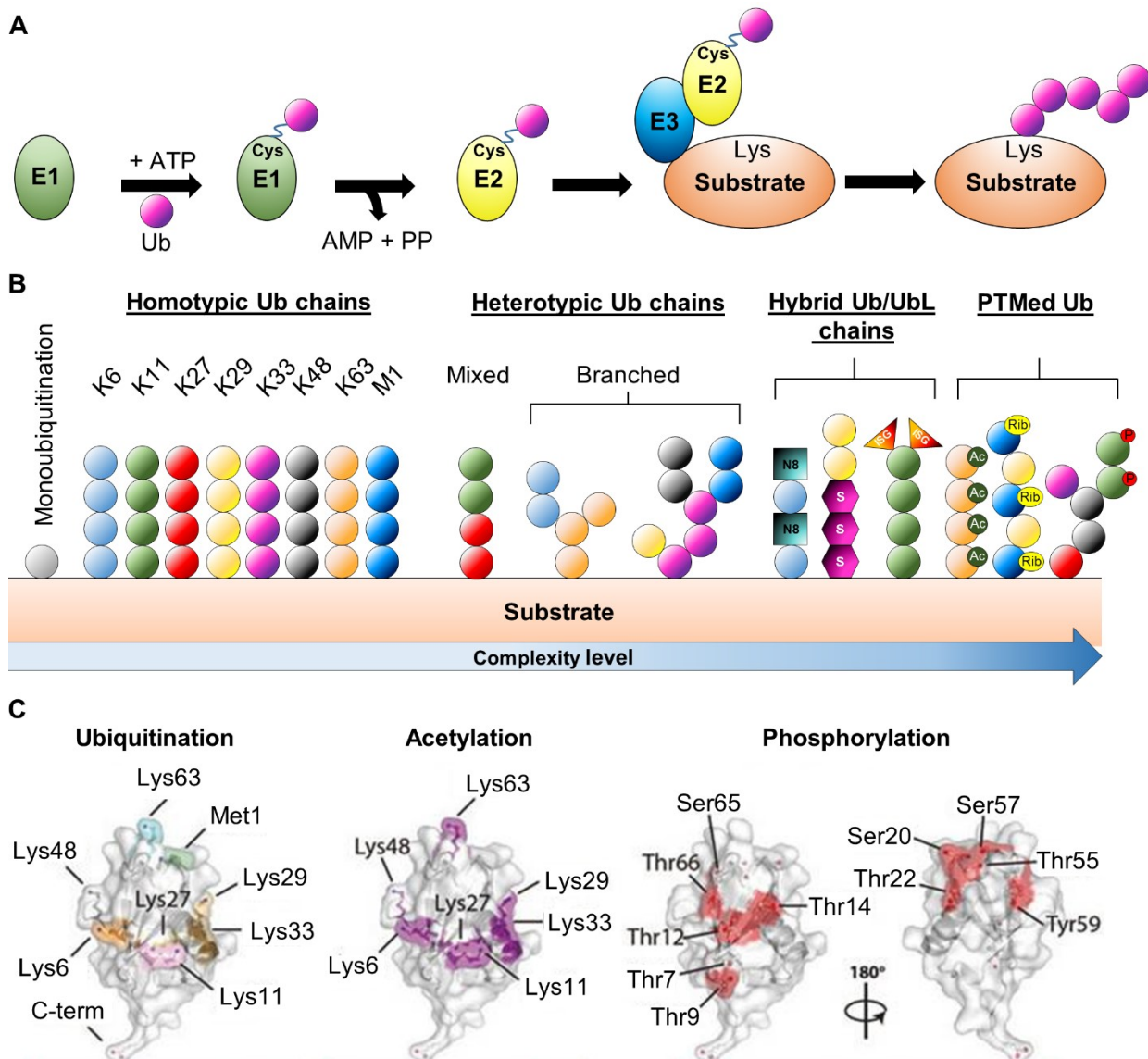


Figure 1 The ubiquitination process and its complexity. **A** At the cost of ATP, E1-activating enzymes (E1) catalyze the adenylation of the C-terminus of ubiquitin, forming an E1-Ub thioester. Afterwards, activated ubiquitin is transferred to an ubiquitin-activating enzyme (E2). An interplay between E2 and E3 ligases (E3) facilitate ubiquitin conjugation to the lysine of the substrate protein. **B** Schematic overview of the ubiquitin code, in ascending order of complexity from left to right. Monoubiquitination as the least complex modification can be further modified with additional ubiquitin molecules at the same lysine, generating eight different homotypic ubiquitin chains. Further on, heterotypic chains, in mixed or branched polymers, increase complexity. Extensive cross-talk between ubiquitin and ubiquitin-like (UbL) proteins, such as neural precursor cell expressed, developmentally downregulated 8 (NEDD8; N8), small ubiquitin-related modifier (SUMO; S), interferon-stimulated gene 15 (ISG15; ISG) or post-translationally modified ubiquitin (PTMed Ub), generates a plethora of complexity levels. **C** Described modifications sites on ubiquitin as a cartoon in ball-and-stick representation in semitransparency. Oxygen atoms are displayed in red, nitrogen atoms in blue. Ubiquitin contains eight different sites for ubiquitination and seven lysine sites for acetylation. Proteomic analysis revealed several different phosphorylation sites of ubiquitin, displayed as red spheres, to indicate phosphorylatable hydroxyl groups on serine/threonine and tyrosine residues. Ubiquitin is shown in a frontal and back view to indicate all phosphorylation sites. Figure adapted and modified from [8, 10].

As an additional way to fine-tune the ubiquitin code, ubiquitin can be acetylated [18], ribosylated [19] or phosphorylated at one of the 11 serine, threonine or tyrosine residues [20-

22] (Figure 1C). In fact, phosphorylated ubiquitin was previously shown to participate in mitophagy initiation. As such, PTEN Induced Kinase 1 (PINK1) phosphorylates ubiquitin at Ser65 [23], thereby creating a recruitment platform for autophagy adaptors [24] and the E3 ubiquitin ligase Parkin [25, 26].

Due to its omnipresence, ubiquitin plays a pivotal role in cellular processes like transcriptional regulation [27], cell cycle regulation [28], DNA repair [29], immune signaling [30], autophagy [31] and cell death [32]. Consequently, dysfunction in ubiquitination drives various pathologies such as neurological disorders like Huntington's [33], Parkinson's [34] and Alzheimer's [35] disease as well as cancer [36].

Collectively, ubiquitination is regarded as one of the most powerful post-translational modifications (PTMs), artfully designed and regulated in a highly complex manner. Various deubiquitinating enzymes (DUBs) exist to dynamically counter-balance these sophisticated ubiquitination events by deconjugating ubiquitin signals from substrates in an equally elaborated way [37, 38].

2.1.2 Deubiquitinating enzymes

Deubiquitinating enzymes (DUBs) dynamically orchestrate the removal of highly complex ubiquitin signals generated throughout the ubiquitination process. Until now, over 100 differential DUBs are described which can be divided into six structurally distinct DUB families due to the architecture of their respective catalytic domains and similarities in amino acid sequences: The ubiquitin C-terminal hydrolases (UCHs), the ubiquitin-specific proteases (USPs), the ovarian tumor proteases (OTUs), the Machado-Josephin domain proteases (MJDs), the JAB1/MPN/MOV34 family (JAMMs) and the motif interacting with Ub-containing novel DUB (MINDY) family [9, 39]. Except for the JAMMs, all other DUB family members are cysteine proteases and can be inactivated by residue substitution of the active cysteine site.

The process of deubiquitination is directed through at least one ubiquitin-binding site, the so-called S1 site, which is present at the DUB surface, guiding the ubiquitin C-terminus as well as the scissile bond to the catalytic center [40]. Subsequently, the peptide bond between the substrate and the ubiquitin C-terminus is hydrolyzed. In general, removal of mono- or poly-ubiquitination by DUBs from a substrate is conducted either by direct substrate binding or by binding to ubiquitin. Direct substrate binding enables DUBs to selectively target signaling pathways through interaction with the substrate, either alone or as part of a macromolecular protein complex such as the proteasome [41] or the Spt-Ada-Gcn5 acetyltransferase (SAGA) complex [42, 43], whereas targeting selective ubiquitin chain types regulates global linkage type abundance.

Apart from ubiquitination, proteins can be modified with ubiquitin-like (UbL) proteins such as ISG15, NEDD8 or SUMO. These UbL modifications are regulated by ubiquitin like proteases

(ULPs), e.g. the NEDD8-specific protease 1 (NEDP1) [41], or the sentrin/SUMO-specific protease 1 (SENP1) [42] which catalyze the removal of NEDDylation or SUMOylation, respectively. Despite the similarity of UbL modification to ubiquitin, DUBs are able to distinguish between Ub and UbL modifications with high accuracy. Unique hydrophobic surfaces on ubiquitin paired with accurate recognition of the C terminus enables a precise DUB interaction and cleavage of ubiquitin chains [8, 44].

A pivotal factor in regulating ubiquitin-dependent processes is the fine-tuning of DUB function. This is warranted by several PTMs, which can act in concert or alone, ensuring correct DUB localization, abundance and activity. Phosphorylation and multiple monoubiquitination events are known to dynamically change DUB localization, leading to nuclear localization or exclusion of the respective DUB [45-49]. DUB abundance can be positively or negatively adjusted in a stimulation-dependent manner. As such, protein levels of the Tumor necrosis factor, alpha-induced protein 3 (A20) were shown to be drastically increased upon NF- κ B activation, whereas USP1 levels were depleted upon UV radiation via autoprocessing [50-52]. The activation or inactivation of DUBs is tightly regulated by various phosphorylation events. Phosphorylation of Ubiquitin carboxyl-terminal hydrolase CYLD (CYLD) by the inhibitor of nuclear factor kappa B kinase subunit beta (IKK β) was shown to positively regulate the DUB-activity of CYLD [53]. On the other hand, valosin-containing protein p97/p47 complex-interacting protein (VCPIP) is inactivated by phosphorylation in early mitosis [54]. Akin to phosphorylation of DUBs, PTMs such as SUMOylation or ubiquitination were shown to interfere with DUB binding and cleavage or they enhanced catalytic activity [55, 56]. Furthermore, PTMed ubiquitin is gaining importance in modulating DUB activity. For example, mitochondrial ubiquitin-specific peptidase 30 (USP30) has less activity towards phospho-ubiquitin compared to unmodified ubiquitin [57, 58].

The physiological role of DUBs is to counterbalance E3 ubiquitin ligases-mediated ubiquitination in order to regulate protein stability and quality as well as to maintain ubiquitin homeostasis. In particular, they can regulate various cellular signaling pathways such as DNA damage response [59, 60], cell cycle [43], inflammation [30, 61] and cell death [44, 62]. DUB-mediated deubiquitination and DUB fine-tuning is accomplished in a highly ingenious way, as described above. Therefore, it is no surprise that dysregulation can have dramatic physiological consequences that contribute to severe diseases, such as several neurological diseases [63-65]. Furthermore, DUBs are well-known to act as oncogenes, tumor suppressors or are associated with tumor progression [66-69].

2.2 Ubiquitin-specific peptidase 22

Ubiquitin-specific peptidase 22 (USP22) belongs to the USP superfamily, which comprise the largest subfamily of the deubiquitinases, consisting of 54 members in humans [9] and being highly conserved in function and in structure. USP22 is ubiquitously expressed and primarily enriched in the nucleus [70, 71]. Two major domains shape the structure of USP22, the N-terminal zinc-finger motif (ZNF; aa 63–134) as well as a catalytically-active C-terminal ubiquitin hydrolase domain (UHD; aa 176–518) (Figure 2A). As a cysteine protease, the ubiquitin hydrolysis activity of USP22 can be inactivated by substitution of the conserved residues Cys185 and His479 [72, 73].

USP22 was initially described as a part of an 11-gene expression signature profile, presumably capable of predicting tumor metastasis, reoccurrence and death after therapy. For this, Glinsky *et al.* tested the prognostic power of the 11-gene expression signature profile in 11 differential types of cancer, including 5 epithelial malignancies (bladder, ovarian, lung, breast and prostate cancer) and 5 nonepithelial malignancies (acute myeloid leukemia (AML), mesothelioma, medulloblastoma, glioma and lymphoma) [74]. Indeed, several studies applying immunohistochemistry and RT-qPCR observed USP22 upregulation in various cancer types, including esophageal, colorectal, breast, ovarian, stomach and pancreatic cancers [75-82]. Contradictory, by utilizing gene sequencing and mRNA expression data analysis, studies could demonstrate a USP22 downregulation, mutation or deletion in the very same cancer types [83, 84]. Nevertheless, both subsets of cancer types seem to exist side by side and contribute to oncogenesis, implying functional implications for cancer development and progression, tightly regulated by variations in USP22 expression levels.

USP22 is well characterized as a transcriptional activator. As such, it participates, together with Ataxin 7 like 3 (ATXN7L3), Ataxin 7 (ATXN7) and ENY2 Transcription and Export Complex 2 Subunit (ENY2), in forming the deubiquitinating module (DUBm) of the human Spt-Ada-Gcn5-acetyltransferase (SAGA) complex [85]. The SAGA complex is a large protein complex (~2MDa), activating transcription by remodeling chromatin. It has two main catalytic activities: Firstly, the acetylation of Histone 3 (H3) and secondly, the deubiquitination of H2A and H2B (Figure 2B). ATXN7 is necessary to anchor the DUBm within the SAGA complex, whereas ATXN7L3 is crucial for directing H2B monoubiquitination (H2Bub1) substrate specificity of the DUBm [86]. Within the DUBm, USP22 deubiquitinates H2A K119 and H2B K120 (Figure 2C), thereby promoting transcriptional activation [43, 87]. Of note, the catalytically active conformation of USP22 in the DUBm is strongly dependent on its assembly [86, 88]. Interestingly, USP27 and USP51 were shown to compete with USP22 for ATXN7L3 and ENY2 binding in order to remove H2Bub1 [89]. However, this compensatory mechanism seems to be restricted to specific cellular functions, as studies could show a lack of compensation for

USP22 mediated H2Bub1 deubiquitination in transcriptional activation and DNA damage repair [87, 90].

USP22 is well described for its capacity to remove monoubiquitination from histone H2B in the human SAGA complex, as described in detail above. Apart from that, little is known regarding the ubiquitin linkage specificity of USP22. Nevertheless, some studies could demonstrate a propensity towards K48- and K63-linked poly-ubiquitin chains, which particularly regulate protein stability and protein interaction [91-94]. Moreover, a recent study demonstrated that USP22 and USP13 form a so-called signalosome to act as negative regulators in the type I interferon pathway. In detail, USP22 recruits USP13 after Herpes-simplex-virus 1 (HSV-1) stimulation, initiating USP13- mediated deubiquitination of K27-linked ubiquitin chains from STING which in turn prevents the recruitment of TANK Binding Kinase 1 (TBK1) to the complex [95]. This study highlights a sophisticated interplay between two DUBs to catalyze the deubiquitination of the target substrate, adding an additional indirect role for USP22 in the removal of K27-linked poly-ubiquitin chains.

Besides inducing gene dysregulation by modifying transcriptional activation, USP22 is implicated in modulating cell cycle progression, another hallmark of cancer. In fact, various studies linked altered USP22 expression with changes in cell cycle progression and checkpoints. Moreover, USP22 silencing could be shown to correlate with a G1 accumulation in lung, colorectal and breast cancer cell lines [91, 96, 97] as well as in human fibroblasts [85]. At the same time, USP22 overexpression facilitates G1/S transition, leading to S-phase accumulation [81]. Various studies tried to shed light on how USP22 is controlling the G1/S transition. For instance, USP22 deubiquitinates Far Upstream Binding Protein 1 (FBP1) by removing K63 linked poly-ubiquitin chains [91], thus preventing FBP1 from repressing its target, the cyclin-dependent kinase (CDK) inhibitor 1 (p21). This in turn blocks the formation of CDK complexes, essential for proper G1/S transition. Interestingly, a different role for USP22 in regulating G2/M progression via controlling CDK1 and Cyclin B1 expression levels could be described in brain glioma cells [98]. This discrepancy may be explained by the use of heterogeneous cellular cancer models. Regardless of these observed variations, USP22 seems to facilitate premature cell cycle transition in a wide range of tumor cell lines.

Intriguingly, apart from its role in regulating transcription and cell cycle progression, USP22 known to be involved in cell death regulation. Several studies could show that USP22 silencing increases apoptosis in multiple cancer cell lines such as colorectal and brain glioma cells as well as in embryonic fibroblasts [59, 97, 98]. Inversely, overexpression of USP22 diminished trichostatin A-induced apoptosis and caused treatment resistance [99, 100]. USP22 primarily regulates apoptosis by catalyzing the removal of poly-ubiquitin chains from sirtuin 1 (SIRT1), protecting it from proteasomal degradation and thereby modulating its abundance. This leads to TP53 deacetylation and transcriptional inhibition of TP53 target genes, impairing apoptosis

[59, 98]. Moreover, SIRT1 was shown to stabilize c-Myc in a deacetylation-dependent manner, restricting apoptosis through a positive feedback loop [100].

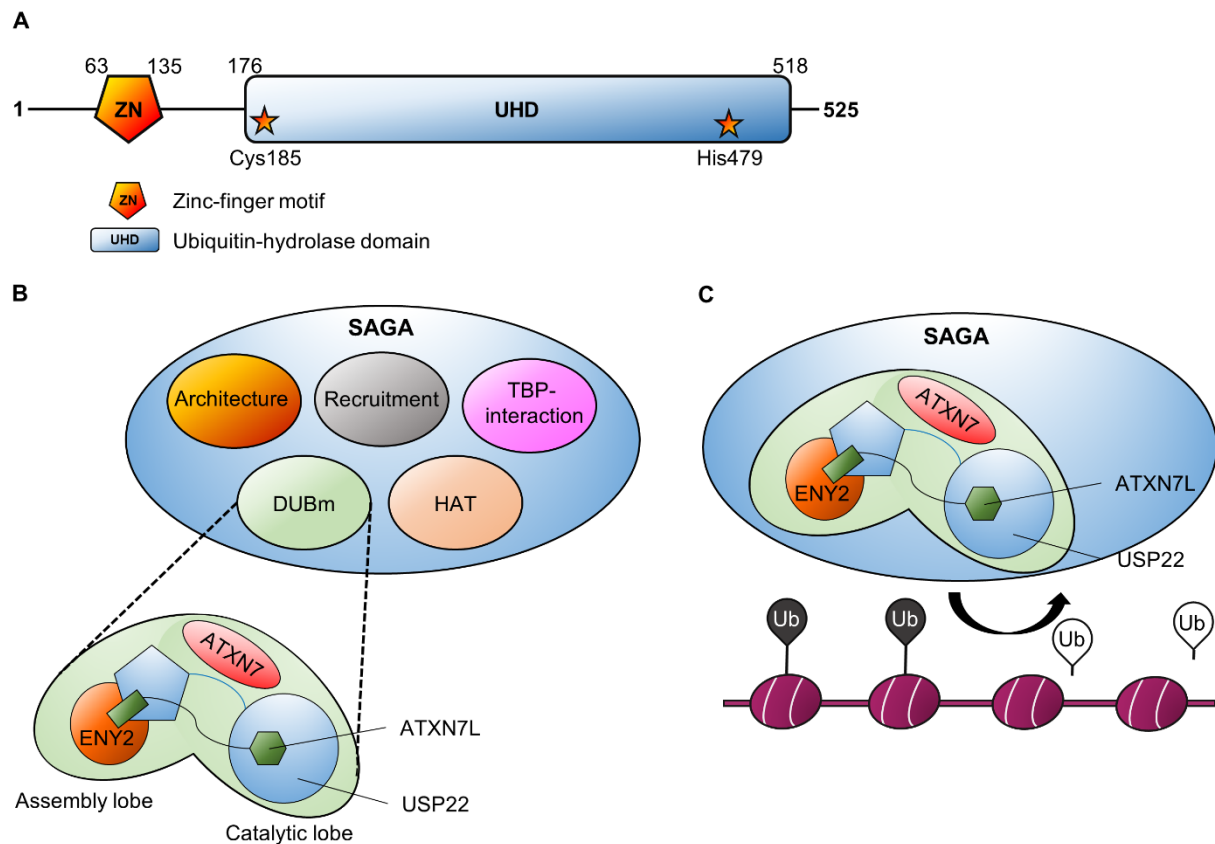


Figure 2 Ubiquitin-specific peptidase 22 (USP22) and its function in Spt-Ada-Gcn5-acetyltransferase (SAGA) complex. **A** Schematic visualization of USP22 and its protein domains. USP22 comprises an N-terminal zinc-finger motif (ZNF; pentagon) and the catalytically-active C-terminal ubiquitin hydrolase domain (UHD; rectangle). Starting and ending positions of each domain are indicated by the respective amino acid number. Asterisks illustrate the evolutionarily-conserved catalytic residues, Cys185 and His479. **B** The multi-module SAGA-complex comprises the deubiquitinase module (DUBm) and the histone acetyl transferase (HAT) module, both catalytically-active, as well as modules for SAGA architecture, recruitment and the TATA-binding protein interaction (TBP). The DUBm is divided into an assembly and a catalytic lobe. Whereas the assembly lobe is formed by the USP22 N-terminal zinc finger motif (blue pentagon) and ENY2, which are structured around the N-terminal helix of ATXN7L3 (green rectangle), the catalytic lobe is formed by the N-terminal zinc-finger domain of ATXN7L3 (green hexagon) and the C-terminal ubiquitin hydrolase domain of USP22 (blue circle). ATXN7 tethers the DUBm to the rest of the SAGA-complex. **C** Schematic illustration of the DUBm, including USP22, removing mono-ubiquitination from a histone. Figure adapted and modified from [84].

Besides apoptosis, USP22 overexpression has also been linked to autophagy. Autophagy is defined as a lysosomal recycling and degradation process, triggered by intra- or extracellular stress conditions, thereby ensuring stable cellular metabolism of the cell [101, 102]. In cancer, sustained autophagy can promote tumor survival, treatment resistance and cell death in a highly context-dependent manner [103, 104]. Mechanistically, USP22 overexpression promotes the activation of the Extracellular signal-regulated protein kinases (ERK) 1/2 pathway and has indirect effects on Autophagy protein 5 (ATG5) and Ubiquitin-like modifier-activating enzyme (ATG7) by modulating SIRT1 abundance, stimulating autophagy [79, 105].

A number of early studies presented a USP22 overexpression in different cancer types, promoting oncogenesis by altering cell cycle progression, transcription, gene expression and cell death. For instance, cancer stem cells, isolated from primary lung adenocarcinomas, displayed elevated levels of USP22, which played a critical role in promoting tumorigenicity and cisplatin resistance [106]. In addition, a USP22-associated loss of H2Bub1 was shown to promote tumor aggressiveness and play a pivotal role in the malignancy and progression of non-small cell lung cancer [107, 108]. Nevertheless, several recent studies identified USP22 to be more frequently downregulated in numerous cancer types than upregulated, indicating a potential oncogenic influence in an attenuated USP22 function and expression [83].

In contrast to its oncogenic role in many different cancer cells, emerging evidence arises that USP22 can also display tumor suppressive roles. For example, by deubiquitinating the transcription factor PU.1, USP22 stabilizes PU.1, thus promoting the expression of myeloid-differentiation genes and thereby impeding with AML development [109]. Kosinsky *et al.* could recently demonstrate that USP22 loss increases colorectal cancer burden by modulating mammalian target of rapamycin (mTOR) activity. They could show a tumor suppressive function of USP22 *in vivo* and highlight a tumor- and context-specific role of USP22 [110].

As USP22 expression is closely associated with neurodegenerative diseases, carcinogenesis and poor patient survival in a wide range of tumor types [74, 76-79, 82, 100, 111-113], targeting USP22 or its downstream effectors is regarded as a promising strategy for cancer therapy. Nevertheless, a recent study could point out a highly tumor- and context-dependent function of USP22 [110], which highlights the complexity in targeting USP22. Since USP22 displays both oncogenic and tumor suppressor-like properties, it will be crucial to assess whether directly targeting USP22 or exploiting reduced expression levels of USP22 may be more therapeutically beneficial.

2.3 Programmed cell death

PCD is an essential regulatory mechanism, involved in tissue homeostasis, embryonic development and pathogenesis by efficiently controlling cell growth and the removal of potentially harmful cells from the organism [114]. To date, 10 different forms of PCD are described, relying on distinct and sometimes overlapping mediators to be activated [115, 116]. Targeting forms of PCD by interfering with or by amplifying the respective signaling cascade, to especially kill cancer cells, is regarded as an auspicious approach for current therapy perspectives [114, 116].

2.3.1 Tumor necrosis factor receptor superfamily

The Tumor Necrosis Factor Receptor Superfamily (TNFR-SF) is part of a series of innate immune receptors, regulating the immune response against invading pathogens. The response is mediated by recognition of specific pathogen-associated molecular patterns. This in turn activates various signaling pathways, including the NF- κ B and the mitogen-activated protein kinase (MAPK) pathway. Consequently, pro-inflammatory cytokines and chemokines are produced [117], modulating the innate immune response by binding and activating for example receptors of the TNFR-SF.

The TNFR-SF, consisting of 29 receptors, can be divided into death receptors (DRs), decoy receptors and TNF α receptor-associated factor (TRAF)-interacting receptors [118, 119]. DRs, such as the prototypical Tumor Necrosis Factor Receptor-1 (TNFR1) are translating death signals from the surface into the cell via their intracellular death domains (DDs), a conserved region of 80 aa. They tightly regulate inflammation, cell proliferation, NF- κ B-mediated pro-survival signaling and PCD [120]. Two of the best studied forms of PCD, apoptosis and necroptosis, can be initiated via the TNFR1 signaling pathway.

2.3.2 NF- κ B pro survival signaling

NF- κ B signaling can either follow a canonical or a non-canonical pro-survival pathway and is based on transcription factors, which regulate gene expression necessary for proliferation, survival and inflammation [121]. TNF α binding to TNFR1 leads to the formation of complex-I and is initiated by binding of the adaptor protein TNFR1-associated via death domain (TRADD) and the Receptor-interacting protein kinase (RIPK1) to the TNFR1 DD via homotypic DD interactions [122, 123]. TRADD then serves as a platform for recruiting TNF receptor-associated factor 2 (TRAF2) [124]. Due to the cIAP interaction motif (CIM) within TRAF2, the two E3 Ub ligases cellular inhibitor of apoptosis (cIAP) protein 1 and 2 (cIAP1/2) can be further incorporated into the complex [124, 125]. Ensuing their recruitment, cIAP1/2 ubiquitinate various components of complex-I such as RIPK1 and cIAP1 itself with K11/48/63-linked ubiquitin chains [32, 126-130]. This facilitates the recruitment of the linear ubiquitin chain-assembly complex (LUBAC), consisting of the central catalytic component E3 ubiquitin-protein ligase RNF31 (HOIL-1), RANBP2-Type and C3HC4-Type Zinc Finger Containing 1 (HOIP), and SHANK Associated RH Domain Interactor (SHARPIN), exclusively generating M1-linked poly-ubiquitin chains on TRADD, TNFR1 and RIPK1 [125, 131]. LUBAC and cIAP1/2-mediated poly-ubiquitination serves as scaffold for recruitment and retention of kinase complexes [125, 130, 132-135] consisting of inhibitor of nuclear factor κ B kinase subunits α/β and NF- κ B essential modulator (NEMO/IKK α /IKK β), transforming growth factor- β -activated

kinase 1 (TAK1) and TAK1-binding proteins 2 and 3 (TAB2/3) [136]. TAK1 subsequently activates IKK β by phosphorylation, leading to phosphorylation and degradation of I κ B α [137]. This abrogates the interaction of I κ B α with NF- κ B proteins in the cytoplasm and leads to translocation of NF- κ B proteins to the nucleus, inducing the expression of several pro-survival genes [138, 139]. cIAP proteins negatively regulate the non-canonical NF- κ B activation in interplay with TRAF2 and TRAF3 by mediating the ubiquitination and successive degradation of the NF- κ B inducing kinase (NIK) [140]. Binding of TNF α to TNFR1 induces the recruitment of cIAP1/2, TRAF2 and TRAF3 to the receptor causing complex formation and successive cIAP mediated K48-linked poly-ubiquitination and proteasomal degradation of TRAF3 [141-143]. Alternatively, cIAP antagonist treatment can reduce cIAP protein levels, leading to NIK stabilization and accumulation. NIK accumulation induces processing of p100 to p52 and NF- κ B p52-RELB heterodimers into the nucleus, activating non-canonical NF- κ B signaling [138].

2.3.3 Apoptosis

Apoptosis is a form of PCD and seizes a pivotal role in maintaining tissue homeostasis such as the clearance of damaged or potentially harmful cells, T-cell development and embryogenesis [144-147]. Multiple groups of executioner and regulatory molecules participate in the correct implementation of this form of PCD. Regarding this high level of complexity, it is no surprise that dysregulation of apoptotic signaling is associated with severe diseases like Parkinson's, Alzheimer's [148] and cancer. Especially in cancer, evasion of apoptosis promotes tumorigenesis, treatment failure and relapse [149, 150]. Apoptotic cell death is typically associated with characteristic morphological changes, such as the condensation of chromatin material, nuclear DNA fragmentation, cell shrinkage, dynamic membrane blebbing and loss of cell adhesion. Biochemically, apoptosis is accompanied by externalization of phosphatidylserine and by activation of cysteine-aspartic proteases (caspases), typically existing as inactive precursors [151-153]. Caspase activation is triggered by induced proximity and subsequent autocatalytic cleavage of inactive pro-caspases, resulting in substrate cleavage and successive cell death [154, 155]. Mechanistically, apoptosis has two core pathways: The DR-mediated extrinsic pathway and the mitochondrial-mediated intrinsic pathway [156, 157] (Fig. 3).

2.3.3.1 Intrinsic apoptosis

Intrinsic apoptosis, also referred to as the mitochondrial pathway of apoptosis, typically emanates due to internal cellular stress such as irradiation-mediated DNA damage, accumulation of unfolded proteins, oxidative stress or growth factor withdrawal in a cell-autonomous manner [115, 116, 156] (Fig. 3). The majority of cytotoxic stimuli intersect at the

mitochondria, leading to mitochondrial outer membrane permeabilization (MOMP), which is considered as a point of no return in intrinsic apoptosis. B-cell lymphoma 2 (BCL-2) family proteins, comprising both pro- and anti-apoptotic proteins, strictly regulate this pivotal step in intrinsic apoptosis. BCL-2 homology 3 (BH3)-only proteins, members of the pro-apoptotic subgroup, are cytotoxic stress sensors and can inhibit anti-apoptotic BCL-2 proteins through direct interaction [114, 116, 158, 159]. Subsequently, the pro-apoptotic effector proteins BCL2 Antagonist/Killer 1 (BAK) and the BCL-2-associated X protein (BAX) are activated, triggering BAK/BAX oligomerization and consequential mitochondrial pore formation [160]. MOMP induces mitochondrial disruption, thereby releasing apoptotic effector proteins such as cytochrome c, Second mitochondria-derived activator of caspases (SMAC) or the apoptosis-inducing factor (AIF) into the cytosol [115, 116, 158, 159]. Following SMAC release, X-linked inhibitor of apoptosis protein (XIAP)-mediated inhibition of caspase-9 is abolished due to SMAC binding to XIAP. At the same time, cytochrome c release initiates the formation of the apoptosome, a cytosolic multiprotein complex. Prerequisite for apoptosome formation is the association of cytochrome c with apoptotic protease-activating factor-1 (Apaf-1) monomers, which facilitates adenosine triphosphate (ATP) binding to Apaf-1 [161, 162]. Heptameric apoptosome formation is completed by recruitment of procaspase-9 via their caspase-recruitment domains (CARDs). Catalyzed by auto-cleavage of procaspase-9 into active caspase-9, the executioner caspases-3 and -7 are activated, leading to subsequent cleavage of cytoskeletal molecules, nuclear envelope proteins, cell adhesion molecules and apoptosis regulators [158, 163, 164]. The combined action of these caspase-mediated cell-encompassing cleavage events ultimately leads to apoptosis execution [115, 155, 156].

2.3.3.2 Extrinsic apoptosis

Extrinsic apoptosis originates from extracellular cytokine binding, such as the CD95 ligand (FAS), TNF-related apoptosis inducing ligand (TRAIL) or tumor necrosis factor α (TNF α) to their respective DR, CD95 (APO1, FAS receptor), TRAIL1/2 or TNFR1/2 [122, 165-167] (Fig. 3). Ligand binding triggers receptor oligomerization and intracellular formation of the so-called death-inducing signaling complex (DISC) multiprotein complex on the intracellular DD of the activated receptor [116, 158]. DISC formation is catalyzed by the recruitment of the cytosolic adaptor proteins cellular FLICE-like inhibitory protein (cFLIP), Fas-associated death domain protein (FADD) and inactive procaspase-8, all harboring DDs and death effector domains (DEDs). DISC assembly drives homodimerization of inactive procaspase-8, activating it through autoproteolytic cleavage [115, 158]. Caspase-8 in turn activates the downstream executioner caspase-3 and -7 or induces the cleavage of BH3-interacting domain death agonist (Bid) into truncated Bid (tBid) [168]. tBid subsequently translocates to mitochondria and promotes cytochrome c release [169], which again converges the extrinsic with the intrinsic

apoptotic pathway. Whereas TRAIL or CD95 ligand binding to their respective receptor promotes DISC formation, ligation of TNFR1 by TNF α induces the formation of the TNFR-SC which is also referred to as complex-I (described in 2.3.2).

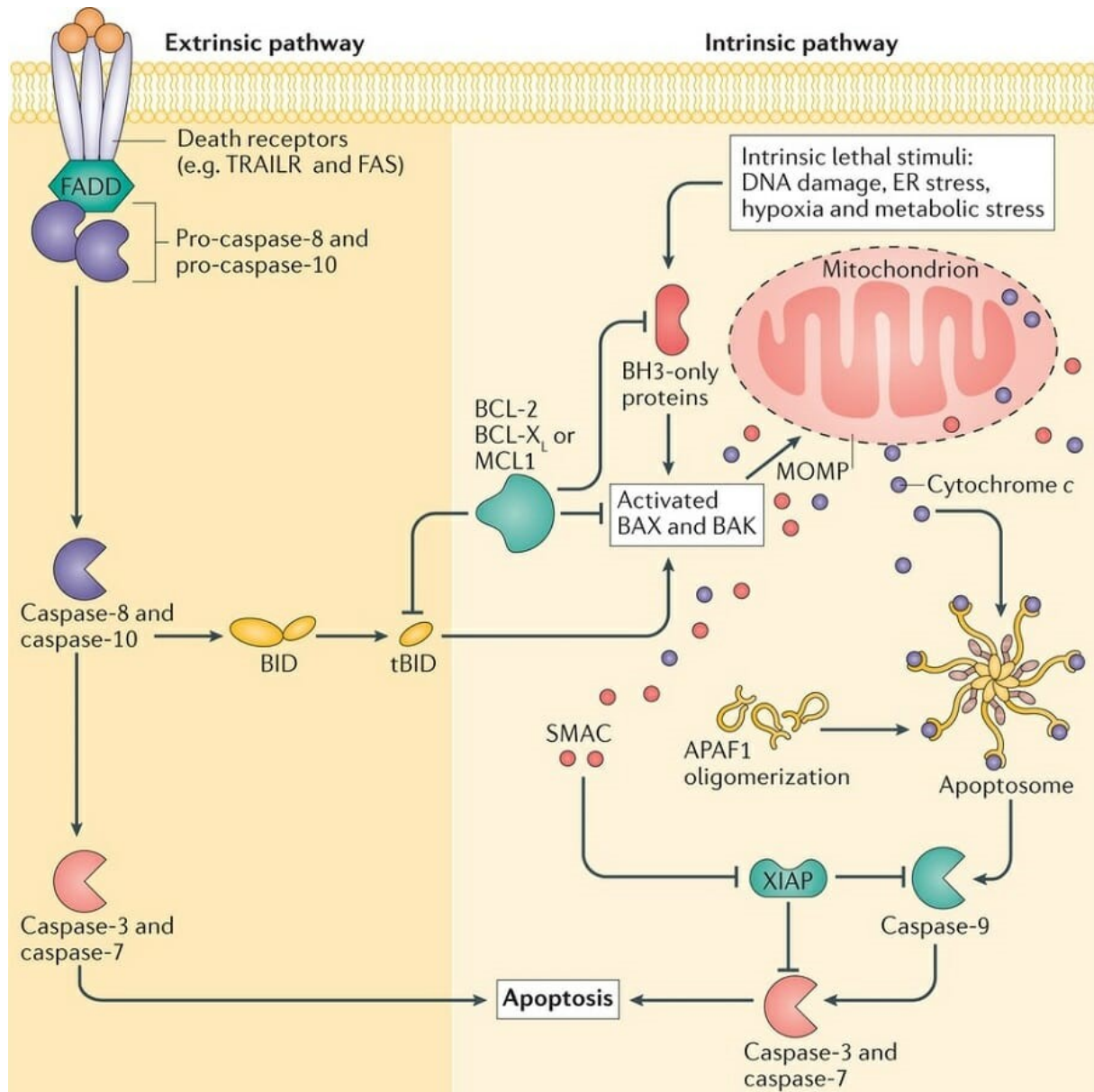


Figure 3 Schematic simplified overview of the extrinsic and intrinsic apoptotic pathway. Ligand binding to the respective death receptor triggers the activation of the extrinsic apoptotic pathway by auto-catalytic cleavage and activation of procaspase-8 or -10, evoked by cytosolic adaptor proteins like FADD-mediated dimerization. Activated caspase-8 or -10 activate caspase-3 and -7 resulting in apoptotic cell death. Active caspase-8 and -10 also cleave BID into tBID, enabling an intersection between the extrinsic and intrinsic apoptotic pathway. Intrinsic apoptosis is initiated by intrinsic lethal stimuli, activating the pro-apoptotic BH3-only proteins BAX and BAK, which induce mitochondrial outer membrane permeabilization (MOMP) through pore formation. This step is counterbalanced by anti-apoptotic BCL-2 family proteins. Following MOMP, cytochrome c is released into the cytosol, mediating apoptosome formation by interacting with APAF1. This activates caspase-9, which in turn activates caspase-3 and -7, eliciting apoptotic cell death. Mitochondrial SMAC release after MOMP facilitates apoptosis by inhibiting XIAP. Adapted from [157].

Extrinsic apoptosis is another possible outcome of $\text{TNF}\alpha$ sensing, requiring the formation of a cytoplasmic caspase-8-activating complex, known as complex-II, in order to switch from a pro-survival to a pro-death response [170]. Cytosolic complex-II is formed after TRADD dissociation from complex-I, engaging the adaptor protein FADD and subsequent recruitment of RIPK1 and caspase-8, thereby activating it [170-172]. Activated Caspase-8 cleaves the effector caspases-3 and -7, inducing apoptotic cell death, which is negatively regulated by FLIP [173].

2.3.4 Necroptosis

Necroptosis, long stigmatized as an accidental form of cell death, is a form of regulated necrosis with a unique and defined signal transduction cascade [174-177]. Morphological hallmarks of necroptosis are defined as a gain in cell volume, cytoplasmic granulation and plasma membrane perforation, resembling the phenotype of necrosis [174, 178, 179]. Membrane perforation is accompanied by the release of inflammatory cytokines and damage-associated molecular patterns (DAMPs), facilitating inflammation [180, 181]. Triggering necroptosis can be achieved by various stimulators, including TRAIL, CD95 (FAS), toll-like receptors (TLRs), polycytidylic acid (polyI:C), double-stranded ribonucleic acid (dsRNA), interferons (IFNs), virus-mediated activation of Z-DNA binding protein-1 (ZBP1) and especially via $\text{TNF}\alpha$ [182-186]. Intriguingly, apoptosis and necroptosis share a vast array of stimulating factors or agents, pointing out the urgent need of specific regulatory events and proteins to guarantee proper execution of necroptosis [187]. The necroptosis pathway is best understood by originating from TNF-ligation of TNFR1.

Prerequisites for necroptotic signaling are two crucial events: Inhibition or depletion of the E3 ubiquitin ligases cIAPs and depletion of the cysteine protease caspase-8 [176]. cIAP depletion abrogates RIPK1 poly-ubiquitination and thereby prevents the activation of kinase complexes required for NF- κ B activation. On the other hand, caspase-8 depletion impedes with the caspase-mediated cleavage of necroptotic downstream effector proteins. Following this interplay of inhibitory events, activated RIPK1 and Receptor-interacting protein kinase 3 (RIPK3) associate via their RIPK homotypic interaction motifs (RHIMs), thus auto- and trans-phosphorylating each other [188-190]. Subsequently, a heteroamyloid complex, composed of kinase-activated RIPK1-RIPK3, is formed, referred to as the necrosome [191]. Of note, canonical necroptosis induction strongly depends on the kinase activities of RIPK1 and RIPK3 [192-194]. By utilizing an inducible dimer system, Wu *et al.* could demonstrate that RIPK1-RIPK1 interaction is expandable for necroptosis execution, whereas RIPK3 dimerization is indispensable and sufficient to induce necroptosis. Moreover, these authors could show that additional RIPK3 is required to be recruited to the RIPK1 and RIPK3 heterodimer to induce necroptosis [195]. Indeed, RIPK3 oligomerization is essential for RIPK3 activation by auto-

phosphorylation and proper necroptosis execution [195]. Accordingly, RIPK3 phosphorylation at S227 induces the recruitment of the mixed lineage kinase domain-like protein (MLKL) into the necrosome, thereby phosphorylating MLKL at T357 and S358 [196-198]. RIPK3-mediated MLKL recruitment and subsequent phosphorylation most likely promotes the transformation of MLKL from a dormant into a pronecrotic, oligomeric form, enabling membrane translocation and permeabilization, ultimately leading to cell demise [176, 199, 200].

2.3.5 The necroptotic core machinery

RIPK1, RIPK3 and MLKL represent the necroptotic core machinery, displaying in the case of RIPK1 and RIPK3, partially overlapping structural domains (Fig. 4). Structurally, RIPK1 is composed of an N-terminal kinase domain (KD) linked to a C-terminal death domain (DD) via an unstructured intermediate domain, harboring a RIP homotypic interaction motif (RHIM) [201, 202].

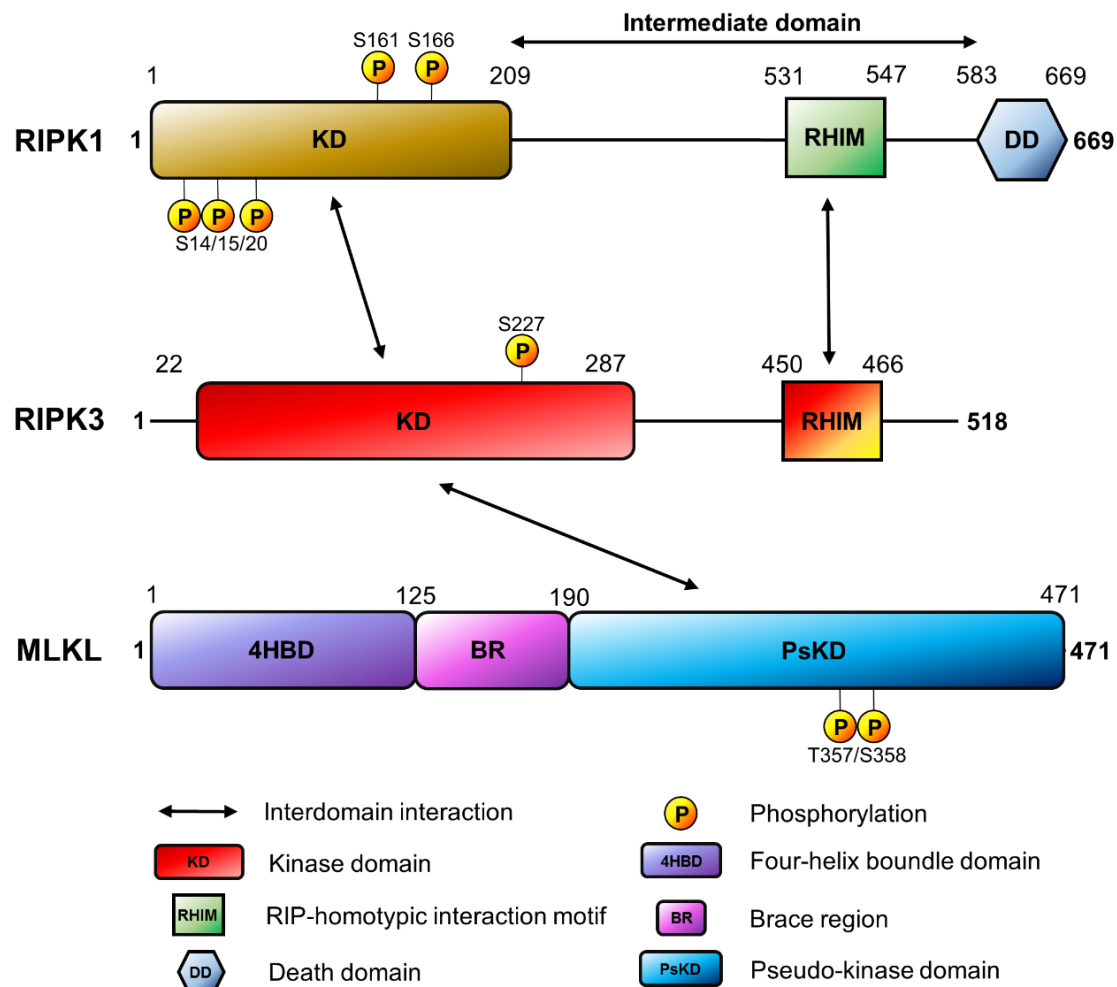


Figure 4 Necroptotic key players and their architecture. Schematic representation showing the domain structure of the necroptotic key players RIPK1, RIPK3 and MLKL. RIPK1 is composed of an N-terminal kinase domain (KD) linked to a C-terminal death domain (DD) by an unstructured intermediate domain, which accommodates the RIP homotypic interaction motif (RHIM). The autophosphorylation sites of RIPK, serine 14, 15, 20, 161 and 166 are highlighted. RIPK3 comprises a KD and a RHIM and the phosphorylation site at S227, necessary for MLKL

interaction, is highlighted. MLKL is composed of a four-helix bundle domain (4HBD), a brace region (BR) and a C-terminal pseudo-kinase domain (PsKD) harboring the phosphorylation sites at T357/S358, essential for necroptosis induction and target of RIPK3. Double-sided arrows indicate established domain interaction between the proteins. Adapted and modified from [176].

RIPK3 consists of an N-terminal kinase domain, as well as a RHIM motif within the unique C-terminus, typical for RIP kinases [176, 201]. The ~16 residue long RHIM motif within RIPK1/3 is conserved among other RIP- containing proteins such as TRIF, ZBP1, mediating fibrillar oligomerization as well as interaction between the RHIM containing proteins [175, 176, 182, 183, 196, 203]. Lastly, MLKL is composed of an N-terminal four helical bundle domain (4HBD), a two α -helices-containing brace region (BR) and a C-terminal pseudo kinase like domain (PsKD), containing an ATP binding pocket and a helical activation loop [204]. An overview of the necroptotic key players and their architecture is shown in Figure 4.

2.3.5.1 Receptor-interacting protein kinase 1

RIPK1, originally identified and named by Stanger *et al.* 1995, has arisen as an essential downstream regulator of a couple of immune receptors, regulating tissue homeostasis, inflammation and cell death kinase dependent and -independent mechanisms [205-207]. Whereas the predominant scaffold function of RIPK1 blocks cell death by driving the expression of several pro-survival and inflammatory genes, the pro-death active kinase function of RIPK1 facilitates apoptosis and especially necroptosis induction, denoting RIPK1 as a molecular switch between life and death of the cell [208]. Several studies in mice could explicitly demonstrate this: RIPK1-deficient mice lack the predominant pro-survival scaffolding role of RIPK1 and die perinatally by cell death-driven inflammation. On the other hand, mice expressing a catalytic dead RIPK1 mutant (K45A / D138N) are healthy and remain unaffected due to the exposure with various necroptosis-inducing compounds [182, 194, 209-211]. Both the scaffold function and the pro-death kinase function of RIPK1 are evolutionary conserved in human, seizing pivotal roles in the human body. As RIPK1 deficiency causes severe intestinal inflammation, immunodeficiency, and arthritis, RIPK1 kinase dependent cell death participates in the removal of infected cells, assisting the immune system [210-214].

RIPK1 can interact with several pivotal TNFR1 signaling components via its RHIM and DD, thereby regulating important checkpoints in apoptotic and necroptotic signaling. Whereas RIPK1 can interact via its DD with TNFR1, TRADD and FADD [215, 216], the RHIM enables interactions with other RHIM containing proteins, like Toll/Interleukin-1 receptor domain-containing adaptor inducing interferon- β (TRIF), ZBP1 and especially RIPK3 [207, 217, 218]. PTMs, such as phosphorylation and ubiquitination, are the master regulators for the pro-death and pro-survival role of RIPK1 [201]. Upon TNFR1 engagement and cIAP depletion, RIPK1 can undergo auto-phosphorylation at S14/15/20/161 and S166 [188, 219], initially presumed

central for later RIPK3 association and necroptosis. Nevertheless, a recent study could demonstrate that phosphorylation at S161 is at least the major if not the only functional phosphorylation site during necroptosis, responsible for RIPK3 recruitment [220]. Moreover, fibroblasts, generated from an Asp138Asn mutation in a mouse model (Ripk1^{D138N/D138N} mice), displayed similar levels of apoptosis compared to the wildtype, but showed a complete protection against necroptosis induction [192, 194]. Additionally, a study could show that dimerization of the DD and subsequent necroptosis could be blocked by a K599R/K843R mutation *in vitro* and *in vivo* [221]. In summary, these studies clearly highlighted the dependency of RIPK1 on its phosphorylation events to activate the necroptotic pathway, such as the hyperphosphorylation-dependent dimerization or functional kinase activity. On the other side, phosphorylation of RIPK1 can also exhibit a pro-survival function. Four independent groups could identify a conserved phosphorylation site of RIPK1 in its intermediate domain at S320 (human) or S321 (mouse), which is described to be either phosphorylated by MAPK-activated protein kinase 2 (MK2) or TAK1, thereby suppressing TNF α -induced cell death [222-225]. Akin to this protective effect, a point mutation at S89 could be shown to amplify RIPK1 kinase activity and subsequent necroptosis, pointing out another cell death-inhibitory phospho-acceptor site [198]. Aside of its pro-survival function, conciliated by phosphorylation events, RIPK1 can also exhibit a protective role through its RHIM domain by competing and interacting with other RHIM domain containing proteins, such as ZBP1. Upon mutation of the RHIM domain, ZBP1 predominantly binds and interacts with RIPK3 to induce ZBP1-mediated necroptosis, highlighting the pro-survival function of the RIPK1 RHIM domain [226, 227]. Similarly, ubiquitination of RIPK1 plays a central role in regulation of cell death. RIPK1 can be ubiquitinated via K48, K63 and M1 chains, thus fine-tuning the outcome of the signaling cascade [175, 228, 229]. cIAPs and LUBAC poly-ubiquitinate RIPK1 to form and stabilize complex-I, whereas CYLD and A20 deubiquitinate RIPK1 to favor complex-II formation [30, 133, 230, 231]. At the same time A20 promotes K48-linked poly-ubiquitination of RIPK1, promoting its proteasomal degradation. A20 and CYLD occupy opposing roles in regulation of cell death. A20 prevents cell death by protecting M1-linked poly-ubiquitin chains on RIPK1 from CYLD mediated deubiquitination, whereas CYLD sensitizes the cell to cell death by cleaving these chains [133, 232]. Pellino E3 Ubiquitin Protein Ligase 1 (PELI1) was identified as a RIPK1 E3 ligase, generating K63-linked poly-ubiquitin chains on K115, directly dependent on the functional kinase activity of RIPK1. Moreover, PELI1 deficiency disrupted RIPK1-RIPK3 interaction and abrogated subsequent necroptosis, pointing towards a mediator function of PELI1 in this interaction process [233]. Taken together, various PTMs on RIPK1, such as phosphorylation and ubiquitination as well as DD-induced dimerization control necroptotic signaling.

2.3.5.2 Receptor-interacting protein kinase 3

Following extensive studies of death receptor induced necroptotic signaling, Receptor-interacting protein kinase 3 (RIPK3) was unraveled as a downstream mediator of RIPK1 [188-190]. In contrast to RIPK1, RIPK3 is missing the C-terminal death domain, but is defined by an unique C-terminus, which stands out from the rest of the RIP kinase family [201]. The typical RHIM domain within the C-terminus mediates the interaction with other RHIM containing proteins such as ZBP1, TRIF and especially RIPK1 [183, 196, 203, 207, 234]. Upon necroptosis induction, recruitment of RIPK3 by activated RIPK1 creates an initial heterodimer, leading RIPK3 phosphorylation and activation [217, 234]. Subsequently, more RIPK3 is recruited by the formation of the initial heterodimer, inducing homodimerization and thereby activating RIPK3 via auto-phosphorylation [195, 234]. This triggers the phosphorylation of RIPK3 at Ser227, which is crucial for mediating the interaction with the necroptosis executioner pseudokinase MLKL [196]. McQuade *et al.* could further demonstrate that a phosphomimetic S204D mutation in RIPK3 could trigger programmed necroptosis unaffected by pharmacological RIPK1 inhibition or knockdown [198]. The Protein Phosphatase, Mg²⁺/Mn²⁺ Dependent 1B (PPM1B) was described to dephosphorylate mouse RIPK3 at T231/S232, thereby negatively regulating necroptosis [235]. Another recent study generated mice with dramatically reduced ADAM Metallopeptidase Domain 17 (ADAM17) expression levels. Murine embryonic fibroblasts (MEFs) generated from these mice were completely protected against TNF α -induced necroptosis. Moreover, RIPK3 and MLKL phosphorylation was completely absent in these cells [236]. However, whether PPM1B and ADAM17 both exhibit a similar function in human cell necroptosis is still unclear. To date and contrary to RIPK1, only pro-death phosphorylation events are described for RIPK3 [188, 189, 196, 217, 234].

Apart from phosphorylation, RIPK3 is modified with ubiquitin chains. Several DUBs and E3 ligases are fine tuning RIPK3 ubiquitination levels and thereby influencing the necroptotic signaling cascade [62, 175, 237, 238]. For example, the DUB A20 negatively regulates necroptosis by deubiquitinating K63-conjugated poly-ubiquitin chains from RIPK3 at K5, thereby interfering with RIPK1-RIPK3 interaction [62]. Furthermore, the E3 ligase Parkin has been described to suppress necrosome formation as well by promoting K33-poly-ubiquitination of RIPK3 [239]. PELI seizes a dual role in the regulation of necroptotic signaling. Besides its role in ubiquitinating RIPK1 on K115 [233], thus promoting necroptosis, PELI1 is also described to add K48-conjugated poly-ubiquitin chains to K363 of kinase-active RIPK3, marking it for proteasomal degradation [240, 241]. Additionally, HSC70-interacting protein (CHIP) has been described to negatively regulate RIPK3 expression levels as well by adding K48-conjugated poly-ubiquitin chains at K55 and K363 of RIPK3, targeting it for lysosomal degradation [242]. Finally, studies with the proteasome inhibitors MG132 and bortezomib could demonstrate an accumulation of K48-conjugated poly-ubiquitin chains of RIPK3 at K264, resulting in the

formation of RIPK3 homo-oligomers and subsequent MLKL recruitment to execute necroptosis independently of caspase-8 inactivation [243]. Thus, in summary, ubiquitination events can either mark RIPK3 for degradation or prime for necroptosis, contingent on the position of ubiquitination.

Beyond its regulation by PTMs, other proteins regulate proper necroptotic signaling and especially RIPK3. For example, the chaperone Heat Shock Protein 90 (HSP90) and its co-chaperone Hsp90 co-chaperone Cdc37 (CDC37) are seizing an auxiliary function in the activation of RIPK3 [188, 244, 245], as well as RIPK1 [246-251] and MLKL [252-254], facilitating correct folding, oligomerization and/or localization.

Of note, RIPK3 is described to be able to induce apoptosis aside to its widely described and pivotal function in necroptosis. Two individual studies in mice could demonstrate that *Ripk3*^{K51A/K51A} mice were born healthy and resistant to necroptotic stimuli, whereas *Ripk3*^{D161/D161} mice displayed unusual high levels of caspase-8- and RIPK1-dependant apoptosis [192, 193]. High doses of GSK'843 and GSK'872, two specific RIPK3 inhibitors, allosterically activated RIPK3 in murine cell lines, triggering complex-II formation and subsequent apoptosis [193]. Interestingly, further studies could show that *Ripk1*^{-/-}*Ripk3*^{+D161N} mice die at late gestation during embryogenesis [255], whereas heterozygosity of *Ripk3* does not induce embryonic lethality in RIPK1 null mice [192, 256]. Amalgamation of these findings suggest that the D161N mutation locks RIPK3 in a state that favors homodimerization through the KD and the allosteric activation of wild-type RIPK3, despite abolishing its kinase activity [175].

Apart from its role in necroptosis, RIPK3 plays a role in inflammatory responses. Moriwaki *et al.* could show that RIPK3 promotes cytokine expression by two complementary mechanisms, namely either by processing of Interleukin-1 β (IL-1 β) or by NF- κ B dependent gene transcription [257]. Furthermore, RIPK3 promotes NACHT, LRR and PYD domains-containing protein 3 (NLRP3) inflammasome formation independent of necroptotic cell death or MLKL [258].

Taken together, RIPK3 seizes a central role in necroptotic signaling by potentiating and relaying the incoming death signal to the executioner pseudo kinase MLKL, regulated by diverse phosphorylation and ubiquitination events. At the same time, new studies describe additional important roles for RIPK3 beyond its pivotal function in necroptosis, like the regulation of proinflammatory cytokine production.

2.3.5.3 Mixed lineage kinase domain-like protein

MLKL is the ubiquitously expressed downstream executioner of necroptosis. As described in 2.3.5, MLKL consists of a four-helix bundle domain (4HBD) bridged to a C-terminal pseudo-kinase domain (PsKD) by an auto-inhibitory bridge-region (BR). Once activated, RIPK3 undergoes auto-phosphorylation triggering phosphorylation of MLKL in the activation loop of

the PsKD at human T357/S358 [204, 259]. Consequently, dormant monomeric MLKL undergoes a conformational change, exposing the 4HBD which normally interacts with the PsKD by an interface centered around the α C helix, mitigating its killing activity [260]. Thioredoxin-1 (Trx1) has been proposed to regulate this oligomerization step, maintaining MLKL in the dormant state by inhibiting the formation of 4HBD disulfide bonds [261]. Additionally, the chaperone HSP90, in interplay with the co-chaperone CDC37, has been shown to serve an auxiliary function in necrosome formation and MLKL oligomerization by binding the PsKD [252-254]. Exposing the 4HBD enables formation of a necroptosis-inducing MLKL tetramer which is recruited to the plasma membrane [204, 260, 262-264]. Upon its recruitment, MLKL induces pore formation and the release of cellular contents (like ions), leading to destructive osmotic pressure and as a result, disruption of membrane integrity and cell death [176, 181, 200, 263].

The transition from a dormant monomeric MLKL form to a necroptotic active oligomeric form most likely differs between species. Transient interaction with RIPK3 and subsequent phosphorylation at S345 is sufficient for mouse MLKL to initiate oligomerization, ensuing membrane translocation and cell death [204, 208]. Studies using phosphomimetic mutants, substitutions in the adjacent pseudoactive site or simple overexpression of the 4HB domain in RIPK3-depleted cells proved the sufficiency of the activation loop phosphorylation [204, 208, 262, 265]. Of note, necroptotic fine tuning in mouse MLKL is regulated by additional phosphorylation sites, though the responsible kinases still remain elusive [208]. Contrarily, overexpression studies of human MLKL 4HBD in human cells proved to be insufficient for necroptosis induction and cell death [266]. Nevertheless, forced dimerization of full length MLKL or the MLKL 4HBD caused an augmentation of necroptotic cell death [200, 266], highlighting the oligomerization of MLKL as a central event in both human and mouse cells. The exact mechanism how RIPK3 activates human MLKL is still unknown. However, RIPK3 still plays an obligate role in its activation by presumably scaffolding the conformational reorganization of MLKL oligomers or by dissociation of pro-necroptotic MLKL oligomers from the necrosome [176].

While the appearance of oligomeric phosphorylated MLKL at the plasma membrane is a hallmark of necroptotic cells, the exact structure of oligomeric MLKL at the plasma membrane has remained elusive. Small-angle X-ray scattering, analytical ultra-centrifugation and native mass spectrometry reported mouse MLKL to be assembled into trimers [262, 267], whereas human MLKL is assembled into tetramers [260], although several studies also describe higher-order killer species, like hexamers [200], octamers [268] and polymers [269]. Interestingly, Petrie *et al.* utilized a MLKL D107A/E110A mutation in the 4HBD α 4 helix to demonstrate that oligomerization of MLKL alone is insufficient for necroptosis induction. MLK D170A/E110A could still oligomerize and maintain lipid binding at the membrane [260].

Intriguingly, translocation of activated MLKL to the plasma membrane does not constitute a point of no return in execution of necroptotic signaling, as previously thought. Recently, several proteins and complexes have been described to further regulate and guide the killing of the cell at the cell membrane. These are, for example, the two lipid kinases inositol polyphosphate multikinase (IPMK) and inositol-tetrakisphosphate 1-kinase (ITPK1). Both are controlling the synthesis of highly phosphorylated inositol phosphate 6 (IP6) from IP3 and have been described as essential auxiliary proteins in human HT-29 and HAP1 cell necroptosis [270]. Binding of these highly phosphorylated IPs to the MLKL 4HBD, displaced the BR and augmented RIPK3-mediated phosphorylation [270]. Furthermore, positively charged amino acids in the 4HB of MLKL have been shown to interact with Phosphatidylinositol phosphates (PIPs) to mediate MLKL binding to the plasma membrane [199, 259, 264]. Whereas PIPs facilitate membrane association of MLKL, the repulsive guidance molecule b (RGMb) has been shown to block MLKL membrane association in proximal kidney tubular cells [271]. Moreover, the endosomal sorting complexes required for transport (ESCRT)-III machinery was shown to counteract necroptosis by accumulating at the damaged plasma membrane and facilitating shedding of phosphorylated MLKL oligomers in necroptotic vesicles [272-274]. Additionally, the authors could show that the ESCRT-III complex enables plasma membrane repair, further negating MLKL-induced plasma membrane rupture [272-274]. The ESCRT-III complex pathway thereby functions as a threshold for necroptotic killing by counteracting MLKL-induced pore formation through its repair activity [175].

To date, ubiquitination, being a key PTM of other necroptotic core players, like RIPK1 or RIPK3, could not be identified for MLKL yet. Nevertheless, a proteome-scale protein-interaction screen of the human liver revealed the interaction of MLKL with the E3 ubiquitin-protein ligase RAD18, which could be the first hint towards a modification of MLKL with ubiquitin [275].

In summary, despite apparent differences in MLKL between the two species, various regulation steps of MLKL throughout necroptotic signaling exist with multiple commonalities (Fig. 5): In the absence of a necroptotic signaling event, MLKL resides in the cytoplasm in its dormant, monomeric form. Upon activation the brace helices mediate the oligomerization into higher-order complexes, necessary for killing. Phosphorylated RIPK3 plays the key role in this activation step and subsequent necroptotic cell death. Over the past few years, a multitude of auxiliary proteins and cofactors have been identified in fine tuning MLKL activation, oligomerization membrane translocation and pore formation. Nevertheless, ubiquitination, as one of the key PTMs in necroptosis, remained elusive for MLKL.

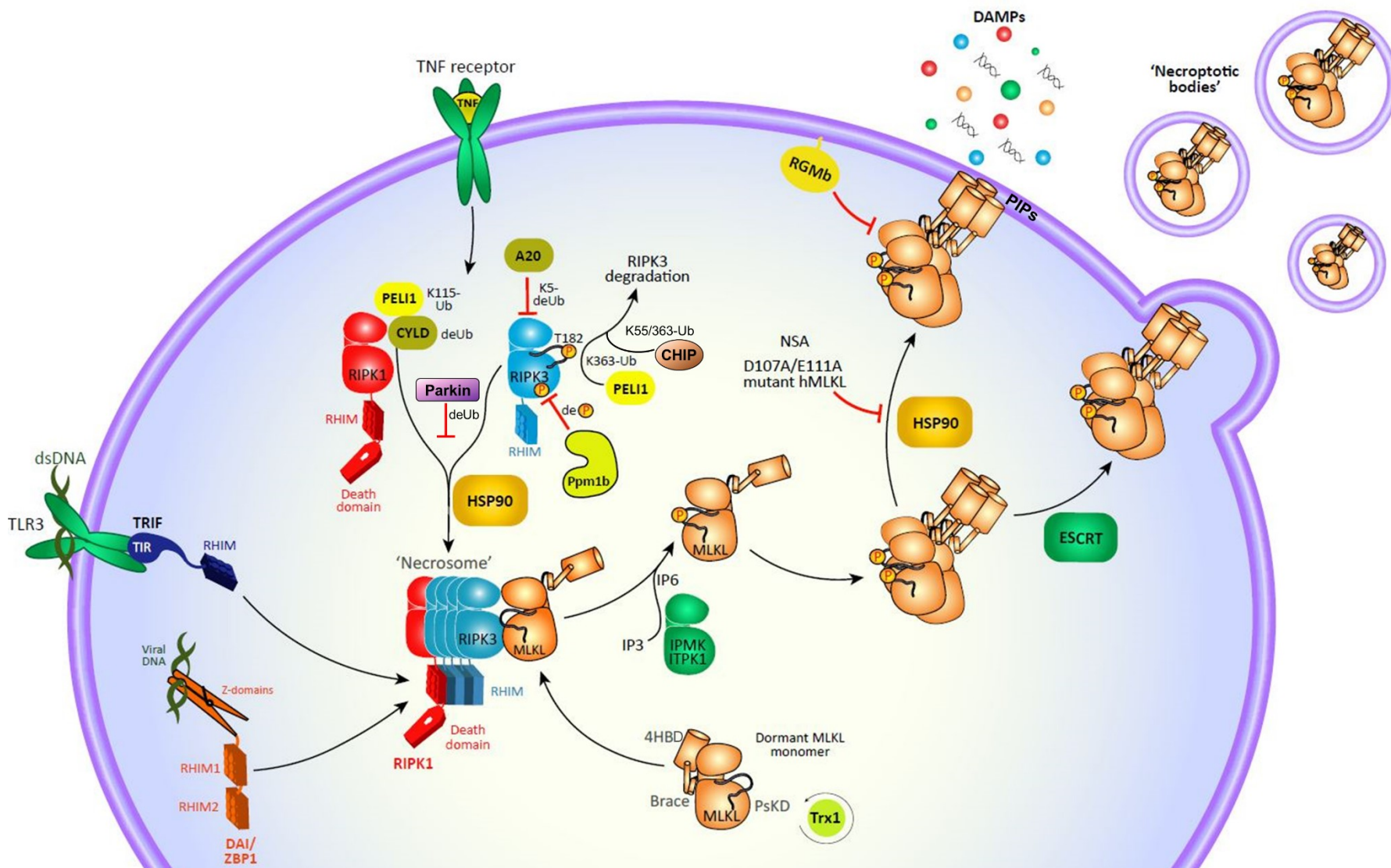


Figure legend is located on the next page.

Figure 5 Schematic overview of necroptotic signaling and its regulation via ubiquitin. Activation of Tumor necrosis factor receptor 1 (TNFR1) via $\text{TNF}\alpha$ triggers subsequent RIPK1-RIPK3 oligomerization and necrosome assembly. Necrosome assembly can be initiated and promoted by other RIPK homotypic interaction motifs (RHIMs) containing proteins such as TIR-domain-containing adapter-inducing interferon- β (TRIF) which is activated by double-stranded(ds)-RNA binding to Toll-like receptor 3 (TLR3) or Z-DNA binding protein-1 (ZBP1), activated by virus DNA sensing. The necrosome serves as a platform for MLKL conversion, from a dormant into a pronecroptotic, phosphorylated oligomeric form. Oligomerization of MLKL is inhibited and regulated by Thioredoxin-1 (Trx1). Subsequently, oligomerized MLKL translocates to the plasma membrane and induces pore formation, thereby releasing inflammatory cytokines and damage-associated molecular patterns (DAMPs), ultimately leading to cell demise. Necroptosis is facilitated by several auxiliary proteins at various stages of the signaling cascade. The chaperone Heat Shock Protein 90 (HSP90), promotes RIPK1, RIPK3 and MLKL activation, whereas the inositol polyphosphate multikinase (IPMK) and inositol-tetrakisphosphate 1-kinase (ITPK1), are synthesizing the MLKL ligand and activator inositol phosphate 6 (IP6). The endosomal sorting complexes required for transport (ESCRT)-III machinery counteracts necroptosis by shedding phosphorylated MLKL oligomers in necroptotic vesicles, enabling membrane repair. Moreover, the repulsive guidance molecule b (RGMB) is reported to counter MLKL membrane association in kidney tubular cells, whereas the Protein Phosphatase, $\text{Mg}^{2+}/\text{Mn}^{2+}$ Dependent 1B (PPM1B) was shown to impede with RIPK3 phosphorylation and successive necrosome formation in mouse cells. Multiple E3-ligases and DUBs regulate the necroptotic signaling. Necrosome assembly can be promoted the DUB Ubiquitin carboxyl-terminal hydrolase CYLD (CYLD) by deubiquitinating RIPK1. PELI1 seizes a dual role in necroptosis, by deubiquitinating RIPK1 at K115 it promotes necrosome assembly, whereas it counteracts necroptotic signaling by adding K48-conjugated poly-ubiquitin chains to K363 of kinase-active RIPK3, marking it for proteasomal degradation. Furthermore, necroptosis is negatively regulated by the TNF Alpha Induced Protein 3 (A20), which deubiquitinates K63-conjugated poly-ubiquitin chains from RIPK3 at K5 and by the E3-ligase Parkin, which promotes K33-poly-ubiquitination. Adapted and modified from [176].

2.3.6 Necroptosis in cancer

Necroptotic signaling strongly relies on the expression of the necroptotic core proteins RIPK1 [186], RIPK3 [217] and MLKL [196] and is involved in a wide array of human diseases, including infectious diseases [182, 183, 276, 277], autoimmune diseases, ischemic injury [278], multiple sclerosis [279, 280] and especially cancer [281, 282].

However, several studies demonstrated that the expression levels of RIPK1, RIPK3 and MLKL fluctuate among different cancer cell lines. RIPK1, as critical mediator of $\text{TNF}\alpha$ -induced NF- κB activation and apoptosis, is widely expressed among cancer cell lines. Nonetheless, RIPK1 expression was shown to be elevated in pancreatic ductal adenocarcinoma (PDA), hepatocellular carcinoma (HCC), melanoma, lung cancer and glioblastoma [283-287], related to a poor prognosis and unfavorable outcome [284-287]. Contrarily to RIPK1 expression levels, RIPK3 expression is frequently diminished in a wide variety of cancer cell lines. Ubiquitin-Like PHD And RING Finger Domain-Containing Protein 1 (UHRF1), a key epigenetic regulator, suppresses RIPK3 expression by sustaining the methylation status of the RIPK3 promoter, whereas the Transcription Factor Sp1 (Sp1) counteracts UHRF1 and positively regulates the expression [288]. Interestingly, B-Raf Proto-Oncogene, Serine/Threonine Kinase (BRAF) and AXL Receptor Tyrosine Kinase (AXL), two oncogenic drivers, were identified as pivotal factors in driving loss of RIPK3 expression, suggesting an oncogenic driven loss of RIPK3 expression levels during tumor growth [289]. Several studies support this hypothesis by demonstrating decreased RIPK3 expression levels in various human cancer samples, such as colorectal cancer, breast cancer, AML and chronic lymphocytic leukemia (CLL) [290-295] with decreased survivability rate in colorectal, ovarian and breast cancers [290, 291, 295]. Nevertheless, some

cancer subtypes, like serous ovarian cancer display elevated RIPK3 expression levels [296]. Furthermore, human PDA samples showed high expression levels of RIPK1, RIPK3 and MLKL, whereas RIPK1 and RIPK3 levels could be further increased by the chemotherapy drug gemcitabine [282]. A transgenic mouse model carrying the mouse mammary tumor virus (MMTV) long terminal repeat upstream of a cDNA sequence encoding the Polyoma Virus middle T antigen (PyVT), called MMTV-PyMT, displayed enhanced RIPK3 and MLKL expression levels in late stage breast cancer [297]. MLKL expression could be monitored in a variety of cancer cell lines and several subtypes of cancer. While higher MLKL expression levels correlated with a favorable outcome condition in cervical squamous cancer [298], low expression was associated with a decreased patient survivability rate in ovarian, gastric and colon cancer [299-301]. In contrast, high levels of phosphorylated MLKL favored a poor patient survival for esophageal and colon cancer patients [295, 302].

Execution of necroptotic signaling ultimately leads to membrane rupture and release of DAMPs, triggering DAMP-induced inflammation and activation of the NF- κ B or MAPK pathway. Several studies could demonstrate the pro-tumor effects of necroptosis. For example, a study with a MMTV-PyMT mouse model could show that necroptosis was ubiquitous in tumor necrotic areas [297]. Furthermore, MLKL depletion revealed a drastically reduced lung metastasis corresponding with decreased levels of inflammatory cytokines [297]. Strilic *et al.* could demonstrate that murine and human tumor cells can induce necroptosis of endothelial cells, thereby promoting tumor cell extravasation and metastasis [303]

Nevertheless, necroptosis also exhibits anti-tumor effects. For example, necroptosis mediated DAMP release induces anti-tumor immunity through CD8⁺ T cell cross-priming or generates cytotoxic Interleukin-12 (IL-12) in the tumor microenvironment [185, 304, 305]. Moreover, RIPK3-PGAM5(Phosphoglycerate Mutase Family Member 5)-Drp1(Dynamin 1 Like)/Nuclear factor of activated T-cells signaling has been reported to be involved in Natural killer T (NKT) activation and mediate crosstalk between immune signaling and mitochondrial function [306], further supporting the anti-tumor effects of necroptosis.

De-regulated apoptotic signaling in cancer facilitates uncontrolled cell proliferation and tumor survival. Chemotherapeutic drugs like 5-Fluorouracil (FU), etoposide and cisplatin in interplay with caspase inhibitors, like carbobenzoxy-valyl-alanyl-aspartyl-[O-methyl]-fluoromethylketone (zVAD.fmk), could be utilized to induce necroptosis of tumor cells, thereby overcoming apoptosis resistance [307-309]. Since overexpression of IAP proteins is associated with apoptosis resistance and poor prognosis, the IAP antagonist BV6 could be shown to induce necroptotic cell death in apoptosis resistant cancer cells [310-312]. Additionally, BV6 could be shown to induce the production of TNF α , subsequently initiating necrosome formation and cell death in pancreatic carcinoma and AML cells [313, 314].

In summary, the necroptotic core proteins RIPK1, RIPK3 and MLKL display temporal and spatial expression patterns in different cancer subtypes, mediating differential tumor activity and thereby impacting overall survival. Necroptosis seizes a dual role in cancer by exhibiting anti- and pro-tumor activity in the tumor microenvironment during tumor progression. Lastly, necroptosis can be utilized as an attractive mechanism to overcome apoptosis-evasion in tumor cells [315]. Although the number of therapeutic approaches to examine the anti-tumor efficacy of necroptosis is rising, necroptotic signaling is still not fully understood. Exact breakdown of the necroptotic signaling pathway is pivotal to evaluate its precise role in modulating cancer development, cancer progression as well as to assess its clinical applicability.

3 Aim of the study

Apoptosis is a form of programmed cell death that is widely used as a therapeutic strategy to ensure efficient elimination of malignant cancer cells in the human body. However, dysregulation of the apoptotic signaling pathway, in particular the pro-apoptotic machinery, is a hallmark of cancer and ensures unrestricted cell proliferation and consequently, tumor survival. Necroptosis induction, as a caspase-independent form of programmed cell death, has emerged as a new experimental therapeutic approach to overcome apoptosis-resistance and efficiently kill cancer cells, thereby holding auspicious therapeutic potential for cancer treatment. Consequently, a deeper understanding of the necroptotic machinery and its regulators is indispensable for future targeted cancer therapies.

Several Deubiquitinating enzymes (DUBs) are well-known for their role in fine tuning the necroptotic signaling pathway. To identify novel DUBs involved in controlling necroptotic signaling, our research group recently performed a siRNA-mediated screen in HT-29 colon carcinoma cells to identify DUBs that could rescue TNF α (T), Smac mimetics (BV6; B) and zVAD.fmk (Z), mediated necroptosis. Among the identified DUBs, USP22 prominently inhibited TBZ-mediated necroptosis in HT-29 cells. USP22 is widely described for its predominant role in the human Spt-Ada-Gcn5 acetyltransferase (SAGA) complex, regulating gene transcription by monoubiquitination of Histone 2B. At the same time, several studies point out the involvement of USP22 in the regulation of apoptosis in several different cancer cell lines.

With this study we aimed to investigate a potential role of USP22 in regulating TBZ-induced-necroptosis in various cancer cell lines. We intended to uncover the molecular mechanisms behind the predominant inhibition of TBZ-induced necroptotic cell death, mediated by Clustered Regularly Interspaced Short Palindromic Repeats(CRISPR)/Cas9-induced USP22 depletion. By employing mass spectrometry-based ubiquitin remnant profiling we intended to identify potential targets for USP22-dependent deubiquitination during TBZ-induced necroptosis. Finally, we focused on the USP22 mediated changes on RIPK3 ubiquitination and phosphorylation patterns during TBZ-induced necroptosis and the resulting changes in necroptotic cell death signaling.

4 Materials and Methods

4.1 Materials

4.1.1 Cell lines

Cell lines were authenticated by STR profiling/DNA fingerprinting at Leibniz Institute, German Collection of Microorganisms and Cell Cultures (DSMZ, *Deutsche Sammlung von Mikroorganismen und Zellkulturen*). All cells were regularly tested for mycoplasma contamination by PCR.

4.1.1.1 Human cell lines

Table 1 Human cell lines

Cell line	Entity	Source
HT-29	colon	American Type Culture Collection (ATCC)
HeLa	epithelial	ATCC
T-Rex™-HeLa Cell Line	epithelial	Thermo Fisher Scientific #R71407
HEK293T	2nd generation retrovirus-producing cell line	ATCC
NB4	human acute promyelocytic leukemia	Deutsche Sammlung von Mikroorganismen und Zellkulturen (DSMZ)
Jurkat	human ALL (T-Cell)	DSMZ

4.1.1.2 Stable transfected human cell lines

Table 2 Stable transfected human cell lines

Cell line	Transgene	Vector Source	Selection
HT-29 RIPK3 KO	Strep-RIPK3-WT PAM	Addgene #60509	G418 (1 mg/ml)
HT-29 RIPK3 KO	Strep-RIPK3-D160N PAM	Addgene #60509	G418 (1 mg/ml)
HT-29 RIPK3 KO	Strep-RIPK3-K518R PAM	Addgene #60509	G418 (1 mg/ml)
HT-29 RIPK3 KO	Strep-RIPK3-3xKR PAM	Addgene #60509	G418 (1 mg/ml)
HT-29 RIPK3 KO	Empty vector	Addgene #60509	G418 (1 mg/ml)

Cell line	Transgene	Vector Source	Selection
HT-29 USP22 KO 2 guide	Empty vector	Addgene #60526	Blasticidin (15 µg/ml)
HT-29 USP22 KO 2 guide	3xFLAG-HA-USP22 PAM	Addgene #60526	Blasticidin (15 µg/ml)
HT-29 USP22 KO 2 guide	3xFLAG-HA-USP22 PAM C185S	Addgene #60526	Blasticidin (15 µg/ml)
HT-29 USP22 KO 2 guide	3xFLAG-HA-USP22 PAM C185A	Addgene #60526	Blasticidin (15 µg/ml)
HeLa	Strep-RIPK3-WT	Addgene #60507	Puromycin (10 µg/ml)
HeLa	Strep-RIPK3-D160N	Addgene #60507	Puromycin (10 µg/ml))
HeLa	Strep-RIPK3-K42R	Addgene #60507	Puromycin (10 µg/ml)
HeLa	Strep-RIPK3-K351R	Addgene #60507	Puromycin (10 µg/ml)
HeLa	Strep-RIPK3-K518R	Addgene #60507	Puromycin (10 µg/ml)
HeLa	Strep-RIPK3-2xKR	Addgene #60507	Puromycin (10 µg/ml)
HeLa	Strep-RIPK3-3xKR	Addgene #60507	Puromycin (2 µg/ml), blasticidin (15 µg/ml)
HeLa-T-REx	Strep-RIPK3-WT	Thermo Fisher Scientific # 12301016	G418 (1 mg/ml)

4.1.2 Murine cell lines

Table 3 Murine cell lines

Cell line	Type	Source
RAW 264.7	macrophage; Abelson murine leukemia virus transformed	ATCC
J774A1	monocyte; macrophage	ATCC
MEF	fibroblast	ATCC

4.1.3 Cell culture reagents

4.1.3.1 Media

Table 4 Media

Medium	Company
Dulbecco's Modified Eagle Medium (DMEM) GlutaMAX™	Thermo Fisher Scientific
McCoy's 5A (Modified) Medium GlutaMAX™-I	Thermo Fisher Scientific
Roswell Park Memorial Institute (RPMI) 1640	Thermo Fisher Scientific
McCoy's 5A Media for SILAC	Thermo Fisher Scientific

4.1.3.2 Media supplements and additional cell culture reagents

Table 5 Media supplements and additional cell culture reagents

Reagent	Company
Fetal calf serum (FCS)	Thermo Fisher Scientific
Blasticidin	Sigma
HEPES (4-(2-hydroxyethyl)-1-piperazineethanesulfonic acid)	Thermo Fisher Scientific
G418 (Geneticin)	Thermo Fisher Scientific
Penicillin/Streptomycin (P/S)	Thermo Fisher Scientific
Puromycin	Clontech Laboratories
Phosphate-buffered saline (PBS)	Thermo Fisher Scientific
Trypan blue solution	Thermo Fisher Scientific
0.05 % Trypsin/EDTA	Thermo Fisher Scientific
Sodium pyruvate (100 mM)	Thermo Fisher Scientific
Doxycycline hydrochloride	Sigma-Aldrich
Dialyzed FCS	Sigma Life Science
Lys 0	Sigma (L8662-100G, Lot#1447507V)
Arg 0	Sigma (A6969-100G, Lot#SLBR2260V)
Lys 8	Cambridge Isotope Laboratories (CNLM-291-H)
Arg 10	Cambridge Isotope Laboratories (CNLM-539-H)

4.1.3.3 Cell death-inducing drugs

Table 6 Cell death-inducing drugs

Reagent	Company
BV6 (Smac mimetic)	Genentech
Tumor necrosis factor α (TNF α) human	Biochrom

4.1.3.4 Inhibitors

Table 7 Inhibitors and reagents

Reagent	Company
GSK 872	Merck
Dabrafenib	Selleckchem
Necrostatin-1s	Merck
N-benzyloxycarbonyl-Val-Ala-Asp(O-Me)fluoromethylketone (zVAD.fmk)	Bachem
Necrosulfonamide (NSA)	Merck
λ -phosphatase	Santa Cruz
Recombinant human USP2 catalytic domain	RND Systems
FLAG-hTNF	Enzo Life Sciences

4.1.3.5 Fluorescent dyes

Table 8 Fluorescent dyes

Reagent	Company
Hoechst 33342	Thermo Fisher Scientific
Propidium iodide (PI)	Sigma

4.1.4 Western blot-related materials

4.1.4.1 Western blot reagents

Table 9 Western Blot reagents

Reagent	Company
Albumin Fraction V (BSA)	Carl Roth
Amersham™ Protran 0.2 nitrocellulose Western blotting membrane	GE Lifesciences

Reagent	Company
Ammonium persulfate (APS)	Carl Roth
Bromphenolblue	Amersham
cOmplete™ Protease Inhibitor Cocktail (PIC)	Roche
Dithiothreitol (DTT)	Merck
PageRuler™ Plus Prestained Protein Ladder	Thermo Fisher Scientific
Phenylmethylsulfonyl fluoride (PMSF)	Carl Roth
Rotiphorese® Gel 30	Carl Roth
Sodium dodecyl sulfate (SDS)	Carl Roth
Sodium orthovanadate	Sigma
Starter for x-ray developer	TETENAL
Superfix MRP x-ray fixing solution	TETENAL
Tetramethylethylenediamine (TEMED)	Carl Roth
Tris HCl	Carl Roth
Whatman paper	Carl Roth
β-glycerophosphate	Sigma

4.1.4.2 Buffers for Western blotting

Table 10 Buffers for Western blotting

Buffer	Ingredients
Blocking buffer	5 % Milk powder in PBS-Tween (0.1 % Tween)
Blotting buffer	5.8 g/l Tris Base 2.9 g/l Glycine 0.04 % SDS 20 % Methanol
Loading buffer (6x)	350 mM Tris Base, pH 6.8 3.8 % Glycerol 10 % SDS 0.12 mg/ml Bromphenolblue
Phosphate-buffered saline (PBS, 10x, pH 7.4)	80 g/l NaCl 2 g/l KCl 2 g/l KH ₂ PO ₄ 14.4 g/l Na ₂ HPO ₄
RIPA buffer	20 mM Tris HCl pH, 8.0 1 % NP-40

Buffer	Ingredients
	0.5 % Na-deoxycholate 150 mM NaCl 2 mM MgCl ₂ 1 % SDS Protease Inhibitor Cocktail (PIC) 1 mM Sodium orthovanadate 1 mM β-glycerophosphate 5 mM Sodium fluoride 250 U/ml Pierce Universal Nuclease
NP-40 buffer	20 mM Tris HCl, pH 7.5 50 mM NaCl 1 % NP-40 10 % Glycerol 5 mM EDTA Protease Inhibitor Cocktail (PIC) 1 mM Sodium orthovanadate 5 mM Sodium fluoride 1 mM β-glycerophosphate 250 U/ml Pierce Universal Nuclease
DUB buffer	50 mM HEPES, pH 8.0 150 mM NaCl 0.1 mM EDTA fresh 1 mM DTT
Ni-NTA lysis buffer	6 M Guanidine HCl 0.1 M NaH ₂ PO ₄ /Na ₂ HPO ₄ 100 mM Tris, pH 8.0
Ni-NTA washing buffer 1	6 M Guanidine HCl 0.1 M NaH ₂ PO ₄ /Na ₂ HPO ₄ 10 mM Tris 0.05 % TritonX-100, pH 8
Ni-NTA washing buffer 2	8 M UREA 0.1 M NaH ₂ PO ₄ /Na ₂ HPO ₄ 10 mM Tris 0.05 % TritonX-100, pH 8
Ni-NTA washing buffer 3	8 M UREA 0.1 M NaH ₂ PO ₄ /Na ₂ HPO ₄

Buffer	Ingredients
	10 mM Tris-HCl 0.05 % TritonX-100, pH 6.3
Ni-NTA elution buffer	3x Laemmli loading buffer 200 mM Imidazole
Stripping buffer	0.4 M NaOH
Running buffer (5x)	15.1 g/l Tris Base, 94 g/l Glycine, 0.5 % SDS
Wash buffer	PBS-Tween (0.1 % Tween)
TBST	20 mM Tris-HCl 0.15 M NaCl 0.1 % Tween-20, pH 8

4.1.4.3 Primary antibodies for Western blotting

Table 11 Primary antibodies for Western blotting

Target protein	Dilution	Species	Company
RIPK1	1:1000	Mouse	BD Bioscience
pRIPK1	1:1000	Rabbit	Cell Signaling
RIPK3	1:1000	Rabbit	Cell Signaling
pRIPK3 (#ab195117)	1:1000	Rabbit	Abcam
pRIPK3 (#ab209384)	1:1000	Rabbit	Abcam
MLKL	1:1000	Rabbit	Cell Signaling
pMLKL	1:1000	Rabbit	Cell Signaling
GAPDH	1:5000	Mouse	Biotrend
GFP	1:1000	Rabbit	ChromoTek
β -Actin	1:2000	Mouse	Merck
USP22	1:1000	Rabbit	Abcam
USP22	1:1000	Rabbit	Novus Biologicals
Strep-tag II	1:1000	Rabbit	Abcam
Flag	1:1000	Mouse	Merck
H2B	1:1000	Rabbit	Merck
H2Bub1	1:1000	Mouse	Merck
Cas9	1:1000	Mouse	Merck
Vinculin	1:2000	Mouse	Sigma
His-tag	1:1000	Mouse	Santa Cruz
Caspase-8	1:1000	Mouse	Cell Signaling

Target protein	Dilution	Species	Company
Caspase-8	1:1000	Mouse	Enzo Life Sciences
TRADD	1:1000	Mouse	Abcam
FADD	1:1000	Mouse	BD Bioscience
TNFR1	1:1000	Rabbit	Cell Signaling
I κ B α	1:1000	Rabbit	Cell Signaling
pI κ B α	1:1000	Mouse	Cell Signaling

All primary antibodies were diluted in PBS-Tween (0.1 %) with 2 % BSA.

4.1.4.4 Secondary antibodies for Western blotting

Table 12 Secondary antibodies for Western blotting

Target species	Dilution	Conjugate	Company
Goat-anti-mouse-IgG	1:10000	Horseradish peroxidase	Santa Cruz Technologies
Goat-anti-rabbit-IgG	1:10000	Horseradish peroxidase	Santa Cruz Technologies

“Goat-anti-mouse-IgG” and “Goat-anti-rabbit-IgG” were diluted in PBS-Tween (0.1 %) with 5 % milk powder.

4.1.5 Mass spectrometry buffers and materials

Table 13 Mass spectrometry buffers

Buffer	Ingredients
Denaturation buffer	6 M Urea 2 M Thiourea in 10 mM HEPES pH, 8.0
Immunoprecipitation buffer	10 mM Sodium phosphate 50 mM Sodium chloride in 50 mM MOPS pH, 7.2

Table 14 Mass spectrometry reagents and equipment

Reagent & equipment	Supplier
Acetonitrile	Sigma
Chloroacetamide	Sigma
C18 reversed-phase columns (15 cm length, 75 μ m inner diameter, 1.9 μ m bead size)	Thermo Scientific
Di-glycine-lysine antibody resin	Cell Signaling Technology

Dithiothreitol	Sigma
Endoproteinase Lys-C	Wako Chemicals
Formic acid	Sigma
Micro-column-based strong-cation exchange chromatography (SCX)	See PMID:23954790
Quadrupole Orbitrap mass spectrometer	Thermo Scientific
Reversed-phase C18 StageTips	See PMID:17703201
Reversed-phase Sep-Pak C18 cartridges	Waters
Sequencing grade modified trypsin	Sigma
Trifluoroacetic	Sigma
Ultra-High-Performance-Liquid-Chromatography (UHPLC) system	Thermo Scientific

4.1.6 Immunofluorescence-related materials

4.1.6.1 Buffers for immunofluorescence

Table 15 Buffers for immunofluorescence

Buffer	Ingredients
Antibody dilution buffer	0,9 % NaCl 10 mM Tris HCl, pH 7.5 5 mM EDTA 1 mg/ml BSA

4.1.6.2 Primary antibodies for immunofluorescence

Table 16 Primary antibodies for immunofluorescence

Target protein	Dilution	Species	Company
USP22	1:100	Rabbit	Abcam
RIPK3	1:100	Mouse	Santa Cruz
MLKL	1:500	Rabbit	Cell Signaling

4.1.6.3 Secondary antibodies for immunofluorescence

Table 17 Secondary antibodies for immunofluorescence

Target species	Dilution	Conjugate	Company
Donkey-anti-mouse	1:800	FITC	Jackson ImmunoResearch
Donkey-anti-rabbit	1:800	Cy3	Jackson ImmunoResearch

4.1.7 Material for cloning, DNA transfection and transduction

4.1.7.1 Plasmids

Table 18 Plasmids

Transgene	Vector backbone	Source
FLAG-HA-USP22	pcDNA3.1	Thermo Fisher Scientific #V79020
FLAG-HA-USP22 C185S	pcDNA3.1	Thermo Fisher Scientific #V79020
empty	pcDNA3.1	Thermo Fisher Scientific #V79020
empty	pSBbi-blast	Addgene #60526
FLAG-HA-USP22	pSBbi-blast	Addgene #60526
FLAG-HA-USP22 C185S	pSBbi-blast	Addgene #60526
FLAG-HA-USP22 PAM	pSBbi-blast	Addgene #60526
FLAG-HA-USP22 C185S PAM	pSBbi-blast	Addgene #60526
Strep-RIPK3-WT	pSBtet-puro	Addgene #60507
Strep-RIPK3-D160N	pSBtet-puro	Addgene #60507
Strep-RIPK3-K42R	pSBtet-puro	Addgene #60507
Strep-RIPK3-K351R	pSBtet-puro	Addgene #60507
Strep-RIPK3-K518R	pSBtet-puro	Addgene #60507
Strep-RIPK3-2xKR	pSBtet-puro	Addgene #60507
Strep-RIPK3-3xKR	pSBtet-puro	Addgene #60507
Strep-RIPK3-WT	pSBtet-neo	Addgene #60509
Strep-RIPK3-D160N	pSBtet-neo	Addgene #60509
Strep-RIPK3-K518R	pSBtet-neo	Addgene #60509
Strep-RIPK3-3xKR	pSBtet-neo	Addgene #60509
(CAT)T7-SB100	pCMV	Addgene #34879
HA-Ubiquitin	pRK5	Addgene #17608
His-Ubiquitin	pRK5	AG Müller (Frankfurt am Main)

Transgene	Vector backbone	Source
Strep-RIPK3 WT	pDest30	Thermo Fisher Scientific #12301016
Strep-RIPK3 D160N	pDest30	Thermo Fisher Scientific #12301016
Strep-RIPK3 K42R	pDest30	Thermo Fisher Scientific #12301016
Strep-RIPK3 K351R	pDest30	Thermo Fisher Scientific #12301016
Strep-RIPK3 K518R	pDest30	Thermo Fisher Scientific #12301016
Cas9	plentiCRISPRv2	Addgene #52961
Cas9 / sgRNA USP22_1	plentiCRISPRv2	Addgene #52961
Cas9 / sgRNA USP22_2	plentiCRISPRv2	Addgene #52961
Cas9 / sgRNA USP22_3	plentiCRISPRv2	Addgene #52961
Cas9 / sgRNA USP22_1_m	plentiCRISPRv2	Addgene #52961
Cas9 / sgRNA USP22_2_m	plentiCRISPRv2	Addgene #52961
Cas9 / sgRNA USP22_3_m	plentiCRISPRv2	Addgene #52961
Cas9 / sgRNA USP22_4_m	plentiCRISPRv2	Addgene #52961
Cas9 / sgRNA RIPK3_1	plentiCRISPRv2	Addgene #52961

4.1.7.2 Mutagenesis primer

Table 19 List of mutagenesis primers

Name	Sequence (5' → 3')	Supplier
RIPK3 K518R fwd	GGTATAATCATAGCGGGAGGTTAGTC GAGATATCTAGAC	Eurofins Genomics
RIPK3 K518R rev	GTCTAGATATCTCGACTACCTCCCG CTATGATTATACC	Eurofins Genomics
RIPK3 K351R fwd	CTGAGTGGCTAAACAGACTGAATCT AGAGG	Eurofins Genomics
RIPK3 K351R rev	CCTCTAGATTCAGTCTGTTTAGCCA CTCAG	Eurofins Genomics
RIPK3 K42R fwd	GGCGCAACATAGGAGATGGGGCTA CGATG	Eurofins Genomics
RIPK3 K42R rev	CATCGTAGCCCCATCTCCTATGTTG CGCC	Eurofins Genomics

RIPK3D160N fwd	GAGCTGCACGTCAAGCTGGCAAATT TTGGCCTGTCCACATTTTC	Eurofins Genomics
RIPK3D160N rev	GAAATGTGGACAGGCCAAAATTTGC CAGCTTGACGTGCAGCTC	Eurofins Genomics
RIPK3 PAM2 fwd	GTTTGTTAACGTAAACCGGAAAGCC TCCACAGCCAGTGACGTC	Eurofins Genomics
RIPK3 PAM2 rev	GACGTCACTGGCTGTGGAGGCTTTC CGGTTTACGTTAACAAAC	Eurofins Genomics
USP22 C185S fwd	GGGAACACATCCTTCATGAAC	Eurofins Genomics
USP22 C185S rev	AAGGTTGATCAGTCCACG	Eurofins Genomics
USP22 C185A fwd	TGGGAACACAGCCTTCATGAACTGC ATC	Eurofins Genomics
USP22 C185S rev	AGGTTGATCAGTCCACGC	Eurofins Genomics
USP22 PAM2 fwd	CATAGGTCTGCGTGGACTGATCAAC CTTGGG	Eurofins Genomics
USP22 PAM2 rev	CCCAAGGTTGATCAGTCCACGCAGA CCTATG	Eurofins Genomics
USP22 PAM3 fwd	GTGGACCCACGCGAGACACCTAGC AGGCTAC	Eurofins Genomics
USP22 PAM3 rev	GTAGCCTGCTAGGTGTCTCGCGTG GGTCCAC	Eurofins Genomics

4.1.7.3 Cloning reagents and kits

Table 20 Cloning reagents

Reagent	Company
Ampicillin	Carl Roth
<i>Sfi</i> 1 restriction enzyme	NEB
DH5 α competent E.coli	Thermo Fisher Scientific
peqGOLD Gel Extraction kit	Peqlab
Glycerol	Carl Roth
Kanamycin	Carl Roth
Chloramphenicol	Merck
LB medium	Carl Roth
Ligation kit	Thermo Fisher Scientific

Reagent	Company
PureLink™ HiPure Plasmid filter Maxiprep kit	Thermo Fisher Scientific
GeneJET plasmid Miniprep kit	Thermo Fisher Scientific
Gene Art Site Directed Mutagenesis System kit	Thermo Fisher Scientific
GenElute PCR clean-up kit	Sigma
Phusion polymerase kit	NEB
QIAamp DNA Mini kit	Qiagen
Quick DNA extraction kit	Biozym
Taq polymerase kit	NEB

4.1.7.4 Bacterial growth media

Table 21 Bacterial growth media

Buffer	Ingredients
LB agar	15 g agar dissolved in 800 ml LB medium

4.1.7.5 Oligonucleotides for generation of CRISPR/Cas9 knockout cells

Table 22 List of oligonucleotides for generation of small guide RNAs (sgRNAs)

sgRNA target	Sequence (5' → 3')
USP22_1	GCCATTGATCTGATGTACGG
USP22_2	CCTCGAACTGCACCATAGGT
USP22_3	ACCTGGTGTGGACCCACGCG
USP22_1_mouse	CCGTACATCAGGTCGATGGC
USP22_2_mouse	ACCCGTAAAGATCTGGTCAA
USP22_3_mouse	CAGGTTGATCAGTCCACGCA
USP22_4_mouse	CTGTGAGATGCAGAGCCCCA
RIPK3_1	GTTTGTTAACGTAAACCGGA
MLKL_3	TTCCCTTAGCAGAATCCACG

4.1.7.6 Reagents for transfection and transduction

Table 23 List of reagents for transfection and transduction

Reagent	Company
FuGENE® HD	Promega

Reagent	Company
Lipofectamine [®] 2000	Thermo Fisher Scientific
OptiMEM transfection medium	Thermo Fisher Scientific
Polybrene	Sigma

4.1.8 Small-interfering RNA (siRNA)

Table 24 List of siRNA constructs

siRNA	Target	Identifier
siCtrl	non-targeting control	4390843
siUSP22 #1	USP22	s230743
siUSP22 #2	USP22	s230744
siUSP22 #1_mouse	USP22_mouse	s103730
siUSP22 #2_mouse	USP22_mouse	s103729

4.1.9 Kits

Table 25 List of kits

Kit	Company
FuGENE [®] HD Transfection Reagent	Promega
Ligation kit	Thermo Fisher Scientific
PureLink [™] HiPure Plasmid filter Maxiprep kit	Thermo Fisher Scientific
TOPO [™] TA Cloning [™] kit for Sequencing	Thermo Fisher Scientific
GeneJET plasmid Miniprep kit	Thermo Fisher Scientific
GenElute PCR clean-up kit	Sigma
Phusion polymerase kit	NEB
Pierce BCA Protein Assay kit	Thermo Fisher Scientific
Pierce ECL Western Blotting Substrate	Thermo Fisher Scientific
Protein A Dynabeads	Thermo Fisher Scientific
Anti-FLAG [®] M2 Magnetic Beads	Merck
Pierce [™] Anti-HA Magnetic Beads	Thermo Fisher Scientific
HisPur [™] Ni-NTA beads	Thermo Fisher Scientific
Glutathione agarose beads	GE Healthcare Bio-Sciences
Novex [™] DYNAL [™] Dynabeads [™] Protein A	Thermo Fisher Scientific

Kit	Company
MagStrep "type3" XT beads 5 % suspension	IBA Lifesciences
SUPERFIX-MRP x-ray fixer	TETENAL
Starter for x-ray developer	TETENAL
GenElute PCR clean-up kit	Sigma
QIAamp DNA Mini kit	Qiagen
Quick DNA extraction kit	Biozym

4.1.10 Chemicals

Table 26 List of chemicals

Chemical	Company
2-propanol	Carl Roth
Agar-Agar	Carl Roth
Acrylamide mix, 30 %	Carl Roth
Agarose	Sigma
Bovine serum albumin (BSA)	Carl Roth
Ammonium persulfate (APS)	Carl Roth
β -Glycerophosphate	Sigma
Bromphenolblue	Carl Roth
cOmplete™ Protease Inhibitor Cocktail (PIC)	Roche
Dithiothreitol	Carl Roth
Ethanol	Carl Roth
Ethylenediaminetetraacetic acid (EDTA)	Carl Roth
Glycerol	Merck
Glycine	Carl Roth
Guanidine	Merck
Hydrochloric acid (HCl)	Carl Roth
K ₂ PO ₄	Merck
Methanol	Carl Roth
Milk powder	Carl Roth
MgCl ₂	Merck
MOPS	Merck
Na-deoxycholate	Merck

Chemical	Company
NaH ₂ PO ₄	Merck
NP40	Carl Roth
Paraformaldehyde	Merck
Phenylmethylsulfonyl fluoride	Carl Roth
Roenteroll HCx-ray developer	TETENAL
Sodium chloride (NaCl)	Carl Roth
Sodium dodecyl sulfate (SDS)	Carl Roth
Sodium fluoride	Carl Roth
Sodium hydroxide	Carl Roth
Sodium orthovanadate	Merck
Sodium phosphate	Carl Roth
Starter for x-ray developer	TETENAL
Superfix MRP x-ray fixing solution	TETENAL
Tetramethylethylenediamine (TEMED)	Carl Roth
Thiourea	Merck
Tris Base	Carl Roth
Tris HCl	Carl Roth
Triton X-100	Carl Roth
Tween 20	Carl Roth
UREA	Merck

4.1.11 Consumables

Table 27 List of consumables

Consumable	Company
Cell culture flasks (25 cm ² , 75 cm ² , 175 cm ² tissue culture)	Greiner Bio-One
Cell culture dishes (10 cm/145 cm diameter, tissue culture)	Greiner Bio-One
Cell culture plates (96-well, 24-well, 12-well, 6-well)	Greiner Bio-One
CELLSTAR® micro clear black plate (96-well)	Greiner Bio-One
Cell scraper	BD Biosciences

Consumable	Company
Combitips (all sizes, sterile and unsterile)	Eppendorf
Centrifuge tubes (15 ml/50 ml)	Greiner Bio-One
Cryogenic vials	Starlab
Disposal bags	Carl Roth
Filter tips (10 µl, 200 µl, 1000 µl)	Starlab
Gel blot paper	Carl Roth
Hybond ECL nitrocellulose membrane	GE Healthcare
Hyperfilm ECL	GE Healthcare
MicroAmp™ Optical 96-Well Reaction Plate	Thermo Fisher Scientific
MicroAmp™ Optical 384-Well Reaction Plate	Thermo Fisher Scientific
Microcentrifuge tubes (0.5 ml/1.5 ml/2 ml)	Starlab
Microcentrifuge tubes (5 ml)	Eppendorf
Nitrile gloves, sterile, powder-free	Kimberly-Clark
Parafilm	VWR
Pasteur pipettes (15 cm/30 cm)	Carl Roth
Precision cover slips (17 mm)	Carl Roth
Scalpel	B. Braun
Syringe (5 ml, 2 ml)	B. Braun
Sterile filters (0.22 µm)	Merck
Sterile pipettes (5 ml, 10 ml, 25 ml, 50 ml)	Greiner Bio-One
Whatman Paper	Thermo Fisher Scientific

4.1.12 Equipment

Table 28 List of equipment

Equipment	Supplier
Autoclave VX150	Systec
Balances Kern 770/EW	Kern
Biowizard biosafety cabinet	Kojair
Centrifuge MIKRO 200 R	Hettich

Equipment	Supplier
Centrifuge ROTIXA 50 RS	Hettich
CM100bio TEM	FEI
CO ₂ Incubator MCO-19AIC	Sanyo
Easypet© 3	Eppendorf
Electronic analytical balance EW	Kern
Electronic precision balance 770	Kern
FACS Aria II cell sorter	BD Biosciences
Heating block	Eppendorf
Heating magnetic stirrer ARE	VELP scientifica
ImageXpress micro XLS system	Molecular Devices
Infinite M100 microplate reader	Tecan
Inolab© pH 7310	WTW
Leica EM UC7 ultra microtome	Leica Microsystems
Leica SP8 laser-scanning microscope	Leica Microsystems
Micro Centrifuge SD	Carl Roth
Microscope CKX41	Olympus
Mini-PROTEAN Tetra Cell electrophoresis system	Bio-Rad
Multipipette© 4	Eppendorf
Nalgene © Mr. Frosty	Sigma
NanoDrop 1000	Peqlab
Neubauer improved counting chamber	Carl Roth
PerfectBlue™ Gel system	Peqlab
Pipette Research plus (2.5 µl, 10 µl, 20 µl, 100 µl, 200 µl, 1000 µl)	Eppendorf
PowerPac™ Universal power supply	Bio-Rad
Shaker	neoLab
Roller	neoLab
Thermomixer comfort	Eppendorf
Trans-Blot© SD Semi-Dry Transfer Cell	Bio-Rad
Vacuum Pump HLC	Ditabis
Vortex mixer ZX classic	VELP scientifica
Water bath WBT 22	Carl Roth
X-Ray cassette type G	Rego

4.1.13 Software

Table 29 List of software

Software	Version	Supplier
i-control™	1.10	Tecan
ImageJ	1.52e	National Institute of Health
Magellan Data Analysis	7.2	Tecan
Microsoft Office 2013	2013	Microsoft GmbH
MetaXpress®	6.5.1.347	Molecular Devices
NanoDrop	-	Peqlab
SnapGene®	4.2	SnapGene
EndNote	X7	Thomson Reuters
MaxQuant	1.5.2.8	Max-Planck-Institute of Biochemistry
Andromeda search engine	-	Max-Planck-Institute of Biochemistry

4.2 Methods

4.2.1 Cell culture

All cell lines were cultured in humidified incubators with 37 °C and 5 % carbon dioxide (CO₂)-atmosphere. HT-29 cells were maintained in McCoy's 5A Medium GlutaMAX™-I, supplemented with 10 % fetal calf serum (FCS) and 1 % penicillin/streptomycin. HEK293T and HeLa cells were cultured in DMEM GlutaMAX™-I medium, supplemented with 10 % fetal calf serum (FCS), 1 % penicillin/streptomycin and 1 % sodium pyruvate.

For mass spectrometry studies, HT-29 cells were cultivated for at least six passages in McCoy's 5A Media for stable isotope labeling by/with amino acids in cell culture (SILAC). Media were supplemented with 10 % dialyzed FBS and the appropriate isotope-labelled lysine and arginine: Lys 0 and Arg 0 for light condition and Lys 8 and Arg 10 for heavy condition. All SILAC-labelling conditions were performed at a lysine and arginine concentration of 28 mg/l and 48 mg/l, respectively.

Cells were cultivated in cell culture flasks and sub-cultured two or three times until reaching 90 % confluency. For passaging, cells were washed with pre-warmed PBS and exposed to trypsin/EDTA solution at 37 °C, 5 % CO₂ for 5 minutes. Following cell detachment, trypsin was blocked by adding fresh media. An appropriate amount of cells were sub-cultured in a new cell culture flask until next passaging. Upon reaching 30 passages, cell culture was terminated.

4.2.2 Freezing and thawing of cell lines

For long term storage, cells were initially washed and trypsinized as described above, followed by centrifugation for 5 minutes at 1800 rpm. Cells were resuspended in freezing solution, containing 90 % FCS and 10 % DMSO. Resuspended cells were frozen in cryogenic vials in a liquid nitrogen tank at -200 °C until further use. For thawing, frozen cells were quickly thawed at room temperature (RT) and the defrosted cell suspension was added dropwise to 5 ml of pre-warmed growth-media. After centrifugation for 5 minutes at 1800 rpm cells were resuspended with the appropriate growth-media in order to remove DMSO and cultured as described above. The next day, growth-media was changed to remove residual DMSO.

4.2.3 Counting, seeding and treatment of cell lines

Cells were initially detached utilizing washing with pre-warmed PBS and trypsin/EDTA solution at 37 °C, 5 % CO₂ for 5 minutes. The amount of viable cells per ml in the cell suspension was determined by trypan blue staining, which excludes dead cells. For this, 20 µl of cell suspension was added to 60 µl of 0.4 % (v/v) trypan blue dye and counted via a Neubauer counting chamber. Cells were seeded using an appropriate number of cells per cm², preventing cell overgrowth during the experimental procedure. To achieve the correct seeding density, the cell suspension was diluted with fresh growth-media. Total volume for plating of cells varied depending on the experimental setup.

Cells were treated 24 h after seeding. Consumed medium was discarded and replaced by fresh growth medium containing the respective drug in the indicated concentration. Duration of treatment depended on the experimental setup and varied between 4 and 48 h.

4.2.4 Generation of genetically modified cell lines

4.2.4.1 CRISPR/Cas9-derived USP22 and RIPK3 knockout cell lines

In order to generate CRISPR/Cas9 control (targeting eGFP), RIPK3 knockout or USP22 knockout cells, gene specific guide RNAs (Table 19) were cloned into the plentiCRISPRv2 vector [316] (Addgene plasmid #52961). Generation was performed using standard restriction enzyme cloning methods. All plasmids were verified by Sanger DNA sequencing.

For virus production, sgRNAs targeting eGFP, RIPK3 or USP22 were co-transfected into HEK293T cells by using FuGENE HD Transfection Reagent (FuGENE/DNA ratio 3:1) according to the manufacturer's instructions in DMEM lacking penicillin/streptomycin. 24 h after transfection, growth media was changed. Supernatant containing virus were collected and pooled by harvesting cell supernatant 48 h and 72 h after transfection. Supernatants were

sterile filtered (45 µm) and stored at 4 °C until transduction. Target cell lines were transduced by combining 1 ml of fresh growth medium with 1 ml of virus supernatant in the presence of 8 µg/ml polybrene for 48 h. Subsequently, cells were selected using 1-10 µg/ml puromycin for at least 14 days.

If necessary, single-cell dilution was performed utilizing limited dilution into 96-well plates. Dilution was performed in conditioned medium, containing 10 % sterile-filtered medium collected from the corresponding cell line and 90 % fresh medium for 72 h in order to ensure growth under single-cell conditions. Single cell colonies were expanded for 14 days before knockout efficiency was validated by Western blot analysis with the corresponding antibody.

4.2.4.2 Site directed mutagenesis

To generate point mutations in USP22 and RIPK3 plasmids, the GENEART® Site-Directed Mutagenesis system was used according to the manufacturer's instructions. The respective plasmid DNA was methylated before being amplified by mutagenesis PCR using an overlapping primer pair (listed in 4.1.5.2), bearing the desired mutation. Mutagenesis PCR was followed by a recombination reaction, amplifying the colony output 3- to 10-fold. The reaction was stopped by addition of 0.5 M EDTA. 2 µl of the recombination reaction was quickly transformed into OneShot® MAX Efficiency® DH5α™-T1R competent *E. coli* for 12 minutes on ice. The bacteria were heat shocked for exactly 30 seconds at 42 °C and placed again on ice for 2 minutes before addition of 250 µl pre-warmed SOC-medium. After 1 h of incubation time at 37 °C and 220 rpm, bacteria were plated on LB Amp plates and inverted for overnight incubation at 37 °C. The following day, single colonies were picked and transferred into 5 ml of LB medium for an overnight culture at 37 °C and 220 rpm. Plasmid extraction was performed using the GeneJET plasmid Miniprep kit following the manufacturer's instructions. Purified plasmid DNA concentration was determined using a NanoDrop 1000 spectrophotometer. Correct mutagenesis was confirmed by Sanger sequencing by LGC Genomics. Correctly mutated plasmids were transformed in One Shot™ TOP10 Chemically Competent *E. coli* and transferred into 250 ml of LB medium at 37 °C and 220 rpm. The next day, the plasmid extraction was performed using the PureLink™ HiPure Plasmid Filter Maxiprep kit following the manufacturer's instructions. Successful mutagenesis was confirmed Sanger sequencing of purified plasmid DNA, by Laboratory of the Government Chemist (LGC) genomics. The purified plasmid DNA was used for downstream applications.

4.2.4.3 Generation of stable cell lines using the T-REx™ system

HeLa-TREx™ or HEK293-TREx™ cells were genetically modified to express doxycycline (Dox)-inducible RIPK3 or MLKL constructs (listed in 4.1.5.1) with the TREx™ (tetracyclin-

regulated expression) system according to the manufacturer's instructions. In brief, HeLa-TREx™ or HEK293-TREx™ cells, stably expressing the tetracycline repressor protein, were seeded into 6 well dishes, 24 h prior to transfection. For transfection, 200 ng of the respective pTREx plasmid containing geneticin resistance and 1800 ng of pOG44 recombinase transfection vector were co-transfected with FuGENE HD according to the manufacturer's instructions. 48 h after transfection, cells were trypsinized, expanded into 10 cm dishes and selected using 50 µg/ml geneticin. Cells which successfully integrated the gene of interest were expanded and tested for doxycycline inducible expression of the protein of interest. Cloning of the constructs was performed by using standard restriction enzyme cloning and PCR amplification, using either the Taq or phusion polymerase kit following the manufacturer's guidelines. Exemplary cycle conditions for both polymerase kits are shown in table 32 and 33.

Table 30 Taq polymerase PCR cycle conditions

Step	Temperature	Time	Number of cycles
Initial denaturation	94 °C	3 min	1
Denaturation	94 °C	45 s	35
Annealing	58-62 °C	30 s	
Extension	72 °C	3 min	
Final extension	72 °C	10 min	
Pause	4 °C	∞	

Table 31 Phusion polymerase PCR cycle conditions

Step	Temperature	Time	Number of cycles
Initial denaturation	98 °C	120 s	1
Denaturation	98 °C	10 s	35
Annealing	68 °C - 70 °C	30 s	
Extension	72 °C	70 s	
Final extension	72 °C	10 min	
Pause	4 °C	∞	

4.2.4.4 Generation of stable cell lines using the Sleeping Beauty vector system

To generate stable constitutively expressing or Dox-inducible USP22 and RIPK3 expressing cells, full-length human USP22 and RIPK3 PCR products were cloned into different expression vectors of the Sleeping Beauty (SB) vector-system [317]. Briefly, different TOPO™-plasmids were generated with the TOPO™ TA Cloning™ kit according to the manufacturer's

instructions, carrying the gene of interest and flanked by SB-specific *Sfi1* restriction sites. TOPO™-plasmids and destination vectors were *Sfi1*-digested and ligated overnight at 16 °C. Transformation of ligated products, plasmid extraction and sequencing was performed as described above (4.2.4.2). For the integration process, 200 ng of pCMV-(CAT)T7-SB100 was co-transfected with 1800 ng of the appropriate expression vector using FuGENE HD according to the manufacturer's instructions (FuGENE/DNA ratio 3:1), 24h after cell plating. 48 h after transfection, cells were trypsinized, expanded in 10 cm dishes and selected using the respective selection agent (blasticidin 10 µg/ml, geneticin 50 µg/ml, puromycin 10 µg/ml). Selection process was terminated after 14 days and cells were cultivated in normal growth medium. Expression levels of stable constitutive or dox-inducible protein expression was determined by Western blotting.

4.2.5 Transfection of cells

4.2.5.1 Transfection with Lipofectamine

For transfection with Lipofectamine2000® reagent, cells were seeded 24 h prior to transfection in growth medium lacking penicillin/streptomycin. Plasmid DNA concentration used for transfection varied depending on the experimental setup and ranged from 2-6 µg (per 6-well) to 30 µg (per 14.5cm dish). DNA was diluted in 125 up to 1000 µl Opti-MEM® medium. All transfections were carried out at a Lipofectamine2000®/DNA ratio of 3:1. For transfection, Lipofectamine2000® was diluted in the same amount of Opti-MEM® medium as the plasmid DNA and incubated for 5 min at RT. Then, the DNA-containing solution was added at 1:1 ratio to the Lipofectamine2000® solution and incubated for 20 minutes after carefully inverting the reaction tube several times. The transfection mixture was finally added dropwise to the cells and incubated for 24 to 48 h. Transfection efficiency was monitored by Western blot analysis.

4.2.5.2 Transfection with FuGENE HD

Transfection with FuGENE HD was carried out in penicillin/streptomycin-free growth media and cells were plated 24 h prior to transfection. For all transfections, a 3:1 ratio of FuGENE HD/DNA was used. Firstly, plasmid DNA was diluted in Opti-MEM® medium, followed by FuGENE HD. The reaction mixture was inverted several times and incubated for 15 minutes before being added dropwise to the cells. After 24 to 48 h of incubation, transfection efficiency was monitored by Western blotting analysis.

4.2.5.3 Reverse RNAiMAX

Transient genetic silencing was performed by reverse transfection of cells with 20 nM Silencer Select siRNAs using Lipofectamine RNAiMax reagent, and Opti-MEM® medium. For reverse transfection, Lipofectamine RNAiMax reagent, Opti-MEM® medium and the respective siRNA were mixed and incubated for 30 minutes at RT. Following incubation, siRNA transfection mixture was placed at the plate surface and counted cells were seeded on top of the transfection mix at the appropriate cell density/ml growth media lacking penicillin/streptomycin. Knockdown efficiency was confirmed by Western blot analysis.

4.2.6 Western Blot analysis

4.2.6.1 Cell lysis

Cells were plated either in 6 wells, 6 cm, 10 cm or 14.5 cm-dishes and treated as indicated in the experiment. All cells were washed twice with PBS before scraping the remaining cell layer with the corresponding lysis buffer. Lysis buffer volume was adjusted according to the experimental setup. General cell lysis, if not indicated otherwise, was performed using RIPA lysis buffer, supplemented with 1 x protease inhibitor cocktail, phosphatase inhibitors (1 mM sodium orthovanadate, 1 mM β -glycerophosphate, 5 mM sodium fluoride), 0.3 % Sodium Dodecyl Sulfate (SDS) and Pierce Universal Nuclease. Cells were lysed for 30 up to 40 minutes on ice before cell debris was removed by centrifugation at 14.000 rpm for 25 minutes at 4 °C. Supernatant was collected and placed on ice for determination of protein concentration.

4.2.6.2 Determination of protein concentration

Protein concentration of supernatant after cell lysis was determined using the BCA Protein Assay kit from Pierce™ according to the manufacturer's instructions. Quantification was done by measuring absorbance at 550 nm with a Tecan Sunrise™ microplate reader and comparing it to a standard curve generated by diluted BSA in ddH₂O.

4.2.6.3 SDS Page and Western blotting

Proteins were separated for their molecular weight by Sodium dodecyl sulfate polyacrylamide gel electrophoresis (SDS-PAGE). All gels were hand-cast (at a maximum of 14 days in advance of the actual experiment). Polyacrylamide gels were divided into a 5 % stacking and a 10-12 % resolving gel, matching the protein size. Stacking gels consisted of 5 % acrylamide, 125 mM TrisHCl (pH 6.8), 0.1 % APS, 0.1 % SDS and 0.1 % TEMED, resolving gels contained

10 % or 12 % acrylamide, 250 mM TrisHCl (pH 8.8, 0.1 % APS,), 0.1 % SDS and 0.04 % TEMED.

Gel electrophoresis was performed using 20-40 µg of total lysate for each sample, respectively. Prior to gel loading, lysates were boiled for 5 min at 95 °C in 1x Laemmli loading buffer (listed in Table 10). In addition to lysates, a protein ladder, ranging from 10 kDa to 250 kDa, was loaded to allow correlation of proteins at later detection. Gel electrophoresis was performed in 1 x running buffer (listed in Table 10) under constant voltage (stacking gel: 100 mV, resolving gel: 140 mV) until the proteins were separated as desired.

Protein transfer from the resolving gel onto a nitrocellulose membrane was performed using a semi-dry blotting system. The resolving gel, a nitrocellulose membrane and four Whatman papers were equilibrated in 1x blotting buffer (listed in Table 10). The resolving gel, saturated with 1x blotting buffer, was placed directly onto nitrocellulose membrane placed on the blotting chamber. Two Whatman papers covered the resolving gel and the nitrocellulose membrane from both sides, before proteins were blotted for 1 h and 40 minutes at 1 mA/cm².

4.2.6.4 Detection of proteins

Unspecific antibody binding to the membranes was blocked by incubation with PBS-T (PBS containing 0.1 % Tween) containing milk powder (5 %) and tween (0.1 %) for 1 h. Subsequently, membranes were washed three times with PBS-T for at least 5 minutes under constant rotation. Primary antibody, diluted 1:1000 in PBS-T and containing 2 % BSA, was incubated overnight on an orbital shaker at 4 °C. The next day, the primary antibody was recovered and stored at -20 °C until further needed. Membranes were washed 3 times with PBS-T for at least 10 min with constant rotation at RT. Secondary antibodies were diluted 1:10,000 in 5 % milk in PBS-T and incubated for 1 h under constant shaking. Secondary antibody dilutions were discarded and the membranes again washed with PBS-T for at least 10 minutes with constant rotation. Detection of HRP-conjugated secondary antibodies was performed using enhanced chemo-luminescence (ECL) with Pierce™ ECL Western Blot Substrate and developing solutions. If additional antibody detections were required, membranes were washed three times with PBS-T and stripped for 10 minutes using 0.4 M NaOH solution (listed in Table 10). Stripping buffer was removed by washing the membrane 3 times with PBS-T for 10 min. Finally, membranes were again blocked with 5 % milk in PBS-T for another 30 minutes, washed with PBS-T 3 times for 10 minutes and incubated with new primary antibody overnight at 4 °C. Representative blots of at least two independent experiments are shown.

4.2.7 Determination of cell death

For cell death analysis, the indicated cell lines were seeded in appropriate densities in sterile 96-well plates 24 h prior to stimulation with the respective drug. Cell death was measured by fluorescence-based microscopic quantification of the fraction of propidium iodide (PI)-positive cells, compared to total cells, using Hoechst 33342 and PI double staining. Imaging and quantification were performed using the ImageXpress Micro XLS Widefield High-Content Analysis System and MetaXpress Software according to the manufacturer's instructions.

4.2.8 Immunoprecipitations

For immunoprecipitations, cells were lysed in NP-40 lysis buffer (listed in Table 10), supplemented with protease inhibitor cocktail, phosphatase inhibitors (1 mM sodium orthovanadate, 1 mM β -glycerophosphate, 5 mM sodium fluoride) and Pierce Universal Nuclease as described above (see 4.2.6.1). Following determination of protein concentration, 1 to 1.5 mg of protein was loaded onto the respective beads and incubated overnight at 4 °C on a rotating wheel. The next day, beads were separated from the supernatant via centrifugation or with a magnetic rack and washed 5 times with lysis buffer. Afterwards, beads were mixed with 15 μ l of 2x Loading Buffer and boiled for 6 minutes at 96 °C in order to remove proteins from the beads. The remaining supernatant was used for Western blot analysis.

4.2.9 *In vivo* (de)ubiquitination immunoprecipitations

For *in vivo* (de)ubiquitination immunoprecipitations under denaturing conditions, cells were either lysed in NP-40 lysis buffer, supplemented with 1% SDS, or in RIPA lysis buffer, supplemented with 2 % SDS and 25 mM NEM. Cells were directly sonicated (3 cycles, 10 seconds burst, amplitude 25, 30 seconds rest) before being boiled at 95 °C for 10 minutes. Following 30 minutes incubation time at 4 °C, NP-40 buffer lysates were diluted with regular lysis buffer (1:10), whereas RIPA lysates were diluted 1:10 in Ni-NTA lysis buffer. At least 1.5 mg of protein lysate was incubated with either anti-HA Magnetic Beads or HisPur™ Ni-NTA beads and rotated overnight at 4 °C. Beads were prewashed twice with either NP-40 lysis buffer or Ni-NTA lysis buffer, respectively. The next day, Anti-HA Magnetic Beads were washed 5 times with NP-40 buffer and boiled for 5 minutes at 95 °C in 2x Laemmli loading buffer. Ni-NTA beads were washed twice with Ni-NTA washing buffer 1, 2 and 3, before being washed once in PBS. Beads were centrifuged at 3000 rpm for 1 minute before being eluted by constantly vortexing the beads for 30 min with Ni-NTA elution buffer at RT.

4.2.10 Complex-I and -II immunoprecipitations

For TNFR1 complex-I (CI) immunoprecipitations, cells were initially washed twice with PBS followed by starvation in serum free DMEM for 2 h. Successively, starved cells were stimulated with 1 µg/ml FLAG-hTNF. For TNFR1 complex-II (CII) immunoprecipitations, cells were pretreated with BV6 for 1 h before being stimulated with TNF α . Cells were washed two times in ice-cold PBS and lysed for 30 minutes in NP-40 lysis buffer. At least 1 mg of protein lysate was incubated with Anti-FLAG® M2 Magnetic Beads and rotated overnight at 4 °C. Novex™ DYNAL™ Dynabeads™ Protein A were used for CII immunoprecipitations and prepared as followed: Three bead washing steps in PBS-Tween (0,05%) using a magnetic separator followed by resuspension in PBS-Tween supplemented with 5 µl Caspase-8 antibody. Beads were incubated with the Caspase-8 antibody for 2 h at 4 °C. For crosslinking, beads were washed in 0.2 M triethanolamine (TEA; pH 8.2), followed by a washing step in TEA, freshly supplemented with 20 mM DMP for 30 minutes. Next, beads were incubated with 50 mM Tris, pH 7.5 for 15 minutes. At last, beads were washed three times with PBS-Tween. At least 1.5 mg of protein was incubated with crosslinked Dynabeads™ overnight at 4 °C. The next day, beads were washed five times with NP-40 lysis buffer before being boiled for 5 minutes at 95 °C in 2x Laemmli loading buffer, followed by Western blot analysis.

4.2.11 Enrichment of ubiquitinated proteins using Tandem Ubiquitin Binding Entities

GST-tagged Tandem Ubiquitin Binding Entities (TUBEs) were expressed and purified from *E. coli* as described previously [318]. Afterwards, GST-tagged TUBEs were immobilized on glutathione agarose beads. Cells were lysed in NP-40 lysis buffer as described above (see 4.2.6.1). Lysis buffer was supplemented with 25 mM N-ethylmaleinimide (NEM) to inhibit deubiquitinase activity. Beads were prewashed with NP-40 lysis buffer twice before incubation with 3.5 mg total protein overnight at 4 °C on a rotating wheel. The next day, GST-TUBE-beads were washed 5 times with NP-40 lysis buffer or TBS-T, supplemented with NEM. Beads were separated from the supernatant by performing 2 minutes centrifugation at 3000x g after each washing step. DUB treatment was conducted for 1 h at 37 °C in DUB buffer, supplemented with 1 µl (50 µM) recombinant catalytic domain of USP2 as indicated. Elution of ubiquitinated proteins was performed with 2x Laemmli loading buffer by boiling the sample 5 minutes at 95 °C, followed by Western blot analysis.

4.2.12 Immunofluorescence

Immunofluorescence staining was performed by seeding cells in black micro-clear 96-well plates. Initially, cells were fixed for 20 minutes with 3.7 % paraformaldehyde at RT, 24 h after cell plating. Cells were permeabilized for 10 minutes with 0.1 % Triton X-100 in PBS, followed by 3 washing steps with PBS for 5 minutes. Then, cells were blocked for 45 minutes with antibody dilution (ABD) buffer, supplemented with 10 % fresh FCS. The desired primary antibody was diluted in ABD buffer and incubated at 4 °C overnight. The next day, primary antibody was recovered, frozen at -20 °C until further use and re-used up to 3 times. Cells were washed 5 times with PBS before being incubated with fluorescently-labeled secondary antibodies (Table 17) and DAPI at a dilution of 1:10,000 for 90 min at RT. Lastly, cells were washed 3 times with PBS and stored in PBS at 4 °C. Analysis was performed using the ImageXpress Micro XLS Widefield High-Content Analysis System by using the 4x or 10x objective and the DAPI, TRITC or FITC filter system. ImageJ was used for image analysis.

4.2.13 Mass spectrometry (MS) analysis

MS analysis and ubiquitin remnant profiling was performed by Thomas Juretschke and Petra Beli at the Institute of Molecular Biology (IMB) (Ackermannweg 4, 55128, Mainz, Germany).

4.2.13.1 Sample preparation

For MS sample preparation, proteins were precipitated with ice-cold acetone in fourfold excess and dissolved in denaturation buffer (Table 13). Then, cysteines were reduced using 1 mM dithiothreitol and alkylated with 5.5 mM chloroacetamide [319]. Subsequently, proteins were digested through sequencing-grade modified trypsin and endoproteinase Lys-C. The reaction was stopped with the addition of trifluoroacetic acid to 0.5 %, followed by centrifugation in order to remove the precipitates. Reversed-phase Sep-Pak C18 cartridges purified the peptides before being eluted in 50 % acetonitrile. Ubiquitin remnant peptide enrichment was performed by re-dissolving 20 mg of peptides in immunoprecipitation buffer (listed in Table 13). Precipitates were removed by centrifugation. Enrichment of modified peptides was performed by using 40 µl of di-glycine-lysine antibody resin. Then, peptides were incubated with the antibodies for 4 h at 4 °C on a rotating wheel. After incubation, beads were washed three times with ice-cold immunoprecipitation buffer followed by three washing steps in water. Enriched peptides were eluted from the beads with 0.15 % trifluoroacetic acid in H₂O. Lastly, peptides were fractionated in six fractions using micro-column-based strong- cation exchange chromatography (SCX) [320], and desalted on reversed-phase C18 StageTips [321].

4.2.13.2 Analysis

A quadrupole Orbitrap mass spectrometer (Q Exactive Plus) equipped with a UHPLC system (EASY-nLC 1000) was used to analyze the peptide fractions as described [322, 323]. For this, peptide samples were loaded onto C18 reversed-phase columns (15 cm length, 75 µm inner diameter, 1.9 µm bead size), followed by elution with a linear gradient from 8 to 40 % acetonitrile containing 0.1 % formic acid over 2 h. The mass spectrometer was operated in data-dependent mode, which allowed automatically switching between MS and MS2 acquisition. Survey full scan MS spectra (m/z 300–1,700) were acquired in the Orbitrap. Higher energy C-trap dissociation (HCD) was used to sequentially isolate and fragment the 10 most intense ions [324]. Ion selection threshold was set to 5,000. Peptides with either unassigned charge states, or with charge states $<+2$, were excluded from the fragmentation process. Ultimately, fragment spectra were acquired in the Orbitrap mass analyzer.

4.2.13.3 Peptide identification

MaxQuant (development version 1.5.2.8) was used to analyze raw data files [325]. A database containing 88,473 human protein sequences obtained from the UniProtKB released in December 2016 was used to search against parent ion and MS2 spectra using. The comparison was performed by the Andromeda search engine [326]. The mass tolerance for spectra was set to 6 ppm in MS mode, 20 ppm in HCD MS2 mode and strict trypsin specificity. Additionally, up to two miscleavages were allowed. Cysteine carbamidomethylation was searched as a fixed modification. Protein N-terminal acetylation, methionine oxidation, N-ethylmaleimide modification of cysteines (mass difference to cysteine carbamidomethylation), and di-glycine- lysine were searched as variable modifications.

MaxQuant using the PTM scoring algorithm was used to determine the site localization probabilities as previously described [325, 327]. A target-decoy approach [328] was used to filter the dataset based on posterior error probability (PEP) to arrive at a false discovery rate of below 1 % estimated. Minimum score was set to 40 whereas delta score was set to 6. Only di-glycine lysine-modified peptides matching these requirements are reported and used for the analysis.

5 Results

The main parts of the results written in 5.1 are described in the publication “USP22 controls necroptosis by regulating receptor-interacting protein kinase 3 ubiquitination”, published in the peer-reviewed journal EMBO Reports in 2020 (#EMBOR-2020-50163V3; accepted for publication on 03.11.2020). Where indicated, experiments were conducted by the PhD students Lisa Kowald or Rebekka Karlowitz. Thomas Juretschke and Petra Beli (Institute of Molecular Biology, Mainz, Germany) analyzed the LC-MS/MS data.

5.1 USP22 governs necroptotic signaling by regulating RIPK3 ubiquitination and phosphorylation

USP22 is an ubiquitin hydrolase, dynamically counterbalancing ubiquitin-modifications by deconjugating ubiquitin signals from substrates, thereby regulating various proteins and interlinked signaling pathways [59, 91, 94, 329]. So far, research focused on the role of USP22 in the human SAGA-complex, catalyzing the removal of monoubiquitination events from H2B, thus regulating gene transcription [85].

On the other hand, USP22 is described to control cell death regulation, mediating apoptosis resistance in various colon cancer cell lines [59]. Necroptosis is regarded as an attractive alternative for overcoming apoptosis resistance in colon cancer [315]. So far, several DUBs are implicated in fine-tuning necroptosis [62, 239-241, 330]. In order to identify novel DUBs involved in controlling necroptotic signaling, a previous study from our research group performed a siRNA-mediated screen in HT-29 colon carcinoma cells to identify DUBs that could rescue TNF α (T), Smac mimetic (BV6; B) and the broad-range caspase inhibitor zVAD.fmk (Z), mediated necroptosis. Among the identified DUBs, USP22 prominently inhibited TBZ-mediated necroptosis in HT-29 cells. Therefore, we decided to investigate the functional role of USP22 during necroptosis.

5.1.1 USP22 regulates necroptosis in HT-29 cells

In order to investigate the functional role of USP22 during necroptosis, USP22 expression was diminished by siRNA-mediated knockdown in the HT-29 human colon carcinoma cell line followed by TBZ-induced necroptosis induction. Subsequently, the amount of resulting cell death was measured by quantification of propidium iodide (PI) uptake, a marker for plasma membrane permeabilization and cell death. siRNA-mediated knockdown of USP22

significantly reduced TBZ-induced necroptotic cell death, as measured by high-throughput fluorescence microscopy 18 h after treatment (Fig. 6A and B).

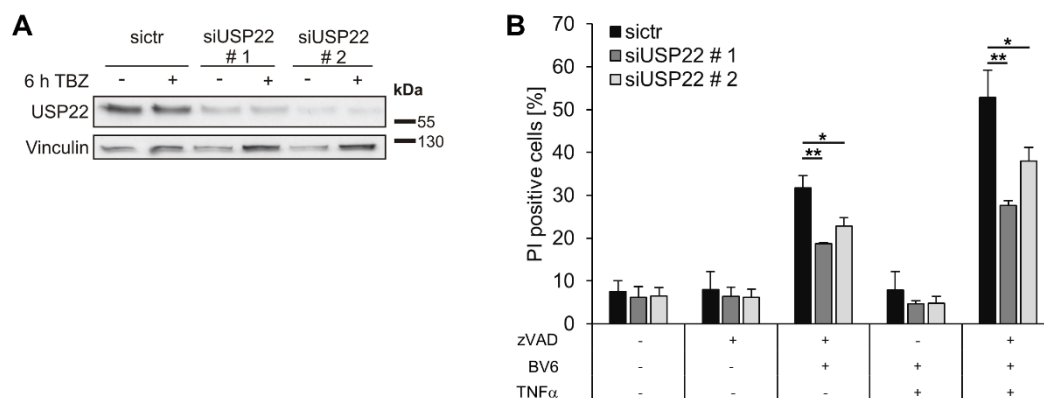


Figure 6 USP22 knockdown decreases TBZ-induced necroptotic cell death in HT-29 cells. A-B HT-29 cells were transfected with non-silencing control siRNA (sict) or siRNAs against USP22 (siUSP22) for 48 h at 20 nM. After transfection, cells were treated with 20 μ M zVAD.fmk, 0.5 μ M BV6 and 1 ng/ml TNF α either for 6 h and analyzed by Western blotting (A) or for 18 h, and the percentage of PI-positive cells was assessed by fluorescence-based PI staining (B). Vinculin served as a loading control. Both experiments were performed by Lisa Kowald. Data information: Data represent mean \pm SD; *P < 0.05; **P < 0.01, by unpaired 2 tailed Student's t-test. Three independent experiments performed in triplicate are shown.

To further substantiate our findings, we generated USP22 knockout (KO) HT-29 cells using CRISPR/Cas9 genome editing. Single clones were generated and isolated using limited dilution technique. Following Western blot analysis, single clones were selected based on USP22 expression levels: HT-29 clones with undetectable USP22 levels (clone # 1, # 2 and # 3), intermediate (clone # 4) or normal USP22 expression, compared to control CRISPR/Cas9 (clone # 5) and wildtype (WT) HT-29 cell lines (Fig. 7A and B). By choosing Clone # 5, we excluded possible side effects conveyed by CRISPR/Cas9 artifacts or puromycin resistance from our analysis. As anticipated, HT-29 cells subjected to CRISPR/Cas9 genome editing displayed Cas9 protein expression, whereas Cas9 was absent in WT parental HT-29, confirming successful genome editing (Fig. 7B). In line with previous publications, USP22 KO HT-29 cells exhibited increased levels of ubiquitinated histone H2B at K120, whereas total H2B levels remained mostly unchanged (Fig. 7B).

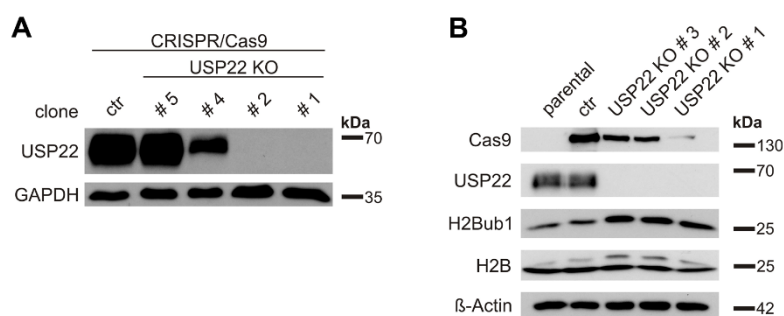


Figure 7 CRISPR/Cas9-mediated knockout (KO) of USP22 in HT-29 cells increases H2Bub1 levels. A HT-29 CRISPR/Cas9 control (ctr) and USP22 KO cells were analyzed by Western blotting for USP22 expression. GAPDH served as loading control. This experiment was performed by Rebekka Karlowitz. **B** Whole cell lysates of HT-29 parental, CRISPR/Cas9 control (ctr) and USP22 KO cells were analyzed by Western blotting for the indicated protein expression levels. β -Actin was used as a loading control.

Consistently with our siRNA experiments, HT-29 clones # 1, # 2 and # 3, lacking USP22 expression, displayed a significant reduction in TBZ-induced necroptotic cell death, compared to control CRISPR/Cas9 HT-29 cells after treatment (Fig. 8A-C). Interestingly, HT-29 clone # 4 cells with intermediate USP22 expression levels showed only a partial rescue upon TBZ-induced cell death, implying that USP22 expression quantitatively corresponds with the extend of necroptosis (Fig. 8A). At the same time, HT-29 clone # 5 cells, expressing near-normal USP22 expression levels, displayed the same extend of necroptotic cell death compared to WT HT-29 cells (Fig. 8C). This implicates that USP22 expression, and not CRISPR/Cas9 artifacts, clonal effects or the puromycin resistance, is the sole determinant for the delay in necroptotic cell death. To guarantee canonical necroptotic signaling in our system, mediated by the necroptotic core proteins RIPK1, RIPK3 and MLKL, we utilized several necroptosis inhibitors to block cell death. Independently of USP22 expression levels, TBZ-induced cell death could be rescued by inhibiting RIPK1 with necrostatin-1 (Nec1-s), RIPK3 with GSK'872 and Dabrafenib (Dab), or MLKL with necrosulfonamide (NSA) (Fig. 8A and C).

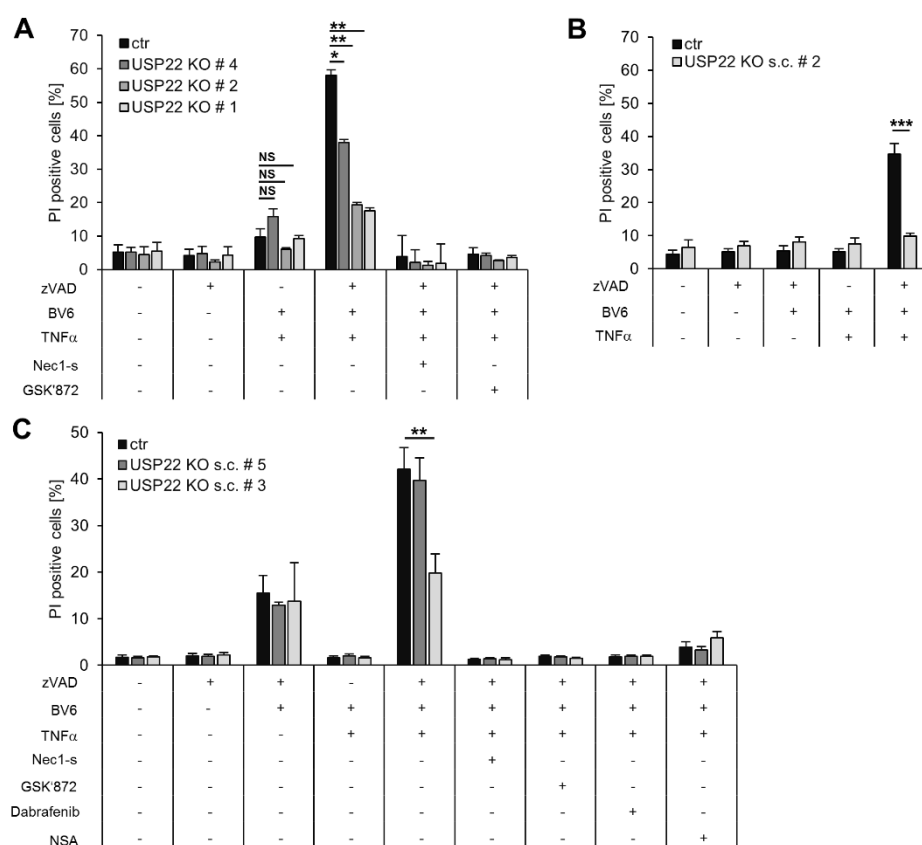


Figure 8 USP22 knockout (KO) decreases TBZ-induced necroptotic cell death in HT-29 cells. **A** HT-29 control and USP22 KO cells were treated with 20 μ M zVAD.fmk, 0.5 μ M BV6 and 1 ng/ml TNF α after pre-incubation with 30 μ M Nec1-s and 20 μ M GSK'872 for 1 h and incubated for 18 h before fluorescence-based quantification of PI-positive cells. **B** HT-29 control and USP22 KO cells were treated with 20 μ M zVAD.fmk, 0.5 μ M BV6 and 1 ng/ml TNF α for 6 h and cell death was determined by analysis of PI-positive nuclei. **C** HT-29 control and USP22 KO cells were stimulated with 20 μ M zVAD.fmk, 0.5 μ M BV6 and 1 ng/ml TNF α for 18 h. Cells were additionally treated with 30 μ M Nec1-s, 20 μ M GSK'872, 20 μ M Dab and 10 μ M NSA, as indicated. Cell death was determined by analysis

of PI-positive nuclei. Data information: Data represent mean \pm SD; *P < 0.05; **P < 0.01; ***P < 0.001, NS: not significant, by unpaired 2-tailed Student's t-test. Three independent experiments performed in triplicate are shown.

TNF α sensing by TNFR1 triggers complex-I formation and ultimately NF- κ B activation, inducing the expression of several pro-survival genes mediated by an interplay between TAK1, I κ B α and IKK β [137-139]. TBZ-induced necroptosis relies on TNFR1 activation by TNF α . In order to investigate the role of USP22 on TNF α -mediated NF- κ B activation, USP22 KO control HT-29 cells were stimulated with TNF α for 5 and 15 minutes, revealing no differences in I κ B α phosphorylation and degradation patterns between USP22 KO and control HT-29 cells, thereby ruling out USP22 mediated effects on TNFR1 activation or NF- κ B activation upstream of I κ B α (Fig. 9).

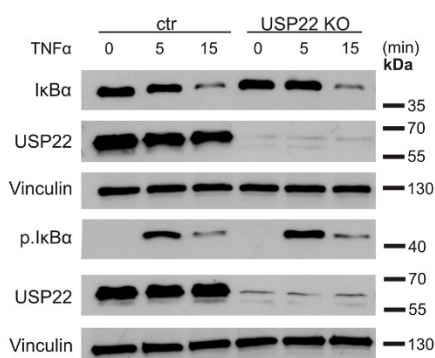


Figure 9 Loss of USP22 in HT-29 cells does not affect NF- κ B activation upstream of I κ B α . HT-29 control and USP22 KO cells were stimulated with 10 ng/ml TNF α for 5 and 15 minutes. Protein expression of I κ B α , phosphorylated I κ B α and USP22 were examined by Western blotting. Vinculin was used as a loading control.

Since USP22 expression has been shown in previous publications to increase apoptosis in some cancer cell lines, like the colorectal cell line HCT116 [97], we decided to investigate a potential effect of USP22 KO on apoptotic cell death. However, we could not detect differences in TB-induced extrinsic apoptotic cell death between USP22 KO and control HT-29 cells (Fig. 8A-C, Fig. 9A and B). We were unable to induce high levels of TB-induced apoptotic cell death in the HT-29 cells, which is however in line with preceding publications [331], demonstrating a resistance against TB-induced cell death in HT-29 cells.

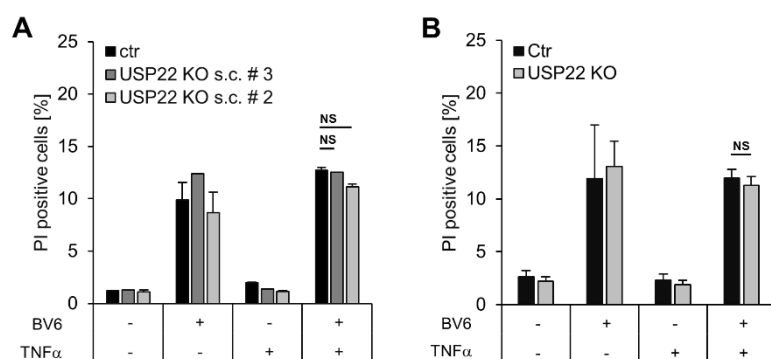


Figure 10 Loss of USP22 in HT-29 cells does not affect TB-induced apoptosis. A-B HT-29 CRISPR/Cas9 control (Ctr) and USP22 KO cells were treated for 48 h (A) or 72 h (B), as indicated, with 0.5 μ M BV6 and 1 ng/ml TNF α . Cell death was determined by analysis of PI-positive nuclei. Data information: Data represent mean \pm SD; NS: not significant, by unpaired 2-tailed Student's t-test. Three independent experiments are shown.

These findings suggest, that USP22 specifically regulates TBZ-induced necroptosis without affecting TNF α -dependent pro-survival response or TB-induced apoptotic cell death.

To consolidate our findings and confirm that loss of USP22 and not any off-target effects are responsible for the effects on necroptotic cell death, we argued that stable re-expression of USP22 in USP22 KO HT-29 cells should re-sensitize the cells for TBZ-induced necroptosis induction. The protospacer adjacent Motif (PAM) is an essential targeting component immediately following the Cas9 target DNA sequence, ensuring successfully binding to or cleavage of the target DNA sequence by Cas9 [332].

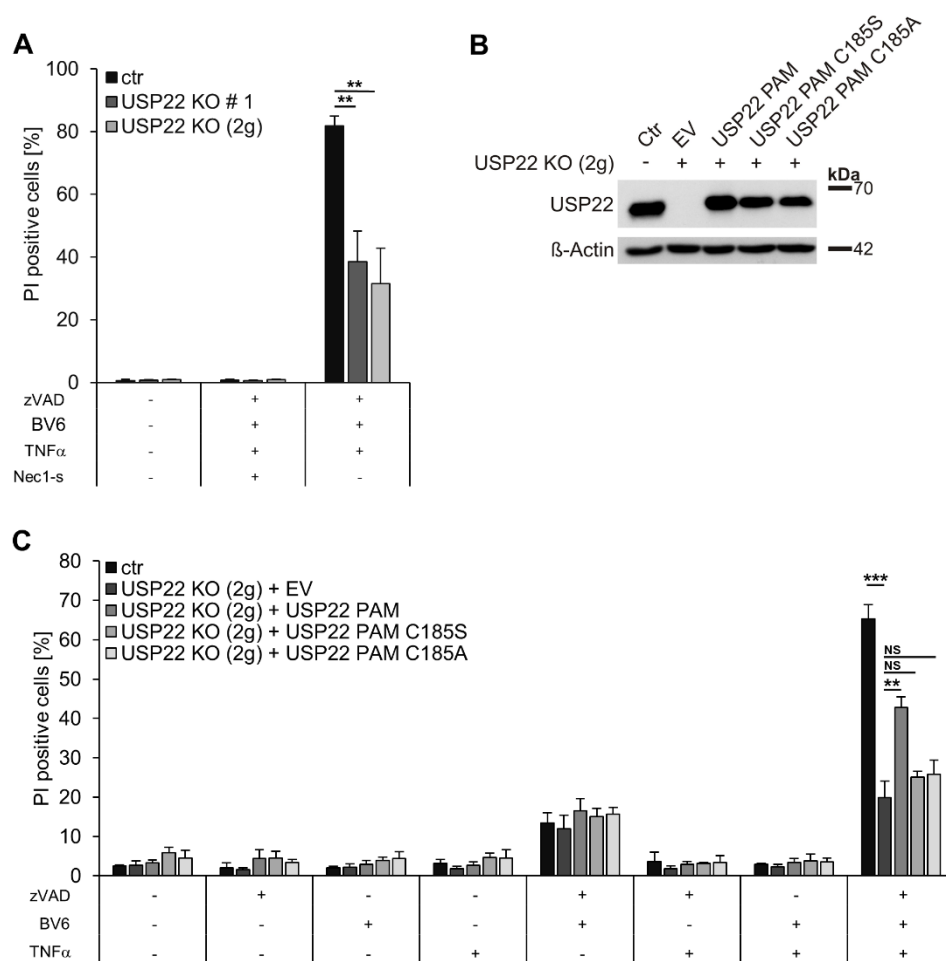


Figure 11 Stable reconstitution of USP22 in USP22 KO HT-29 cells re-sensitizes USP22 KO HT-29 cells for TBZ-induced necroptosis. A HT-29 control cells and USP22 KO cells, generated with three (USP22 KO #1) or with two (USP22 KO (2g)) USP22 gRNAs, were stimulated with 20 μ M zVAD.fmk, 0.5 μ M BV6, 1 ng/ml TNF α and 30 μ M Nec1-s for 18 h. The percentage of PI-positive cells was assessed by fluorescence-based PI staining. B HT-29 control and USP22 KO cells, generated with 2 guide RNAs (2g), expressing empty vector (EV) or PAM mutated 3xFLAG-HA-USP22 WT (USP22 PAM), C185S (USP22 PAM C185S) or C185A (USP22 PAM C185A) were analyzed by Western blotting for USP22 expression levels. β -Actin was used as a loading control. C HT-29 control and USP22 KO cells, generated with 2 guide RNAs (2g), expressing empty vector (EV) or PAM mutated 3xFLAG-HA-USP22 WT (USP22 PAM), C185S (USP22 PAM C185S) or C185A (USP22 PAM C185A) were stimulated with 20 μ M zVAD.fmk, 0.5 μ M BV6, 1 ng/ml TNF α for 18 h. The percentage of PI-positive cells was assessed by fluorescence-based PI staining. Data information: Data represent mean \pm SD; **P < 0.01; ***P < 0.001, NS: not significant, by unpaired 2 tailed Student's t-test. Three independent experiments performed in triplicate are shown.

For this purpose, PAM-mutated WT and catalytically inactive C185S or C185A USP22 mutants were stably re-expressed in USP22 KO HT-29 cells generated with two guide RNAs (2g). USP22 KO (2g) HT-29 cells showed the same necroptotic resistance as cells generated with three guide RNAs (Fig. 11A), thereby excluding potential differences between the different USP22 KO HT-29 cells. Stable re-expression of PAM-mutated WT and USP22 C185S/A in USP22 KO HT-29 cells restored USP22 expression (Fig. 11B, Fig. 12 A and B). As expected, only reconstitution with PAM-mutated WT USP22 and not with empty vector (EV), was able to re-sensitize USP22 KO (2g) HT-29 cells to TBZ-induced necroptotic cell death (Fig. 11C). Noteworthy, reconstitution of C185S or C185A USP22 into USP22 KO (2g) HT-29 cells could

not re-establish necroptosis sensitivity (Fig. 11C), suggesting that the catalytic DUB activity of USP22 is vital for TBZ-induced necroptosis.

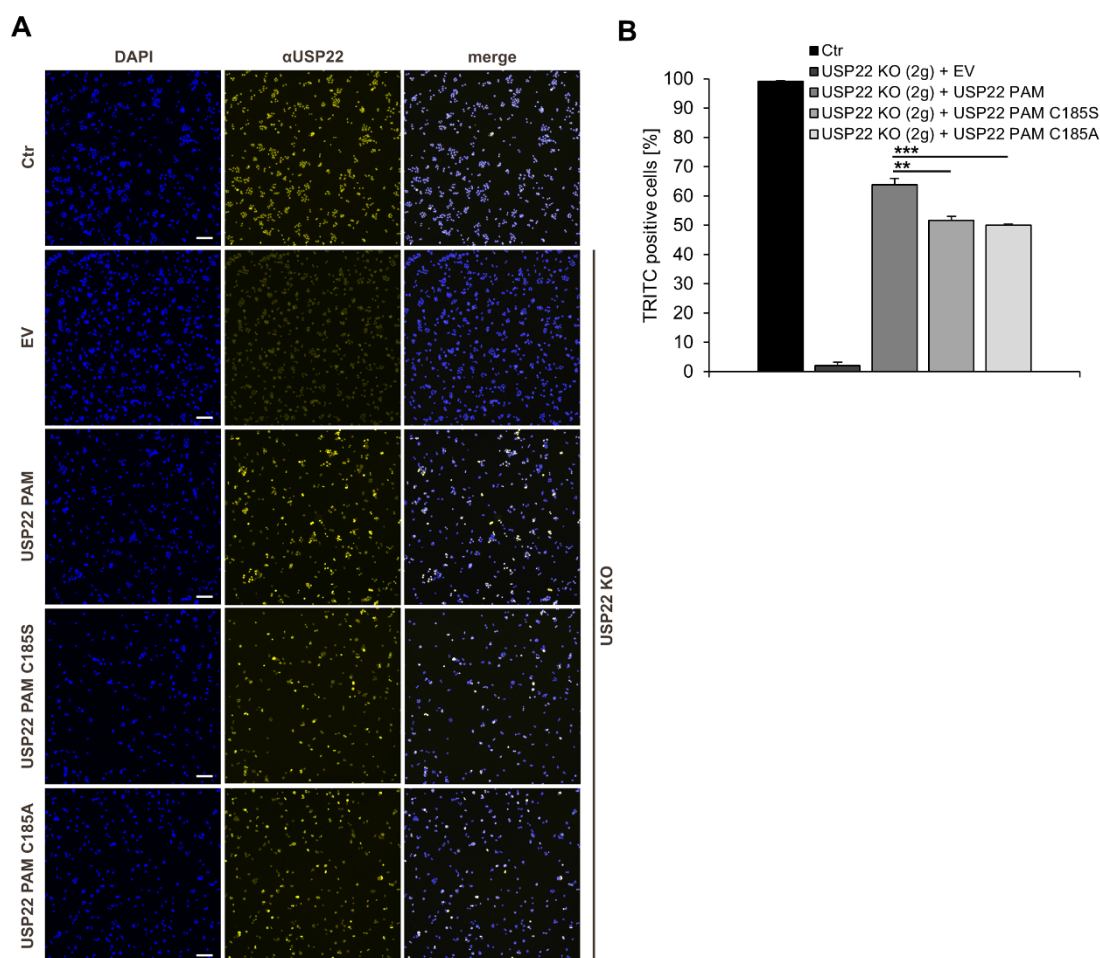


Figure 12 HT-29 USP22 KO (2g) cells display a comparable number of cells re-expressing USP22 PAM, USP22 PAM C185S or USP22 PAM C185A. **A** USP22 expression was quantified using anti-USP22 immunofluorescence staining in HT-29 CRISPR/Cas9 control (Ctr) cells and in USP22 KO cells re-expressing empty vector (EV), FLAG-HA-USP22 PAM (USP22 PAM) or the corresponding mutants C185S and C185A. Scale bar represents 100 μ m. **B** Quantification of the percentage of TRITC-positive HT-29 cells after anti-USP22 immunofluorescence staining. Data information: Data represent mean \pm SD; ***P < 0.001; **P < 0.01, by unpaired 2-tailed Student's t-test. Three independent experiments are shown.

We further substantiated our findings by extending our set of cancer cells with the human acute lymphoblastic leukemia (ALL) Jurkat cell line. CRISPR/Cas9-mediated USP22 depletion in Jurkat cells prominently reduced TBZ-induced necroptosis, compared to CRISPR/Cas9 control Jurkat cells (Fig. 13A-C). At the same time, USP22 KO and control Jurkat ALL displayed equal amounts of TB-induced apoptotic cell death, which is in line with the previously observed effects of USP22 depletion in the HT-29 cells (Fig. 13A and C).

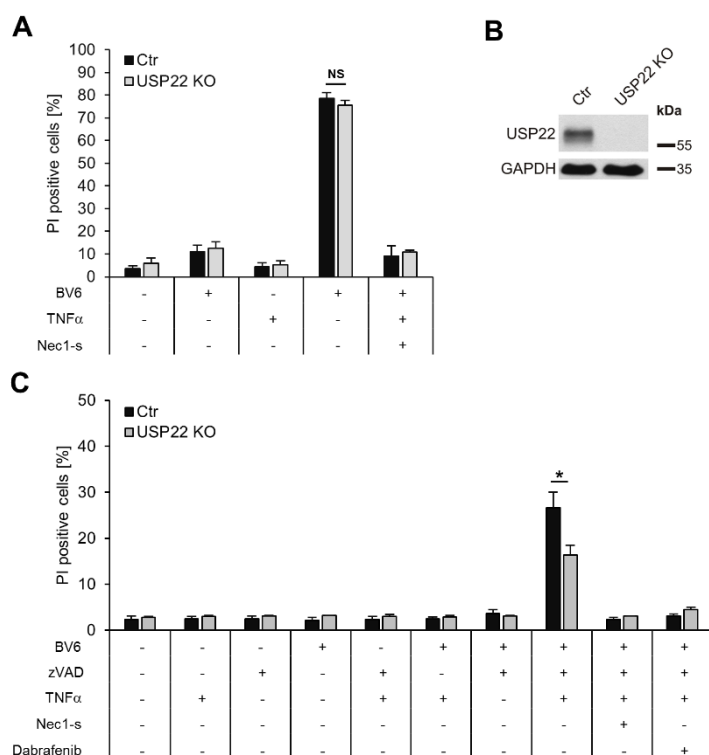


Figure 13 USP22 KO reduces TBZ-induced necroptotic cell death in acute lymphoblastic leukemia (ALL) Jurkat cells. **A** Jurkat CRISPR/Cas9 control (Ctr) control and USP22 KO cells were analyzed for USP22 expression by Western blotting. β -Actin served as loading control. **B** Jurkat control and USP22 KO cells were pre-treated with 10 μ M Nec1-s before stimulation with 1 μ M BV6 and 10 ng/ml TNF α . Cell death was measured after 18 h by analysis of PI-positive nuclei. This experiment was performed by Rebekka Karlowitz. **C** Jurkat control and USP22 KO cells were pre-treated with 10 μ M Nec1-s or 20 μ M Dabrafenib before stimulation with 1 μ M BV6 and 10 ng/ml TNF α for 8 h. Cell death was determined by analysis of PI-positive nuclei. This experiment was performed by Rebekka Karlowitz. Data information: Data represent mean \pm SD; *P < 0.05; NS: not significant, by unpaired 2-tailed Student's t-test. Three independent experiments performed in triplicate are shown.

Additionally, we examined acute promyelocytic leukemia (APL) NB4 cells for potential TBZ-induced differences in apoptotic cell death between upon CRISPR/Cas9-mediated USP22 depletion. Similar to HT-29 and Jurkat ALL cells, no differences in the amount of TBZ-induced apoptotic cell death could be detected between USP22 KO and control APL NB4 cells (Fig. 14A and B).

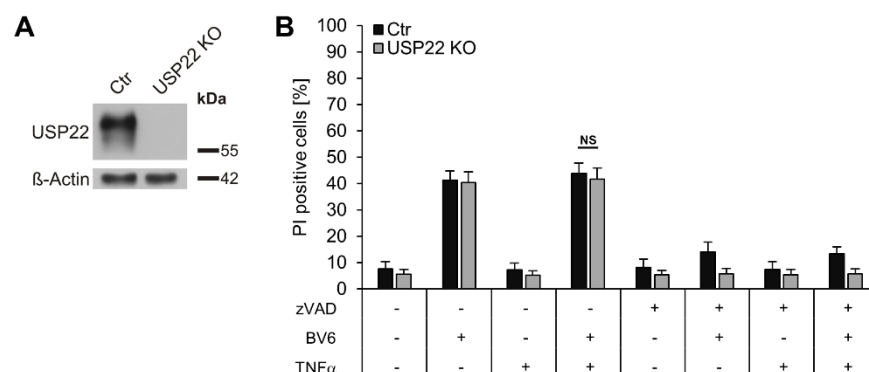


Figure 14 CRISPR/Cas9-mediated knockout of USP22 in NB4 cells does not affect TB-induced apoptotic cell death. **A** NB4 CRISPR/Cas9 control (Ctr) and USP22 KO cells were analyzed for USP22 expression by Western blotting. β -Actin served as loading control. **B** NB4 control and USP22 KO cells were stimulated with 20 μ M zVAD.fmk, 1 μ M BV6 and 10 ng/ml TNF α . Cell death was measured after 48 h by analysis of PI-positive nuclei.

Both experiments were performed by Lisa Kowald. Data information: Data represent mean \pm SD; NS: not significant, by unpaired 2-tailed Student's t-test. Three independent experiments are shown.

In order to investigate if the regulatory role of USP22 is conserved among murine cancer cell lines, we employed siRNA- or CRISPR/Cas9-mediated knockdown or KO of USP22 in mouse embryonic fibroblasts (MEFs) or the macrophage lines Raw264.7 or J774A1, which both are commonly used to investigate necroptotic signaling [333-335]. Though, the analysis of the amount of TB- or TBZ-induced apoptotic or necroptotic cell death, confirmed by utilizing Nec1s, Dabrafenib or GSK'872 as specific inhibitors, revealed no differences between USP22 KO and control cells (Fig. 15A-F).

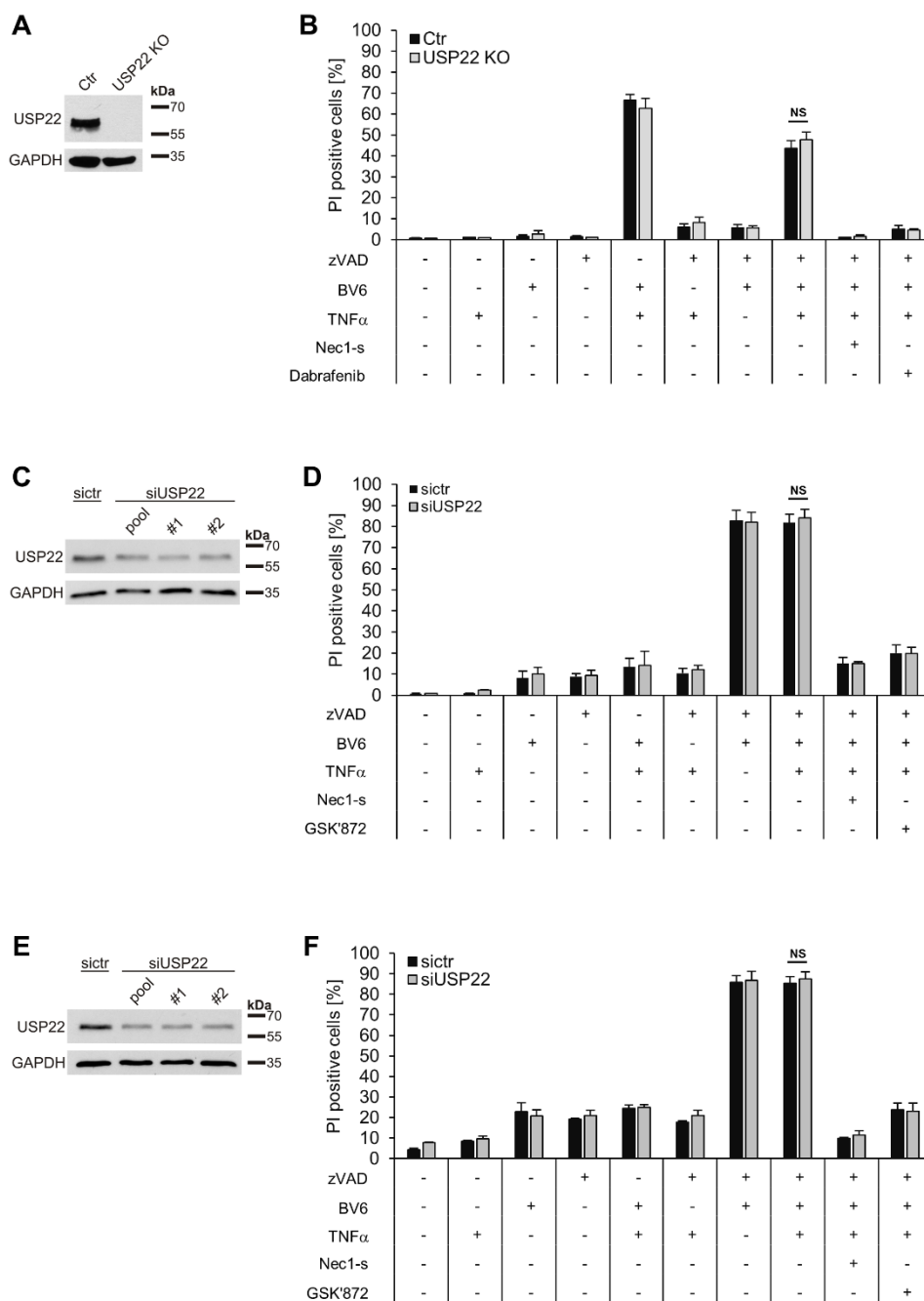


Figure 15 CRISPR/Cas9-mediated knockout of USP22 does not alter TBZ-induced cell death in MEF cells and the macrophage cell lines Raw264.7 or J774A.1. **A** MEF CRISPR/Cas9 control (Ctr) and USP22 KO cells

were analyzed by Western blotting for USP22 expression. GAPDH served as loading control. **B** MEF control and USP22 KO cells were pre-treated with 10 μ M Nec1-s and 20 μ M Dabrafenib for 1 h. Cells were stimulated with 20 μ M zVAD, 5 μ M BV6 and 10 ng/ml TNF α for 24h. Cell death was determined by analysis of PI-positive nuclei. **C** Raw264.7 CRISPR/Cas9 control (Ctr) and USP22 KO cells were transfected with non-silencing control siRNA (sictr) or siRNAs against USP22 (siUSP22) for 48 h at 20 nM. USP22 expression was monitored by Western blotting. GAPDH served as loading control. **D** Raw264.7 control and USP22 KO cells were transfected with non-silencing control siRNA (sictr) or pooled siRNAs against USP22 (siUSP22) for 48 h at 20 nM. Cells were pre-treated with 10 μ M Nec1-s and 20 μ M GSK'872 for 1 h before being stimulated with 20 μ M zVAD, 5 μ M BV6 and 10 ng/ml TNF α for 24h. The percentage of PI-positive cells was assessed by fluorescence-based PI staining. **E** J774A.1 CRISPR/Cas9 control (Ctr) and USP22 KO cells were transfected with non-silencing control siRNA (sictr) or siRNAs against USP22 (siUSP22) for 48 h at 20 nM. USP22 expression was monitored by Western blotting. GAPDH served as loading control. **F** J774A.1 control and USP22 KO cells were transfected with non-silencing control siRNA (sictr) or pooled siRNAs against USP22 (siUSP22) for 48 h at 20 nM. Cells were pre-treated with 10 μ M Nec1-s and 20 μ M GSK'872 for 1 h prior to stimulation with 20 μ M zVAD, 5 μ M BV6 and 10 ng/ml TNF α for 24h. The percentage of PI-positive cells was assessed by fluorescence-based PI staining. Data information: Data represent mean \pm SD; NS: not significant, by unpaired 2-tailed Student's t-test. Three independent experiments are shown.

Necroptosis can be initiated by various stimuli, including TNF α , FasL and TRAIL, triggering respective death receptor ligation and subsequent RIPK1-RIPK3 mediated necrosome formation [182-186]. In order to investigate, whether the functional role of USP22 in necroptosis is indeed a broader necroptotic mechanism and not specific for TNFR1 mediated necroptosis, we subjected USP22 KO and control HT-29 cells to FasL(BZ)- and TRAIL(BZ)-induced necroptosis. Remarkably, USP22 KO HT-29 cells displayed a significant reduction in TRAIL(BZ)- and FasL(BZ)-induced necroptotic cell death, compared to control CRISPR/Cas9 HT-29 cells, whereas the effect was more pronounced in TRAIL(BZ)-treated HT-29 cells (Fig. 16A-D).

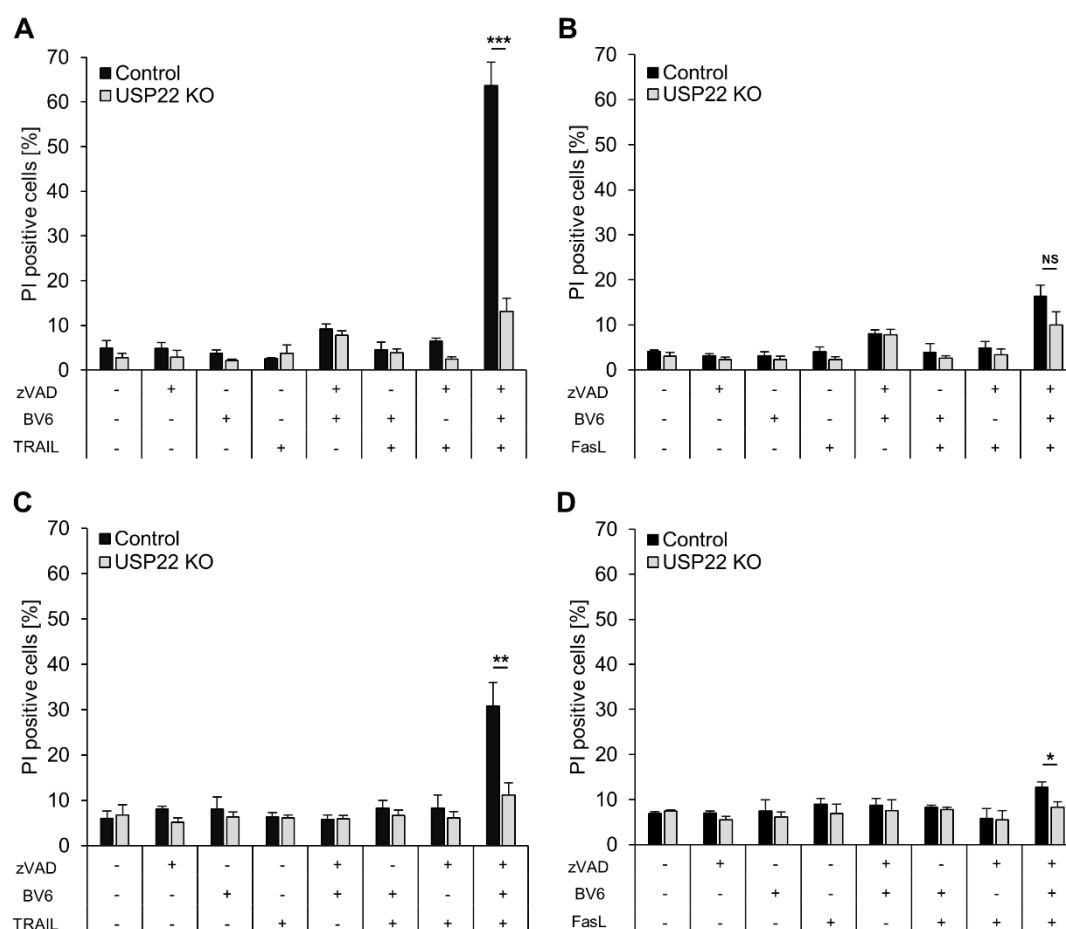


Figure 16 USP22 KO reduces TRAIL(BZ)-and FasL(BZ)-induced necroptotic cell death in HT-29 cells. A-D HT-29 control and USP22 KO cells were treated with 20 μ M zVAD.fmk, 0.5 μ M BV6 and 20 ng/ml TRAIL (A and C) or 200 ng/ml FasL (B and D) and incubated for 18 h (A-B) or 6 h (C-D) before fluorescence-based quantification of PI-positive cells. Data information: Data represent mean \pm SD; *P < 0.05; **P < 0.01; ***P < 0.001; NS: not significant, by unpaired 2-tailed Student's t-test. Three independent experiments performed in triplicate are shown.

Taken together these experiments suggest, that USP22 specifically regulates necroptosis in human tumor cell lines and most likely not in murine tumor cells. Furthermore, the observed regulatory role of USP22 in human tumor cells seems to be dependent on the active DUB function of USP22.

In order to dissect how USP22 regulates necroptosis, the expression and phosphorylation levels of the necroptotic core machinery, RIPK1, RIPK3 and MLKL, was monitored in USP22 KO and control HT-29 cells upon TBZ exposure in a time-dependent manner. As anticipated, USP22-dependent differences in MLKL and RIPK1 phosphorylation appeared after two to three hours of prolonged TBZ treatment (Fig. 17A). Importantly, USP22 KO HT-29 cells displayed a prominent 'smear' of slower-migrating RIPK3 bands, almost absent in the control HT-29 cells, which was maintained over the whole experimental time-frame. RIPK3 is massively modified with various types of PTMs, such as ubiquitination and phosphorylation during necroptosis progression [62, 188, 189]. To confirm, that indeed USP22 depletion alters

levels of phosphorylated RIPK3 during TBZ-induced necroptosis, we utilized two phospho-RIPK3-specific antibodies (recognizing RIPK3 S227 phosphorylation), both demonstrating increased levels of phosphorylated RIPK3 in the USP22 KO condition (Fig. 17B).

In order to confirm increased levels of phosphorylated RIPK3 in USP22 KO HT-29 cells upon TBZ-induced necroptosis progression, we subjected cell lysates of TBZ-treated control and USP22 KO HT-29 cells to λ -phosphatase treatment. Indeed, λ -phosphatase treatment almost completely reduced the TBZ-induced slower-migrating RIPK3 in the USP22 KO HT-29 cells (Fig. 17C). Notably, high molecular weight RIPK3 signals were shown to be increased in USP22 KO HT-29 cells as shown by densitometric quantification of high-molecular weight RIPK3 smears, normalized to total RIPK3 and β -Actin levels. (Fig. 17C). As anticipated, utilizing the necroptosis inhibitors Nec1-s and Dab almost completely blocked slower-migrating RIPK3 bands in both the control and USP22 KO HT-29 cells, suggesting various types of necroptosis-induced PTMs. Together, these findings indicate that USP22 specifically regulates TBZ-induced necroptosis, affecting post-translational modifications of the necroptotic key player RIPK3.

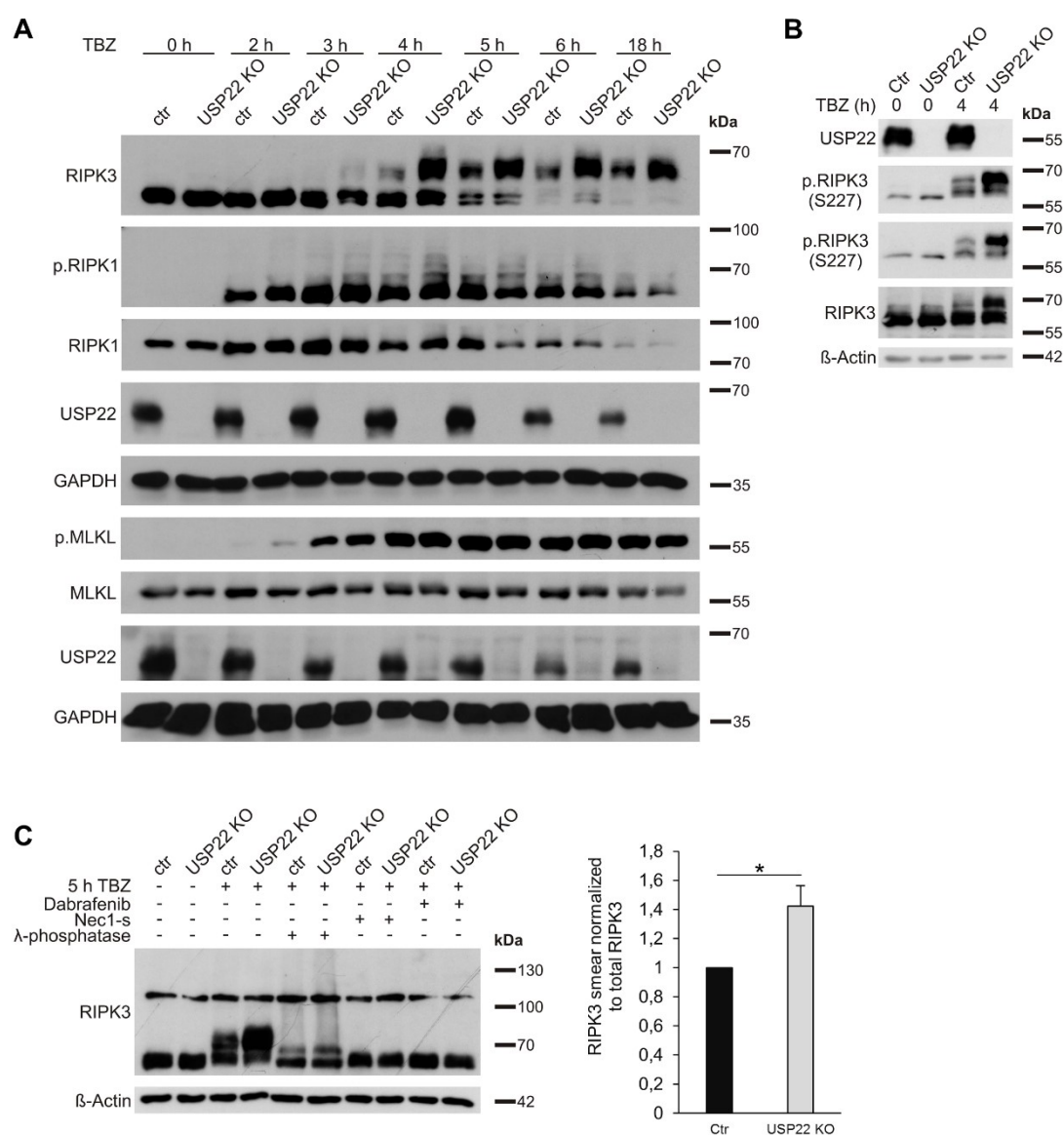


Figure 17 USP22 KO leads to increased TBZ-induced RIPK3 phosphorylation in HT-29 cells. **A** HT-29 control and USP22 KO cells were stimulated with 20 μ M zVAD.fmk, 0.5 μ M BV6 and 1 ng/ml TNF α for the indicated time points. Detection of indicated proteins was carried out by Western blotting. GAPDH served as a loading control. **B** HT-29 control and USP22 KO cells were stimulated with 20 μ M zVAD.fmk, 0.5 μ M BV6 and 1 ng/ml TNF α for 4 h. Detection of indicated proteins was carried out by Western blotting. β -Actin served as a loading control. **C** HT-29 control and USP22 KO cells were incubated with 30 μ M Nec1-s or 20 μ M Dab for 18 h, as indicated. Cells were stimulated with 20 μ M zVAD.fmk, 0.5 μ M BV6 and 1 ng/ml TNF α for 5 h. 100 μ g of each lysate were incubated with 400 U/ μ l λ -phosphatase for 30 min at 30 $^{\circ}$ C. Protein expression of RIPK3 was monitored by Western blotting. β -Actin was used as a loading control. High molecular weight RIPK3 'smears' were quantified after λ -phosphatase treatment and normalized to total RIPK3 and β -Actin levels. Data information: Data represent mean \pm SD; *P < 0.05; by unpaired 2-tailed Student's t-test. Three independent experiments performed in triplicate are shown. In panel C, quantification of blots from three independent experiments is shown.

5.1.2 Loss of USP22 induces resistance to necroptotic cell death in RIPK3-expressing HeLa cells

HeLa TRex cells lack endogenous RIPK3 expression and are therefore resistant to TBZ-induced necroptosis. In order to further understand the functional roles of USP22 during TBZ-induced necroptosis and on the necroptosis-induced post-translational modification of RIPK3, HeLa TRex cells were modified to express doxycycline (Dox)-inducible RIPK3, rendering them vulnerable to necroptosis induction (Fig. 18A). Moreover, we generated HeLa TRex RIPK3 USP22 KO cells by applying CRISPR/Cas9 technology (Fig. 18A). Upon Dox induction, control and USP22 KO HeLa TRex RIPK3 cells express largely comparable RIPK3-expression patterns, implying a most likely redundant role for USP22 in regulating basal RIPK3 protein stability (Fig. 18A).

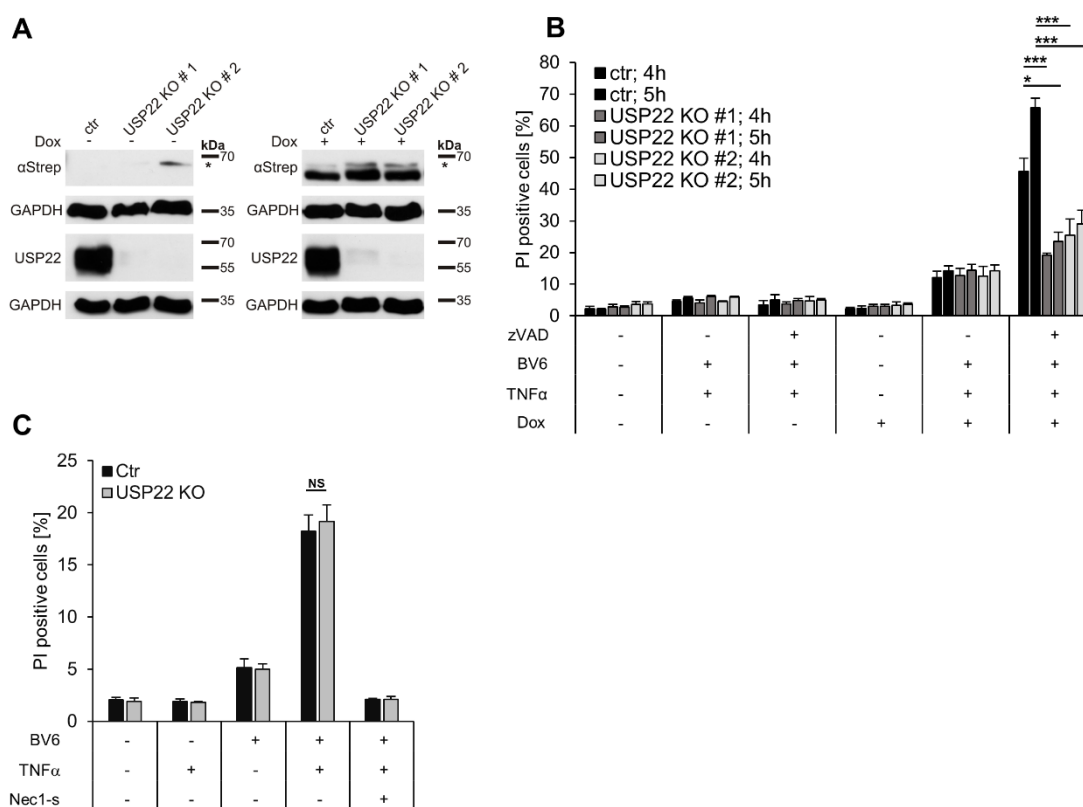


Figure 18 USP22 knockdown in RIPK3-expressing HeLa cells induces resistance to TBZ-induced necroptotic cell death. **A** HeLa TRex RIPK3 CRISPR/Cas9 control (ctr) and USP22 KO cells were treated with 1 μ g/ml Dox overnight. Protein expression of induced Strep-RIPK3 was analyzed by Western blotting. GAPDH served as loading control. The asterisk marks an unspecific band. **B** HeLa TRex RIPK3 control and USP22 KO cells were incubated with 1 μ g/ml Dox for 18 h before pre-treatment with 20 μ M zVAD.fmk, 5 μ M BV6 for 1 h. After pre-treatment, 10 ng/ml TNF α was added and cell death was measured after 4 and 5 h by analysis of PI-positive nuclei. **C** HeLa TRex RIPK3 CRISPR/Cas9 control (Ctr) and USP22 KO cells were treated with 5 μ M BV6 and 10 ng/ml TNF α for 24h. Cell death was determined by analysis of PI-positive nuclei. Data information: Data represent mean \pm SD; *P < 0.05; ***P < 0.001; NS: not significant, by unpaired 2-tailed Student's t-test. Three independent experiments performed in triplicate are shown.

Following Dox-inducible RIPK3-expression, TBZ treatment substantially increased cell death in control and USP22 KO HeLa TRex RIPK3 cells. At the same time, USP22 KO HeLa TRex RIPK3 cells displayed significantly less TBZ-induced necroptotic cell death compared to control HeLa TRex RIPK3 cells (Fig. 18B), indicating a functional role for USP22 in controlling necroptotic cell death in necroptosis-sensitive HeLa cells, akin to its role in HT-29 cells. In line with previous experiment in HT-29 cells, control and USP22 KO HeLa TRex cells displayed the same amount of TB-induced apoptotic cell death (Fig. 18B and C).

Additionally, and congruent to preceding experiments in Jurkat, NB4 and HT-29 cells, USP22 depletion did not affect the formation of the apoptotic signaling complex-II, as shown through Caspase-8 immunoprecipitations from control and USP22 KO HeLa TRex cells upon TB-treatment (Fig. 19A). Of interest, TNF α -induced complex-I formation remained unaffected due to USP22 depletion as demonstrated by TNFR1 immunoprecipitations from control and USP22 KO HeLa TRex cells stimulated with TNF α (Fig.19B). Both experiments correspond to the previously conducted experiments in HT-29, NB4 and Jurkat cells, demonstrating a lack of function for USP22 in TNF α -induced NF- κ B signaling and TB-induced apoptotic cell death.

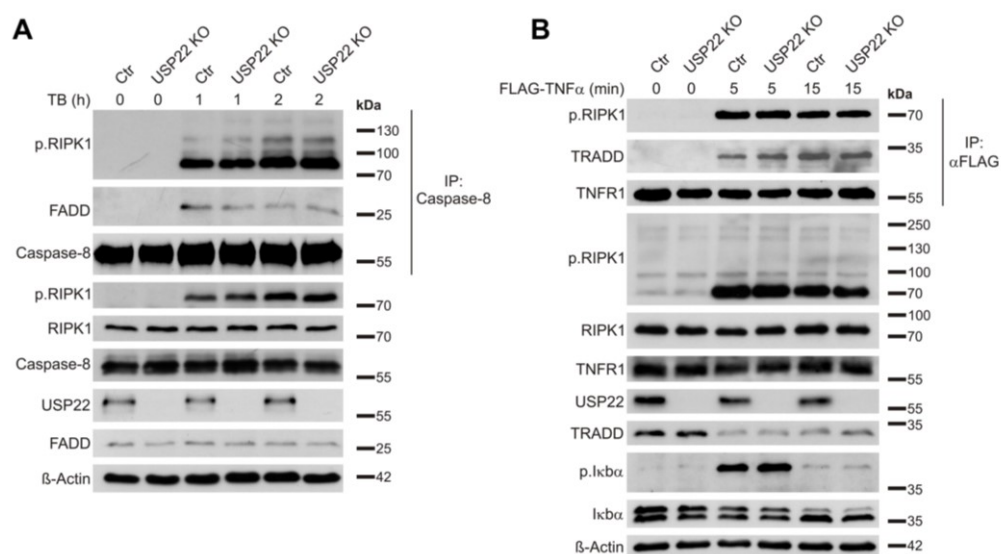


Figure 19 USP22 KO in HeLa TRex RIPK3 does not affect complex-I or -II formation. **A** HeLa TRex RIPK3 CRISPR/Cas9 control (Ctr) and USP22 KO cells were pre-treated with 5 μ M BV6 for 1 h before being stimulated with 10 ng/ml TNF α for 1 and 2 h, after which caspase-8 was immunoprecipitated, followed by analysis by Western blotting with the indicated antibodies. β -Actin served as loading control. **B** HeLa TRex RIPK3 CRISPR/Cas9 control (Ctr) and USP22 KO cells were starved in serum-free DMEM for 2 h. Cells were stimulated with 1 μ g/ml FLAG-hTNF for 5 and 15 minutes as indicated in the Methods section. FLAG-hTNF was immunoprecipitated and analyzed by Western blotting with the indicated antibodies. β -Actin served as loading control.

In order to investigate whether USP22 depletion affects necroptotic signaling in HeLa TRex cells, control and USP22 KO HeLa TRex RIPK3 cells, with and without Dox-induced RIPK3 expression, were monitored for RIPK1, RIPK3 and MLKL expression and phosphorylation status upon TBZ-induced necroptosis. As expected, upon TBZ treatment and in the absence of Dox, RIPK3 expression as well as MLKL phosphorylation were both absent, whereas RIPK1 gets phosphorylated (Fig. 20A, left). Remarkably, and similar to USP22 KO HT-29 cells,

slower-migrating RIPK3 bands were detected in a TBZ-, time-, and USP22-dependent manner upon Dox-induced RIPK3 expression (Fig. 20A, right). Moreover, slower-migrating RIPK3 species were more pronounced and occurred earlier in USP22 depleted HeLa TRex RIPK3 cells compared to control cells, expressing normal USP22 levels (Fig. 20A, right). At the same time, slight alterations in RIPK1 phosphorylation could be detected in USP22 KO HeLa TRex cells following TBZ-induced necroptosis (Fig. 20A, right). Strikingly, USP22 depletion reduced the levels of phosphorylated MLKL under necroptotic conditions in a RIPK3-dependent way. The extend of MLKL phosphorylation was quantified and normalized to β -Actin levels and to the 0 h time point of HeLa TRex CRISPR/Cas9 control cells. By doing so, a prominent, USP22-dependent decrease in phosphorylated MLKL levels could be observed among three biological independent experiments, which further increases with progression of necroptosis, corresponding to the decrease in cell death (Fig. 20A and Fig. 20B).

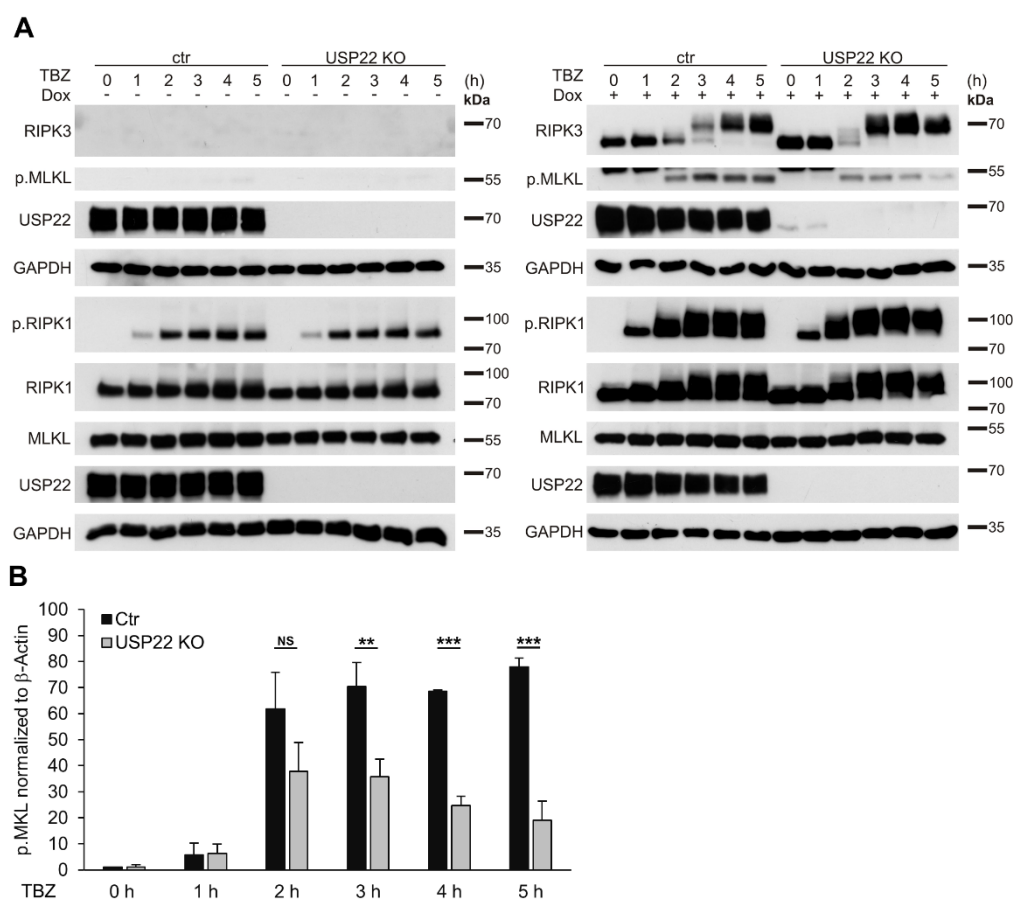


Figure 20 USP22 KO leads to increased TBZ-induced RIPK3 phosphorylation in HT-29 cells. **A** HeLa TRex RIPK3 control and USP22 KO cells were pre-treated with 20 μ M zVAD.fmk, 5 μ M BV6 for 1 h. After pre-treatment, 10 ng/ml TNF α were added for 1, 2, 3, 4 and 5 h. Protein expression of phosphorylated RIPK1, total RIPK1, total RIPK3, phosphorylated MLKL, total MLKL and USP22, without (left) or with (right) 1 μ g/ml Dox treatment overnight, was monitored by Western blotting. GAPDH was used as a loading control. **B** RIPK3 expression in HeLa TRex CRISPR/Cas9 control and USP22 KO cells was induced by Dox treatment. For quantification, phosphorylated MLKL levels of both cell lines were first normalized to β -Actin levels followed by normalization to the 0 h time point of HeLa TRex CRISPR/Cas9 control cells. Data information: Data represent mean \pm SD; **P < 0.01; ***P < 0.001; NS: not significant, by unpaired 2-tailed Student's t-test. Three independent experiments performed in triplicate are shown. In panel D, quantification of blots from three independent experiments.

Finally, we sought to prove the interaction between USP22 and RIPK3 by performing reciprocal immunoprecipitation experiments. Endogenous USP22 could be co-immunoprecipitated with RIPK3 from RIPK3 KO HT-29 cells re-expressing Dox-inducible Strep-tagged RIPK3 WT, independently of TBZ stimulation (Fig. 21A), phosphorylated MLKL could only be co-immunoprecipitated upon TBZ-induced necroptosis. On the other hand, endogenous RIPK3 could be co-immunoprecipitated with USP22 from USP22 KO HT-29 (2g) cells, re-expressing 3xFLAG-HA-tagged USP22 PAM, independently of TBZ-induced necroptosis (Fig. 21B).

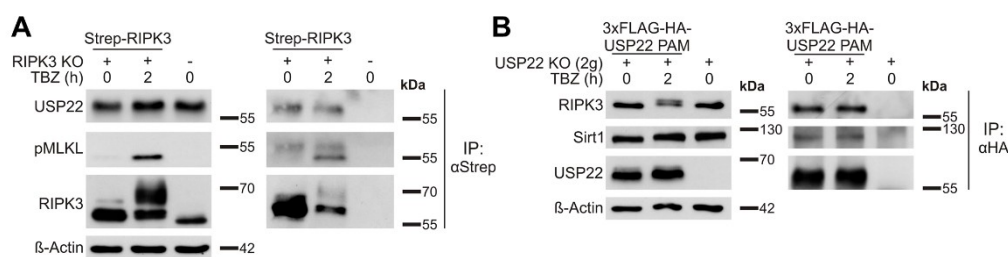


Figure 21 USP22 interacts with RIPK3 independently of TBT treatment. **A** HT-29 RIPK3 KO cells and RIPK3 KO cells re-expressing PAM-mutated Dox-inducible RIPK3 WT were incubated overnight with 1 μ M Dox. Cells were pre-treated with 20 μ M zVAD.fmk, 5 μ M BV6 for 1 h. After pre-treatment, 10 ng/ml TNF α were added for 2 h, as indicated. Strep-RIPK3 was immunoprecipitated using anti Strep-beads and the indicated co-immunoprecipitated proteins were analyzed by Western blotting. β -Actin served as a loading control. **B** USP22 KO HT-29 cells and USP22 KO cells re-expressing PAM-mutated 3xFLAG-HA-USP22 were pre-treated with 20 μ M zVAD.fmk, 5 μ M BV6 for 1 h. After pre-treatment, 10 ng/ml TNF α was added for 2 h, as indicated. 3xFLAG-HA-USP22 was immunoprecipitated using anti-HA-beads and the indicated co-immunoprecipitated proteins were analyzed by Western blotting. β -Actin served as a loading control.

Conclusively, USP22 specifically regulates TBZ-induced necroptosis as well as RIPK3 phosphorylation levels in RIPK3-expressing HeLa cells, corresponding to its previously observed role in HT-29 cells. Furthermore, USP22-RIPK3 interactions could be identified, independently of TBZ treatment.

5.1.3 USP22 controls RIPK3 ubiquitination during necroptosis induction

Necroptosis is regulated by various PTMs, such as ubiquitination, ensuring fine-tuning of necroptotic cell death [228, 330, 336]. Especially RIPK3 is targeted by various E3 ligases and DUBs at different necroptotic signaling check points, dynamically balancing its ubiquitination status [62, 238, 239]. At the same time, USP22 regulates multiple signaling pathways by deubiquitination [59, 91, 92, 337, 338]. In order to investigate whether USP22 is involved in regulating RIPK3 ubiquitination, HT-29 control, USP22 KO and USP22 KO cells re-expressing PAM-mutated WT or C185S USP22, were exposed to TBZ treatment, followed by enrichment of ubiquitinated proteins using Tandem Ubiquitin Binding Entities (TUBE) pull-downs. USP22 KO HT-29 cells and USP22 KO HT-29 cells re-expressing USP22 C185S displayed a profound increase in ubiquitinated RIPK3 upon TBZ-induced necroptosis when compared to control and WT USP22 re-expressing HT-29 cells (Fig. 22A).

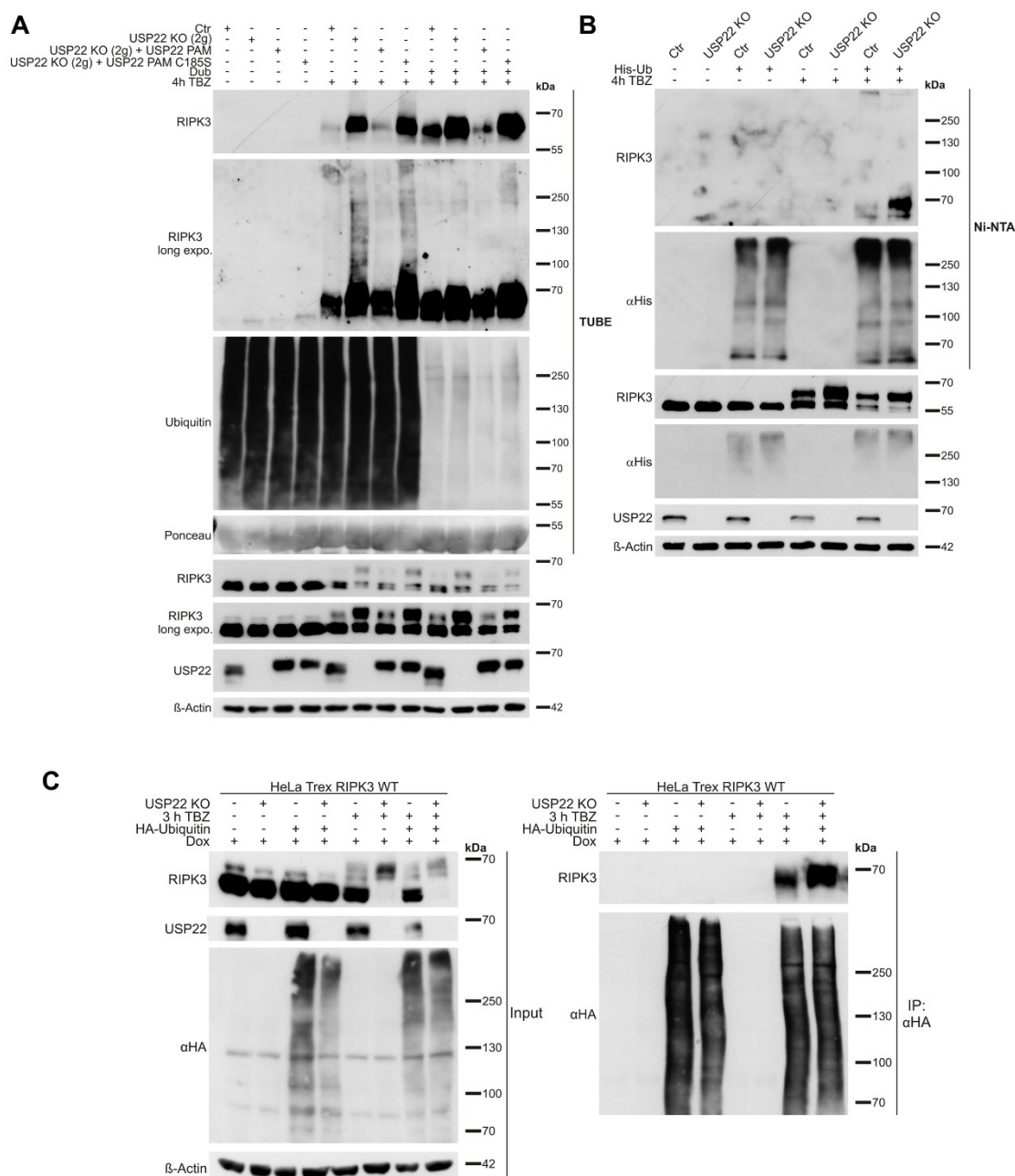


Figure 22 Increased RIPK3 ubiquitination in USP22 KO HT-29 cells during TBZ-induced necroptosis. A HT-29 control, USP22 KO and USP22 KO cells re-expressing PAM-mutated 3xFLAG-HA-USP22 WT or C185S were stimulated with 20 μ M zVAD.fmk, 0.5 μ M BV6 and 1 ng/ml TNF α for 4 h. Poly-ubiquitinated proteins were enriched by GST-TUBE pull-down, followed by incubation with the catalytic domain of USP2, as indicated. RIPK3 and USP22 expression and levels of ubiquitinated RIPK3 were monitored using Western blotting with the indicated antibodies. β -Actin served as loading control. Ponceau-staining was used to confirm equal loading of GST-TUBE. **B** HT-29 control and USP22 KO cells were transfected with His-ubiquitin for 24 h, as indicated. Cells were pre-stimulated with 20 μ M zVAD.fmk, 0.5 μ M BV6 for 1 h. Following pre-treatment, 1 ng/ml TNF α was added for 4 h. His-ubiquitin was immunoprecipitated using Ni-NTA beads and detection of indicated proteins was performed by Western blotting. β -Actin served as loading control for the input, whereas His-ubiquitin levels served as loading control for immunoprecipitated ubiquitin. **C** HeLa TRex RIPK3 control and USP22 KO cells were incubated with 1 μ g/ml Dox and transfected with HA-ubiquitin for 24 h, as indicated. Cells were pre-stimulated with 20 μ M zVAD.fmk, 5 μ M BV6 for 1 h. Following pre-treatment, 10 ng/ml TNF α were added for 3 h. HA-ubiquitin was immunoprecipitated using anti-HA-beads and detection of indicated proteins was performed by Western blotting. β -Actin served as loading control for the input, whereas HA-levels served as loading control for immunoprecipitated ubiquitin.

TUBE-enriched ubiquitin fractions were incubated with a recombinant human protein, encompassing the catalytic domain of ubiquitin-specific peptidase 2 (USP2), a non-specific

DUB [339], reducing the levels of poly-ubiquitinated RIPK3 and thereby confirming direct ubiquitin modification of RIPK3 in our TUBE-system (Fig. 22A). Interestingly, re-expression of the catalytic inactive USP22 mutant C185S into the USP22 KO background was unable to rescue increased levels of TBZ-induced phosphorylation of RIPK3 (Fig. 22A). On the other hand, re-expression of WT USP22 into USP22 depleted HT-29 cells reduced necroptosis-induced RIPK3 phosphorylation (Fig. 22A). Notably, ubiquitinated RIPK1 levels remained mostly unaffected by USP22 depletion and TBZ-induced necroptosis (Fig. 23).

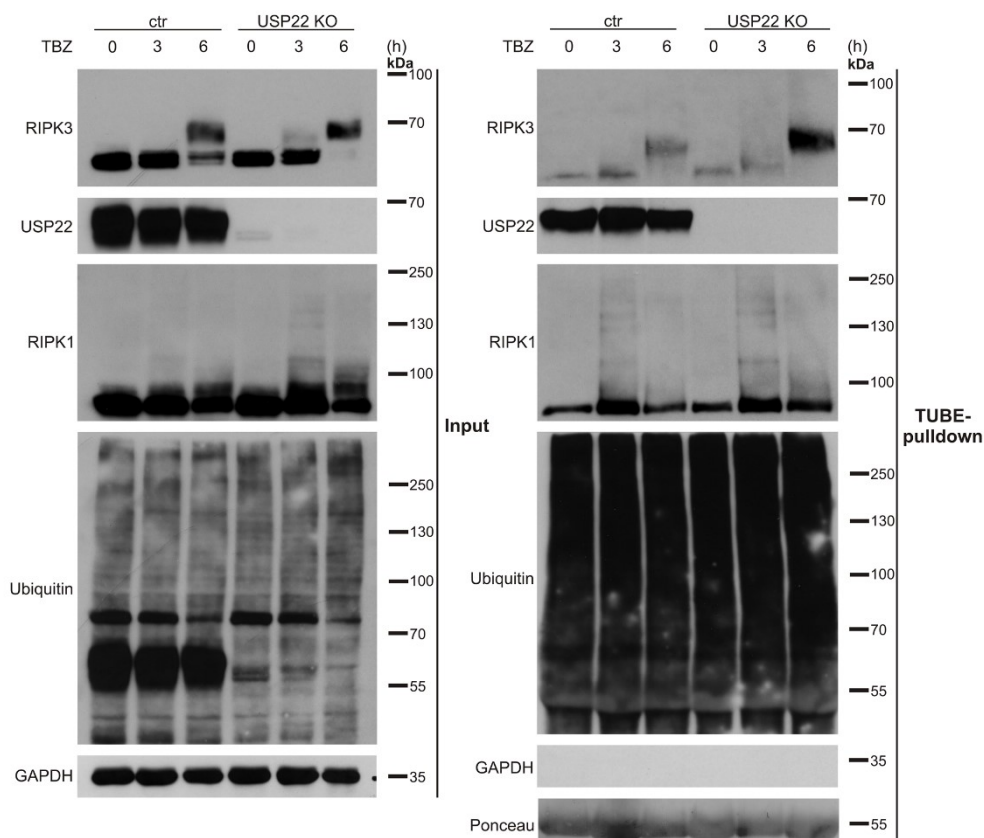


Figure 23 USP22 KO in HT-29 cells does not alter TBZ-induced RIPK1 ubiquitination. HT-29 control and USP22 KO cells were stimulated with 20 μ M zVAD.fmk, 0.5 μ M BV6 and 1 ng/ml TNF α for 3 and 6 h. Ubiquitinated proteins were enriched by GST-TUBE pull-down. Protein expression of RIPK1, RIPK3, USP22 and ubiquitinated RIPK1, RIPK3 and USP22 was monitored using Western blotting with the indicated antibodies. GAPDH served as a loading control. Ponceau-staining was used to confirm equal loading of GST-TUBE.

To further substantiate our findings, we performed denaturing His- and HA-tagged ubiquitin immunoprecipitations on Dox- and TBZ-induced HeLa TRex RIPK3 USP22 WT and USP22 KO cells as well as on TBZ-treated control and USP22 KO HT-29 cells. In both experiments, we could identify increased levels of RIPK3 ubiquitination in USP22 KO cells compared to control cells (Fig. 22B and C).

Collectively, this set of experiments highlights a regulatory role for USP22 in controlling RIPK3 ubiquitination during TBZ-induced necroptosis and implies a critical function for the DUB activity of USP22 in regulating RIPK3 modification.

5.1.4 USP22 mediates RIPK3 ubiquitination and controls necroptosis through RIPK3 K518 ubiquitination

Multiple lysine residues at RIPK3 are being modified by different DUBs and E3 ligases, thereby fine-tuning necroptotic signaling. For example, the E3 ligase PELI1 is described to add K48-conjugated poly-ubiquitin chains to K363 of kinase-active RIPK3, marking it for proteasomal degradation [241], whereas A20 deubiquitinates K63-conjugated poly-ubiquitin chains from RIPK3 at K5, interfering with RIPK1-RIPK3 interaction, thus negatively regulating necroptosis [62]. To investigate the functional consequences of loss of USP22 for total cellular ubiquitination and for necroptosis-specific ubiquitin events, mass spectrometry-based ubiquitin remnant profiling was performed on control and USP22 KO HT-29 cells in untreated and necroptosis-induced conditions (supplementary Excel file; "GlyGly (K) sites all experiments").

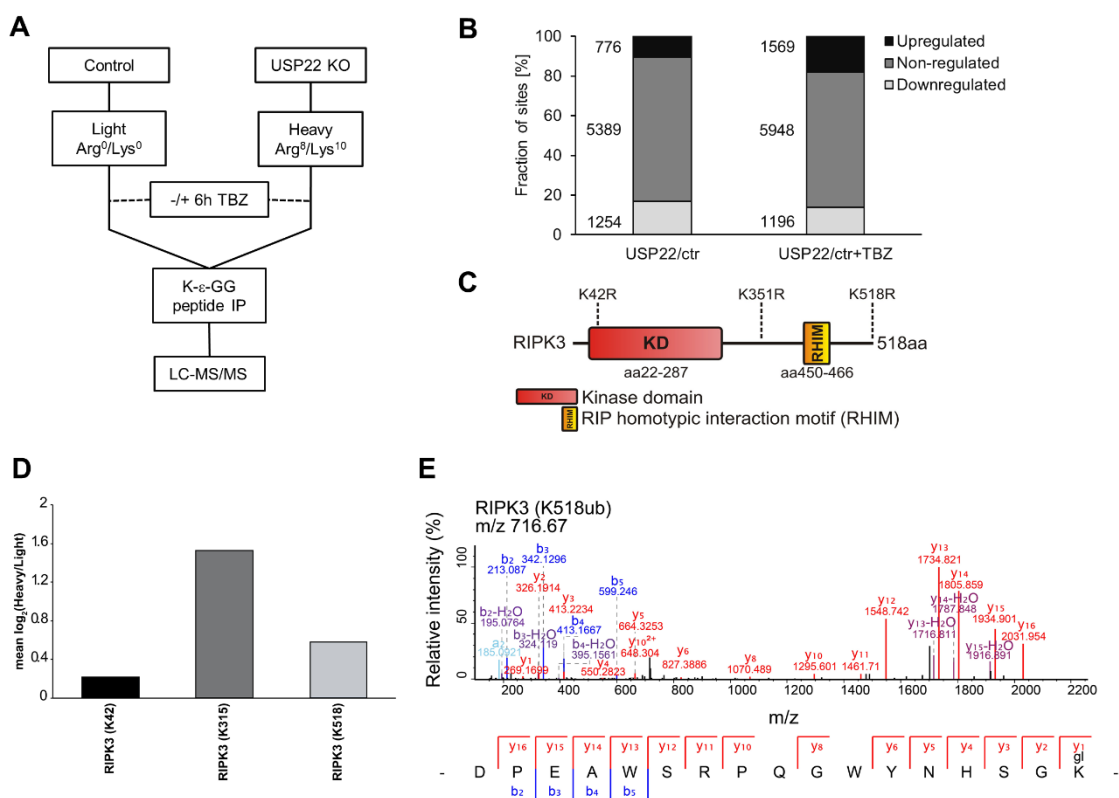


Figure 24 Ubiquitin remnant profiling identifies RIPK3 K518 as USP22-dependent ubiquitin target during necroptosis. **A** Schematic representation of the experimental strategy for quantitative analysis of ubiquitination sites in USP22 KO HT-29 cells versus HT-29 CRISPR/Cas9 control (ctr) cells under untreated and necroptosis-induced conditions. Control cells were grown in SILAC medium containing Arg⁰/Lys⁰ ("Light") labeled, whereas USP22 KO cells were labeled in SILAC medium containing Arg¹⁰/Lys⁸ ("heavy") labeled. In the treated conditions, cells were incubated with 20 μM zVAD.fmk, 0.5 μM BV6 and 1 ng/ml TNF α for 6 h. Cells were lysed, and equal amounts of extracted proteins extracted from "Light" or "Heavy" were pooled and digested in-solution with trypsin. Ubiquitin remnant peptides were enriched using di-glycine-lysine-specific antibodies, fractionated by Micro-SCX and analyzed by LC-MS/MS. **B** Bar graphs demonstrating the number of up-, non-, and downregulated ubiquitination sites in USP22 KO HT-29 cells versus control under TBZ-treated conditions. **C** Schematic representation of RIPK3. Indicated are the two major protein domains, the kinase domain (KD), the RHIM and the three different potential ubiquitination sites identified by ubiquitin remnant profiling. **D** RIPK3 ubiquitination sites detected by ubiquitin remnant profiling upon USP22 KO and TBZ treatment. The mean of two biological replicates is depicted. Only RIPK3 sites are shown that were identified in both replicates. **E** Fragment spectrum of TBZ-treated RIPK3 diglycine-modified peptide corresponding to K518. The b- and y-ions detected are highlighted. These experiments were analyzed and performed by Thomas Juretschke and Petra Beli.

For this purpose, cells were grown in stable isotope labeling with amino acids in cell culture (SILAC)-medium, followed by immunoprecipitation-based enrichment and quantification of ubiquitin remnant-modified lysine abundance (Fig. 24A). Ubiquitin remnant profiling revealed 7,419 total unique endogenous ubiquitin sites in untreated HT-29 cells and 8,713 sites upon TBZ treatment. In untreated USP22 HT-29 KO cells, 776 (10.4%) sites were upregulated and 1,254 (16.9%) sites downregulated compared to control cells. TBZ-mediated induction of necroptosis in USP22 HT-29 KO cells increased the number of upregulated sites to 1,569 (18.0%), whereas 1,198 (13.7%) sites were downregulated compared to control HT-29 cells (Fig. 24B, see USB flash drive for raw data). Strikingly, upon TBZ-induced necroptosis, we could identify three novel modified lysine residues (K42, K352 and K518) in RIPK3, directly dependent on USP22 expression (Fig. 24C-E). Maintaining control and USP22 HT-29 KO cells in SILAC medium did not affect necroptotic cell death (Fig. 25A) or expression levels and phosphorylation status of RIPK1, RIPK3 and MLKL (Fig. 25B).

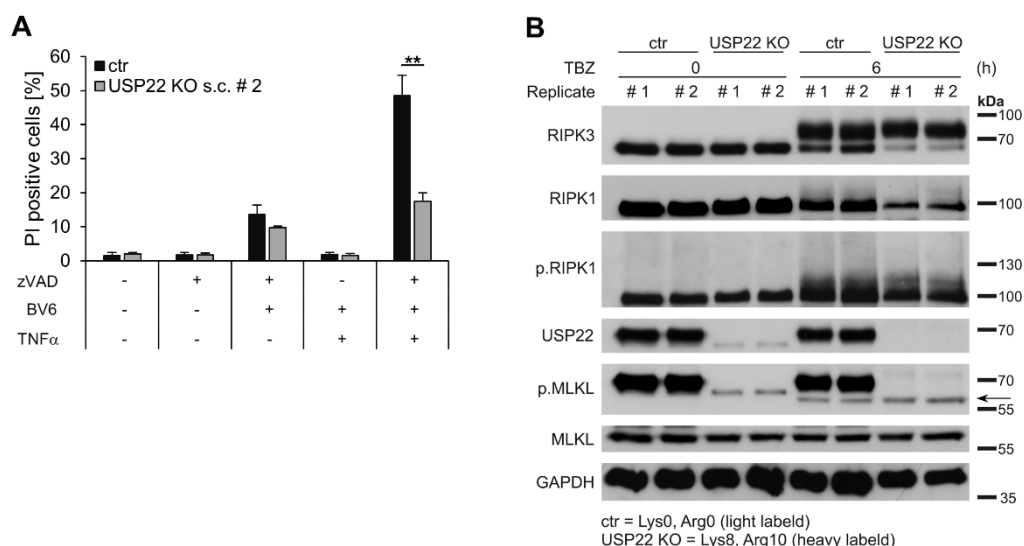


Figure 25 SILAC incorporation does not alter the resistance of HT-29 USP22 KO cells to TBZ-induced necroptosis or the expression levels of necroptotic core proteins. **A** SILAC-labeled HT-29 CRISPR/Cas9 control (ctr) and USP22 KO cells were stimulated with 20 μ M zVAD.fmk, 0.5 μ M BV6 and 1 ng/ml TNF α for 6 h. The percentage of PI-positive cells was assessed by fluorescence-based PI staining. **B** SILAC-labeled HT-29 control and USP22 KO cells were treated with 20 μ M zVAD.fmk, 0.5 μ M BV6 and 1 ng/ml TNF α for 6 h and analyzed by Western blotting with the indicated antibodies. GAPDH served as a loading control. The arrow marks specific phosphorylated MLKL bands.

Of note, ubiquitination of the necroptotic key players RIPK1 and RIPK3 plays a crucial role in regulating necroptosis. Nevertheless, for MLKL, as the third crucial necroptotic player, ubiquitination as a regulatory event in fine-tuning necroptosis could not be identified yet. In our analysis we could identify three novel lysine residues in MLKL, directly dependent on USP22 expression levels and TBZ-induced necroptosis. These novel lysine residues in MLKL are being investigated by another PhD student from our group (Isabelle Gollin) and are part of an upcoming study.

In order to investigate the functional relevance of the TBZ- and USP22-dependent RIPK3 lysine residues for RIPK3 ubiquitination and necroptotic signaling, we generated single RIPK3 K-to-R mutants (K42R, K351R and K518R), double mutants (K42R/K351R; 2xKR) and triple RIPK3 mutations (K42R/K351R/K518R; 3xKR). These RIPK3 K-to-R mutants were stably expressed in HeLa cells under Dox regulation. Alongside the RIPK3 K-to-R mutants, we expressed WT RIPK3 and catalytic-inactive D160N RIPK3 [188] to adequately monitor potential effects on necroptosis and RIPK3 ubiquitination levels. In these cells, RIPK3 expression was induced and the extent of necroptotic cell death was evaluated in the presence or absence of $\text{TNF}\alpha$, BV6 and zVAD, with and without pre-treatment by Dabrafenib and NSA. Dox-mediated ectopic expression of RIPK3 WT, K42, K351R, 2xKR in HeLa cells triggered a large, but homogeneously amount of necroptotic cell death in response to TBZ treatment (Fig. 26A). In contrast, HeLa cells expressing RIPK3 K518R and 3xKR displayed significantly more necroptotic cell death induced by TBZ treatment compared to RIPK3 WT, K42, K351R, 2xKR (Fig. 26A). Notably, neither expression of RIPK3 WT, K42, K351R, 2xKR nor RIPK3 K518R or 3xKR triggered spontaneous necroptotic cell death (Fig. 26A). As anticipated, HeLa cells expressing catalytic-inactive RIPK3 D160N, were resistant towards TBZ-induced necroptosis (Fig. 26A). Prominent TBZ-induced necroptotic cell death could be blocked by Dab and NSA in all cases, confirming proper necroptotic signaling (Fig. 26A).

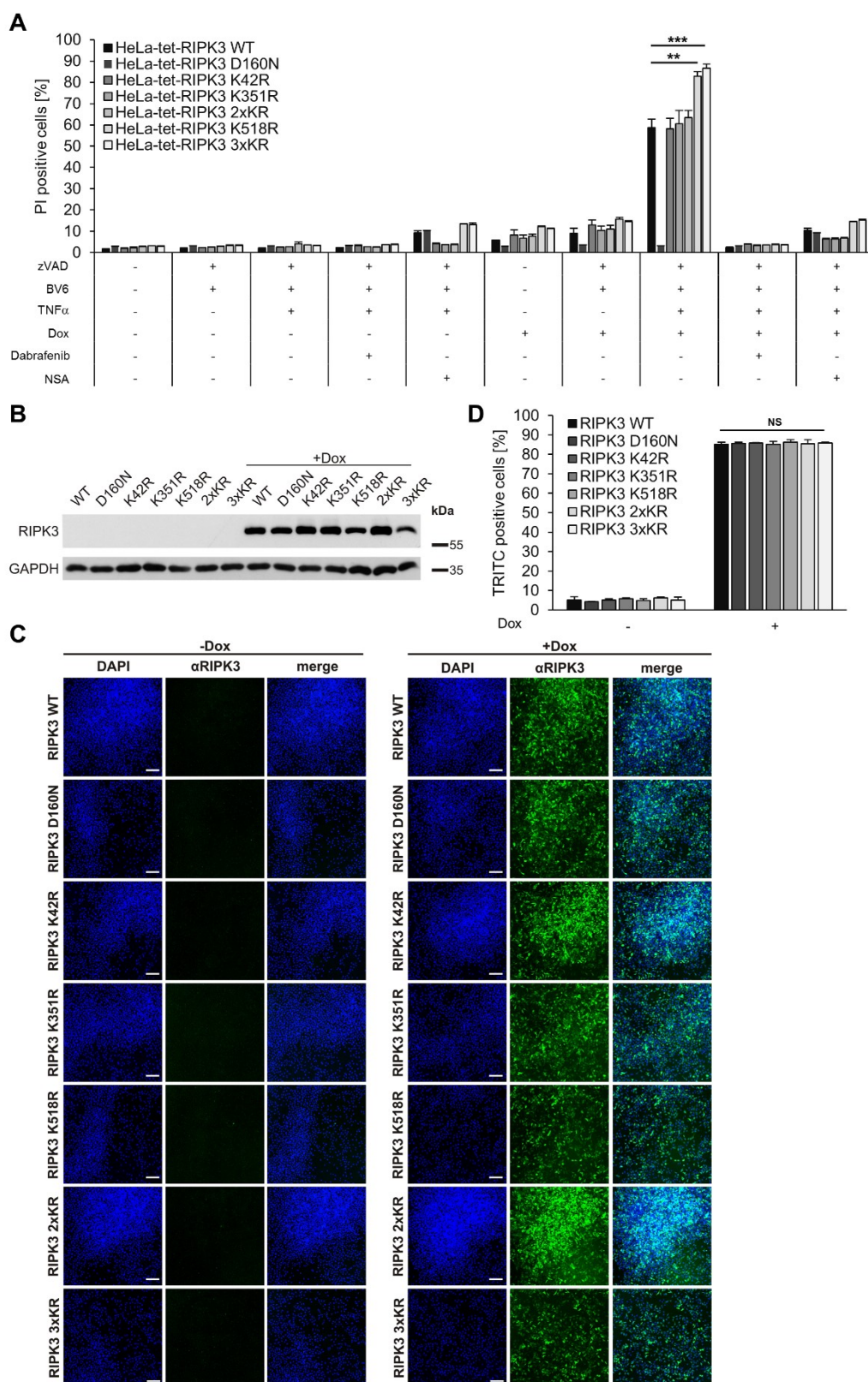


Figure 26 USP22-dependent modification of RIPK3 lysine residue 518 amplifies TBZ-induced necroptotic responses in RIPK3-reconstituted HeLa cells. **A** HeLa cells expressing Dox-inducible RIPK3 WT, D160N, K42R, K351, K518R, 2xKR or 3xKR were pre incubated with 1 μ g/ml Dox, 20 μ M Dab, or 10 μ M NSA overnight, followed by pre-treatment with 20 μ M zVAD.fmk, 5 μ M BV6 for 1 h. After pre-treatment, 10 ng/ml TNF α were added for 4 h. Cell death was measured by analysis of PI-positive nuclei. **B** HeLa cells expressing Dox-inducible RIPK3 mutants were treated with 1 μ g/ml Dox overnight. Protein levels of inducible RIPK3 expression were analyzed by Western blotting. GAPDH served as loading control. **C** HeLa cells expressing Dox-inducible RIPK3 WT, D160N, K42R, K351R, K518R, 2xKR and 3xKR were treated with 1 μ g/ml Dox overnight. RIPK3 expression was imaged using

FITC-labeled anti-RIPK3 immunofluorescence staining. Scale bars represent 250 μm . **D** Quantification of the percentage of FITC-positive cells treated with 1 $\mu\text{g}/\text{ml}$ Dox overnight after anti-RIPK3 immunofluorescence staining. Data information: Data represent mean \pm SD; ** $P < 0.01$; *** $P < 0.001$; NS: not significant, by unpaired 2-tailed Student's t-test. Three independent experiments are shown.

Quantification of FITC-positive cells after RIPK3 immunofluorescence staining and analysis of Dox-mediated RIPK3 expression levels by Western blot analysis confirmed largely comparable expression patterns among the different RIPK3 expressing cell lines (Fig. 26B-D), thereby ruling out that the differences in cell death are due to variations in RIPK3 expression levels. To prove, that indeed RIPK3 K518R ubiquitination is mediated by USP22, we performed a siRNA-mediated knockdown of USP22 in RIPK3 WT, 2xKR, K518R and 3xKR expressing HeLa cells, followed by quantification of PI positive cells. As expected, siRNA-mediated knockdown of USP22 in HeLa cells expressing RIPK3 WT and 2xKR resulted in a significant reduction of necroptotic cell death (Fig. 27A and B). On the other hand, HeLa cells expressing RIPK3 K518R and 3xKR displayed no further reduction in the extend of necroptotic cell death in response to USP22 knockdown, confirming the relevance of USP22 in controlling RIPK3 K518 ubiquitination during TBZ-induced necroptosis (Fig. 27A and B).

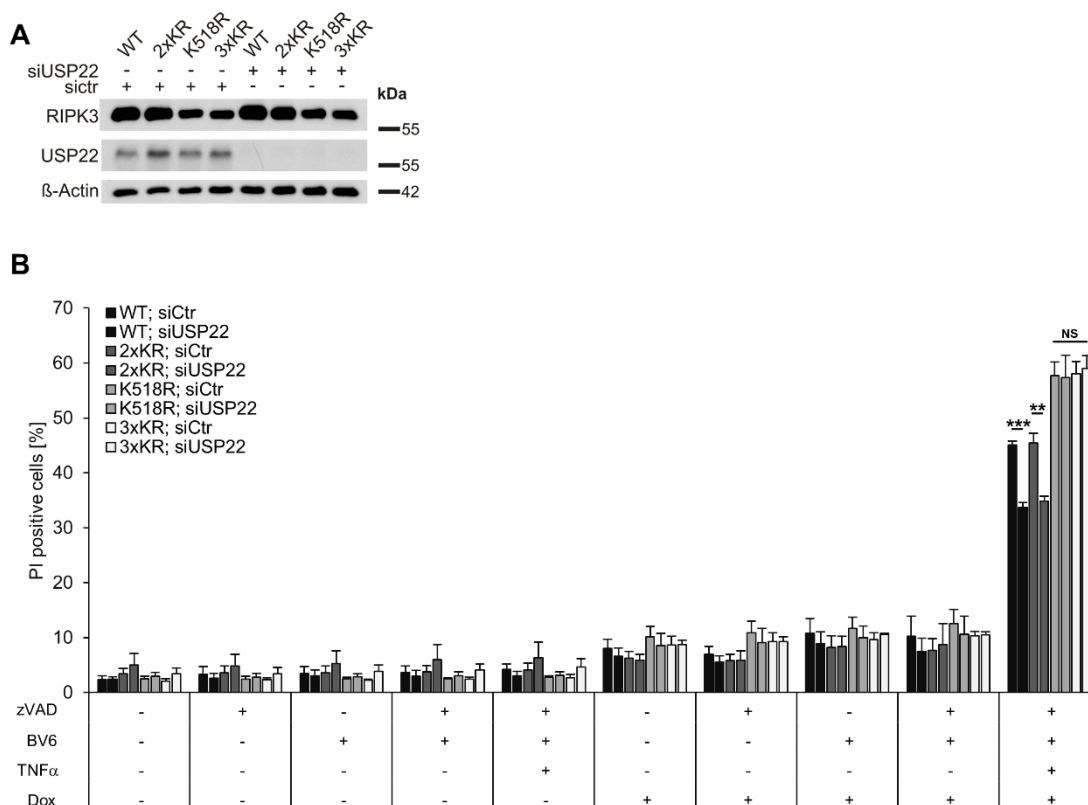


Figure 27 siRNA-mediated knockdown of USP22 in RIPK3-K518R or RIPK3 3xKR reconstituted HeLa cells does not affect sensitivity to TBZ-induced necroptotic cell death. **A** HeLa cells expressing Dox-inducible RIPK3 WT, K518R, 2xKR or 3xKR were transfected with non-silencing control siRNA (sict) or siRNAs against USP22 (siUSP22) for 48 h at 20 nM and treated with 1 $\mu\text{g}/\text{ml}$ Dox. RIPK3 and USP22 expression was analyzed by Western blotting. β -Actin served as a loading control. **B** HeLa cells expressing Dox-inducible RIPK3 WT, K518R, 2xKR or 3xKR were transfected with non-silencing control siRNA (sict) or pooled siRNAs against USP22 (siUSP22) for 48 h at 20 nM and treated with 1 $\mu\text{g}/\text{ml}$ Dox, as indicated. Cells were pre-treated with 20 μM zVAD.fmk and 5 μM BV6 for 1 h after 10 ng/ml TNF α was added for 4 h. The percentage of PI-positive cells was assessed by fluorescence-based PI staining.

Remarkably, Dox-induced expression of RIPK3 WT, K518R and 3xKR already induced MLKL phosphorylation in the absence of a necroptotic stimulus, but was still unable to trigger necroptotic cell death. Furthermore, MLKL phosphorylation was more prominent in RIPK3 K518R and RIPK3 3xKR cells compared to cells expressing wild-type RIPK3 (Fig. 28A and B). Of note, RIPK3-induced MLKL phosphorylation could be blocked by using Dab, but by using NSA (Fig. 28A). This is due to the fact that NSA covalently binds MLKL Cys86, thus blocking MLKL oligomerization, but not its phosphorylation [196]. Upon early progression of TBZ-induced necroptosis, HeLa cells expressing WT or 3xKR RIPK3 demonstrated a constant increase in MLKL phosphorylation. HeLa RIPK3 3xKR-expressing cells exhibited a stronger MLKL phosphorylation at earlier time-points when compared to RIPK3 WT-expressing cells (Fig. 28B). At late phase necroptosis, in both the HeLa RIPK3 WT and 3xKR-expressing cells, levels of phosphorylated MLKL decreased, however this deduction in phosphorylated MLKL due to necroptosis progression was more pronounced in RIPK3 3xKR-expressing cells (Fig. 28B). In accordance with previous experiments, TBZ-induced necroptosis significantly elevated the levels of phosphorylated RIPK3 in HeLa RIPK3 WT cells, inducing typical higher molecular weight RIPK3 band shifts (Fig. 28B). λ -phosphatase treatment almost completely reduced these RIPK3 shift, suggesting that the higher molecular weight RIPK3 bands probably are phosphorylated forms of RIPK3 (Fig. 28C). Strikingly, the slower-migrating RIPK3 species were hardly detectable in HeLa RIPK3 3xKR cells (Fig. 28B), contradictory to HeLa RIPK3 WT and 2xKR cells (Fig. 28B and D). At the same time, RIPK3 3xKR levels diminished upon prolonged necroptosis when compared to WT RIPK3 (Fig. 28B). Subsequently, we performed lysis of TBZ-treated cells expressing RIPK3 WT, K518R and 3xKR under denaturing conditions observing RIPK3 K518R and RIPK3 3xKR expression and modification in the insoluble fraction, suggesting that RIPK3 K518R and 3xKR become more and earlier insoluble due to progressing necroptosis, compared to WT RIPK3 (Fig. 28E).

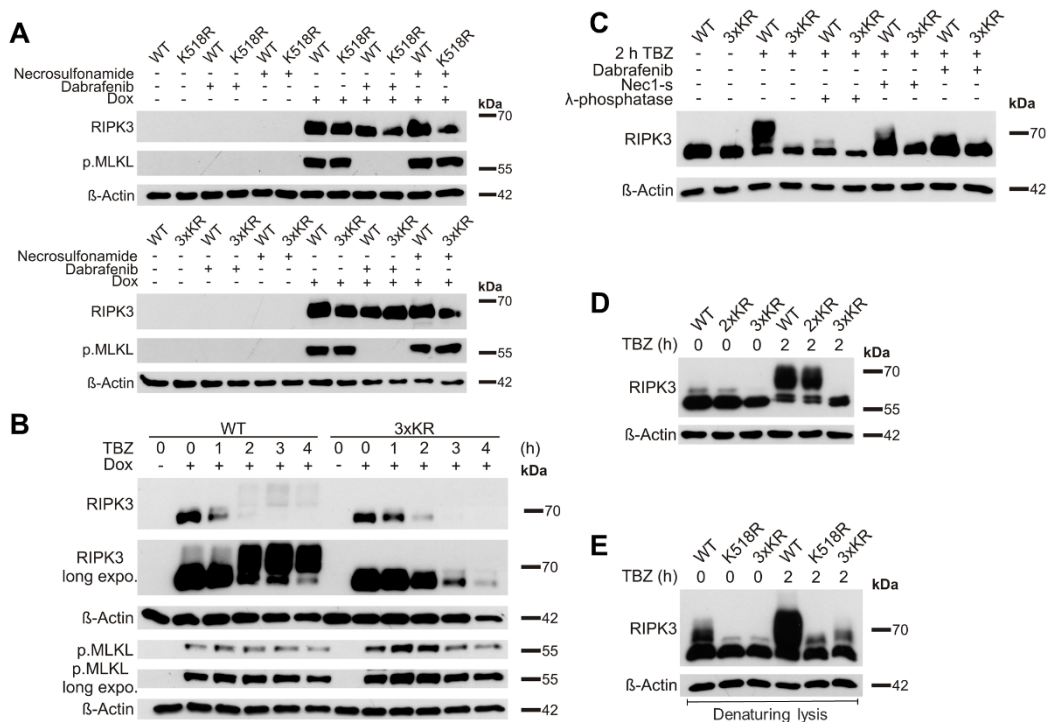


Figure 28 Mutation of RIPK3 lysine residue 518 alter RIPK3 phosphorylation upon TBZ-induced necroptosis in RIPK3-reconstituted HeLa cells. **A** HeLa cells expressing Dox-inducible RIPK3 WT, K518R or 3xKR were treated with 1 μ g/ml Dox and/or 10 μ M NSA and 20 μ M Dab overnight. Protein levels of inducible RIPK3 expression and phosphorylated MLKL were examined by Western blotting. β -Actin was used as a loading control. **B** HeLa cells expressing Dox-inducible RIPK3 WT or 3xKR were treated with 1 μ g/ml Dox overnight before pre-treatment with 20 μ M zVAD.fmk, 5 μ M BV6 for 1 h. After pre-treatment, 10 ng/ml TNF α were added for 1, 2, 3 and 4 h. Protein levels of inducible RIPK3 expression and phosphorylated MLKL were analyzed by Western blotting. β -Actin served as loading control. **C** HeLa cells expressing Dox-inducible RIPK3 WT or 3xKR were incubated with 30 μ M Nec1-s or 20 μ M Dab and 1 μ g/ml Dox overnight, as indicated. Cell were stimulated with 20 μ M zVAD.fmk, 0.5 μ M BV6 and 1 ng/ml TNF α for 2 h. 100 μ g of each lysate was incubated with 400 U/ μ l λ -phosphatase for 30 min at 30 $^{\circ}$ C. RIPK3 protein expression was monitored by Western blotting. β -Actin was used as loading control. **D** HeLa cells expressing Dox-inducible RIPK3 WT, 2xKR or 3xKR were treated with 1 μ g/ml Dox overnight before pre-treatment with 20 μ M zVAD.fmk, 5 μ M BV6 for 1 h. After pre-treatment, 10 ng/ml TNF α was added for 2 h. Protein levels of inducible RIPK3 expression was analyzed by Western blotting. β -Actin served as loading control. **E** HeLa cells expressing Dox-inducible RIPK3 WT, K518R or 3xKR were treated with 1 μ g/ml Dox overnight before pre-treatment with 20 μ M zVAD.fmk, 5 μ M BV6 for 1 h. After pre-treatment, 10 ng/ml TNF α were added for 2 h. Whole cell lysates were generated using RIPA lysis buffer containing 2% SDS. Protein levels of inducible RIPK3 expression were analyzed by Western blotting. β -Actin served as loading control.

Necrosome formation is a central process in necroptotic signaling [234, 340]. RIPK3-mediated MLKL recruitment and subsequent phosphorylation enables MLKL transformation from a dormant into a pronecrotic oligomeric form, facilitating MLKL membrane translocation, permeabilization and subsequent cell death [176, 196, 260, 268, 340]. In order to dissect the relevance of lysine-specific RIPK3 ubiquitination for necrosome formation, we performed necrosome immunoprecipitations from RIPK3 WT, D160N, K518R and 3xKR-expressing HeLa cells upon TBZ-induced necroptosis and analyzed MLKL and RIPK1 co-immunoprecipitation. Based on the interaction between RIPK3 and phosphorylated MLKL, we could detect increased necrosome formation in HeLa cells expressing RIPK3 K518R and 3xKR (Fig. 29A). Corresponding to previous experiments, RIPK3 K518R and 3xKR-expressing cells demonstrated increased levels of phosphorylated MLKL upon TBZ-induced necroptosis,

compared to WT RIPK3 cells (Fig. 29A). As expected, HeLa cells expressing RIPK3 D160N were resistant to TBZ-induced MLKL phosphorylation, whereas basal MLKL expression remained largely unaffected by Dox-mediated expression of either RIPK3 WT, D160N, K518R or 3xKR (Fig. 29A). Interestingly, RIPK1 binding to WT RIPK3 was elevated upon TBZ-induced necroptosis. This interaction was increased in RIPK3 K518R-expressing cells and even more elevated in cells expressing RIPK3 D160N. Contradictory, upon TBZ-induced necroptosis and Dox-mediated expression of RIPK3 3xKR, this RIPK3-RIPK1 interaction was decreased (Fig. 29A). Moreover, we could detect changes in RIPK1 phosphorylation in HeLa cells expressing RIPK3 D160N, K518R and 3xKR when compared to RIPK3 WT-expressing cells, suggesting mutational-, cell line- and TBZ-dependent effects on RIPK1 phosphorylation (Fig. 29A).

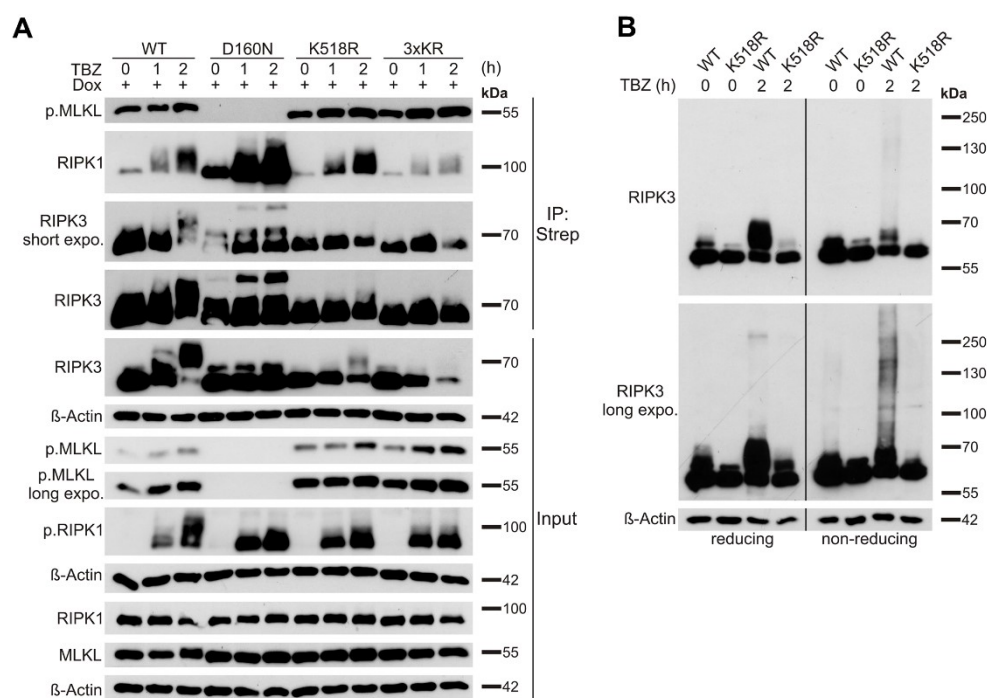


Figure 29 Mutation of RIPK3 lysine residue 518 amplifies necrosome formation upon TBZ-induced necroptosis in RIPK3-reconstituted HeLa cells. **A** HeLa cells expressing Dox-inducible RIPK3 WT, D160N, K518R or 3xKR were incubated overnight with 1 $\mu\text{g/ml}$ Dox and pre-treated with 20 μM zVAD.fmk, 5 μM BV6 for 1 h. After pre-treatment, 10 ng/ml $\text{TNF}\alpha$ were added for 1 and 2 h. Strep-RIPK3 was immunoprecipitated by using anti-Strep-beads. Co-immunoprecipitated phosphorylated MLKL and RIPK1, as well as protein expression of indicated proteins were analyzed by Western blotting. β -Actin served as a loading control. **B** HeLa cells expressing Dox-inducible RIPK3 WT or K518R were incubated with 1 $\mu\text{g/ml}$ Dox overnight. Cells were pre-treated with 20 μM zVAD.fmk and 5 μM BV6 for 1 h. After pre-treatment, 10 ng/ml $\text{TNF}\alpha$ was added for 2 h. Levels of inducible RIPK3 expression were analyzed by Western blotting under reducing and non-reducing conditions. β -Actin served as loading control. The asterisk marks putative RIPK3 dimers.

Homodimerization of RIPK3 is a prerequisite for RIPK3 auto-phosphorylation and subsequent recruitment of MLKL [195, 234]. Therefore, we compared RIPK3 WT and K518R-expressing cells under reducing and non-reducing conditions for their ability to form RIPK3 homodimers upon TBZ-induced necroptosis. Surprisingly, RIPK3 WT and K518R homodimerization occurred evenly. Nevertheless, RIPK3 WT-expressing cells displayed a noticeable 'smear' which was absent in RIPK3 K518R-expressing cells. In fact, this 'smear' most likely consists

of oligomers, or various PTMs, induced by TBZ-induced RIPK3 modification (Fig. 29B). Lastly, we performed denaturing immunoprecipitations of HA-tagged ubiquitin upon TBZ treatment in RIPK3 WT, K518R and 3xKR-expressing cells, demonstrating decreased levels of ubiquitinated RIPK3 in RIPK3 K518R and 3xKR compared with RIPK3 WT (Fig. 30).

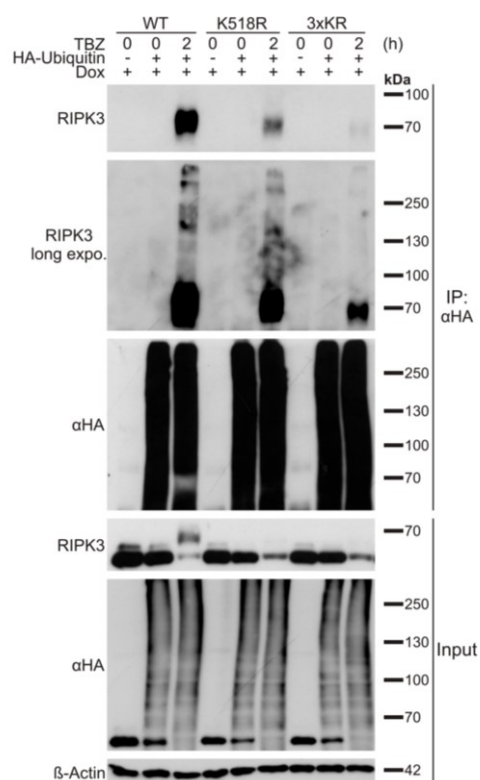


Figure 30 Mutation of RIPK3 lysine residue 518 decreases RIPK3 ubiquitination upon TBZ-induced necroptosis in RIPK3-reconstituted HeLa cells. HeLa cells expressing Dox-inducible RIPK3 WT, K518R or 3xKR were incubated with 1 μ g/ml Dox and transfected with HA-ubiquitin for 24 h, as indicated. Cells were pre-treated with 20 μ M zVAD.fmk, 5 μ M BV6 for 1 h. After pre-treatment, 10 ng/ml TNF α were added for 2 h. HA-ubiquitin was immunoprecipitated using anti-HA-beads and detection of indicated proteins was performed by Western blotting. β -Actin served as loading control for the input, whereas HA-ubiquitin levels served as loading control for immunoprecipitated ubiquitin.

In summary, these experiments imply residue K518 in RIPK3 as a new and primary USP22-dependent (de)ubiquitination site during TBZ-induced necroptosis. Furthermore, our data suggest that dynamic (de)ubiquitination at RIPK3 K518 strongly affects necroptosis-induced RIPK3 phosphorylation.

5.1.5 RIPK3 K518R hypersensitizes HT-29 cells to TBZ-induced necroptosis

In order to further validate the pro-necroptotic functions of RIPK3 K518 modification, we utilized CRISPR/Cas9-mediated genome editing to generate RIPK3 KO HT-29 cells (Fig. 31A). As expected, RIPK3 KO HT-29 cells were resistant towards TBZ-induced necroptosis (Fig. 31B).

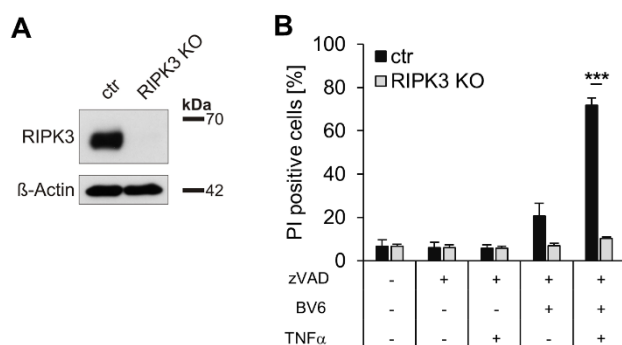


Figure 31 RIPK3 KO HT-29 cells are resistant against TBZ-induced necroptosis. A HT-29 CRISPR/Cas9 control (ctr) and RIPK3 KO cells were analyzed by Western blotting for RIPK3 expression. β -Actin served as loading control. B HT-29 control and RIPK3 KO cells were stimulated with 20 μ M zVAD.fmk, 0.5 μ M BV6 and 1 ng/ml TNF α for 18 h. The percentage of PI-positive cells was assessed by fluorescence-based PI staining. Data information: Data represent mean \pm SD; ***P < 0.001, by unpaired 2-tailed Student's t-test. Three independent experiments are shown.

Subsequently, we stably reconstituted RIPK3 WT, D160N, K518R and 3xKR with CRISPR/Cas9-resistant PAMs under Dox regulation in the RIPK3 depleted HT-29 cells. Reconstitution of RIPK3 successfully restored necroptosis sensitivity in RIPK3 WT, K518R and 3xKR-expressing cells. Importantly, TBZ-induced necroptotic cell death was significantly increased in cells expressing RIPK3 K518R and RIPK3 3xKR compared to RIPK3 WT-expressing cells (Fig. 32A), matching previous results obtained in HeLa RIPK3-expressing cells. As expected, RIPK3 KO cells reconstituted with catalytic inactive RIPK3 D160N were entirely resistant against TBZ-induced necroptotic cell death (Fig. 32A). All reconstituted RIPK3 KO HT-29 cell lines displayed a homogenous RIPK3 expression (Fig. 32C and D) as well as equivalent RIPK3 protein expression levels (Fig. 32B), eliminating the possibility that the observed increase in necroptotic cell death is due to variations in RIPK3 expression. In accordance to the increase in necroptotic cell death, with RIPK3 K518R and 3xKR reconstituted RIPK3 KO cell lines displayed elevated levels of phosphorylated MLKL upon TBZ-induced necroptosis and compared to cells reconstituted with WT RIPK3 (Fig. 32B). Furthermore, cells expressing K518R and 3xKR displayed a reduction in RIPK3 phosphorylation, consistent with previously performed experiments (Fig. 32B).

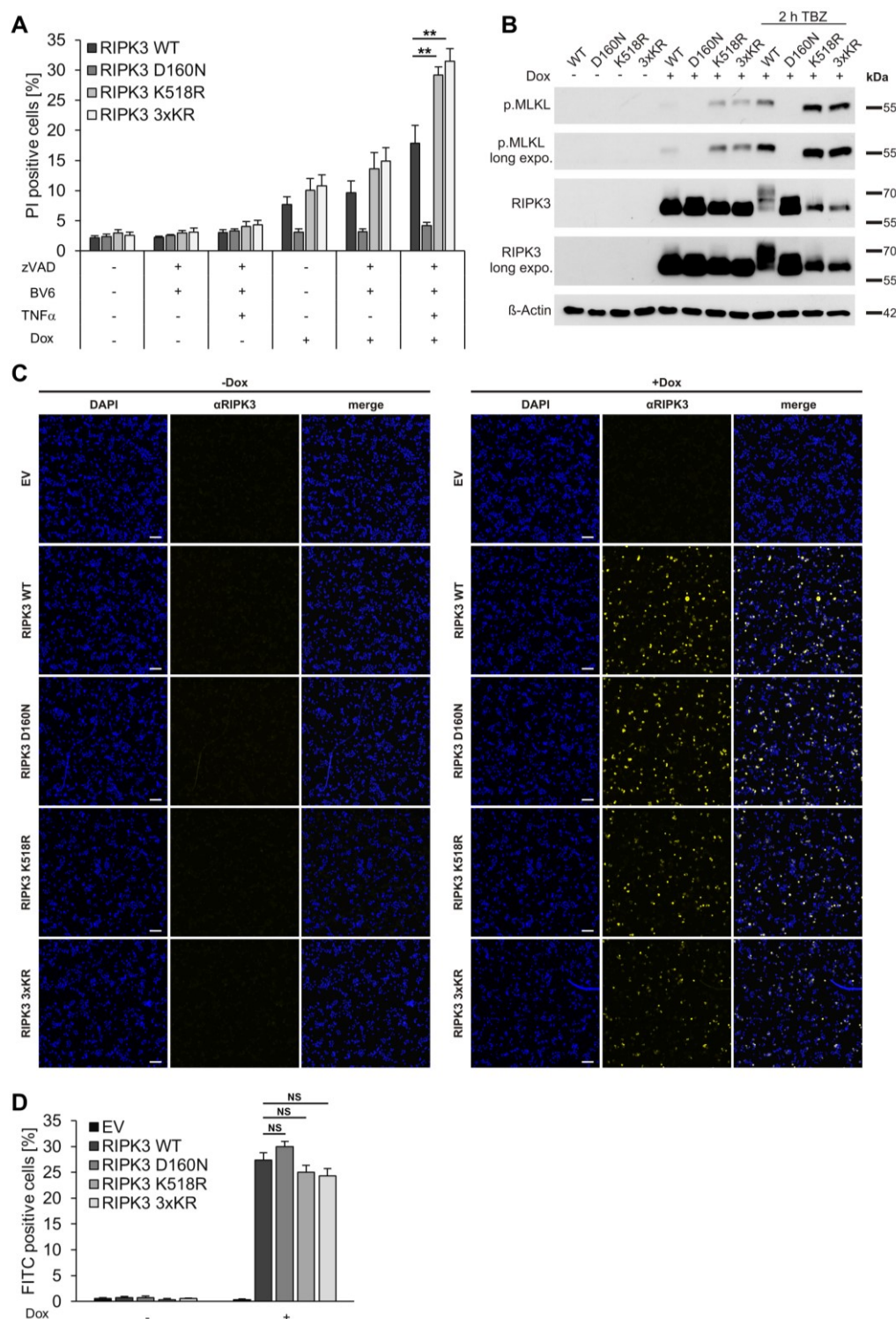


Figure 32 RIPK3 K518R hypersensitize HT-29 cells for TBZ-induced necroptosis. **A** HT-29 RIPK3 KO cells re-expressing Dox-inducible WT RIPK3 or the indicated RIPK3 mutants were incubated with 1 μ g/ml Dox overnight. Cells were treated with 20 μ M zVAD.fmk, 5 μ M BV6 and 10 ng/ml TNF α for 4 h. Cell death was measured by analysis of PI-positive nuclei. **B** HT-29 RIPK3 KO cells re-expressing Dox-inducible WT RIPK3 or the indicated RIPK3 mutants were incubated with 1 μ g/ml Dox overnight, as indicated. Cells were treated with 20 μ M zVAD.fmk, 5 μ M BV6 and 10 ng/ml TNF α for 2 h and analyzed by Western blotting for RIPK3 and phosphorylated MLKL expression levels. β -Actin served as a loading control. **C** HT-29 cells expressing EV and Dox-inducible RIPK3 WT, D160N, K518R and 3xKR were treated with 1 μ g/ml Dox overnight. Strep-RIPK3 expression was imaged using anti-RIPK3 immunofluorescence staining. Scale bars represent 100 μ m. **D** Quantification of FITC-positive cells after RIPK3 immunofluorescence staining of HT-29 cells expressing Dox-inducible RIPK3 WT, D160N, K518R and 3xKR. Data information: Data represent mean \pm SD; **P < 0.01; NS: not significant, by unpaired 2 tailed Student's t-test. Three independent experiments performed in triplicate are shown.

Finally, we performed necrosome immunoprecipitations from RIPK3 KO HT-29 cells reconstituted with RIPK3 WT, K518R or 3xKR upon TBZ-induced necroptosis and analyzed phosphorylated RIPK1 and MLKL co-immunoprecipitation. In cells reconstituted with RIPK3 K518R or 3xKR necrosome formation occurred faster and more pronounced based on the interaction between phosphorylated MLKL and RIPK3 upon TBZ-induced necroptosis (Fig. 33). Moreover, this increase in necrosome formation corresponded with elevated levels of phosphorylated MLKL in RIPK3 KO HT-29 cells reconstituted with RIPK3 K518R or 3xKR upon TBZ-induced necroptosis compared to cells reconstituted with RIPK3 WT (Fig. 33). As anticipated, RIPK3 D160N was unable to co-immunoprecipitate phosphorylated MLKL, congruent with the absence of phosphorylated MLKL upon TBZ-induced necroptosis (Fig. 33). MLKL expression remained largely unaltered by reconstitution of RIPK3 WT, D160N, K518R or 3xKR (Fig. 33). Akin to previously performed experiment in HeLa RIPK3-expressing cells, we could detect alterations in RIPK1 phosphorylation upon TBZ-induced necroptosis in cells expressing RIPK3 D160N, K518R or 3xKR compared to cells reconstituted with WT RIPK3 (Fig. 33). Moreover, the changes in RIPK1 phosphorylation was congruent to the amount of by RIPK3 co-immunoprecipitated phosphorylated RIPK1, suggesting cell line-, mutational- and TBZ-dependent effects on RIPK1 phosphorylation and interaction with RIPK3 (Fig. 33).

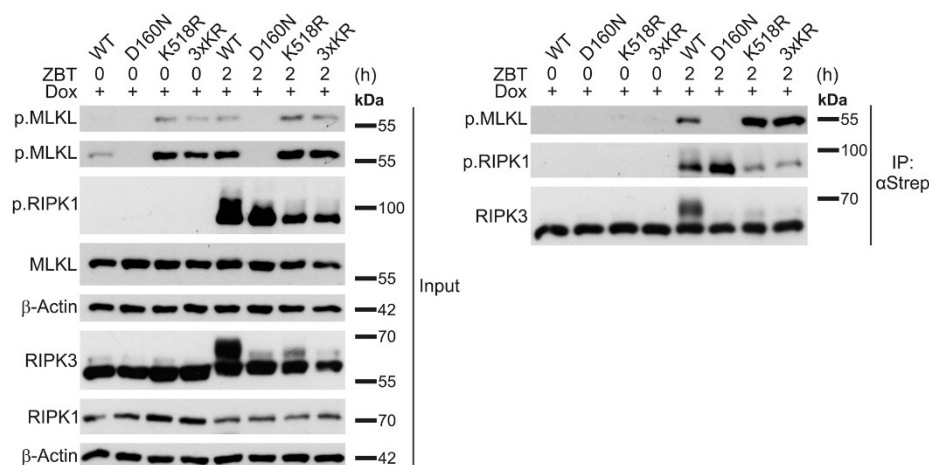


Figure 33 RIPK3 K518R amplifies necrosome formation upon TBZ-induced necroptosis in HT-29 cells. RIPK3 KO HT-29 cells reconstituted with Dox-inducible RIPK3 WT, D160N, K518R or 3xKR were incubated overnight with 1 μ g/ml Dox and pre-treated with 20 μ M zVAD.fmk, 5 μ M BV6 for 1 h. After pre-treatment, 10 ng/ml TNF α was added for 2 h. Strep-RIPK3 was immunoprecipitated by using anti-Strep-beads. Co-immunoprecipitated phosphorylated MLKL and phosphorylated RIPK1, as well as protein expression of indicated proteins were analyzed by Western blotting. β -Actin served as a loading control.

In summary, these experiments highlight a central role for USP22 in regulating TBZ-induced necroptosis. We provide evidence that USP22 regulates RIPK3 ubiquitination and phosphorylation and that USP22-dependent RIPK3 ubiquitination at K518 is a crucial step in fine-tuning necroptotic cell death signaling.

6 Discussion

Numerous studies highlight the ever-growing importance of ubiquitination as an essential regulative PTM in programmed cell death signaling [239, 241, 330, 341]. Several E3 ligases and DUBs have been described to tightly regulate the outcome of apoptotic and necroptotic signaling by dynamically changing the abundance and composition of ubiquitin chains on the target substrate [62, 237, 330, 341-344]. USP22, as part of the DUBm of the human SAGA complex, is well-characterized in its function in regulating H2A and H2B mono-ubiquitination, thereby controlling gene transcription. However, several studies recently described novel biological functions for USP22 [93, 337, 338]. For instance, USP22 participates in the regulation of cell death signaling by deubiquitination and stabilization of SIRT1, subsequent TP53 deacetylation and transcriptional activation of TP53 target genes or deacetylation-dependent c-Myc stabilization, thereby inhibiting apoptosis [59, 100]. In this study, we identify USP22 as a novel pro-necroptotic player, controlling necroptotic cell death in various human tumor cell lines by regulating RIPK3 phosphorylation and ubiquitination. By utilizing ubiquitin remnant profiling we could identify three novel potential USP22-regulated RIPK3 ubiquitination sites K42, K351 and K518 upon TBZ-induced necroptosis. Finally, we demonstrate that USP22-mediated RIPK3 K518 ubiquitination regulates necroptotic signaling by amplifying necrosome formation.

6.1 USP22 controls TBZ-induced necroptotic cell death in human tumor cell lines

In the present study we could show that loss of USP22 expression delays prototypical TBZ-induced necroptosis in several human tumor cell lines and that necroptosis resistance positively correlates with USP22 expression levels, as shown by partial USP22 knockdown cell lines. The fact that re-expression of C185S or C185A USP22 could not rescue necroptosis sensitivity suggests a pivotal role for the catalytic USP22 DUB activity in controlling necroptotic signaling. Interestingly, loss of USP22 expression did not affect necroptotic signaling in necroptosis-proficient mouse cell lines, implying a human specificity for USP22 in controlling necroptotic signaling. CRISPR/Cas9-mediated loss of USP22 expression did not influence TNFR1-mediated NF- κ B activation or TNF α -induced complex-I formation, suggesting that USP22 controls necroptotic cell death regulators downstream in signaling. Moreover, we could demonstrate that loss of USP22 expression also delays TRAIL(BZ)- and FasL(BZ)-induced necroptosis, further substantiating this hypothesis, since TRAIL- and FasL-induced

necroptosis act independently of TNF α -induced complex-I formation [345]. In contrast to previously described anti-apoptotic functions of USP22 [59], USP22 depletion did not affect apoptotic complex-II formation. Accordingly, ubiquitin remnant profiling revealed three potential USP22-regulated ubiquitination sites in RIPK3, whereas other complex-I and -II associated proteins remained unaffected in their ubiquitination status upon USP22 depletion and TBZ-induced necroptosis, suggesting highly specific, novel pro-necroptotic functions of USP22. In fact, dual roles in cell fate control have also been reported for other DUBs, like CYLD, which controls pro-survival and pro-death functions, depending on caspase-8-dependent, TNF α -mediated processing [237].

Interestingly, loss of USP22 expression only delays TBZ-induced necroptosis, but does not completely block cell death. This might be due to functional compensatory or cooperative mechanisms, triggered by additional, USP22-redundant DUBs, which take over upon USP22 depletion. Indeed, this redundancy has indeed been described for USP22 within the context of the SAGA complex. USP27X and USP51 are described to compete with USP22 for ENY2- and ATXN7L3- dependent activation [89], suggesting at least partial compensatory mechanisms. Furthermore,

USP13 is described to cooperate with USP22 in order to mediate the deubiquitination of STING [95], emphasizing the compensatory interplay between USP22 and other DUBs, which could be induced upon USP22 depletion, preventing a complete resistance against necroptosis.

In agreement with previous studies we could detect increased H2Bub1 levels in HT-29 colon carcinoma cells upon USP22 depletion [76, 87]. However, the protein expression levels of the necroptotic core machinery, consisting of RIPK1, RIPK3 and MLKL, were largely unaffected by USP22 depletion, suggesting that the observed effects of USP22 on necroptotic signaling are most likely not linked to global USP22-dependent changes in gene transcription.

6.2 USP22-mediated deubiquitination of RIPK3

At first sight, RIPK3 and USP22 seem to reside in separate cellular compartments. Necrosome formation and subsequent necroptosis execution occurs in the cytoplasm [188, 200], whereas the majority of USP22 and USP22 substrates are located in the nucleus [87, 92, 338]. However, several substrates such as Regulator of Calcineurin 1 (RCAN1), Programmed cell death 1 ligand 1 (PD-L1) or COP9 signalosome 5 (CSN5), are located and deubiquitinated in the cytoplasm or at the plasma membrane, respectively [93, 337, 346], suggesting unexplored extra-nuclear functions of USP22. Our interaction studies could demonstrate that RIPK3 and USP22 are able to interact independently of the presence of a necroptotic stimulus. Although it is tempting to speculate that USP22 directly deubiquitinates RIPK3, it might be more likely that USP22 indirectly affects RIPK3 modification through DUB activity-dependent direct or

indirect modulation of the activity of additional E3 ligases. Various DUBs have been shown to deubiquitinate E3 ligases, such as A20 or CYLD, which both target K63-linked poly-ubiquitin chains TRAF2 and TRAF6, thus negatively regulating the NF- κ B pathway [347, 348]. Along this line, similar mechanisms have been reported for USP8. By catalyzing the removal of K6-conjugated poly-ubiquitin chains from the E3 ligase parkin, USP8 negatively regulates mitophagy [349, 350]. Given the fact that MLKL and RIPK3 are able to shuttle between the cytoplasm and the nucleus during necroptosis, potential molecular contacts with USP22- and RIPK3-associated E3 ligases are further increased [272, 351]. So far, potential E3 ligase candidates that are able to interact with USP22 in order to modify RIPK3 remain to be identified, although several E3 ligases are implicated in RIPK3 ubiquitination. For instance, the E3 ligase parkin negatively regulates necrosome formation by adding K33-conjugated poly-ubiquitin chains on RIPK3 [239], whereas A20 deubiquitinates K63-conjugated poly-ubiquitin chains from RIPK3 at K5, thus negatively regulating necroptosis [62]. Moreover, both PELI1 and CHIP have been described to add K48-conjugated poly-ubiquitin chains on RIPK3, thus negatively regulating RIPK3 expression levels [238, 241].

Currently, USP22 has been associated with catalyzing the removal of mono-ubiquitination as well as K6-, K11-, K27-, K29-, K33-, K48- and K63-conjugated poly-ubiquitin chains [87, 91, 93, 346]. Even though Wang *et al.* demonstrated the ability for USP22 to remove K6-, K11-, K27-, K29-, K33- and K63-conjugated poly-ubiquitin chains from both CSN5 and PD-L1 [346], the vast majority of literature associates USP22 only with hydrolyzing mono-ubiquitination as well as K48- and K63-conjugated ubiquitin chains [84, 91-94]. Although USP22 has been shown to cooperate with USP13 to catalyze the hydrolysis of K27-linked ubiquitin chains, a potential role of USP13 in necroptosis remains yet to be determined. We were unable to characterize the type of the USP22-dependent ubiquitin signal on RIPK3 during necroptosis. However, when considering the fact that the expression levels of RIPK3 remained unaffected due to USP22 depletion, the type of ubiquitin signal on RIPK3 is most likely a non-proteolytic form of ubiquitination, regulating protein interactions and signaling [8].

6.3 USP22-mediated RIPK3 K518 ubiquitination regulates necroptosis progression

In the present study we identified K42, K351 and K518 in RIPK3 as novel USP22-regulated ubiquitination sites during TBZ-induced necroptosis in the HT-29 cells. Importantly, RIPK3 K518R could be shown to be a crucial ubiquitination site, regulating necrosome formation and necroptosis progression. Throughout necroptosis progression, activated RIPK1 and RIPK3 associate via their RHIMs, auto- and trans-phosphorylating each other, leading to the creation of extended, hetero-amyloid-like structures [188-191, 340]. RIPK3 K518 is located at the very

end of the C-terminus of RIPK3 and, based on primary sequence, not in close proximity to the RHIM. This might potentially isolate the RIPK3 ubiquitination site and could facilitate ubiquitination during necroptosis, although this remains to be determined experimentally, since no structural data is present that explains the localization of the C-terminus of RIPK3 during necrosome formation. However, it is tempting to speculate that RIPK3 K518 ubiquitination mechanistically interferes with necrosome formation. Depending on the actual localization of the C-terminus of RIPK3 in the necrosome, it is conceivable that increased ubiquitination at K518 upon USP22 depletion could either hide or sterically hinder the RIPK3 RHIM or could impede with protein-protein interactions. This is supported by the line of evidence demonstrating widely unstructured sequences surrounding the RIPK1 and RIPK3 RHIM domains, affecting spontaneous RHIM-dependent clustering [234].

Interestingly, our analysis could show that the extent of RIPK1 phosphorylation as well as RIPK1-RIPK3 D160N, K518R and 3xKR interactions were altered upon TBZ-induced necroptosis when compared to RIPK WT-expressing cells. The D160N mutation renders RIPK3 catalytically inactive [188], blocking RIPK3 phosphorylation and subsequent interaction with MLKL, which in turn might lead to an accumulation of phosphorylated RIPK1 and thus, increased RIPK3 binding, akin to previous studies utilizing RHIM-mutated RIPK3 V448P [352]. Additionally, necrosome formation involving RIPK3 K518R displayed increased RIPK1 and phosphorylated MLKL binding, which is line with the increased amount of necroptotic cell death. Interestingly, necrosome immunoprecipitations from RIPK3 3xKR-expressing HeLa cells demonstrated reduced RIPK1 binding, despite immunoprecipitated phosphorylated MLKL levels being similar to those found in the RIPK3 K518R necrosome. Accordingly, experiments investigating necrosome formation in HT-29 cells demonstrated reduced levels of phosphorylated RIPK1 both in the K518R- and 3xKR-expressing cells. One possible explanation could be the notion that RIPK3 K518R and 3xKR both become rapidly insoluble upon necroptosis progression and that RIPK3 K518R- and 3xKR-associated phosphorylated RIPK1 might be complexed and trapped in the insoluble fractions.

In the present study, increased RIPK1 phosphorylation could be detected in HeLa and HT-29 cells expressing RIPK3 D160N. At the same time, increased RIPK1 phosphorylation could be detected in HeLa cells expressing RIPK3 K518R and 3xKR, whereas on the other hand RIPK1 phosphorylation was reduced in HT-29 cells expressing RIPK3 K518R and 3xKR. Even though RIPK3 D160 could affect RIPK1 phosphorylation by inhibiting RIPK3 phosphorylation, we cannot exclude retrograde signaling towards RIPK1 from RIPK3 K518R and 3xKR or upon USP22 depletion. Furthermore, cell line-specific effects on necrosome formation and RIPK1 phosphorylation might be involved too, although RIPK3-expressing HeLa cells are able to execute TBZ-induced necroptosis. Given the fact that ubiquitinated RIPK1 levels remained unchanged upon loss of USP22, necrosome formation is most likely not affected by altered

RIPK1 ubiquitination levels. As several E3 ligases are known to negatively regulate necroptosis via ubiquitination [238, 341], USP22 could also regulate necrosome formation by dynamically exchanging the composition or abundance of poly-ubiquitin chains on RIPK3, thereby affecting RIPK1/RIPK3 complex formation and subsequent MLKL phosphorylation.

6.4 USP22 affects RIPK3 phosphorylation during TBZ-induced necroptosis

Up to date only two studies further describe a prominent RIPK3 band shift upon necroptosis progression in detail [189, 197]. Interestingly, we could identify a TBZ- and USP22-dependent RIPK3 phosphorylation, marked by a prominent slower migrating RIPK3 band shift, matching these observations. Since re-expression of USP22 WT, but not C185S, into the USP22 KO background could reduce RIPK3 phosphorylation to its normal levels, it is quite likely that the DUB activity of USP22 plays a crucial role in regulating this RIPK3 modification. He *et al.* could show that the high molecular weight RIPK3 signals might correspond to S199 phosphorylated RIPK3 [189]. Hence, it would be interesting to elucidate whether USP22 depletion might lead to increased RIPK3 S199 phosphorylation in future studies.

RIPK3 phosphorylation was markedly reduced upon inhibition of RIPK3 ubiquitination in RIPK3 K518R and even further decreased in cells expressing RIPK3 3xKR, whereas necroptotic cell death was increased. This suggests that USP22-dependent RIPK3 (de)ubiquitination might be a prerequisite for TBZ-induced necrosome formation and RIPK3 phosphorylation. Moreover, as the K518R and 3xKR mutant became more rapidly insoluble compared to RIPK3 WT, USP22-dependent changes in RIPK3 phosphorylation and ubiquitination might affect RIPK3 oligomerization and localization during necroptosis. However, if this is partially responsible for the changes in necroptotic signaling needs to be further elucidated. Furthermore, USP22-mediated changes in RIPK3 phosphorylation do most likely not restrict the ability of RIPK3 to induce necroptotic cell death, as RIPK3 K518R and 3xKR-expressing cells displayed increased necroptotic cell death, whereas the RIPK3 shift was dramatically reduced. This matches to previous studies using a RIPK3 S199A mutant, which was still able to induce necroptotic cell death, despite absent RIPK3 shift [197].

Murine RIPK3 displays a band shift of RIPK3 under resting conditions, which is absent in human RIPK3 and can only be induced by extracellular stimuli [197], such as TBZ. Unlike murine RIPK3, human RIPK3 phosphorylation that leads to the mobility shift is not critical for its necroptotic function [197], highlighting evolutionary-dependent differences in RIPK3 modifications and necroptotic signaling. In line with this, we could not identify a role for USP22 in regulating necroptosis in murine cell lines, suggesting USP22-dependent changes on RIPK3 phosphorylation and necroptotic signaling specifically for human tumor cells.

The collective results are presented in our working model (Fig. 34). In conclusion, we have deciphered a novel role of USP22 in controlling necroptotic cell death as well as RIPK3 ubiquitination and phosphorylation. In detail, TBZ-induced necroptosis is delayed upon loss of USP22 in human tumor cell lines, which is accompanied by an increase in RIPK3 phosphorylation and ubiquitination of RIPK3 K518. We identified RIPK3 K518 as a crucial USP22-dependent ubiquitin acceptor site for regulating necroptosis. The USP22-mediated changes in necroptotic signaling are either caused by direct (de)ubiquitination of RIPK3 by USP22 or indirectly, for instance, by regulating RIPK3 autophosphorylation and/or the activity of RIPK3-associated E3 ligases or kinases. The present study further highlights the pivotal role of DUBs in controlling necroptosis and cell fate and provide novel insights in how PTMs of RIPK3 alter necroptotic signaling in human diseases.

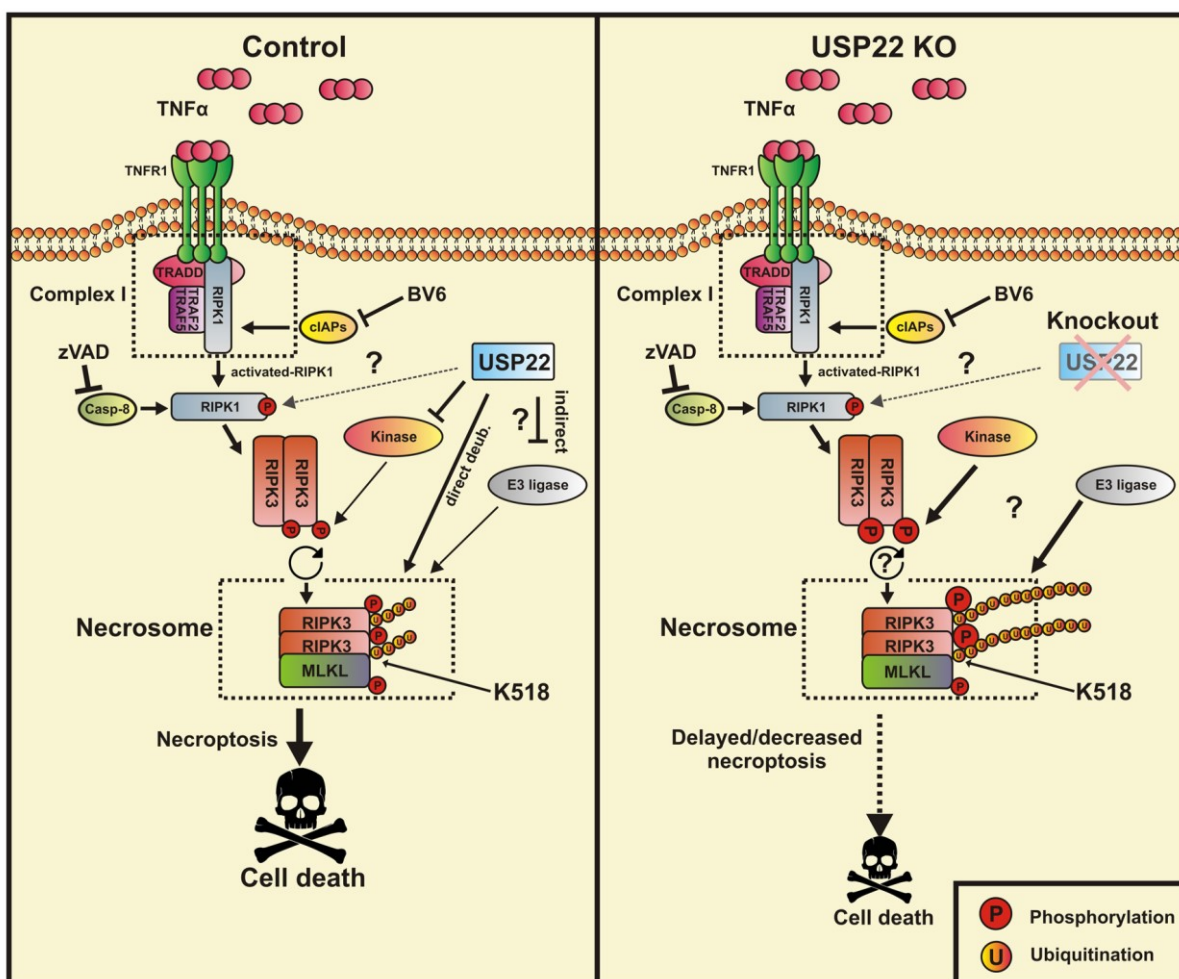


Figure 34 USP22 controls necroptotic cell death by regulating RIPK3 phosphorylation and RIPK3 K518 ubiquitination. Schematic overview of the putative mechanistic roles of USP22 in necroptosis. Activation of TNFR1 by TNF α upon caspase-8 inhibition by zVAD.fmk and cIAP1/2 inactivation by BV6, induces RIPK1/3 activation, necrosome formation and execution of necroptosis. In the absence of USP22 KO, TBZ-induced necroptosis is delayed, accompanied by increased RIPK3 phosphorylation and ubiquitination of RIPK3 at lysine 518. This USP22-mediated necroptotic signaling could be caused either by direct USP22-mediated (de)ubiquitination of RIPK3 and/or indirectly by, for example, regulating RIPK3 autophosphorylation or the activity of RIPK3-associated E3 ligases or kinases. Additionally, USP22-mediated retrograde effects on RIPK1 phosphorylation and RIPK3 oligomerization might be involved as well.

6.5 Limitations and outlook

6.5.1 Dissecting the signaling cascade leading to delayed necroptotic cell death upon loss of USP22

In order to dissect the mechanisms behind the delayed TBZ-induced necroptotic cell death upon loss of USP22, we investigated the classical necroptotic signaling pathway and its central players, including TNFR1 activation, complex-II formation as well as the necrosome, which is indeed a pivotal checkpoint for necroptotic signaling [231, 234]. However, necrosome formation does not represent a point of no return in the execution of necroptotic signaling [175, 176]. Following necrosome formation, pro-necroptotic MLKL presumably dissociates from the necrosome and translocates to the plasma membrane where several proteins and complexes are described to further guide and regulate MLKL-induced necroptotic cell death [176]. For instance, PIPs have been shown to interact with positively charged amino acids in the 4HB of MLKL, mediating MLKL plasma membrane binding [199, 259, 264]. On the other hand, RGMb has been shown to block MLKL membrane association [271]. At the same time, several studies could demonstrate an accumulation of the ESCRT-III machinery at the damaged plasma membrane, facilitating the shedding of phosphorylated MLKL oligomers in necroptotic vesicles and enabling plasma membrane repair, thus counteracting necroptosis [272-274]. Future studies should therefore investigate the potential effects of USP22 on downstream signaling components of necroptotic signaling. As ubiquitin remnant profiling also revealed three novel USP22- and TBZ-dependent modified lysine residues in MLKL, it is tempting to speculate that potential USP22-dependent MLKL ubiquitination plays a role in the above mentioned downstream signaling, possibly being partially responsible for the delayed necroptotic cell death. Nevertheless, a potential USP22-dependent MLKL ubiquitination during TBZ-induced necroptosis needs to be experimentally confirmed and functionally characterized in detail. USP22 is described to compete with other DUBs, such as USP27x or USP51, for ENY2- and ATXN7L3- dependent activation or to cooperate with USP13 to regulate interferon signaling. Hence, compensatory mechanisms are quite conceivable in mediating the delay in necroptotic cell death. Double KO cells, targeting USP22 and DUBs known to cooperate or to compete with USP22, could be utilized to determine if possible compensatory mechanisms are involved in mediating the delay in necroptotic cell death.

6.5.2 Detailed investigation of USP22-mediated RIPK3 ubiquitination during necroptosis progression

As ubiquitin remnant profiling revealed three novel USP22- and TBZ-dependent modified lysine residues in RIPK3 (K42, K352 and K518), we therefore utilized *in vivo* deubiquitinating

assays and TUBEs to confirm increased ubiquitination of RIPK3 upon loss of USP22 expression and TBZ-induced necroptosis. Moreover, we identified RIPK3 K518 as a pivotal USP22-dependent ubiquitin acceptor site for regulation of necroptotic signaling. However, with this approach, we were still unable to identify the ubiquitin linkage type deposited on RIPK3 upon loss of USP22 and TBZ-induced necroptosis. In particular, performing an *in vitro* deubiquitinating assay could be performed to determine if USP22 is directly deubiquitinating RIPK3, whereas an Ubiquitin Chain Restriction Analysis (UbiCREST) could be used to decipher the ubiquitin linkages present in the poly-ubiquitin chains conjugated to RIPK3 upon necroptosis progression. However, it should be noted that, the analysis of recombinant *in vitro* protein extracts are often limited due to lack of PTMs, such as phosphorylation [353, 354]. Furthermore, this assay would also exclude potential cooperative interplays between USP22 and other DUBs, since USP22 is also described to cooperate with USP13 in interferon signaling [95]. Nevertheless, since phosphorylation driven activity for USP22 has not yet been described and a potential role for USP13 in necroptosis needs to be determined, we can only speculate if this could play a role in mediating the TBZ-dependent (de)ubiquitination of RIPK3. On the other hand, the potential of UbiCREST lies in the usage of mammalian cell lysates or live cells, retaining the DUB in its native form, including interacting proteins required for correct folding or multimeric assembly, as well as potential modification such as phosphorylation, allowing to monitor the DUB activity within the intracellular environment [353]. USP22 is widely described to catalyze the removal of mono-ubiquitination as well as K48- and K63-conjugated poly-ubiquitin chains [84, 91-94], whereas a recent study described the removal of K6-, K11-, K27-, K29-, K33- and K63-conjugated poly-ubiquitin chains [346]. At the same time, RIPK3 is described to be regulated by K33-, K48- and K63-conjugated poly-ubiquitin chains in necroptotic signaling. Since the USP22-mediated ubiquitin signal on RIPK3 is most likely a non-proteolytic form of ubiquitination, it is conceivable that RIPK3 is modified with K33- and K63-linked poly-ubiquitination upon loss of USP22 and TBZ-induced necroptosis. Conclusively, this would provide a detailed analysis of the role of USP22 in necroptotic signaling, potentially narrowing down the ubiquitin linkage type and potential E3 ligases or DUBs involved in RIPK3 (de)ubiquitination upstream in signaling which could be affected by USP22.

6.5.3 Unraveling the effects of USP22-mediated changes on RIPK3 phosphorylation

One limitation of this study is that we have not yet deciphered the USP22-mediated changes on RIPK3 phosphorylation. In the absence of USP22, phosphorylated RIPK3 was prominently increased, however this RIPK3 band shift and its consequences are barely studied in the current literature [189, 197]. We could detect a delay in TBZ-induced necroptosis accompanied

with increased RIPK3 phosphorylation in the USP22 KO background, which implies that the increase in RIPK3 phosphorylation is most likely not connected to its ability to induce necroptotic cell death. As it is highly unlikely that USP22, as a DUB, is directly responsible for the changes in RIPK3 phosphorylation, future studies should therefore investigate which upstream kinases trigger USP22-dependent RIPK3 phosphorylation upon necroptosis induction. It could therefore be promising to perform mass-spectrometry (MS)-based phosphoproteomic analysis of necroptotic players. This would not only help to identify which phospho-sites are modified in RIPK3 upon loss of USP22 and TBZ-induced necroptosis, but would also help to clarify if there is less active phosphorylated MLKL (T357/S358), as we could see a decrease in phosphorylated MLKL in USP22 KO HeLa cells, whereas USP22 KO HT-29 cells displayed comparable levels of phosphorylated MLKL. Moreover, we could monitor effects on potential other upstream kinases or components which are involved in mediating the USP22-dependent changes on necroptotic signaling. Finally, performing phospho-proteomic analysis in the context of RIPK3 K518R- or 3xKR-expressing cells would help to monitor mutational-, cell line- and TBZ-dependent effects on RIPK3 and RIPK1 phosphorylation.

6.5.4 Evaluating the effects of USP22 on necroptosis-induced antitumor immunity

To date, two strategies have been widely described to trigger antitumor immunity by necroptosis induction. Vaccination with necroptotic tumor cells initiates a severe DAMP release by the necroptotic cells, facilitating the maturation of bone marrow-derived dendritic cells (BMDCs), CD8⁺ T cell cross-priming and excessive IFN- γ production, triggering cytotoxic anticancer effects [355]. On the other hand, vaccination with necroptotic fibroblasts initiates, independently of DAMPs, the release of NF- κ B-derived signals and subsequent dendritic cell activation as well as elevated antigen loading and robust CD8⁺ T cell-mediated tumor control [356]. Nevertheless, since we could not demonstrate a functional role for USP22 in murine cells, current mice based necroptotic animal models are unsuitable to monitor the effects of USP22 on necroptotic signaling and antitumor immunity. Future studies should therefore involve tumor spheroids generated from, for instance, human HT-29, HCT116 or Caco-2 cells, which all have been previously described to be able to form spheroids in culture [357, 358]. Tumor spheroids not only more closely resemble *in vivo* tumors but they can also be used to monitor changes in the tumor microenvironment and may thus be a superior *in vitro* cancer model compared to monolayer cultures [357].

Several studies could demonstrate pro-tumoral effects of necroptosis. For instance, the induction of necroptosis in human endothelial cells is described to promote tumor cell extravasation and metastasis [303]. Moreover, soluble E-cadherin is released from the

necroptotic cell surface, interfering with intercellular adhesion junctions, enhancing angiogenesis and matrix metalloproteinases activity, thus promoting tumor cell invasion and metastasis [359]. Since we could demonstrate a perturbed necroptotic signaling upon loss of USP22, it would be interesting to investigate potential USP22-mediated effects on the pro-tumoral effects of necroptosis, either in the context of aberrant USP22 expression or utilizing a USP22 specific inhibitor. However, as a cysteine protease, the catalytic domain of USP22 is conserved amongst the USP family members. Hence, the generation of a specific USP22 inhibitor is challenging and up to date, no specific inhibitor has been described yet. Conclusively, this approach would provide a detailed analysis of the potential functional relevance of USP22 in necroptosis-induced antitumor immunity and clarifying a possible exploitation for clinical studies.

7 Summary (Deutsche Zusammenfassung)

Ubiquitinierung, d.h. die kovalente post-translationale Modifikation von Substraten mit einem oder mehreren Ubiquitin-Molekülen, kontrolliert den Proteinabbau, die zelluläre Signaltransduktion, Transkription und viele weitere zelluläre Prozesse. Die überwiegende Mehrheit der zellulären Proteine wird während seiner Lebensdauer ubiquitiniert. Die Ubiquitinierung kann als einzelne Modifikation (Mono-Ubiquitinierung) oder durch Verknüpfung in Poly-Ubiquitin-Ketten über interne Lysin(K)-Reste oder über den Initiator Methionin (lineare Ketten) erfolgen. Eine hochentwickelte enzymatische Kaskade, bestehend aus E1 Ubiquitin-aktivierenden Enzymen, E2 Ubiquitin-konjugierenden Enzymen und E3 Ubiquitin-Ligasen, reguliert die kovalente Bindung von Mono-Ubiquitin- oder Poly-Ubiquitin-Molekülen an das Zielsubstrat. Ubiquitin selbst besitzt acht Ubiquitinierungsstellen – sieben Lysin-Reste (K6, K11, K27, K29, K33, K48 und K63) sowie ein primäres Amin am N-Terminus (M1) – von denen alle an der Bildung von Poly-Ubiquitinketten beteiligt sein können. Da die internen Lysine sich alle an verschiedenen Positionen auf der Oberfläche des Proteins befinden, nimmt jede der acht möglichen Ubiquitin-Verknüpfungen eine strukturell unterschiedliche Konformation ein und erzeugt dadurch einen komplexen und vielschichtigen Ubiquitin-Code. Proteine mit Ubiquitin-Bindungsdomänen (UBDs) erkennen spezifisch strukturell unterschiedliche Poly-Ubiquitinketten und übersetzen damit den Ubiquitin-Code in unterschiedliche zelluläre Funktionen und Signale. Demgegenüber stehen mehrere spezialisierte Familien von Proteasen, die deubiquitinierenden Enzyme (DUBs). DUBs katalysieren die Entfernung von hochkomplexen Ubiquitin-Signalen, die während des Ubiquitinierungsprozesses erzeugt wurden und fungieren somit als dynamischer Gegenspieler zum Prozess der Ubiquitinierung. Durch Modulierung der Ubiquitin-Abundanz innerhalb der Poly-Ubiquitinketten oder am Protein selbst, werden zuvor spezifische Konformationen und Strukturen verändert, was die Bindung und die damit einhergehende Signalweiterleitung durch z.B. UBD Proteinen unterbricht.

Die Ubiquitin-spezifische Protease 22 (USP22) gehört zur USP-Superfamilie. USPs bilden die größte Unterfamilie der DUBs, bestehend aus 54 Mitgliedern beim Menschen, hoch konserviert in Funktion und Struktur. USP22 wird ubiquitär exprimiert und hauptsächlich im Zellkern angereichert. Zwei Hauptdomänen prägen die Struktur von USP22, das N-terminale Zink-Finger-Motiv sowie eine katalytisch aktive, C-terminale, Ubiquitinhydrolase Domäne. USP22 wurde ursprünglich als Teil eines 11-Gen-Expressions-Signaturprofils beschrieben, dass die Metastasierung, das Wiederauftreten und den Tod des Tumors nach Therapie in einer Vielzahl von Tumorentitäten vorhersagen konnte. Während einige Studien in Speiseröhren-, Darm-, Brust-, Eierstock-, Magen- und Bauchspeicheldrüsenkrebs eine USP22-Hochregulierung beobachten konnten, zeigten andere Studien unter Verwendung von

Gensequenzierungs- sowie mRNA-Expressionsdatenanalysen eine USP22-Deregulierung, -Mutation oder -Deletion in den gleichen Krebsarten. Dennoch scheinen beide Untergruppen von Krebsarten nebeneinander zu existieren und zur Onkogenese beizutragen, was auf funktionelle Implikationen für die Krebsentstehung und -Progression hindeutet, die durch Variationen der USP22-Expressionsniveaus streng reguliert werden. Da die Expression von USP22 eng mit neurodegenerativen Erkrankungen, Karzinogenese und einer niedrigen Überlebensrate von Patienten bei einer Vielzahl von Tumorarten assoziiert ist, wird die gezielte Beeinflussung von USP22 oder seiner nachgeschalteten Effektoren als eine vielversprechende Strategie für die Krebstherapie angesehen. Heute ist klar, dass USP22 starke tumor- und kontextabhängige Funktionen aufweist und abhängig von der Tumorentität, entweder onkogene oder Tumorsuppressor-ähnliche Eigenschaften besitzt.

USP22 ist zusammen mit ATXN7L3, ATXN7 und ENY2 Teil des deubiquitinierenden Moduls (DUBm) des humanen Spt-Ada-Gcn5-Acetyltransferase(SAGA)-Komplexes. Innerhalb dieses Komplexes besteht die Hauptfunktion von USP22 in der Deubiquitinierung des Histons H2B K120 und des Histons H2A K119. Durch der daraus resultierenden Remodellierung von Chromatin wird die Gentranskription reguliert. Darüber hinaus konnten kürzlich veröffentlichte Studien weitere funktionale Rollen für USP22 nachweisen. Beispielsweise konnte gezeigt werden, dass USP22 zelluläre Prozesse wie Zellwachstum und -differenzierung, Tumorentwicklung und Zelltod steuert. Die von USP22 vermittelte Regulation von apoptotischem Zelltod wird durch die Deubiquitinierung und Stabilisierung von SIRT1 initiiert. SIRT1-Stabilisierung führt zur Deacetylierung und transkriptionellen Aktivierung von TP53-Zielgenen oder zur deacetylierungsabhängigen c-Myc-Stabilisierung, wodurch Apoptose inhibiert wird.

Eines der Markenzeichen von Krebs ist die Umgehung von Zelltod, insbesondere der Apoptose, einer Form des programmierten Zelltods. Ein vielversprechender therapeutischer Ansatz zur Überwindung von Apoptose-Resistenz in Tumorzellen ist die Induktion von Nekroptose. Nekroptose, lange Zeit als zufällige Form des Zelltods stigmatisiert, ist eine Form der regulierten Nekrose mit einer einzigartigen und definierten Signaltransduktionskaskade. Jedoch ist die komplette nekroptotische Signalkaskade bis heute nicht völlig aufgeklärt. Voraussetzung für die nekroptotische Signalweiterleitung ist zunächst die Hemmung oder Deletion der E3-Ubiquitin-Ligasen cIAPs und der Cysteinprotease Caspase-8. Nekroptose ist durch ein reguliertes, phosphorylierungsabhängiges Wechselspiel zwischen RIPK1, RIPK3 und MLKL gekennzeichnet. Aktivierung von TNFR1 durch Bindung des TNF α -Liganden induziert die Aktivierung von RIPK1. Anschließend interagieren aktiviertes RIPK1 und RIPK3 durch ihre RHIM-Domänen, was eine gegenseitige Auto- und Trans-Phosphorylierung bewirkt. Nachfolgend bildet sich ein Heteroamyloid-Komplex, bestehend aus Kinase-aktiviertem RIPK1-RIPK3, auch bekannt als Nekrosom. Dementsprechend induziert die RIPK3-

Phosphorylierung an S227 die Rekrutierung von MLKL in das Nekrosom, wodurch MLKL an T357 und S358 phosphoryliert wird. Die RIPK3-vermittelte MLKL-Rekrutierung und anschließende Phosphorylierung fördert höchstwahrscheinlich die Umwandlung von MLKL aus einer ruhenden in eine pro-nekroptotische, oligomere Form, wodurch Membrantranslokation und Permeabilisierung ermöglicht werden, was letztlich zum Tod der Zelle führt. Abgesehen von Phosphorylierungen werden auch die nekroptotischen Schlüsselakteure RIPK1 und RIPK3 durch Poly-Ubiquitinketten modifiziert, wodurch die nekroptotische Signaltransduktion beeinflusst wird. Beispielsweise wurde gezeigt, dass RIPK3-Ubiquitinierung an K5 die RIPK1-RIPK3-Komplexbildung fördert und Nekroptose verstärkt, was wiederum von der DUB A20 negativ reguliert wird. Darüber hinaus ist bekannt, dass die E3-Ubiquitin-Protein-Ligase PELI1 die K48-konjugierte Poly-Ubiquitinierung von Kinase-aktiviertem RIPK3 vermittelt und dadurch zum proteasomalen Abbau von RIPK3 führt.

Unsere Forschungsgruppe führte kürzlich einen siRNA-basierten DUB Screen in HT-29 Kolonkarzinomzellen durch, bei dem $\text{TNF}\alpha$ (T), Smac-Mimetika (BV6; B) und zVAD.fmk (Z) vermittelte Nekroptose induziert wurde. Dies ermöglichte die Identifikation von neuen DUBs, die an der Kontrolle der nekroptotischen Signalübertragung beteiligt sind. Unter den dadurch identifizierten DUBs hemmte USP22 die durch TBZ-vermittelte Nekroptose in HT-29 Zellen am stärksten. Das Ziel dieser Arbeit war, basierend auf den Ergebnissen des siRNA-Screens, die funktionelle Rolle von USP22 im nekroptotischen Zelltodsignalweg zu charakterisieren.

Um die Ergebnisse des siRNA-Screens zunächst zu validieren, wurden, unter Verwendung von CRISPR/Cas9 Technologie, USP22 knockout (KO) Zellen generiert. Diese wurden im Anschluss auf TBZ-induzierten nekroptotischen Zelltod mittels fluoreszenzbasierter Mikroskopie getestet. USP22 KO HT-29 Zellen zeigten einen stark reduzierten und verzögerten TBZ-induzierten nekroptotischen Zelltod im Vergleich zu HT-29 Kontrollzellen. Um zu beweisen, dass es sich bei der beobachteten Reduktion im TBZ-induzierten Zelltod tatsächlich um Nekroptose handelte, wurde Zelltod in der Anwesenheit pharmakologischer Nekroptoseinhibitoren ermittelt. Tatsächlich konnten die Inhibitoren zeigen, dass es sich bei dem Zelltod spezifisch um Nekroptose handelte. Interessanterweise konnte eine Reexpression des USP22-Wildtyps (WT) in USP22 KO HT-29 Zellen die Zellen für TBZ-induzierte Nekroptose resensibilisieren, während eine Rekonstitution mit der katalytisch inaktiven USP22 Mutante Cys185Ser die Anfälligkeit der Zellen für TBZ-induzierte Nekroptose nicht wiederherstellen konnte, was der DUB-Funktion von USP22 eine zentrale Rolle bei der Regulierung des nekroptotischen Zelltodsignalwegs zusprach. Durch weitere Zelltodmessungen sowie Western Blotting Analysen konnten wir weiterhin ausschließen, dass der Knockout von USP22 $\text{TNF}\alpha$ -induzierte Nuklearfaktor-Kappa B ($\text{NF-}\kappa\text{B}$)-Signaltransduktion oder $\text{TNF}\alpha$ -vermittelte extrinsische Apoptose beeinträchtigt. Wir erweiterten unsere

Untersuchungen auf RIPK3-exprimierende HeLa Zellen sowie auf akute lymphoblastische Leukämie (ALL) Jurkat Zellen. In beiden Fällen führte ein USP22 KO zu einer signifikanten Reduktion von TBZ-induzierter Nekroptose. Um zu untersuchen, ob die regulatorische Funktion von USP22 in Krebszelllinien der Maus konserviert ist, untersuchten wir den Effekt einer USP22 Deletion auf TBZ-induzierte Nekroptose in embryonalen Fibroblasten der Maus (MEF) bzw. in den Makrophagenzelllinien Raw264.7 oder J774A1. Tatsächlich konnten wir keine Unterschiede zwischen USP22 KO und Kontrollzellen ermitteln, was die Schlussfolgerung ermöglichte, dass USP22 sehr wahrscheinlich spezifisch Nekroptose in humanen Tumorzelllinien und nicht in murinen Tumorzellen reguliert.

Im nächsten Schritt interessierten wir uns dafür, wie USP22 den molekularen Signalweg der Nekroptose reguliert. Hierfür untersuchten wir neben dem Expressionslevel das Phosphorylierungsniveau und den Ubiquitinierungsstatus der nekroptotischen Kernmaschinerie (RIPK1, RIPK3 und MLKL) in HT-29 USP22 KO Zellen während TBZ-induzierter Nekroptose. Interessanterweise förderte eine USP22 Deletion nicht nur die Ubiquitinierung von RIPK3, sondern auch dessen Phosphorylierung während TBZ-induzierter Nekroptose, wohingegen basale Expressionslevel größtenteils unbeeinflusst blieben. RIPK3 wird während voranschreitender Nekroptose stark mit verschiedenen posttranslationalen Modifikationen, wie Ubiquitinierung und Phosphorylierung, modifiziert. Festzustellen war dies durch mehrfache, langsamere migrierende Western Blot Banden, die deutlich verstärkt in mit TBZ-behandelten USP22 KO Zellen auftraten. Durch einen Phosphatase-Verdau mit anschließender Western Blot Analyse bestätigten wir, dass es sich hierbei hauptsächlich um erhöhte RIPK3 Phosphorylierung handelte. Ko-Immunpräzipitationsexperimente in HT-29 und HeLa Zellen konnten eine TBZ-unabhängige Interaktion zwischen RIPK3 und USP22 zeigen, was eine funktionelle Relevanz von USP22 auf RIPK3 Phosphorylierung und Ubiquitinierung untermauerte. Durch *in vivo* (De)Ubiquitinierungs-Immunpräzipitationen sowie Tandem-Ubiquitin-Bindungseinheiten (TUBE)-Pulldowns konnten wir eine erhöhte RIPK3 Ubiquitinierung in USP22 KO Zellen schließlich während TBZ-induzierter Nekroptose bestätigen. Um diese Ergebnisse weiter zu untermauern, führten wir eine massenspektrometrische Untersuchung zur Bestimmung des globalen Ubiquitinierungsstatus in HT-29 USP22 KO Zellen während TBZ-induzierter Nekroptose durch. Bemerkenswerterweise konnten wir drei neue potentielle USP22-regulierte Ubiquitinierungsstellen in RIPK3 (K42, K351 und K518) während TBZ-induzierter Nekroptose identifizieren. Um die funktionelle Bedeutung der TBZ- und USP22-abhängigen RIPK3-Lysinreste für die RIPK3-Ubiquitinierung und die nekroptotische Signalgebung zu untersuchen, generierten wir RIPK3-K-zu-R-Mutanten (K42R, K351R und K518R), Doppelmutanten (K42R/K351R; 2xKR) und dreifach RIPK3-Mutanten (K42R/K351R/K518R; 3xKR). Neben den RIPK3-K-zu-R-Mutanten exprimierten wir weiterhin WT RIPK3 und

katalytisch-inaktives D160N RIPK3, um mögliche Auswirkungen auf das RIPK3-Ubiquitinierungslevel sowie den nekroptotischen Signalweg genauer beurteilen zu können. Der genetische Knock-in von RIPK3 K518R sowie 3xKR bewirkte nicht nur einen Anstieg an phosphoryliertem MLKL, sondern damit einhergehend auch einen prägnanten Anstieg an TBZ-induziertem, nekroptotischen Zelltod. Erstaunlicherweise konnten wir, im Vergleich zu WT exprimierenden RIPK3 Zellen, eine Reduktion der RIPK3 Phosphorylierung feststellen, was sich durch eine deutliche Verminderung des markanten, TBZ-induzierten, höhermolekularen RIPK3 Bandenmuster bemerkbar machte. Darüber hinaus zeigten *in vivo* Ubiquitinierungs-Immunpräzipitationen, dass eine Mutation von K518 in RIPK3 die nekroptose-assoziierte RIPK3-Ubiquitinierung deutlich reduzierte. Wie erwartet, führte der siRNA-vermittelte Knockdown von USP22 in RIPK3 WT und 2xKR-exprimierenden HeLa-Zellen, zu einer Reduktion des nekroptotischen Zelltods, wohingegen in RIPK3 K518R- und 3xKR-exprimierende Zellen keine zusätzliche Verringerung feststellbar war, was die Relevanz von USP22 bei der Kontrolle der RIPK3 K518-Ubiquitinierung während TBZ-induzierter Nekroptose bestätigte. Abschließend konnten wir, gemessen an der Interaktion zwischen phosphoryliertem MLKL und RIPK3, eine verstärkte Nekrosombildung in RIPK K518R- und 3xKR-exprimierenden Zellen durch Immunpräzipitationsexperimente demonstrieren.

Die vorliegende Studie ermöglichte die Identifizierung von USP22 als neuen, pro-nekroptotischen Regulator. Wir konnten zeigen, dass USP22 sowohl RIPK3 Ubiquitinierung als auch RIPK3 Phosphorylierung in menschlichen Tumorzellen reguliert. Wir identifizierten RIPK3 K518 als eine entscheidende USP22-abhängige Ubiquitin-Akzeptorstelle des nekroptotischen Zelltodsignalwegs. Die USP22-vermittelten Veränderungen in der nekroptotischen Signalübertragung werden entweder durch direkte (De)Ubiquitinierung von RIPK3 durch USP22 oder indirekt durch Regulation der RIPK3-Autophosphorylierung und/oder der Aktivität von RIPK3-assoziierten E3-Ligasen, bzw. Kinasen verursacht. Die vorliegende Studie unterstreicht nicht nur die zentrale Rolle von DUBs in der Regulation von Nekroptose und Zellschicksal, sie liefert darüber hinaus neue Erkenntnisse, wie PTMs an RIPK3 die nekroptotische Signalübertragung verändern. Da Nekroptose eine zentrale Rolle in verschiedensten Krankheitsbildern, wie beispielsweise Krebs, axonalen Degenerationen, Ischämie und akuten sowie chronischen Entzündungen einnimmt, hat die Identifikation von USP22 als pro-nekroptotischer Regulator sehr wahrscheinlich Implikationen für weitere Studien, die diesen Krankheitsbildern zu Grunde liegen.

8 References

1. Schulman, B.A. and J.W. Harper, Ubiquitin-like protein activation by E1 enzymes: the apex for downstream signalling pathways. *Nat Rev Mol Cell Biol*, 2009. 10(5): p. 319-31.
2. Ye, Y. and M. Rape, Building ubiquitin chains: E2 enzymes at work. *Nat Rev Mol Cell Biol*, 2009. 10(11): p. 755-64.
3. Buetow, L. and D.T. Huang, Structural insights into the catalysis and regulation of E3 ubiquitin ligases. *Nat Rev Mol Cell Biol*, 2016. 17(10): p. 626-42.
4. Ciechanover, A., et al., "Covalent affinity" purification of ubiquitin-activating enzyme. *J Biol Chem*, 1982. 257(5): p. 2537-42.
5. Hunt, L.T. and M.O. Dayhoff, Amino-terminal sequence identity of ubiquitin and the nonhistone component of nuclear protein A24. *Biochem Biophys Res Commun*, 1977. 74(2): p. 650-5.
6. Hershko, A., et al., Components of ubiquitin-protein ligase system. Resolution, affinity purification, and role in protein breakdown. *J Biol Chem*, 1983. 258(13): p. 8206-14.
7. Akutsu, M., I. Dikic, and A. Bremm, Ubiquitin chain diversity at a glance. *J Cell Sci*, 2016. 129(5): p. 875-80.
8. Komander, D. and M. Rape, The ubiquitin code. *Annu Rev Biochem*, 2012. 81: p. 203-29.
9. Mevissen, T.E.T. and D. Komander, Mechanisms of Deubiquitinase Specificity and Regulation. *Annu Rev Biochem*, 2017. 86: p. 159-192.
10. Swatek, K.N. and D. Komander, Ubiquitin modifications. *Cell Res*, 2016. 26(4): p. 399-422.
11. Hershko, A. and A. Ciechanover, The ubiquitin system. *Annu Rev Biochem*, 1998. 67: p. 425-79.
12. Chen, Z.J. and L.J. Sun, Nonproteolytic functions of ubiquitin in cell signaling. *Mol Cell*, 2009. 33(3): p. 275-86.
13. Haas, A.L., et al., Interferon induces a 15-kilodalton protein exhibiting marked homology to ubiquitin. *J Biol Chem*, 1987. 262(23): p. 11315-23.
14. Flotho, A. and F. Melchior, Sumoylation: a regulatory protein modification in health and disease. *Annu Rev Biochem*, 2013. 82: p. 357-85.
15. Enchev, R.I., B.A. Schulman, and M. Peter, Protein neddylation: beyond cullin-RING ligases. *Nat Rev Mol Cell Biol*, 2015. 16(1): p. 30-44.
16. Guzzo, C.M., et al., RNF4-dependent hybrid SUMO-ubiquitin chains are signals for RAP80 and thereby mediate the recruitment of BRCA1 to sites of DNA damage. *Sci Signal*, 2012. 5(253): p. ra88.
17. Maghames, C.M., et al., NEDDylation promotes nuclear protein aggregation and protects the Ubiquitin Proteasome System upon proteotoxic stress. *Nat Commun*, 2018. 9(1): p. 4376.
18. Ohtake, F., et al., Ubiquitin acetylation inhibits polyubiquitin chain elongation. *EMBO Rep*, 2015. 16(2): p. 192-201.
19. Qiu, J., et al., Ubiquitination independent of E1 and E2 enzymes by bacterial effectors. *Nature*, 2016. 533(7601): p. 120-4.
20. Herhaus, L. and I. Dikic, Expanding the ubiquitin code through post-translational modification. *EMBO Rep*, 2015. 16(9): p. 1071-83.
21. Swaney, D.L., et al., Global analysis of phosphorylation and ubiquitylation cross-talk in protein degradation. *Nat Methods*, 2013. 10(7): p. 676-82.
22. Hornbeck, P.V., et al., PhosphoSitePlus, 2014: mutations, PTMs and recalibrations. *Nucleic Acids Res*, 2015. 43(Database issue): p. D512-20.
23. Kazlauskaitė, A., et al., Parkin is activated by PINK1-dependent phosphorylation of ubiquitin at Ser65. *Biochem J*, 2014. 460(1): p. 127-39.

24. Lazarou, M., et al., The ubiquitin kinase PINK1 recruits autophagy receptors to induce mitophagy. *Nature*, 2015. 524(7565): p. 309-314.
25. Shiba-Fukushima, K., et al., Phosphorylation of mitochondrial polyubiquitin by PINK1 promotes Parkin mitochondrial tethering. *PLoS Genet*, 2014. 10(12): p. e1004861.
26. Okatsu, K., et al., Phosphorylated ubiquitin chain is the genuine Parkin receptor. *J Cell Biol*, 2015. 209(1): p. 111-28.
27. Hochstrasser, M. and A. Varshavsky, In vivo degradation of a transcriptional regulator: the yeast alpha 2 repressor. *Cell*, 1990. 61(4): p. 697-708.
28. Ciechanover, A., D. Finley, and A. Varshavsky, Ubiquitin dependence of selective protein degradation demonstrated in the mammalian cell cycle mutant ts85. *Cell*, 1984. 37(1): p. 57-66.
29. Jentsch, S., J.P. McGrath, and A. Varshavsky, The yeast DNA repair gene RAD6 encodes a ubiquitin-conjugating enzyme. *Nature*, 1987. 329(6135): p. 131-4.
30. Kovalenko, A., et al., The tumour suppressor CYLD negatively regulates NF-kappaB signalling by deubiquitination. *Nature*, 2003. 424(6950): p. 801-5.
31. Nakatogawa, H., Y. Ichimura, and Y. Ohsumi, Atg8, a ubiquitin-like protein required for autophagosome formation, mediates membrane tethering and hemifusion. *Cell*, 2007. 130(1): p. 165-78.
32. Park, S.M., J.B. Yoon, and T.H. Lee, Receptor interacting protein is ubiquitinated by cellular inhibitor of apoptosis proteins (c-IAP1 and c-IAP2) in vitro. *FEBS Lett*, 2004. 566(1-3): p. 151-6.
33. Ciechanover, A. and Y.T. Kwon, Degradation of misfolded proteins in neurodegenerative diseases: therapeutic targets and strategies. *Exp Mol Med*, 2015. 47: p. e147.
34. McNaught, K.S., et al., Failure of the ubiquitin-proteasome system in Parkinson's disease. *Nat Rev Neurosci*, 2001. 2(8): p. 589-94.
35. Ciechanover, A. and P. Brundin, The ubiquitin proteasome system in neurodegenerative diseases: sometimes the chicken, sometimes the egg. *Neuron*, 2003. 40(2): p. 427-46.
36. Du, W. and Q.B. Mei, Ubiquitin-proteasome system, a new anti-tumor target. *Acta Pharmacol Sin*, 2013. 34(2): p. 187-8.
37. Clague, M.J., et al., Deubiquitylases from genes to organism. *Physiol Rev*, 2013. 93(3): p. 1289-315.
38. Reyes-Turcu, F.E., K.H. Ventii, and K.D. Wilkinson, Regulation and cellular roles of ubiquitin-specific deubiquitinating enzymes. *Annu Rev Biochem*, 2009. 78: p. 363-97.
39. Abdul Rehman, S.A., et al., MINDY-1 Is a Member of an Evolutionarily Conserved and Structurally Distinct New Family of Deubiquitinating Enzymes. *Mol Cell*, 2016. 63(1): p. 146-55.
40. Zhu, X., R. Menard, and T. Sulea, High incidence of ubiquitin-like domains in human ubiquitin-specific proteases. *Proteins*, 2007. 69(1): p. 1-7.
41. Verma, R., et al., Role of Rpn11 metalloprotease in deubiquitination and degradation by the 26S proteasome. *Science*, 2002. 298(5593): p. 611-5.
42. Henry, K.W., et al., Transcriptional activation via sequential histone H2B ubiquitylation and deubiquitylation, mediated by SAGA-associated Ubp8. *Genes Dev*, 2003. 17(21): p. 2648-63.
43. Zhang, X.Y., et al., USP22, an hSAGA subunit and potential cancer stem cell marker, reverses the polycomb-catalyzed ubiquitylation of histone H2A. *Cell Cycle*, 2008. 7(11): p. 1522-4.
44. Komander, D., M.J. Clague, and S. Urbe, Breaking the chains: structure and function of the deubiquitinases. *Nat Rev Mol Cell Biol*, 2009. 10(8): p. 550-63.
45. Herhaus, L., et al., Casein kinase 2 (CK2) phosphorylates the deubiquitylase OTUB1 at Ser16 to trigger its nuclear localization. *Sci Signal*, 2015. 8(372): p. ra35.
46. Mueller, T., et al., CK2-dependent phosphorylation determines cellular localization and stability of ataxin-3. *Hum Mol Genet*, 2009. 18(17): p. 3334-43.
47. Yuan, J., et al., USP10 regulates p53 localization and stability by deubiquitinating p53. *Cell*, 2010. 140(3): p. 384-96.

48. Zhang, L., et al., USP4 is regulated by AKT phosphorylation and directly deubiquitylates TGF-beta type I receptor. *Nat Cell Biol*, 2012. 14(7): p. 717-26.
49. Mashtalir, N., et al., Autodeubiquitination protects the tumor suppressor BAP1 from cytoplasmic sequestration mediated by the atypical ubiquitin ligase UBE2O. *Mol Cell*, 2014. 54(3): p. 392-406.
50. Hymowitz, S.G. and I.E. Wertz, A20: from ubiquitin editing to tumour suppression. *Nat Rev Cancer*, 2010. 10(5): p. 332-41.
51. Dixit, V.M., et al., Tumor necrosis factor-alpha induction of novel gene products in human endothelial cells including a macrophage-specific chemotaxin. *J Biol Chem*, 1990. 265(5): p. 2973-8.
52. Huang, T.T., et al., Regulation of monoubiquitinated PCNA by DUB autocleavage. *Nat Cell Biol*, 2006. 8(4): p. 339-47.
53. Thein, S., et al., IKK regulates the deubiquitinase CYLD at the postsynaptic density. *Biochem Biophys Res Commun*, 2014. 450(1): p. 550-4.
54. Zhang, X. and Y. Wang, Cell cycle regulation of VCIP135 deubiquitinase activity and function in p97/p47-mediated Golgi reassembly. *Mol Biol Cell*, 2015. 26(12): p. 2242-51.
55. Todi, S.V., et al., Ubiquitination directly enhances activity of the deubiquitinating enzyme ataxin-3. *EMBO J*, 2009. 28(4): p. 372-82.
56. Meulmeester, E., et al., Mechanism and consequences for paralog-specific sumoylation of ubiquitin-specific protease 25. *Mol Cell*, 2008. 30(5): p. 610-9.
57. Wauer, T., et al., Ubiquitin Ser65 phosphorylation affects ubiquitin structure, chain assembly and hydrolysis. *EMBO J*, 2015. 34(3): p. 307-25.
58. Bingol, B., et al., The mitochondrial deubiquitinase USP30 opposes parkin-mediated mitophagy. *Nature*, 2014. 510(7505): p. 370-5.
59. Lin, Z., et al., USP22 antagonizes p53 transcriptional activation by deubiquitinating Sirt1 to suppress cell apoptosis and is required for mouse embryonic development. *Mol Cell*, 2012. 46(4): p. 484-94.
60. Wang, A., et al., USP22 Induces Cisplatin Resistance in Lung Adenocarcinoma by Regulating gamma H2AX-Mediated DNA Damage Repair and Ku70/Bax-Mediated Apoptosis. *Frontiers in Pharmacology*, 2017. 8.
61. Peng, L., et al., Ubiquitin specific peptidase 21 regulates interleukin-8 expression, stem-cell like property of human renal cell carcinoma. *Oncotarget*, 2016. 7(27): p. 42007-42016.
62. Onizawa, M., et al., The ubiquitin-modifying enzyme A20 restricts ubiquitination of the kinase RIPK3 and protects cells from necroptosis. *Nat Immunol*, 2015. 16(6): p. 618-27.
63. Bhattacharyya, B.J., et al., Altered neurotransmitter release machinery in mice deficient for the deubiquitinating enzyme Usp14. *Am J Physiol Cell Physiol*, 2012. 302(4): p. C698-708.
64. Imai, S., et al., Ubiquitin-specific peptidase 46 (Usp46) regulates mouse immobile behavior in the tail suspension test through the GABAergic system. *PLoS One*, 2012. 7(6): p. e39084.
65. Xilouri, M., et al., Selective neuroprotective effects of the S18Y polymorphic variant of UCH-L1 in the dopaminergic system. *Hum Mol Genet*, 2012. 21(4): p. 874-89.
66. Carneiro, A.P., et al., A putative OTU domain-containing protein 1 deubiquitinating enzyme is differentially expressed in thyroid cancer and identifies less-aggressive tumours. *Br J Cancer*, 2014. 111(3): p. 551-8.
67. Zhao, Y., et al., The deubiquitinase CYLD targets Smad7 protein to regulate transforming growth factor beta (TGF-beta) signaling and the development of regulatory T cells. *J Biol Chem*, 2011. 286(47): p. 40520-30.
68. Saldana, M., et al., Otubain 1: a non-canonical deubiquitinase with an emerging role in cancer. *Endocr Relat Cancer*, 2019. 26(1): p. R1-R14.
69. Coombs, N., et al., Helicobacter pylori affects the cellular deubiquitinase USP7 and ubiquitin-regulated components TRAF6 and the tumour suppressor p53. *Int J Med Microbiol*, 2011. 301(3): p. 213-24.

70. Uhlen, M., et al., Proteomics. Tissue-based map of the human proteome. *Science*, 2015. 347(6220): p. 1260419.
71. Lee, H.J., et al., The expression patterns of deubiquitinating enzymes, USP22 and Usp22. *Gene Expr Patterns*, 2006. 6(3): p. 277-84.
72. Samara, N.L., et al., Structural insights into the assembly and function of the SAGA deubiquitinating module. *Science*, 2010. 328(5981): p. 1025-9.
73. Kohler, A., et al., Structural basis for assembly and activation of the heterotetrameric SAGA histone H2B deubiquitinase module. *Cell*, 2010. 141(4): p. 606-17.
74. Glinsky, G.V., O. Berezovska, and A.B. Glinskii, Microarray analysis identifies a death-from-cancer signature predicting therapy failure in patients with multiple types of cancer. *J Clin Invest*, 2005. 115(6): p. 1503-21.
75. Liu, Y.L., et al., Increased expression of ubiquitin-specific protease 22 can promote cancer progression and predict therapy failure in human colorectal cancer. *J Gastroenterol Hepatol*, 2010. 25(11): p. 1800-5.
76. Wang, Z., et al., Decreased H2B monoubiquitination and overexpression of ubiquitin-specific protease enzyme 22 in malignant colon carcinoma. *Hum Pathol*, 2015. 46(7): p. 1006-14.
77. Yang, D.D., et al., The co-expression of USP22 and BMI-1 may promote cancer progression and predict therapy failure in gastric carcinoma. *Cell Biochem Biophys*, 2011. 61(3): p. 703-10.
78. Wang, H., et al., Prognostic significance of USP22 as an oncogene in papillary thyroid carcinoma. *Tumour Biol*, 2013. 34(3): p. 1635-9.
79. Liang, J.X., et al., Ubiquitinspecific protease 22induced autophagy is correlated with poor prognosis of pancreatic cancer. *Oncol Rep*, 2014. 32(6): p. 2726-34.
80. Liu, Y.L., et al., Aberrant expression of USP22 is associated with liver metastasis and poor prognosis of colorectal cancer. *J Surg Oncol*, 2011. 103(3): p. 283-9.
81. Ning, Z., et al., USP22 promotes the G1/S phase transition by upregulating FoxM1 expression via beta-catenin nuclear localization and is associated with poor prognosis in stage II pancreatic ductal adenocarcinoma. *Int J Oncol*, 2014. 45(4): p. 1594-608.
82. Li, J., Z. Wang, and Y. Li, USP22 nuclear expression is significantly associated with progression and unfavorable clinical outcome in human esophageal squamous cell carcinoma. *J Cancer Res Clin Oncol*, 2012. 138(8): p. 1291-7.
83. Cerami, E., et al., The cBio cancer genomics portal: an open platform for exploring multidimensional cancer genomics data. *Cancer Discov*, 2012. 2(5): p. 401-4.
84. Jeusset, L.M. and K.J. McManus, Ubiquitin Specific Peptidase 22 Regulates Histone H2B Mono-Ubiquitination and Exhibits Both Oncogenic and Tumor Suppressor Roles in Cancer. *Cancers (Basel)*, 2017. 9(12).
85. Zhang, X.Y., et al., The putative cancer stem cell marker USP22 is a subunit of the human SAGA complex required for activated transcription and cell-cycle progression. *Mol Cell*, 2008. 29(1): p. 102-11.
86. Morgan, M.T., et al., Structural basis for histone H2B deubiquitination by the SAGA DUB module. *Science*, 2016. 351(6274): p. 725-8.
87. Zhao, Y., et al., A TFTC/STAGA module mediates histone H2A and H2B deubiquitination, coactivates nuclear receptors, and counteracts heterochromatin silencing. *Mol Cell*, 2008. 29(1): p. 92-101.
88. Lang, G., et al., The tightly controlled deubiquitination activity of the human SAGA complex differentially modifies distinct gene regulatory elements. *Mol Cell Biol*, 2011. 31(18): p. 3734-44.
89. Atanassov, B.S., et al., ATXN7L3 and ENY2 Coordinate Activity of Multiple H2B Deubiquitinases Important for Cellular Proliferation and Tumor Growth. *Mol Cell*, 2016. 62(4): p. 558-71.
90. Ramachandran, S., et al., The SAGA Deubiquitination Module Promotes DNA Repair and Class Switch Recombination through ATM and DNAPK-Mediated gammaH2AX Formation. *Cell Rep*, 2016. 15(7): p. 1554-1565.
91. Atanassov, B.S. and S.Y. Dent, USP22 regulates cell proliferation by deubiquitinating the transcriptional regulator FBP1. *EMBO Rep*, 2011. 12(9): p. 924-30.

92. Ao, N., et al., Ubiquitin-specific peptidase USP22 negatively regulates the STAT signaling pathway by deubiquitinating SIRT1. *Cell Physiol Biochem*, 2014. 33(6): p. 1863-75.
93. Hong, A., J.E. Lee, and K.C. Chung, Ubiquitin-Specific Protease 22 (USP22) Positively Regulates RCAN1 Protein Levels Through RCAN1 De-Ubiquitination. *Journal of Cellular Physiology*, 2015. 230(7): p. 1651-1660.
94. Kobayashi, T., et al., Deubiquitinating enzymes regulate Hes1 stability and neuronal differentiation. *FEBS J*, 2015. 282(13): p. 2411-23.
95. Sun, H., et al., USP13 negatively regulates antiviral responses by deubiquitinating STING. *Nat Commun*, 2017. 8: p. 15534.
96. Liu, Y.L., et al., USP22 Acts as an Oncogene by the Activation of BMI-1-Mediated INK4a/ARF Pathway and Akt Pathway. *Cell Biochemistry and Biophysics*, 2012. 62(1): p. 229-235.
97. Xu, H., et al., Knock-down of ubiquitin-specific protease 22 by micro-RNA interference inhibits colorectal cancer growth. *Int J Colorectal Dis*, 2012. 27(1): p. 21-30.
98. Li, Z.H., et al., RNA interference-mediated USP22 gene silencing promotes human brain glioma apoptosis and induces cell cycle arrest. *Oncol Lett*, 2013. 5(4): p. 1290-1294.
99. Xiong, J., et al., USP22 transcriptional activity is negatively regulated by the histone deacetylase inhibitor trichostatin A. *Mol Med Rep*, 2014. 10(6): p. 3343-7.
100. Li, L., et al., SIRT1 activation by a c-MYC oncogenic network promotes the maintenance and drug resistance of human FLT3-ITD acute myeloid leukemia stem cells. *Cell Stem Cell*, 2014. 15(4): p. 431-446.
101. Johansen, T. and T. Lamark, Selective Autophagy: ATG8 Family Proteins, LIR Motifs and Cargo Receptors. *J Mol Biol*, 2020. 432(1): p. 80-103.
102. Munch, C. and I. Dikic, Publisher Correction: Hitchhiking on selective autophagy. *Nat Cell Biol*, 2018. 20(8): p. 990.
103. Levine, B. and G. Kroemer, Autophagy in the pathogenesis of disease. *Cell*, 2008. 132(1): p. 27-42.
104. Yang, Z.J., et al., The role of autophagy in cancer: therapeutic implications. *Mol Cancer Ther*, 2011. 10(9): p. 1533-41.
105. Xiong, H., et al., LncRNA HULC triggers autophagy via stabilizing Sirt1 and attenuates the chemosensitivity of HCC cells. *Oncogene*, 2017. 36(25): p. 3528-3540.
106. Yun, X., et al., Targeting USP22 Suppresses Tumorigenicity and Enhances Cisplatin Sensitivity Through ALDH1A3 Downregulation in Cancer-Initiating Cells from Lung Adenocarcinoma. *Mol Cancer Res*, 2018. 16(7): p. 1161-1171.
107. Zhang, K., et al., Ubiquitin-specific protease 22 is critical to in vivo angiogenesis, growth and metastasis of non-small cell lung cancer. *Cell Commun Signal*, 2019. 17(1): p. 167.
108. Zhang, K., et al., Loss of H2B monoubiquitination is associated with poor-differentiation and enhanced malignancy of lung adenocarcinoma. *Int J Cancer*, 2017. 141(4): p. 766-777.
109. Melo-Cardenas, J., et al., USP22 deficiency leads to myeloid leukemia upon oncogenic Kras activation through a PU.1-dependent mechanism. *Blood*, 2018. 132(4): p. 423-434.
110. Kosinsky, R.L., et al., USP22 exerts tumor-suppressive functions in colorectal cancer by decreasing mTOR activity. *Cell Death Differ*, 2019.
111. Ji, M., et al., Ubiquitin specific protease 22 promotes cell proliferation and tumor growth of epithelial ovarian cancer through synergy with transforming growth factor beta1. *Oncol Rep*, 2015. 33(1): p. 133-40.
112. Ning, J., et al., Overexpression of ubiquitin-specific protease 22 predicts poor survival in patients with early-stage non-small cell lung cancer. *Eur J Histochem*, 2012. 56(4): p. e46.
113. Zhang, Y., et al., Elevated expression of USP22 in correlation with poor prognosis in patients with invasive breast cancer. *J Cancer Res Clin Oncol*, 2011. 137(8): p. 1245-53.

114. Fuchs, Y. and H. Steller, Live to die another way: modes of programmed cell death and the signals emanating from dying cells. *Nat Rev Mol Cell Biol*, 2015. 16(6): p. 329-44.
115. Green, D.R. and F. Llambi, Cell Death Signaling. *Cold Spring Harb Perspect Biol*, 2015. 7(12).
116. Galluzzi, L., et al., Molecular mechanisms of cell death: recommendations of the Nomenclature Committee on Cell Death 2018. *Cell Death Differ*, 2018. 25(3): p. 486-541.
117. Kumar, H., T. Kawai, and S. Akira, Pathogen recognition by the innate immune system. *Int Rev Immunol*, 2011. 30(1): p. 16-34.
118. Dempsey, P.W., et al., The signaling adaptors and pathways activated by TNF superfamily. *Cytokine Growth Factor Rev*, 2003. 14(3-4): p. 193-209.
119. Locksley, R.M., N. Killeen, and M.J. Lenardo, The TNF and TNF receptor superfamilies: integrating mammalian biology. *Cell*, 2001. 104(4): p. 487-501.
120. Annibaldi, A. and P. Meier, Checkpoints in TNF-Induced Cell Death: Implications in Inflammation and Cancer. *Trends Mol Med*, 2018. 24(1): p. 49-65.
121. Gasparini, C., et al., NF-kappaB pathways in hematological malignancies. *Cell Mol Life Sci*, 2014. 71(11): p. 2083-102.
122. Ashkenazi, A. and V.M. Dixit, Death receptors: signaling and modulation. *Science*, 1998. 281(5381): p. 1305-8.
123. Schulze-Osthoff, K., et al., Apoptosis signaling by death receptors. *Eur J Biochem*, 1998. 254(3): p. 439-59.
124. Vince, J.E., et al., TRAF2 must bind to cellular inhibitors of apoptosis for tumor necrosis factor (tnf) to efficiently activate nf-kappaB and to prevent tnf-induced apoptosis. *J Biol Chem*, 2009. 284(51): p. 35906-15.
125. Haas, T.L., et al., Recruitment of the linear ubiquitin chain assembly complex stabilizes the TNF-R1 signaling complex and is required for TNF-mediated gene induction. *Mol Cell*, 2009. 36(5): p. 831-44.
126. Bertrand, M.J., et al., cIAP1 and cIAP2 facilitate cancer cell survival by functioning as E3 ligases that promote RIP1 ubiquitination. *Mol Cell*, 2008. 30(6): p. 689-700.
127. Mahoney, D.J., et al., Both cIAP1 and cIAP2 regulate TNFalpha-mediated NF-kappaB activation. *Proc Natl Acad Sci U S A*, 2008. 105(33): p. 11778-83.
128. Varfolomeev, E., et al., c-IAP1 and c-IAP2 are critical mediators of tumor necrosis factor alpha (TNFalpha)-induced NF-kappaB activation. *J Biol Chem*, 2008. 283(36): p. 24295-9.
129. Dynek, J.N., et al., c-IAP1 and Ubch5 promote K11-linked polyubiquitination of RIP1 in TNF signalling. *EMBO J*, 2010. 29(24): p. 4198-209.
130. Gerlach, B., et al., Linear ubiquitination prevents inflammation and regulates immune signalling. *Nature*, 2011. 471(7340): p. 591-6.
131. Gerlach, K., et al., Transcription factor NFATc2 controls the emergence of colon cancer associated with IL-6-dependent colitis. *Cancer Res*, 2012. 72(17): p. 4340-50.
132. Tokunaga, F., et al., Involvement of linear polyubiquitylation of NEMO in NF-kappaB activation. *Nat Cell Biol*, 2009. 11(2): p. 123-32.
133. Draber, P., et al., LUBAC-Recruited CYLD and A20 Regulate Gene Activation and Cell Death by Exerting Opposing Effects on Linear Ubiquitin in Signaling Complexes. *Cell Rep*, 2015. 13(10): p. 2258-72.
134. Smit, J.J., et al., The E3 ligase HOIP specifies linear ubiquitin chain assembly through its RING-IBR-RING domain and the unique LDD extension. *EMBO J*, 2012. 31(19): p. 3833-44.
135. Wang, C., et al., TAK1 is a ubiquitin-dependent kinase of MKK and IKK. *Nature*, 2001. 412(6844): p. 346-51.
136. Kirisako, T., et al., A ubiquitin ligase complex assembles linear polyubiquitin chains. *EMBO J*, 2006. 25(20): p. 4877-87.
137. Traenckner, E.B., et al., Phosphorylation of human I kappa B-alpha on serines 32 and 36 controls I kappa B-alpha proteolysis and NF-kappa B activation in response to diverse stimuli. *EMBO J*, 1995. 14(12): p. 2876-83.

138. Sun, S.C., The non-canonical NF-kappaB pathway in immunity and inflammation. *Nat Rev Immunol*, 2017. 17(9): p. 545-558.
139. Mercurio, F., et al., IKK-1 and IKK-2: cytokine-activated I kappaB kinases essential for NF-kappaB activation. *Science*, 1997. 278(5339): p. 860-6.
140. Woronicz, J.D., et al., I kappaB kinase-beta: NF-kappaB activation and complex formation with I kappaB kinase-alpha and NIK. *Science*, 1997. 278(5339): p. 866-9.
141. Vallabhapurapu, S., et al., Nonredundant and complementary functions of TRAF2 and TRAF3 in a ubiquitination cascade that activates NIK-dependent alternative NF-kappaB signaling. *Nat Immunol*, 2008. 9(12): p. 1364-70.
142. Zarnegar, B.J., et al., Noncanonical NF-kappaB activation requires coordinated assembly of a regulatory complex of the adaptors cIAP1, cIAP2, TRAF2 and TRAF3 and the kinase NIK. *Nat Immunol*, 2008. 9(12): p. 1371-8.
143. Sun, S.C., The noncanonical NF-kappaB pathway. *Immunol Rev*, 2012. 246(1): p. 125-40.
144. Kerr, J.F., A.H. Wyllie, and A.R. Currie, Apoptosis: a basic biological phenomenon with wide-ranging implications in tissue kinetics. *Br J Cancer*, 1972. 26(4): p. 239-57.
145. Meier, P., A. Finch, and G. Evan, Apoptosis in development. *Nature*, 2000. 407(6805): p. 796-801.
146. Giovannetti, A., et al., Apoptosis in the homeostasis of the immune system and in human immune mediated diseases. *Curr Pharm Des*, 2008. 14(3): p. 253-68.
147. Brill, A., et al., The role of apoptosis in normal and abnormal embryonic development. *J Assist Reprod Genet*, 1999. 16(10): p. 512-9.
148. Mattson, M.P., Apoptosis in neurodegenerative disorders. *Nat Rev Mol Cell Biol*, 2000. 1(2): p. 120-9.
149. Hanahan, D. and R.A. Weinberg, Hallmarks of cancer: the next generation. *Cell*, 2011. 144(5): p. 646-74.
150. Fulda, S. and K.M. Debatin, Targeting apoptosis pathways in cancer therapy. *Curr Cancer Drug Targets*, 2004. 4(7): p. 569-76.
151. Nicholson, D.W. and N.A. Thornberry, Caspases: killer proteases. *Trends Biochem Sci*, 1997. 22(8): p. 299-306.
152. Budihardjo, I., et al., Biochemical pathways of caspase activation during apoptosis. *Annu Rev Cell Dev Biol*, 1999. 15: p. 269-90.
153. Riedl, S.J. and Y. Shi, Molecular mechanisms of caspase regulation during apoptosis. *Nat Rev Mol Cell Biol*, 2004. 5(11): p. 897-907.
154. Nunez, G., et al., Caspases: the proteases of the apoptotic pathway. *Oncogene*, 1998. 17(25): p. 3237-45.
155. Fischer, U., R.U. Janicke, and K. Schulze-Osthoff, Many cuts to ruin: a comprehensive update of caspase substrates. *Cell Death Differ*, 2003. 10(1): p. 76-100.
156. Fulda, S. and K.M. Debatin, Extrinsic versus intrinsic apoptosis pathways in anticancer chemotherapy. *Oncogene*, 2006. 25(34): p. 4798-811.
157. Ichim, G. and S.W. Tait, A fate worse than death: apoptosis as an oncogenic process. *Nat Rev Cancer*, 2016. 16(8): p. 539-48.
158. Cavalcante, G.C., et al., A Cell's Fate: An Overview of the Molecular Biology and Genetics of Apoptosis. *Int J Mol Sci*, 2019. 20(17).
159. Czabotar, P.E., et al., Control of apoptosis by the BCL-2 protein family: implications for physiology and therapy. *Nat Rev Mol Cell Biol*, 2014. 15(1): p. 49-63.
160. Westphal, D., et al., Apoptotic pore formation is associated with in-plane insertion of Bak or Bax central helices into the mitochondrial outer membrane. *Proc Natl Acad Sci U S A*, 2014. 111(39): p. E4076-85.
161. Du, C., et al., Smac, a mitochondrial protein that promotes cytochrome c-dependent caspase activation by eliminating IAP inhibition. *Cell*, 2000. 102(1): p. 33-42.
162. Shimizu, S., M. Narita, and Y. Tsujimoto, Bcl-2 family proteins regulate the release of apoptogenic cytochrome c by the mitochondrial channel VDAC. *Nature*, 1999. 399(6735): p. 483-7.
163. Deveraux, Q.L., et al., X-linked IAP is a direct inhibitor of cell-death proteases. *Nature*, 1997. 388(6639): p. 300-4.

164. Adrain, C., et al., Regulation of apoptotic protease activating factor-1 oligomerization and apoptosis by the WD-40 repeat region. *J Biol Chem*, 1999. 274(30): p. 20855-60.
165. Park, Y.H., M.S. Jeong, and S.B. Jang, Death domain complex of the TNFR-1, TRADD, and RIP1 proteins for death-inducing signaling. *Biochem Biophys Res Commun*, 2014. 443(4): p. 1155-61.
166. Kischkel, F.C., et al., Cytotoxicity-dependent APO-1 (Fas/CD95)-associated proteins form a death-inducing signaling complex (DISC) with the receptor. *EMBO J*, 1995. 14(22): p. 5579-88.
167. Walczak, H. and P.H. Krammer, The CD95 (APO-1/Fas) and the TRAIL (APO-2L) apoptosis systems. *Exp Cell Res*, 2000. 256(1): p. 58-66.
168. Li, H., et al., Cleavage of BID by caspase 8 mediates the mitochondrial damage in the Fas pathway of apoptosis. *Cell*, 1998. 94(4): p. 491-501.
169. Luo, X., et al., Bid, a Bcl2 interacting protein, mediates cytochrome c release from mitochondria in response to activation of cell surface death receptors. *Cell*, 1998. 94(4): p. 481-90.
170. Micheau, O. and J. Tschopp, Induction of TNF receptor I-mediated apoptosis via two sequential signaling complexes. *Cell*, 2003. 114(2): p. 181-90.
171. Feoktistova, M., P. Geserick, and M. Leverkus, Ripoptosome Analysis by Caspase-8 Coimmunoprecipitation. *Cold Spring Harb Protoc*, 2016. 2016(3): p. pdb prot087403.
172. Wang, L., F. Du, and X. Wang, TNF-alpha induces two distinct caspase-8 activation pathways. *Cell*, 2008. 133(4): p. 693-703.
173. Feoktistova, M., et al., cIAPs block Ripoptosome formation, a RIP1/caspase-8 containing intracellular cell death complex differentially regulated by cFLIP isoforms. *Mol Cell*, 2011. 43(3): p. 449-63.
174. Vandenabeele, P., et al., Molecular mechanisms of necroptosis: an ordered cellular explosion. *Nat Rev Mol Cell Biol*, 2010. 11(10): p. 700-14.
175. Peltzer, N. and H. Walczak, Cell Death and Inflammation - A Vital but Dangerous Liaison. *Trends Immunol*, 2019. 40(5): p. 387-402.
176. Petrie, E.J., P.E. Czabotar, and J.M. Murphy, The Structural Basis of Necroptotic Cell Death Signaling. *Trends Biochem Sci*, 2019. 44(1): p. 53-63.
177. Vanden Berghe, T., et al., Molecular crosstalk between apoptosis, necroptosis, and survival signaling. *Mol Cell Oncol*, 2015. 2(4): p. e975093.
178. Festjens, N., T. Vanden Berghe, and P. Vandenabeele, Necrosis, a well-orchestrated form of cell demise: signalling cascades, important mediators and concomitant immune response. *Biochim Biophys Acta*, 2006. 1757(9-10): p. 1371-87.
179. Zong, W.X. and C.B. Thompson, Necrotic death as a cell fate. *Genes Dev*, 2006. 20(1): p. 1-15.
180. Newton, K. and G. Manning, Necroptosis and Inflammation. *Annu Rev Biochem*, 2016. 85: p. 743-63.
181. Weinlich, R., et al., Necroptosis in development, inflammation and disease. *Nat Rev Mol Cell Biol*, 2017. 18(2): p. 127-136.
182. Upton, J.W. and W.J. Kaiser, DAI Another Way: Necroptotic Control of Viral Infection. *Cell Host Microbe*, 2017. 21(3): p. 290-293.
183. Kaiser, W.J., J.W. Upton, and E.S. Mocarski, Viral modulation of programmed necrosis. *Curr Opin Virol*, 2013. 3(3): p. 296-306.
184. Thapa, R.J., et al., Interferon-induced RIP1/RIP3-mediated necrosis requires PKR and is licensed by FADD and caspases. *Proc Natl Acad Sci U S A*, 2013. 110(33): p. E3109-18.
185. Takemura, R., et al., PolyI:C-Induced, TLR3/RIP3-Dependent Necroptosis Backs Up Immune Effector-Mediated Tumor Elimination In Vivo. *Cancer Immunol Res*, 2015. 3(8): p. 902-14.
186. Holler, N., et al., Fas triggers an alternative, caspase-8-independent cell death pathway using the kinase RIP as effector molecule. *Nat Immunol*, 2000. 1(6): p. 489-95.
187. Grootjans, S., T. Vanden Berghe, and P. Vandenabeele, Initiation and execution mechanisms of necroptosis: an overview. *Cell Death Differ*, 2017. 24(7): p. 1184-1195.

188. Cho, Y.S., et al., Phosphorylation-driven assembly of the RIP1-RIP3 complex regulates programmed necrosis and virus-induced inflammation. *Cell*, 2009. 137(6): p. 1112-23.
189. He, S., et al., Receptor interacting protein kinase-3 determines cellular necrotic response to TNF-alpha. *Cell*, 2009. 137(6): p. 1100-11.
190. Zhang, D.W., et al., RIP3, an energy metabolism regulator that switches TNF-induced cell death from apoptosis to necrosis. *Science*, 2009. 325(5938): p. 332-6.
191. Mompean, M., et al., The Structure of the Necrosome RIPK1-RIPK3 Core, a Human Hetero-Amyloid Signaling Complex. *Cell*, 2018. 173(5): p. 1244-1253 e10.
192. Newton, K., et al., Activity of protein kinase RIPK3 determines whether cells die by necroptosis or apoptosis. *Science*, 2014. 343(6177): p. 1357-60.
193. Mandal, P., et al., RIP3 induces apoptosis independent of pronecrotic kinase activity. *Mol Cell*, 2014. 56(4): p. 481-95.
194. Polykratis, A., et al., Cutting edge: RIPK1 Kinase inactive mice are viable and protected from TNF-induced necroptosis in vivo. *J Immunol*, 2014. 193(4): p. 1539-1543.
195. Wu, X.N., et al., Distinct roles of RIP1-RIP3 hetero- and RIP3-RIP3 homo-interaction in mediating necroptosis. *Cell Death Differ*, 2014. 21(11): p. 1709-20.
196. Sun, L., et al., Mixed lineage kinase domain-like protein mediates necrosis signaling downstream of RIP3 kinase. *Cell*, 2012. 148(1-2): p. 213-27.
197. Chen, W., et al., Diverse sequence determinants control human and mouse receptor interacting protein 3 (RIP3) and mixed lineage kinase domain-like (MLKL) interaction in necroptotic signaling. *J Biol Chem*, 2013. 288(23): p. 16247-61.
198. McQuade, T., Y. Cho, and F.K. Chan, Positive and negative phosphorylation regulates RIP1- and RIP3-induced programmed necrosis. *Biochem J*, 2013. 456(3): p. 409-15.
199. Quarato, G., et al., Sequential Engagement of Distinct MLKL Phosphatidylinositol-Binding Sites Executes Necroptosis. *Mol Cell*, 2016. 61(4): p. 589-601.
200. Wang, H., et al., Mixed lineage kinase domain-like protein MLKL causes necrotic membrane disruption upon phosphorylation by RIP3. *Mol Cell*, 2014. 54(1): p. 133-146.
201. Zhang, D., J. Lin, and J. Han, Receptor-interacting protein (RIP) kinase family. *Cell Mol Immunol*, 2010. 7(4): p. 243-9.
202. Duprez, L., et al., Intermediate domain of receptor-interacting protein kinase 1 (RIPK1) determines switch between necroptosis and RIPK1 kinase-dependent apoptosis. *J Biol Chem*, 2012. 287(18): p. 14863-72.
203. Upton, J.W., W.J. Kaiser, and E.S. Mocarski, Virus inhibition of RIP3-dependent necrosis. *Cell Host Microbe*, 2010. 7(4): p. 302-13.
204. Murphy, J.M., et al., The pseudokinase MLKL mediates necroptosis via a molecular switch mechanism. *Immunity*, 2013. 39(3): p. 443-53.
205. Stanger, B.Z., et al., RIP: a novel protein containing a death domain that interacts with Fas/APO-1 (CD95) in yeast and causes cell death. *Cell*, 1995. 81(4): p. 513-23.
206. Silke, J., J.A. Rickard, and M. Gerlic, The diverse role of RIP kinases in necroptosis and inflammation. *Nat Immunol*, 2015. 16(7): p. 689-97.
207. Pasparakis, M. and P. Vandenabeele, Necroptosis and its role in inflammation. *Nature*, 2015. 517(7534): p. 311-20.
208. Tanzer, M.C., et al., Necroptosis signalling is tuned by phosphorylation of MLKL residues outside the pseudokinase domain activation loop. *Biochem J*, 2015. 471(2): p. 255-65.
209. Berger, S.B., et al., Cutting Edge: RIP1 kinase activity is dispensable for normal development but is a key regulator of inflammation in SHARPIN-deficient mice. *J Immunol*, 2014. 192(12): p. 5476-80.
210. Saleh, D. and A. Degterev, Emerging Roles for RIPK1 and RIPK3 in Pathogen-Induced Cell Death and Host Immunity. *Curr Top Microbiol Immunol*, 2017. 403: p. 37-75.
211. Peterson, L.W., et al., RIPK1-dependent apoptosis bypasses pathogen blockade of innate signaling to promote immune defense. *J Exp Med*, 2017. 214(11): p. 3171-3182.
212. Li, Y., et al., Human RIPK1 deficiency causes combined immunodeficiency and inflammatory bowel diseases. *Proc Natl Acad Sci U S A*, 2019. 116(3): p. 970-975.

213. Cuchet-Lourenco, D., et al., Biallelic RIPK1 mutations in humans cause severe immunodeficiency, arthritis, and intestinal inflammation. *Science*, 2018. 361(6404): p. 810-813.
214. Uchiyama, Y., et al., Primary immunodeficiency with chronic enteropathy and developmental delay in a boy arising from a novel homozygous RIPK1 variant. *J Hum Genet*, 2019. 64(9): p. 955-960.
215. Hsu, H., et al., TNF-dependent recruitment of the protein kinase RIP to the TNF receptor-1 signaling complex. *Immunity*, 1996. 4(4): p. 387-96.
216. Varfolomeev, E.E., et al., A potential mechanism of "cross-talk" between the p55 tumor necrosis factor receptor and Fas/APO1: proteins binding to the death domains of the two receptors also bind to each other. *J Exp Med*, 1996. 183(3): p. 1271-5.
217. Sun, X., et al., Identification of a novel homotypic interaction motif required for the phosphorylation of receptor-interacting protein (RIP) by RIP3. *J Biol Chem*, 2002. 277(11): p. 9505-11.
218. Kaiser, W.J., J.W. Upton, and E.S. Mocarski, Receptor-interacting protein homotypic interaction motif-dependent control of NF-kappa B activation via the DNA-dependent activator of IFN regulatory factors. *J Immunol*, 2008. 181(9): p. 6427-34.
219. Degterev, A., et al., Identification of RIP1 kinase as a specific cellular target of necrostatins. *Nat Chem Biol*, 2008. 4(5): p. 313-21.
220. Zhang, Y., et al., RIP1 autophosphorylation is promoted by mitochondrial ROS and is essential for RIP3 recruitment into necrosome. *Nat Commun*, 2017. 8: p. 14329.
221. Meng, H., et al., Death-domain dimerization-mediated activation of RIPK1 controls necroptosis and RIPK1-dependent apoptosis. *Proc Natl Acad Sci U S A*, 2018. 115(9): p. E2001-E2009.
222. Dondelinger, Y., et al., MK2 phosphorylation of RIPK1 regulates TNF-mediated cell death. *Nat Cell Biol*, 2017. 19(10): p. 1237-1247.
223. Jaco, I., et al., MK2 Phosphorylates RIPK1 to Prevent TNF-Induced Cell Death. *Mol Cell*, 2017. 66(5): p. 698-710 e5.
224. Menon, M.B., et al., p38(MAPK)/MK2-dependent phosphorylation controls cytotoxic RIPK1 signalling in inflammation and infection. *Nat Cell Biol*, 2017. 19(10): p. 1248-1259.
225. Geng, J., et al., Regulation of RIPK1 activation by TAK1-mediated phosphorylation dictates apoptosis and necroptosis. *Nat Commun*, 2017. 8(1): p. 359.
226. Newton, K., et al., RIPK1 inhibits ZBP1-driven necroptosis during development. *Nature*, 2016. 540(7631): p. 129-133.
227. Lin, J., et al., RIPK1 counteracts ZBP1-mediated necroptosis to inhibit inflammation. *Nature*, 2016. 540(7631): p. 124-128.
228. Dondelinger, Y., et al., Poly-ubiquitination in TNFR1-mediated necroptosis. *Cell Mol Life Sci*, 2016. 73(11-12): p. 2165-76.
229. Kang, K., et al., Post-translational modification of the death receptor complex as a potential therapeutic target in cancer. *Arch Pharm Res*, 2019. 42(1): p. 76-87.
230. Dondelinger, Y., et al., RIPK3 contributes to TNFR1-mediated RIPK1 kinase-dependent apoptosis in conditions of cIAP1/2 depletion or TAK1 kinase inhibition. *Cell Death Differ*, 2013. 20(10): p. 1381-92.
231. Vanlangenakker, N., et al., cIAP1 and TAK1 protect cells from TNF-induced necrosis by preventing RIP1/RIP3-dependent reactive oxygen species production. *Cell Death Differ*, 2011. 18(4): p. 656-65.
232. Kupka, S., et al., Formation and removal of poly-ubiquitin chains in the regulation of tumor necrosis factor-induced gene activation and cell death. *FEBS J*, 2016. 283(14): p. 2626-39.
233. Wang, H., et al., PELI1 functions as a dual modulator of necroptosis and apoptosis by regulating ubiquitination of RIPK1 and mRNA levels of c-FLIP. *Proc Natl Acad Sci U S A*, 2017. 114(45): p. 11944-11949.
234. Li, J., et al., The RIP1/RIP3 necrosome forms a functional amyloid signaling complex required for programmed necrosis. *Cell*, 2012. 150(2): p. 339-50.

235. Chen, W., et al., Ppm1b negatively regulates necroptosis through dephosphorylating Rip3. *Nat Cell Biol*, 2015. 17(4): p. 434-44.
236. Fuchslocher Chico, J., et al., The enhanced susceptibility of ADAM-17 hypomorphic mice to DSS-induced colitis is not ameliorated by loss of RIPK3, revealing an unexpected function of ADAM-17 in necroptosis. *Oncotarget*, 2018. 9(16): p. 12941-12958.
237. O'Donnell, M.A., et al., Caspase 8 inhibits programmed necrosis by processing CYLD. *Nat Cell Biol*, 2011. 13(12): p. 1437-42.
238. Seo, J., et al., CHIP controls necroptosis through ubiquitylation- and lysosome-dependent degradation of RIPK3. *Nat Cell Biol*, 2016. 18(3): p. 291-302.
239. Lee, S.B., et al., The AMPK-Parkin axis negatively regulates necroptosis and tumorigenesis by inhibiting the necrosome. *Nature Cell Biology*, 2019. 21(8): p. 940-+.
240. Park, H.H., et al., Regulation of RIP3 protein stability by PELI1-mediated proteasome-dependent degradation. *BMB Rep*, 2018. 51(10): p. 484-485.
241. Choi, S.W., et al., PELI1 Selectively Targets Kinase-Active RIP3 for Ubiquitylation-Dependent Proteasomal Degradation. *Mol Cell*, 2018. 70(5): p. 920-935 e7.
242. Seo, J., et al., CHIP controls necroptosis through ubiquitylation- and lysosome-dependent degradation of RIPK3. *Nature Cell Biology*, 2016. 18(3): p. 291-+.
243. Moriwaki, K. and F.K. Chan, Regulation of RIPK3- and RHIM-dependent Necroptosis by the Proteasome. *J Biol Chem*, 2016. 291(11): p. 5948-59.
244. Li, D., et al., A cytosolic heat shock protein 90 and cochaperone CDC37 complex is required for RIP3 activation during necroptosis. *Proc Natl Acad Sci U S A*, 2015. 112(16): p. 5017-22.
245. Park, S.Y., J.H. Shim, and Y.S. Cho, Distinctive roles of receptor-interacting protein kinases 1 and 3 in caspase-independent cell death of L929. *Cell Biochem Funct*, 2014. 32(1): p. 62-9.
246. Chen, W.W., et al., RIP1 mediates the protection of geldanamycin on neuronal injury induced by oxygen-glucose deprivation combined with zVAD in primary cortical neurons. *J Neurochem*, 2012. 120(1): p. 70-7.
247. Fearn, C., et al., Triad3A regulates ubiquitination and proteasomal degradation of RIP1 following disruption of Hsp90 binding. *J Biol Chem*, 2006. 281(45): p. 34592-600.
248. Gentle, I.E., et al., In TNF-stimulated cells, RIPK1 promotes cell survival by stabilizing TRAF2 and cIAP1, which limits induction of non-canonical NF-kappaB and activation of caspase-8. *J Biol Chem*, 2011. 286(15): p. 13282-91.
249. Lewis, J., et al., Disruption of hsp90 function results in degradation of the death domain kinase, receptor-interacting protein (RIP), and blockage of tumor necrosis factor-induced nuclear factor-kappaB activation. *J Biol Chem*, 2000. 275(14): p. 10519-26.
250. Pantano, C., et al., Hydrogen peroxide signaling through tumor necrosis factor receptor 1 leads to selective activation of c-Jun N-terminal kinase. *J Biol Chem*, 2003. 278(45): p. 44091-6.
251. Vanden Berghe, T., et al., Disruption of HSP90 function reverts tumor necrosis factor-induced necrosis to apoptosis. *J Biol Chem*, 2003. 278(8): p. 5622-9.
252. Bigenzahn, J.W., et al., An Inducible Retroviral Expression System for Tandem Affinity Purification Mass-Spectrometry-Based Proteomics Identifies Mixed Lineage Kinase Domain-like Protein (MLKL) as an Heat Shock Protein 90 (HSP90) Client. *Mol Cell Proteomics*, 2016. 15(3): p. 1139-50.
253. Jacobsen, A.V., et al., HSP90 activity is required for MLKL oligomerisation and membrane translocation and the induction of necroptotic cell death. *Cell Death Dis*, 2016. 7: p. e2051.
254. Zhao, X.M., et al., Hsp90 modulates the stability of MLKL and is required for TNF-induced necroptosis. *Cell Death Dis*, 2016. 7: p. e2089.
255. Zhao, Q., et al., RIPK3 Mediates Necroptosis during Embryonic Development and Postnatal Inflammation in Fadd-Deficient Mice. *Cell Rep*, 2017. 19(4): p. 798-808.
256. Dillon, C.P., et al., RIPK1 blocks early postnatal lethality mediated by caspase-8 and RIPK3. *Cell*, 2014. 157(5): p. 1189-202.

257. Moriwaki, K., S. Balaji, and F.K. Chan, Border Security: The Role of RIPK3 in Epithelium Homeostasis. *Front Cell Dev Biol*, 2016. 4: p. 70.
258. Lawlor, K.E., et al., RIPK3 promotes cell death and NLRP3 inflammasome activation in the absence of MLKL. *Nat Commun*, 2015. 6: p. 6282.
259. Su, L., et al., A plug release mechanism for membrane permeation by MLKL. *Structure*, 2014. 22(10): p. 1489-500.
260. Petrie, E.J., et al., Conformational switching of the pseudokinase domain promotes human MLKL tetramerization and cell death by necroptosis. *Nat Commun*, 2018. 9(1): p. 2422.
261. Reynoso, E., et al., Thioredoxin-1 actively maintains the pseudokinase MLKL in a reduced state to suppress disulfide bond-dependent MLKL polymer formation and necroptosis. *J Biol Chem*, 2017. 292(42): p. 17514-17524.
262. Hildebrand, J.M., et al., Activation of the pseudokinase MLKL unleashes the four-helix bundle domain to induce membrane localization and necroptotic cell death. *Proc Natl Acad Sci U S A*, 2014. 111(42): p. 15072-7.
263. Cai, Z., et al., Plasma membrane translocation of trimerized MLKL protein is required for TNF-induced necroptosis. *Nat Cell Biol*, 2014. 16(1): p. 55-65.
264. Dondelinger, Y., et al., MLKL compromises plasma membrane integrity by binding to phosphatidylinositol phosphates. *Cell Rep*, 2014. 7(4): p. 971-81.
265. Rodriguez, D.A., et al., Characterization of RIPK3-mediated phosphorylation of the activation loop of MLKL during necroptosis. *Cell Death Differ*, 2016. 23(1): p. 76-88.
266. Tanzer, M.C., et al., Evolutionary divergence of the necroptosis effector MLKL. *Cell Death Differ*, 2016. 23(7): p. 1185-97.
267. Davies, K.A., et al., The brace helices of MLKL mediate interdomain communication and oligomerisation to regulate cell death by necroptosis. *Cell Death Differ*, 2018. 25(9): p. 1567-1580.
268. Huang, D., et al., The MLKL Channel in Necroptosis Is an Octamer Formed by Tetramers in a Dyadic Process. *Mol Cell Biol*, 2017. 37(5).
269. Liu, S., et al., MLKL forms disulfide bond-dependent amyloid-like polymers to induce necroptosis. *Proc Natl Acad Sci U S A*, 2017. 114(36): p. E7450-E7459.
270. Dovey, C.M., et al., MLKL Requires the Inositol Phosphate Code to Execute Necroptosis. *Mol Cell*, 2018. 70(5): p. 936-948 e7.
271. Liu, W., et al., RGMb protects against acute kidney injury by inhibiting tubular cell necroptosis via an MLKL-dependent mechanism. *Proc Natl Acad Sci U S A*, 2018. 115(7): p. E1475-E1484.
272. Yoon, S., et al., Necroptosis is preceded by nuclear translocation of the signaling proteins that induce it. *Cell Death Differ*, 2016. 23(2): p. 253-60.
273. Gong, Y.N., et al., ESCRT-III Acts Downstream of MLKL to Regulate Necroptotic Cell Death and Its Consequences. *Cell*, 2017. 169(2): p. 286-300 e16.
274. Gong, Y.N., et al., Biological events and molecular signaling following MLKL activation during necroptosis. *Cell Cycle*, 2017. 16(19): p. 1748-1760.
275. Wang, J., et al., Toward an understanding of the protein interaction network of the human liver. *Mol Syst Biol*, 2017. 13(12): p. 965.
276. Mocarski, E.S., H. Guo, and W.J. Kaiser, Necroptosis: The Trojan horse in cell autonomous antiviral host defense. *Virology*, 2015. 479-480: p. 160-6.
277. Pearson, J.S., et al., EspL is a bacterial cysteine protease effector that cleaves RHIM proteins to block necroptosis and inflammation. *Nat Microbiol*, 2017. 2: p. 16258.
278. Degterev, A., et al., Chemical inhibitor of nonapoptotic cell death with therapeutic potential for ischemic brain injury. *Nat Chem Biol*, 2005. 1(2): p. 112-9.
279. Alvarez-Diaz, S., et al., The Pseudokinase MLKL and the Kinase RIPK3 Have Distinct Roles in Autoimmune Disease Caused by Loss of Death-Receptor-Induced Apoptosis. *Immunity*, 2016. 45(3): p. 513-526.
280. Ofengeim, D., et al., Activation of necroptosis in multiple sclerosis. *Cell Rep*, 2015. 10(11): p. 1836-49.
281. Najafov, A., H. Chen, and J. Yuan, Necroptosis and Cancer. *Trends Cancer*, 2017. 3(4): p. 294-301.

282. Seifert, L., et al., The necrosome promotes pancreatic oncogenesis via CXCL1 and Mincle-induced immune suppression. *Nature*, 2016. 532(7598): p. 245-9.
283. Richards, C.H., et al., The prognostic value of histological tumor necrosis in solid organ malignant disease: a systematic review. *Future Oncol*, 2011. 7(10): p. 1223-35.
284. Park, S., et al., The receptor interacting protein 1 inhibits p53 induction through NF-kappaB activation and confers a worse prognosis in glioblastoma. *Cancer Res*, 2009. 69(7): p. 2809-16.
285. Wang, Q., et al., RIP1 potentiates BPDE-induced transformation in human bronchial epithelial cells through catalase-mediated suppression of excessive reactive oxygen species. *Carcinogenesis*, 2013. 34(9): p. 2119-28.
286. Liu, X.Y., et al., RIP1 Kinase Is an Oncogenic Driver in Melanoma. *Cancer Res*, 2015. 75(8): p. 1736-48.
287. Wang, C., et al., RIP1 upregulation promoted tumor progression by activating AKT/Bcl-2/BAX signaling and predicted poor postsurgical prognosis in HCC. *Tumour Biol*, 2016. 37(11): p. 15305-15313.
288. Yang, C., et al., Regulation of RIP3 by the transcription factor Sp1 and the epigenetic regulator UHRF1 modulates cancer cell necroptosis. *Cell Death Dis*, 2017. 8(10): p. e3084.
289. Najafov, A., et al., BRAF and AXL oncogenes drive RIPK3 expression loss in cancer. *PLoS Biol*, 2018. 16(8): p. e2005756.
290. Koo, G.B., et al., Methylation-dependent loss of RIP3 expression in cancer represses programmed necrosis in response to chemotherapeutics. *Cell Res*, 2015. 25(6): p. 707-25.
291. Nugues, A.L., et al., RIP3 is downregulated in human myeloid leukemia cells and modulates apoptosis and caspase-mediated p65/RelA cleavage. *Cell Death Dis*, 2014. 5: p. e1384.
292. Hockendorf, U., et al., RIPK3 Restricts Myeloid Leukemogenesis by Promoting Cell Death and Differentiation of Leukemia Initiating Cells. *Cancer Cell*, 2016. 30(1): p. 75-91.
293. Liu, P., et al., Dysregulation of TNFalpha-induced necroptotic signaling in chronic lymphocytic leukemia: suppression of CYLD gene by LEF1. *Leukemia*, 2012. 26(6): p. 1293-300.
294. Moriwaki, K., et al., Differential roles of RIPK1 and RIPK3 in TNF-induced necroptosis and chemotherapeutic agent-induced cell death. *Cell Death Dis*, 2015. 6: p. e1636.
295. Bozec, D., et al., Critical function of the necroptosis adaptor RIPK3 in protecting from intestinal tumorigenesis. *Oncotarget*, 2016. 7(29): p. 46384-46400.
296. McCabe, K.E., et al., Triggering necroptosis in cisplatin and IAP antagonist-resistant ovarian carcinoma. *Cell Death Dis*, 2014. 5: p. e1496.
297. Jiao, D., et al., Necroptosis of tumor cells leads to tumor necrosis and promotes tumor metastasis. *Cell Res*, 2018. 28(8): p. 868-870.
298. Ruan, J., et al., Mixed lineage kinase domain-like protein is a prognostic biomarker for cervical squamous cell cancer. *Int J Clin Exp Pathol*, 2015. 8(11): p. 15035-8.
299. Ertao, Z., et al., Prognostic value of mixed lineage kinase domain-like protein expression in the survival of patients with gastric cancer. *Tumour Biol*, 2016. 37(10): p. 13679-13685.
300. He, L., et al., Low expression of mixed lineage kinase domain-like protein is associated with poor prognosis in ovarian cancer patients. *Onco Targets Ther*, 2013. 6: p. 1539-43.
301. Li, X., et al., Association of Mixed Lineage Kinase Domain-Like Protein Expression With Prognosis in Patients With Colon Cancer. *Technol Cancer Res Treat*, 2017. 16(4): p. 428-434.
302. Liu, X., et al., Key roles of necroptotic factors in promoting tumor growth. *Oncotarget*, 2016. 7(16): p. 22219-33.
303. Strilic, B., et al., Tumour-cell-induced endothelial cell necroptosis via death receptor 6 promotes metastasis. *Nature*, 2016. 536(7615): p. 215-8.

304. Schmidt, S.V., et al., RIPK3 expression in cervical cancer cells is required for PolyIC-induced necroptosis, IL-1alpha release, and efficient paracrine dendritic cell activation. *Oncotarget*, 2015. 6(11): p. 8635-47.
305. Yatim, N., et al., RIPK1 and NF-kappaB signaling in dying cells determines cross-priming of CD8(+) T cells. *Science*, 2015. 350(6258): p. 328-34.
306. Kang, Y.J., et al., Regulation of NKT cell-mediated immune responses to tumours and liver inflammation by mitochondrial PGAM5-Drp1 signalling. *Nat Commun*, 2015. 6: p. 8371.
307. Tenev, T., et al., The Ripoptosome, a signaling platform that assembles in response to genotoxic stress and loss of IAPs. *Mol Cell*, 2011. 43(3): p. 432-48.
308. Xu, Y., et al., Cisplatin-induced necroptosis in TNFalpha dependent and independent pathways. *Cell Signal*, 2017. 31: p. 112-123.
309. Brown, M.F., et al., Loss of caspase-3 sensitizes colon cancer cells to genotoxic stress via RIP1-dependent necrosis. *Cell Death Dis*, 2015. 6: p. e1729.
310. Fulda, S., Promises and Challenges of Smac Mimetics as Cancer Therapeutics. *Clin Cancer Res*, 2015. 21(22): p. 5030-6.
311. Cekay, M.J., et al., Smac mimetics and type II interferon synergistically induce necroptosis in various cancer cell lines. *Cancer Lett*, 2017. 410: p. 228-237.
312. Brumatti, G., et al., The caspase-8 inhibitor emricasan combines with the SMAC mimetic birinapant to induce necroptosis and treat acute myeloid leukemia. *Sci Transl Med*, 2016. 8(339): p. 339ra69.
313. Safferthal, C., K. Rohde, and S. Fulda, Therapeutic targeting of necroptosis by Smac mimetic bypasses apoptosis resistance in acute myeloid leukemia cells. *Oncogene*, 2017. 36(11): p. 1487-1502.
314. Hannes, S., B.A. Abhari, and S. Fulda, Smac mimetic triggers necroptosis in pancreatic carcinoma cells when caspase activation is blocked. *Cancer Lett*, 2016. 380(1): p. 31-8.
315. Chromik, J., et al., Smac mimetic primes apoptosis-resistant acute myeloid leukaemia cells for cytarabine-induced cell death by triggering necroptosis. *Cancer Lett*, 2014. 344(1): p. 101-109.
316. Sanjana, N.E., O. Shalem, and F. Zhang, Improved vectors and genome-wide libraries for CRISPR screening. *Nat Methods*, 2014. 11(8): p. 783-784.
317. Kowarz, E., D. Loscher, and R. Marschalek, Optimized Sleeping Beauty transposons rapidly generate stable transgenic cell lines. *Biotechnol J*, 2015. 10(4): p. 647-53.
318. Hjerpe, R., et al., Efficient protection and isolation of ubiquitylated proteins using tandem ubiquitin-binding entities. *EMBO Rep*, 2009. 10(11): p. 1250-8.
319. Nielsen, M.L., et al., Iodoacetamide-induced artifact mimics ubiquitination in mass spectrometry. *Nat Methods*, 2008. 5(6): p. 459-60.
320. Weinert, B.T., et al., Lysine succinylation is a frequently occurring modification in prokaryotes and eukaryotes and extensively overlaps with acetylation. *Cell Rep*, 2013. 4(4): p. 842-51.
321. Rappsilber, J., M. Mann, and Y. Ishihama, Protocol for micro-purification, enrichment, pre-fractionation and storage of peptides for proteomics using StageTips. *Nat Protoc*, 2007. 2(8): p. 1896-906.
322. Kelstrup, C.D., et al., Optimized fast and sensitive acquisition methods for shotgun proteomics on a quadrupole orbitrap mass spectrometer. *J Proteome Res*, 2012. 11(6): p. 3487-97.
323. Michalski, A., et al., Mass spectrometry-based proteomics using Q Exactive, a high-performance benchtop quadrupole Orbitrap mass spectrometer. *Mol Cell Proteomics*, 2011. 10(9): p. M111 011015.
324. Olsen, J.V., et al., Higher-energy C-trap dissociation for peptide modification analysis. *Nat Methods*, 2007. 4(9): p. 709-12.
325. Cox, J. and M. Mann, MaxQuant enables high peptide identification rates, individualized p.p.b.-range mass accuracies and proteome-wide protein quantification. *Nat Biotechnol*, 2008. 26(12): p. 1367-72.

326. Cox, J., et al., Andromeda: a peptide search engine integrated into the MaxQuant environment. *J Proteome Res*, 2011. 10(4): p. 1794-805.
327. Olsen, J.V., et al., Global, in vivo, and site-specific phosphorylation dynamics in signaling networks. *Cell*, 2006. 127(3): p. 635-48.
328. Elias, J.E. and S.P. Gygi, Target-decoy search strategy for increased confidence in large-scale protein identifications by mass spectrometry. *Nat Methods*, 2007. 4(3): p. 207-14.
329. Gao, Y.Y., et al., USP22 is a positive regulator of NFATc2 on promoting IL2 expression. *Febs Letters*, 2014. 588(6): p. 878-883.
330. Moquin, D.M., T. McQuade, and F.K. Chan, CYLD deubiquitinates RIP1 in the TNFalpha-induced necrosome to facilitate kinase activation and programmed necrosis. *PLoS One*, 2013. 8(10): p. e76841.
331. El-Mesery, M., M.E. Shaker, and A. Elgaml, The SMAC mimetic BV6 induces cell death and sensitizes different cell lines to TNF-alpha and TRAIL-induced apoptosis. *Exp Biol Med (Maywood)*, 2016. 241(18): p. 2015-2022.
332. Mojica, F.J.M., et al., Short motif sequences determine the targets of the prokaryotic CRISPR defence system. *Microbiology*, 2009. 155(Pt 3): p. 733-740.
333. Jouan-Lanhouet, S., et al., Necroptosis, in vivo detection in experimental disease models. *Semin Cell Dev Biol*, 2014. 35: p. 2-13.
334. Sawai, H., Characterization of TNF-induced caspase-independent necroptosis. *Leuk Res*, 2014. 38(6): p. 706-13.
335. Zhou, W. and J. Yuan, SnapShot: Necroptosis. *Cell*, 2014. 158(2): p. 464-464 e1.
336. Liu, X., et al., Post-translational modifications as key regulators of TNF-induced necroptosis. *Cell Death & Disease*, 2016. 7.
337. Huang, X., et al., USP22 Deubiquitinates CD274 to Suppress Anticancer Immunity. *Cancer Immunol Res*, 2019.
338. Lin, Z., et al., Ubiquitin-specific protease 22 is a deubiquitinase of CCNB1. *Cell Discov*, 2015. 1.
339. Hospenthal, M.K., T.E.T. Mevissen, and D. Komander, Deubiquitinase-based analysis of ubiquitin chain architecture using Ubiquitin Chain Restriction (UbiCRest). *Nat Protoc*, 2015. 10(2): p. 349-361.
340. Zhao, J., et al., Mixed lineage kinase domain-like is a key receptor interacting protein 3 downstream component of TNF-induced necrosis. *Proc Natl Acad Sci U S A*, 2012. 109(14): p. 5322-7.
341. de Almagro, M.C., et al., Cellular IAP proteins and LUBAC differentially regulate necrosome-associated RIP1 ubiquitination. *Cell Death Dis*, 2015. 6: p. e1800.
342. Hitomi, J., et al., Identification of a molecular signaling network that regulates a cellular necrotic cell death pathway. *Cell*, 2008. 135(7): p. 1311-23.
343. Lork, M., K. Verhelst, and R. Beyaert, CYLD, A20 and OTULIN deubiquitinases in NF-kappaB signaling and cell death: so similar, yet so different. *Cell Death Differ*, 2017. 24(7): p. 1172-1183.
344. Witt, A. and D. Vucic, Diverse ubiquitin linkages regulate RIP kinases-mediated inflammatory and cell death signaling. *Cell Death Differ*, 2017. 24(7): p. 1160-1171.
345. Wajant, H., TRAIL- and TNF-induced signaling complexes-so similar yet so different. *EMBO J*, 2017. 36(9): p. 1117-1119.
346. Wang, Y., et al., The deubiquitinase USP22 regulates PD-L1 degradation in human cancer cells. *Cell Commun Signal*, 2020. 18(1): p. 112.
347. Boone, D.L., et al., The ubiquitin-modifying enzyme A20 is required for termination of Toll-like receptor responses. *Nat Immunol*, 2004. 5(10): p. 1052-60.
348. Sun, S.C., CYLD: a tumor suppressor deubiquitinase regulating NF-kappaB activation and diverse biological processes. *Cell Death Differ*, 2010. 17(1): p. 25-34.
349. Durcan, T.M., et al., The Machado-Joseph disease-associated mutant form of ataxin-3 regulates parkin ubiquitination and stability. *Hum Mol Genet*, 2011. 20(1): p. 141-54.
350. Durcan, T.M., et al., USP8 regulates mitophagy by removing K6-linked ubiquitin conjugates from parkin. *EMBO J*, 2014. 33(21): p. 2473-91.

351. Weber, K., et al., Nuclear RIPK3 and MLKL contribute to cytosolic necrosome formation and necroptosis. *Commun Biol*, 2018. 1: p. 6.
352. Zhang, H., et al., Crucial Roles of the RIP Homotypic Interaction Motifs of RIPK3 in RIPK1-Dependent Cell Death and Lymphoproliferative Disease. *Cell Rep*, 2020. 31(7): p. 107650.
353. Cho, J., et al., Assay Systems for Profiling Deubiquitinating Activity. *Int J Mol Sci*, 2020. 21(16).
354. Xu, D., et al., Phosphorylation and activation of ubiquitin-specific protease-14 by Akt regulates the ubiquitin-proteasome system. *Elife*, 2015. 4: p. e10510.
355. Aaes, T.L., et al., Vaccination with Necroptotic Cancer Cells Induces Efficient Anti-tumor Immunity. *Cell Rep*, 2016. 15(2): p. 274-87.
356. Snyder, A.G., et al., Intratumoral activation of the necroptotic pathway components RIPK1 and RIPK3 potentiates antitumor immunity. *Sci Immunol*, 2019. 4(36).
357. Bruning, S.C., et al., 3D tumour spheroids for the prediction of the effects of radiation and hyperthermia treatments. *Sci Rep*, 2020. 10(1): p. 1653.
358. Courau, T., et al., Cocultures of human colorectal tumor spheroids with immune cells reveal the therapeutic potential of MICA/B and NKG2A targeting for cancer treatment. *J Immunother Cancer*, 2019. 7(1): p. 74.
359. Hu, Q.P., et al., Beyond a tumor suppressor: Soluble E-cadherin promotes the progression of cancer. *Int J Cancer*, 2016. 138(12): p. 2804-12.

9 Acknowledgements

First, I would like to thank Prof. Dr. Simone Fulda for giving me the opportunity to perform this PhD thesis in her well-equipped lab as well as for her supervision and regular discussions. I would also like to thank Prof. Volker Dötsch for accepting to be my supervisor at the Fachbereich 14 and for evaluating this work.

Next, I would like to thank Sjoerd van Wijk for his guidance, the fruitful discussions together, the regular meetings and of course for your special out of the box thinking! Thank you for the many fantastic advices and all the proof-reading work during my time in the lab! And of course not to forget, all the fun we had!

A special thanks goes out to Lisa and Rebekka. Lisa, I want to thank you for helping me to familiarize myself with the project! Rebekka, I want to thank you sharing so many inspiring thoughts on this project. I want to thank both of you for your support and the fun times we had, especially during my revision in the time of Corona. I really enjoyed being part of this USP22 team and I feel very honored for having had the opportunity to work with both of you.

Thanks to all members of the AG Fulda lab for creating this unique working atmosphere. Thanks for all the events inside and outside the lab and the various wise conversations during the countless coffee breaks. Especially, I would like to thank Dani and Sonja for keeping the lab spotless and organized! I also want to thank Christina Hugenberg for her expert help in all administrative and bureaucratic issues.

Thank you to Anne, Anna, Anni, Svenja, Lisa, Meike, Sjoerd, Rebekka and Tanja for the fun times we had in our second floor-office.

Finally, I would like to thank my whole family for believing in me and their continuous support! Heiko, I want to thank you for encouraging me and for all the discussions we had on our way back home. A special thanks goes out to Meriam, my wife! Thank you for being such a wonderful person and backing me up throughout my PhD thesis!

10 Curriculum vitae

Jens Rödиг

Kaiser-Wilhelm-Ring 39, 55118 Mainz

E-mail: jens.roedig@live.de

Mobile: 0157-73818982

Date of birth: 17/12/1989

[LinkedIn Profile](#)



EDUCATION AND RESEARCH EXPERIENCE

- | | |
|-------------------|---|
| 10/2016 – 09/2020 | <p>PhD-Student
 Institute for Experimental Cancer Research in Pediatrics, J.W. Goethe University Hospital Frankfurt am Main
 Supervisor: Prof. Dr. Simone Fulda
 Thesis: Characterization of the ubiquitin specific peptidase 22 in necroptotic signaling
 Key areas: Molecular biology, cancer therapy, ubiquitin, necroptosis,</p> |
| 02/2016 – 04/2016 | <p>Research Assistant
 Johannes Gutenberg-University (JGU) Mainz, Institute of Zoology, Department 1 Cell & Matrix Biology
 Key areas: Interaction studies of GPCRs in the frame of the DFG FOR 2149 project: Elucidation of Adhesion GPCR signaling</p> |
| 04/2013 – 02/2016 | <p>Master of Science in Biology, (Grade: 1.0)
 JGU Mainz
 Master Thesis, (Grade: 1.0)
 JGU Mainz, Institute of Zoology, Department 1 Cell & Matrix Biology</p> |
| 04/2010 – 04/2013 | <p>Bachelor of Science in Biology, (Grade: 2.4)
 JGU Mainz
 Bachelor Thesis, (Grade: 2.7)
 JGU Mainz, Institute of Molecular Genetics, Genetic Engineering Research and Consulting
 Thesis: Comparative analysis of methylation patterns in <i>Chironomus thummi</i> and <i>Chironomus piger</i></p> |

FUNDING

- | | |
|-------------|---|
| 2016 – 2019 | <p>PhD position, supported by the Deutschen Forschungsgemeinschaft (DFG) Project title: "Funktionelle Charakterisierung der Deubiquitinase USP22 als neuer Regulator von Nekroptose"</p> |
|-------------|---|

2015 – 2016 **Master position**, offered by DFG-FOR 2149 – Elucidation of Adhesion-GPCR signaling, Mainz

SCIENTIFIC CONFERENCES AND MEETINGS

09/2019 9th UCT Science Day, Frankfurt am Main **[Audience]**
 10/2018 26th Euroconference on Apoptosis "Cell death in disease: from small molecules to translational medicine", St. Petersburg, Russia **[Poster & Presentation]**
 02/2016 Young Scientist Retreat FOR 2149, Eisenach **[Poster]**
 04/2015 First Meeting of the Research Unit FOR 2149, Kleinlüder **[Audience]**

SPECIAL QUALIFICATIONS

08/2019 **Project management course**, FernUniversität in Hagen
 11/2018 **European Business Competence* License (EBC*L)**, FernUniversität in Hagen
 03/2016 **Experimental procedures with laboratory animals**, Translation Animal Research Center, JGU Mainz
 03/2015 **Safety in genetic engineering**, JGU Mainz

SKILLS

Methodical skills Cell culture, transfection (chemical and physical), CRISPR/Cas9, siRNA, cloning, PCR, RNA isolation, qRT-PCR, ELISA, Pull-down assays, Western blot, fluorescence microscopy, immunohistochemistry, FACS, mass spectrometry
Technical skills Microsoft Word, Excel, OneNote, Outlook and PowerPoint, Adobe Photoshop, CorelDRAW, GraphPad Prism, ImageJ

LANGUAGES

German Native speaker
English Fluent orally and in writing
French Basic knowledge

INTERESTS

since 10/2011 Trainer in trampolining
 since 05/2007 Referee in trampolining
 since 10/2006 Trainer of popular sport and performance training for all ages

LIST OF PUBLICATIONS

Original work

- 1) Jens **Roedig**, Lisa Kowald, Thomas Juretschke, Rebekka Karlowitz, Behnaz Ahangarian Abhari, Heiko Roedig, Simone Fulda, Petra Beli and Sjoerd J. L. van Wijk, 2020. USP22 controls necroptosis by regulating receptor-interacting protein kinase 3 ubiquitination. EMBO Reports (**Accepted for publication on 03.11.2020; EMBOR-2020-50163V3**)
- 2) Barbara Knapp, Jens **Roedig**, Karsten Boldt, Jacek Krzysko, Nicola Horn, Marius Ueffing, Uwe Wolfrum, 2019. Affinity Proteomics Identifies Novel Functional Modules Related to Adhesion GPCRs. Ann N Y Acad Sci 2019 Nov;1456(1):144-167
<https://pubmed.ncbi.nlm.nih.gov/31441075/>

11 Erklärung

Ich erkläre hiermit, dass ich die vorgelegte Dissertation mit dem Titel „Unraveling the functional relevance of the Ubiquitin-specific peptidase 22 for necroptotic cell death“ selbständig angefertigt und mich anderer Hilfsmittel als der in ihr angegebenen nicht bedient habe, insbesondere, dass alle Entlehnungen aus anderen Schriften mit Angabe der betreffenden Schrift gekennzeichnet sind. Alle Beiträge von Kollegen und Kolleginnen werden in der Arbeit explizit erwähnt und sind im Folgenden nochmals aufgeführt:

Figure 6 USP22 knockdown decreases TBZ-induced necroptotic cell death in HT-29 cells. Lisa Kowald (Doktorandin): Durchführung und Auswertung der Versuche; eigener Beitrag: Aufarbeitung der Figure.

Figure 7 CRISPR/Cas9-mediated knockout (KO) of USP22 in HT-29 cells increases H2Bub1 levels. Rebekka Karlowitz (Doktorandin): Durchführung des Western Blots Figure 7A; eigener Beitrag: Generierung der USP22 KO HT-29 Zellen, Aufarbeitung der Figure.

Figure 13 USP22 KO reduces TBZ-induced necroptotic cell death in acute lymphoblastic leukemia (ALL) Jurkat cells. Rebekka Karlowitz (Doktorandin): Durchführung des Western Blots Figure 13B, Durchführung der Zelltodversuches Figure 13C; eigener Beitrag: Zelltodversuch Figure 13A, Aufarbeitung der Figure.

Figure 14 CRISPR/Cas9-mediated knockout of USP22 in NB4 cells does not affect TB-induced apoptotic cell death. Lisa Kowald (Doktorandin): Durchführung und Auswertung der Versuche; eigener Beitrag: Aufarbeitung der Figure, Generierung der USP22 KO NB4 Zellen.

Das unten aufgeführte Material wurde im Rahmen von Forschungsk Kooperationen erstellt:

Figure 24 Ubiquitin remnant profiling identifies RIPK3 K518 as USP22-dependent ubiquitin target during necroptosis; Kollaborationspartner: Thomas Juretschke und Petra Beli, Institut für Molekulare Biologie (IMB), Ackermannweg 4, 55128, Mainz; Beitrag des Kollaborationspartners: Massenspektrometrische Analyse, Aufbereitung der Daten (Quantifizierung und statistische Auswertung); eigener Beitrag: Vorbereitung der Proben für Massenspektrometrische Analyse, Analyse der Daten, Aufbereitung der Figure

Die folgenden Teile der Dissertation sind bereits in Teilen veröffentlicht worden [#EMBOR-2020-50163V3; akzeptiert zur Veröffentlichung am 03.11.2020]:

Vereinzelte Textpassagen aus folgenden Kapiteln:

2.2 Ubiquitin-specific peptidase 22

5.1 USP22 governs necroptotic signaling by regulating RIPK3 ubiquitination and phosphorylation

5.1.1 USP22 regulates necroptosis in HT-29 cells

5.1.2 Loss of USP22 induces resistance to necroptotic cell death in RIPK3-expressing HeLa cells

5.1.3 USP22 controls RIPK3 ubiquitination during necroptosis induction

5.1.4 USP22 mediates RIPK3 ubiquitination and controls necroptosis through RIPK3 K518 ubiquitination

5.1.5 RIPK3 K518R hypersensitizes HT-29 cells to TBZ-induced necroptosis

6.1 USP22 controls TBZ-induced necroptotic cell death in human tumor cell lines

6.2 USP22-mediated deubiquitination of RIPK3

6.3 USP22-mediated RIPK3 K518 ubiquitination regulates necroptosis progression

6.4 USP22 affects RIPK3 phosphorylation during TBZ-induced necroptosis

Teile von Figuren:

- Figure 6 USP22 knockdown decreases TBZ-induced necroptotic cell death in HT-29 cells.
- Figure 7 CRISPR/Cas9-mediated knockout (KO) of USP22 in HT-29 cells increases H2Bub1 levels.
- Figure 8 USP22 knockout (KO) decreases TBZ-induced necroptotic cell death in HT-29 cells.
- Figure 9 Loss of USP22 in HT-29 cells does not affect NF- κ B activation upstream of I κ B α .
- Figure 10 Loss of USP22 in HT-29 cells does not affect TB-induced apoptosis.
- Figure 11 Stable reconstitution of USP22 in USP22 KO HT-29 cells re-sensitizes USP22 KO HT-29 cells for TBZ-induced necroptosis.
- Figure 12 HT-29 USP22 KO (2g) cells display a comparable number of cells re-expressing USP22 PAM, USP22 PAM C185S or USP22 PAM C185A.
- Figure 13 USP22 KO reduces TBZ-induced necroptotic cell death in acute lymphoblastic leukemia (ALL) Jurkat cells.
- Figure 14 CRISPR/Cas9-mediated knockout of USP22 in NB4 cells does not affect TB-induced apoptotic cell death.

- Figure 15 CRISPR/Cas9-mediated knockout of USP22 does not alter TBZ-induced cell death in MEF cells and the macrophage cell lines Raw264.7 or J774A.1. 65
- Figure 17 USP22 KO leads to increased TBZ-induced RIPK3 phosphorylation in HT-29 cells.
- Figure 18 USP22 knockdown in RIPK3-expressing HeLa cells induces resistance to TBZ-induced necroptotic cell death.
- Figure 19 USP22 KO in HeLa TRex RIPK3 does not affect complex-I or -II formation.
- Figure 20 USP22 KO leads to increased TBZ-induced RIPK3 phosphorylation in HT-29 cells.
- Figure 21 USP22 interacts with RIPK3 independently of TBT treatment.
- Figure 22 Increased RIPK3 ubiquitination in USP22 KO HT-29 cells during TBZ-induced necroptosis.
- Figure 23 USP22 KO in HT-29 cells does not alter TBZ-induced RIPK1 ubiquitination.
- Figure 24 Ubiquitin remnant profiling identifies RIPK3 K518 as USP22-dependent ubiquitin target during necroptosis.
- Figure 25 SILAC incorporation does not alter the resistance of HT-29 USP22 KO cells to TBZ-induced necroptosis or the expression levels of necroptotic core proteins.
- Figure 26 USP22-dependent modification of RIPK3 lysine residue 518 amplifies TBZ-induced necroptotic responses in RIPK3-reconstituted HeLa cells.
- Figure 27 siRNA-mediated knockdown of USP22 in RIPK3-K518R or RIPK3 3xKR reconstituted HeLa cells does not affect sensitivity to TBZ-induced necroptotic cell death.
- Figure 28 Mutation of RIPK3 lysine residue 518 alter RIPK3 phosphorylation upon TBZ-induced necroptosis in RIPK3-reconstituted HeLa cells.
- Figure 29 Mutation of RIPK3 lysine residue 518 amplifies necrosome formation upon TBZ-induced necroptosis in RIPK3-reconstituted HeLa cells.
- Figure 30 Mutation of RIPK3 lysine residue 518 decreases RIPK3 ubiquitination upon TBZ-induced necroptosis in RIPK3-reconstituted HeLa cells.
- Figure 31 RIPK3 KO HT-29 cells are resistant against TBZ-induced necroptosis.
- Figure 32 RIPK3 K518R hypersensitize HT-29 cells for TBZ-induced necroptosis.
- Figure 33 RIPK3 K518R amplifies necrosome formation upon TBZ-induced necroptosis in HT-29 cells.
- Figure 34 USP22 controls necroptotic cell death by regulating RIPK3 phosphorylation and RIPK3 K518 ubiquitination.

Ich versichere, die Grundsätze der guten wissenschaftlichen Praxis beachtet, und nicht die Hilfe einer kommerziellen Promotionsvermittlung in Anspruch genommen zu haben.

Frankfurt am Main, den